DAE – BRNS

16th National Symposium and Workshop on Thermal Analysis

Proceedings of the WORKSHOP

held

at IGCAR, Kalpakkam during 7-8, February, 2008

Contents

Thermal Analysis in Materials Research

P.V. Ravindran
Analytical Chemistry Division, Bhabha Atomic Research Centre,
Trombay, Mumbai 400 085

Dr. P.K. Ravindran graduated from University of Kerala on 1969 and joined the Department of Atomic Energy in 1970 after completing orientation course in Chemistry in BARC Training School. He has since been actively engaged in research work in the field of thermal analysis in analytical Chemistry Division of Bhabha Atomic Research Centre. He was awarded Ph.D degree from University of Bombay in 1987 for his work on non-isothermal kinetics of solid sate reactions. His other areas of interest include elucidation of thermal decomposition schemes, chromatographic and electroanalytical methods of analysis and applications of computers in chemistry and in particular, thermoanalytical research. He is presently serving as Head, Thermal and Electrochemical Methods Section of Analytical Chemistry Division. He has over seventy publications in the field of thermal analysis, including several publications in international journals and contribution to chapters in books. He is a founder member of Indian Thermal Analysis Society (ITAS) and has been actively engaged in its activities for promoting the science of thermal analysis in the country as Vice President / Secretary /Treasurer (ITAS), Editor of Bulletin of Thermal Analysis and Convener of National Symposium and Workshop on Thermal Analysis organized by ITAS.

Materials evaluation under conditions of actual application is essential for ensuring optimum use of the materials, especially, to meet demands of newer technologies. One of the procedures with potential for such testing is assessment of thermal stability using thermoanalytical measurements. Although normally thermoanalytical measurements are carried out under atmospheric pressure, techniques like, differential thermal analysis (DTA) are amenable to design adaptation for measurements under high pressure and high temperature. This in situ measurement capability under extreme conditions of temperature and pressure is one of the most attractive features of thermal analysis techniques. Thermoanalytical measurements involve the measurement of physical properties of substances as a function of temperature under controlled conditions. Changes in various physical properties, such as weight, enthalpy, visco-elastic, optical, electrical and magnetic properties, dimension, etc. are followed as functions of temperature. Depending on the physical property being measured, there are a large number of techniques, listed in Table1, that come under the scope of thermal analysis. Such measurements may constitute use of a single technique or simultaneous analysis involving two or more techniques to follow the thermal effects in a given sample. A wide range of temperature from -100 to 2400°C has been considered in some of these studies. Thermogravimetry, Differential Thermal Analysis, Differential Scanning Calorimetry, Evolved Gas Analysis and Thermomechanical Analysis, which are the widely used among these methods, will be considered in some detail in the subsequent sections.

Table 1: Thermoanalytical techniques

| Technique	Abbreviation	Physical property measured
Thermogravimetry	TG	Weight / Change in weight of the sample
Differential thermal analysis	DTA	Difference in temperature between the sample and a thermally inert reference material heated identically
Differential scanning calorimetry	DSC	Rate of change of enthalpy
Evolved gas analysis	EGA	Nature of gases evolved
Thermodilatometry		Change in dimension of the sample under zero load
Thermomechanical analysis	TMA	Change in visco-elastic properties under non-oscillatory load
Dynamic mechanical analysis	DMA	Change in visco-elastic properties under oscillatory load
Thermooptometry		Change in optical properties
Thermomagnetometry		Change in magnetic properties
Themoelectrometry		Change in electrical properties

Thermogravimetry

Thermogravimetry is widely used for the study of solid-gas reactions, e.g.,

Thermogravimetric measurements involve, the recording of weight or change in weight of the sample as a function of time or temperature while heating or cooling it in a controlled manner. Usually, the heating / cooling programme is such that the temperature is varied linearly with time. Further, the sample environment can be static or dynamic, and inert, reactive or of the product gas type. The TG curve (Fig. 1) consisting of constant weight plateaus interspersed with weight change steps are very useful for the study of solid-gas reactions, e.g.,

$$A(s) \rightarrow B(s) + C(g) \quad \text{...} \quad (1)$$

and

$$A(s) + C(g) \rightarrow B(s) \quad \text{...} \quad (2)$$
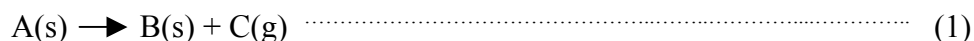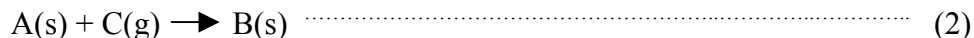
The magnitude of the weight change corresponds to the stoichiometry of the reaction and the length of the constant weight plateau represents the temperature range of stability of the corresponding reaction intermediate. The temperature of inception, T_i, or the temperature at which the weight of the sample starts to deviate from the constant weight plateau, is useful in comparing the thermal stabilities of the various compounds. T_m is the temperature at which the rate of change of weight is a maximum and T_f is the temperature at which the formation of the new intermediate compound is completed.

The TG curves are recorded using a thermobalance, facilitating the recording of weight of the sample continuously as a function of time. It is a combination of the automatic recording balance, the furnace, the temperature programmer controller and the recorder. The automation in weight recording is achieved through the use of appropriate transducers, which convert the net mechanical forces on the balance beam into electrical signals. One of the most sensitive transducers makes use of the electromagnetic compensation of deflection of the balance beam. The beam is suspended using a torsion fiber attached to a solenoid kept between the poles of a permanent magnet. Deflection of the beam is detected by a lamp-shutter-phototube arrangement. The light falling on the phototube is controlled by the shutter fixed at one end of the beam. Hence, a deflection of the beam causes increased or decreased generation of photocurrent with respect to that corresponding to the reference (null) position of the beam. The changed photocurrent generates a counterbalancing force in the solenoid and returns the beam to its reference position. The change in photocurrent generating the counterbalancing force is a measure of the extent of deflection of the beam and hence the change weight of the sample. This arrangement is capable of detecting changes in weight of the order of 0.1 microgram in 1 g. Simpler arrangements, for example, employing changes in inductive pick-ups (LVDT) or capacitance have also been used to monitor weight changes continuously as a function of time.
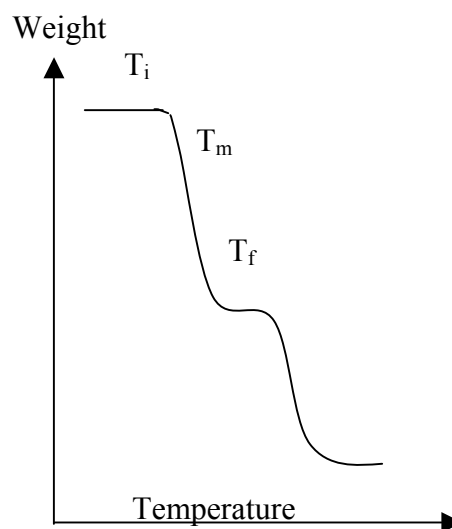

Fig. 1 Typical TG curve

The time derivative of the TG curve is referred to as the derivative thermogravimetric (DTG) curve. It can be easily recorded using simple resistance-capacitance circuits to differentiate the output of the thermobalance. Alternately, the weight change data may be curve-fitted and then differentiated using suitable computer programs. The DTG curve provides information on kinetics of the solid-gas reaction. Overlapping consecutive reaction steps are better resolved on the DTG curve than on TG curve.

The temperature and weight data recorded in thermogravimetry are affected by several experimental variables. The most significant among these are heating rate as well as the buoyancy change and convection currents due to temperature gradients in the environment surrounding the sample. The apparent weight changes caused by these effects are superimposed on the actual change in weight of the sample as it is being heated. The consequent errors in weight change data recorded should be either minimized by suitable experimental design or by appropriate blank correction procedures. The blank data have to be recorded for the specific experimental condition defined by the dimensions of the reaction chamber, nature and flow rate of the sample environment, heating rate as well as the material of construction and geometry of the sample holder. Blank correction is satisfactory only when the desired lowest detection limit of weight
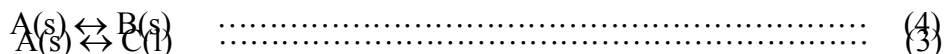
change measurements is 0.5% or more. Symmetric beam balances employing identical heating and gas flow arrangements around both sample and counter-poise are necessary for applications requiring lower detection limits of the order of 0.05%.

Accuracy in temperature measurement is another factor influencing the reliability of thermogravimetric data. Difficulty in the keeping the temperature sensor in contact with the sample without affecting the balance response necessitates a compromise between sensitivity of weight measurement and accuracy of temperature information. The temperature sensor has to be necessarily kept separated from the sample holder while working with sensitive balances. The resulting errors in temperature measurement are dependent on the temperature gradients in and around the sample and hence become more prominent with increasing heating rate and sample weight. The effects of sample environment on the reaction equilibria make calibration of temperature response a difficult task. Alloys undergoing Curie transitions enabling detection of transition point from apparent mass changes observed when the sample is kept in a magnetic field have been recommended as calibrants to overcome this problem.

Reactivity of the sample and/or its reaction products with the sample environment also has to be considered while interpreting the thermogravimetric data. Thus organic compounds like polymers undergo oxidative degradation in oxygen-rich environments, but decompose to monomers in inert atmosphere. Similarly, oxidation of lower valent metal oxide intermediates to higher valent metal oxides observed in oxygen-rich environments as a weight gain step, will be absent from TG data recorded in inert atmosphere. Decomposition reactions in gaseous environments rich in product gas tend to be shifted to higher temperatures.

Differential Thermal Analysis

Differential Thermal Analysis (DTA) provides a direct means of assessing changes in a system by following the energy changes undergone by it. DTA has been used extensively by mineralogists, analytical chemists, polymer chemists, physical chemists, metallurgists, cement technologists and ceramists for identification and characterisation of changes of phase and composition in materials. In combination with thermogravimetry, evolved gas analysis, X-ray diffraction and infra red spectroscopy it provides a powerful means of phase analysis in addition to interpretation of thermal decomposition mechanism and thermal stability of materials. In fact, along with high-temperature X-ray diffraction, DTA and differential scanning calorimetry (DSC) are two important tools available to physical chemists for observation of high-temperature phase changes in situ. DTA can be used for the study of the following equilibria,

$$A(s) \leftrightarrow B(s) \quad \text{\dots\dots\dots\dots\dots\dots\dots\dots\dots\dots\dots\dots\dots} \quad (4)$$
$$A(s) \leftrightarrow C(l) \quad \text{\dots\dots\dots\dots\dots\dots\dots\dots\dots\dots\dots\dots\dots} \quad (3)$$

in addition to the cases represented by eq. (1) and (2). The only condition necessary to be

$$A(s) + B(s) \leftrightarrow D(s) \quad \text{\dots\dots\dots\dots\dots\dots\dots\dots\dots\dots} \quad (5)$$
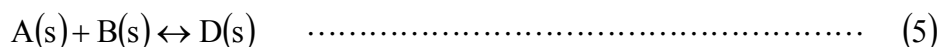
satisfied is that energy changes involved should be of sufficient magnitude to be

detectable. Such energy changes induce self-heating or self-cooling of the sample. The consequent alteration of temperature profile in the sample is the basis of DTA signal. Comparison of the instantaneous temperature at a specified location in the sample with that in a thermally inert reference material maintained in the same thermal regime provides a differential temperature signal which is recorded as a function of temperature of the sample / reference material varied under pre-defined conditions to get the DTA curve. Since the reference temperature is usually varied linearly with time, the differential temperature (T_{sample} - $T_{reference}$) can also be plotted against time to record the DTA curve.

An attractive feature of differential thermal analyser is that the instrumentation involved is simple and cheap. A system for use in static air environment between ambient temperature and 1000°C can easily be set up in any laboratory. A resistive furnace with nichrome wire as heating element, chromel-alumel thermocouples, a temperature-programmer controller, sample crucibles made from platinum, alumina or silica, a pre-amplifier and a millivolt recorder are sufficient to set it up. More advanced versions can be set up by adding facilities for atmosphere control, higher temperature operation and personal computer based data acquisition and processing.

A predictable temperature profile within the system can be achieved only with the use of a carefully designed furnace. Hot spots resulting from non-uniform winding will give rise to spurious peaks. Non-inductive winding is employed to ensure elimination of a.c. pick-ups. The requirement of a fairly large uniform temperature zone necessitates design of relatively large furnaces. The upper limit of temperature of the furnace is determined by the nature of winding, former, furnace atmosphere, etc. Facility for accelerated cooling up to or below room temperature is an added advantage.

Proportional-integral-differential (PID) control and suitability for operation in heating, cooling and isothermal modes are the sought after features for temperature-programmer controllers. The control element (usually, a thermocouple) providing feedback of furnace temperature to the program controller should ideally be placed close to the heating element to prevent `hunting' of temperature around the control value.

The differential temperature signal is affected by the nature of reactions in and around the sample as well as by the rates of heat and mass transfer between the sample and its environment. Several factors, which affect the following processes, must be duly considered before attempting interpretation of the DTA curves:

(i) Chemical or physical transformations in the sample forming solid, liquid and/or gaseous products: The reactions can be well resolved, consecutive or with more than one process occurring simultaneously. Resolution of consecutive reaction peaks can be improved by decreasing the sample weight and reducing the heating rate as these factors decrease the temperature span of the reaction. Annealing of crystal defects in poorly crystallised samples leads to spurious peaks.

(ii) Interaction between the sample or reaction products and other materials in contact with it: Sample-sample holder and sample-thermocouple interactions are of interest in this context. The commonly used platinum sample holders catalyse several gas phase reactions. Sometimes the sample is diluted with a material having thermal characteristics close to those of the reference material

to ensure better baseline characteristics and hence to obtain well defined peaks. In such cases, sample-diluent interactions also become important.

(iii) Interaction between the sample, reaction products, sample holder or thermocouples and the environment: Static atmosphere allows accumulation of product gases and impedes the forward reaction. Variation of gas composition within the sample pores during the reaction affects the thermal conductivity of the sample and hence the temperature gradients within it. Dynamic atmosphere, preferably through the sample, facilitates uniform composition of gaseous mixture in the vicinity of sample particles and ensures better-defined conditions of heat transfer to the specimen.

The chemical interaction between the atmosphere and the sample depends on the nature of the environmental gas (inert, reactive or product-gas type) and the ease of inflow and outflow of gases from the sample. The usefulness of measurements in reactive atmosphere depends on the reaction equilibrium of interest. Side reactions are undesirable and possible reactions with the products will have to be considered. In product-gas atmosphere, the decomposition temperatures are shifted to higher values as compared to inert gas atmosphere or vacuum.

Base-metal thermocouples, preferred as sensors at lower temperatures due to low cost and better sensitivity, are not reliable at high temperatures in oxidising atmospheres. Similarly, Pt/Pt-10%Rh thermocouples usable in oxidising atmospheres up to 1900 K are unreliable in reducing atmospheres.

(iv) Heat transfer: A number of instrumental factors such as heating rate, location of thermocouple, type of specimen holders, temperature-programmer controller and furnace affect the nature of heat transfer between the furnace and the specimen, sample and reference material as well as specimen and sensors. The heat transfer within the sample holder is affected by the characteristics of the sample.

Temperature gradients within the furnace and specimen holder assembly are determined largely by the heating or cooling rate. Heating rates of 6 - 10^oC/min are generally used for qualitative applications. It may be desirable to use a lower heating rate in the range of 2 - 5^oC/min for quantitative work. An increase in heating rate increases the differential temperature signal. The inception temperature, T_i, is not much affected, but the peak temperature, T_p, and final temperature of the peak, T_f, are shifted to higher values with increased heating rate, resulting in poorly resolved peaks for consecutive reactions. The time span of the peak, however, decreases with increase in heating rate. The combined effect of heating rate on differential temperature, ΔT, and time span of the peak is such that the area under the DTA peak, recorded as ΔT versus time, is not affected significantly by changing the heating rate.

The geometry of the sample holder influences the heat transfer within the sample and hence affects the shape of the DTA peaks. Peaks recorded with cylindrical sample holders become sharper on decreasing the radius of the

sample holder. Heat capacity and emissivity of the material of construction of the sample holder also affect the intensity of peaks recorded, endothermic reactions being more intense under conditions ensuring enhanced insulation of the sample, e.g., heat capacity, thermal conductivity, bulk density and particle size also affect heat transfer within it and hence modify the differential temperature signal. However, the effects of these variables are often additive or mutually compensating and hence not easy to predict or interpret. It is therefore advisable to maintain identical conditions of packing and particle size in all the experiments.

Table 2: Calibration standards useful in DTA measurements

Calibrant	Transition temperature (K)	Heat of reaction (J/g)
KNO_3	400.7	54.06
In	430	28.41
Sn	504.9	59.66
SiO_2	846	10.25
K_2SO_4	856	46.61
K_2CrO_4	938	52.63
$BaCO_3$	1083	-
$SrCO_3$	1198	-

The DTA curve, interpreted after giving due considerations to the above factors, can be used to ascertain the thermal stabilities of substances and their thermal decomposition intermediates based on the temperature of transformation. Although peak temperature is sometimes reported as a measure of thermal stability, it is dependent on several experimental factors and hence the inception temperature or the more reproducible extrapolated on-set temperature is the preferred index of thermal stability. Even in this case, the temperature axis must be calibrated using appropriate standards. The standards and the respective transition temperatures recommended by the Standardisation Committee of International Confederation of Thermal Analysis and Calorimetry are given in Table 2. These standards are available from NIST, U.S.A.

The qualitative interpretation of thermal stability and quantitative assessment of heat effects, though approximate, possible with this technique based on energy changes within the sample, facilitate study of a wide variety of substances over a large temperature range in a short time. If appropriate care is exercised in designing the experiment, and if the results are supplemented by additional measurements, like, thermogravimetry, X-ray diffraction, evolved gas analysis and infra red spectroscopy, DTA can be a very useful tool in the hands of a materials scientist.

Differential Scanning Calorimetry

The differential temperature developed between the sample and reference material, due exothermic or endothermic reaction in the sample, is converted into energy

units (mW or mJ/s) in DSC by appropriate calibration against known heat input. The DSC signal may be recorded in power compensated or heat flux modes. In the former case, the instantaneous differential temperature is compensated by additional heat input to the reference holder (for exothermic reaction in the sample) or sample holder (for endothermic reaction in the sample) and the rate of such instantaneous heat input is recorded against time or temperature.

Although the signal recorded using power compensated instruments is in the absence of any heat leakage between the sample and reference material and is directly in energy units, the instrumentation involved in this type of measurement is more complex. In heat flux DSC, on the other hand, the instrumentation involved is simpler as it involves direct measurement of the differential temperature proportional to the difference in heat flux to the sample and reference holders. Although this is similar to DTA, the sensor used is much more sensitive than the simple differential thermocouple used in DTA. This ensures that the differential temperature is small and proportional to the differential heat flux between the sample and reference holders. Further, the differential temperature measured in heat flux DSC is directly in energy units. In the case of both power compensated and heat flux DSC, the DSC signal can be considered to be proportional to rate of change of heat content of the system,

$$dq/dt = K\, dH/dt \quad\quad\quad\quad\quad\quad\quad\quad\quad (6)$$

where K is the calibration constant. Unlike in DTA, the calibration constant in DSC is relatively independent of temperature. A temperature-dependent calibration factor needs to be considered only when high accuracy is expected. It is evident from the above equation that the ordinate of the DSC curve is proportional to heat capacity, i.e.,

$$dq/dt = K\, dH/dT\, dT/dt = K\beta C_p \quad\quad\quad\quad\quad\quad (7)$$

where β is the heating rate maintained constant in DSC measurements. Hence DSC curve can be used for detecting glass transitions, which are accompanied by change in heat capacity rather than enthalpy change. This is helpful in characterising many polymeric materials on the basis of glass transition. Integration of eq. (6) gives the enthalpy change in the reaction as

$$\Delta H = K'\, \Delta Q = K'\, A \quad\quad\quad\quad\quad\quad\quad\quad (8)$$

where $K' = 1/K$ and A is the area enclosed by the DSC peak and the baseline interpolated in the reaction interval.

Evolved Gas Analysis (EGA)

The material of interest may contain several components and more than one component may often contribute to change in a particular physical property. A simple TG measurement or a combination of TG and DTA would not be enough to interpret the corresponding reactions. Additional useful information on the reaction can be obtained in such cases by using evolved gas analysis (EGA) if the different components evolve different gaseous species. It is possible that different components evolve same gaseous

species over the temperature range of interest. Although such processes cannot be completely resolved in EGA, the information on the nature of gaseous species derived from it helps a better understanding of the process than that is possible by using other thermoanalytical techniques. The international Confederation for Thermal Analysis and Calorimetry (ICTAC) has recommended the use of the term `evolved gas analysis (EGA)' whenever the technique involves detection and identification of the gaseous species evolved during heating a substance under controlled conditions.

A closely related technique is evolved gas detection (EGD) in which the evolution of the total gas during heating a substance under controlled conditions is detected. The individual components of the gaseous species are not identified in this case. A simple thermal conductivity detector can be used for EGD measurements. However, the information derivable from EGD measurements does not add significantly to that from simultaneous TG-DTA measurements.

Gas titrimetry, gas chromatography, mass spectrometry and Infra red spectroscopy have been used as EGA systems. Gas titrimetry involves absorption of the volatiles in appropriate reagents and determining the consumption of the reagent in the consequent reaction titrimetrically. The method requires apriori knowledge of the nature of volatiles for selecting the proper reagent. Further, the selectivity of the method is poor.

Gas chromatograph is one of the simplest and most commonly used evolved gas analyzer. The effluents from the pyrolysis chamber are led either to cold traps or an automatic sampling device. The condensed volatiles in the cold traps can later be introduced into a gas-liquid chromatography (GLC) column by flash heating of the traps. Alternatively, the automatic sampling device is used to inject at regular intervals a measured quantity of the sample effluent into the GLC column. The GLC column consists of a liquid (stationery) phase held on an inert support material packed in the column. The components of the volatile sample injected into the column are separated according to the way they partition between the liquid and the gas (mobile) phases. The individual components eluted from the column in accordance with their retention times are detected using a thermal conductivity detector, flame ionization detector, electron capture detector, etc.

The GLC peaks recorded reflect the instantaneous concentration of the volatile corresponding to a mean temperature in the interval of sampling. Either peak area or peak height may be used as a measure of the instantaneous concentration of the volatile and the overall gas evolution profile may be constructed by plotting these as a function of the mean temperature. The reliability of the gas evolution profile so constructed will be best when the sampling rate is high. The retention time of the last component to be eluted by the GLC column and the heating rate should be small to enhance the sampling rate.

Gas chromatographic technique has the disadvantage that there is a significant time delay in the detection of a gaseous species after it has evolved in the reaction zone. The use of a separating column necessarily implies that the gas evolution profile is modified by the rate of elusion of the gaseous component from the separating column. Hence a one-to-one correspondence between gas evolution and gas detection is not possible in this case. In other words, when a gas chromatograph is used for EGA in combination with another thermoanalytical technique, say, thermogravimetry, the

interpretation of the TG curve is vitiated by the absence of one-to-one correspondence between the TG and EGA curves on the time/temperature axis. A mass spectrometer may be used as the gas analyzer to overcome these difficulties because in this case the separation and detection of components of the gaseous mixture injected into the mass spectrometer is achieved almost instantaneously at least with reference to the time scale used in thermoanalytical measurements.

Among the various types of mass spectrometers, the quadrupole mass spectrometer is more commonly employed as the gas analyzer. It is easier to handle and occupies less space compared to the other types of mass spectrometers. However, the resolution between closely lying mass spectral peaks obtainable with this instrument is rather low, of the order of a few thousand atomic mass units. Furthermore, in this case, the resolution varies with mass and is inversely related to the sensitivity.

The need to have a high vacuum (of the order of 10^{-5} mbar) in the mass spectrometer necessitates the use of an interface between the thermal analyser operated at atmospheric pressure and the mass spectrometer. A long heated capillary between the thermal analyser and the mass spectrometer is commonly used for the purpose (Fig. 2). The volatiles evolved in the thermal analyzer are carried to a line splitter. One arm of the line splitter is connected to the capillary and the other arm is open to atmosphere. The other end of the capillary is connected to a chamber evacuated to 1 mbar using a low-capacity, rotary vane pump, such that laminar flow conditions prevail in the capillary. A frit valve between this chamber and the ionization chamber of the mass spectrometer facilitates molecular leak of the volatiles into the mass spectrometer.

The heated capillary interface involves a long transfer line for the evolved gas and hence the conclusions arrived at can often be vitiated by condensation of volatiles in the interface. A micro orifice interface involving two differentially pumped chambers connected through a very fine orifice enables a closer proximity of mass spectrometer to specimen holder assembly of the thermal analyser. This helps to minimize condensation problems and thereby facilitates study of high-temperature volatile systems. Alternately, a jet separator can also be used as the interface between the pyrolysis chamber and the mass spectrometer. In the latter case, however, the carrier gas used is restricted to a light gas like helium or hydrogen. Such a restriction is a drawback when coupling the mass spectrometer with a thermal analyser because thermal analysis measurements have to be carried out under different atmospheric conditions. Further, helium gas, being a good conductor of heat, reduces the sensitivity of DTA measurements.

Fast scanning infra red spectrometers have ensured successful use of infra red spectrometry in combination with thermal analysis. This has the advantage that TG-DTA-EGA measurements can also be carried out in wide variety of environments including oxidizing atmospheres. On the other hand, while using mass spectrometer equipped with electron bombardment-type ion source, oxidizing gases are normally excluded as they shorten the lifetime of the filament of the ion source. In view of the overlap between infra red absorption frequencies of several gases, the costlier Fourier transform infra red spectrometers have to be used to ensure better resolution. Software for handling the large database of infra red spectra is essential for a successful exploitation of the technique.

Thermomechanical analysis (TMA)

Thermomechanical analysis is very useful for the assessment of polymeric materials by following changes in their mechanical strength. Softening of the materials due to exposure to high temperatures and load is the subject of these studies. Various modes of measurement include extension, penetration, flexure (bending), etc. Generally, the sample in the form of a block is held using an appropriate support and the load is applied from above while the sample itself is heated in a controlled manner (Fig. 3). A quartz or boron nitride rod in contact with sample serves as the probe and its movement

Fig. 2. Schematic of a simultaneous Thermal Analysis - Mass Spectrometry system

due to visco-elastic changes in the sample is followed using a linear variable differential transformer (LVDT). The output of the LVDT is proportional to the change in dimension (ΔL) of the sample. A plot of the relative change in dimension ($\Delta L/L_o$) vs. temperature, with L_o as the original dimension, constitutes a TMA curve. The different configurations of sample holder presented in Fig. 3 are useful for following the changes in different modes of visco-elastic properties, like, expansion, penetration, flexure, extension, etc. Themomechanical analyser is used extensively in the characterization of polymers.

Other techniques, like dynamic mechanical analysis, torsional braid analysis, etc. which are broadly classified as thermomechanometry, are also widely used in polymer characterization. In these types of instruments the sample is subjected to oscillations at selected frequencies while being heated and the damping of such oscillations is followed as a function of temperature. The damping depends on the intramolecular forces and hence the results of such studies are useful in the interpreting the structural characteristics of the polymer.

Simultaneous and Complementary Measurements – An Example

TG-DTA-EGA measurements have been successfully used for the phase identification of a number of substances in our laboratry. Use of Thermogravimetry for characterization of high temperature superconducting oxide, $YBa_2Cu_3O_{7-\delta}$, is well recognized. The compound is known to have labile oxygen content which is reversibly lost above 400°C. A TG measurement in oxygen atmosphere to establish the reversibility of this oxygen loss is one of the methods recommended to distinguish a `good' superconducting yttrium-barium-copper oxide from a `bad' one. In one such study, an oxide with poor superconducting properties was observed to have an additional weight loss in the temperature range 150-350°C. X-ray diffraction measurements on the sample showed only insignificant level of impurity phases. Hence the low temperature weight loss was attributed to oxygen loss.

We carried out a TG-DTA-EGA study on the sample. The results presented in Fig. 4 showed that the sample released carbon dioxide and oxygen at temperatures above 150^oC. Oxygen release could be seen only above 400^oC, whereas carbon dioxide loss was observed from EGA data in the temperature ranges of $150\text{-}350^oC$ and $700\text{-}950^oC$. Although the higher temperature loss of carbon dioxide could be attributed to the presence of excess/unreacted barium carbonate which is one of the starting materials for

the preparation of the oxide superconductor, the reason for loss of carbon dioxide in the temperature range 150-350°C was not immediately apparent since the other starting materials were in oxide form. The effect of moisture and carbon dioxide in the ambient atmosphere on these oxides and the superconducting oxide to form basic carbonate of yttrium and its decomposition was assumed to be one of the factors contributing to the low temperature carbon dioxide loss. Accordingly additional experiments with fresh
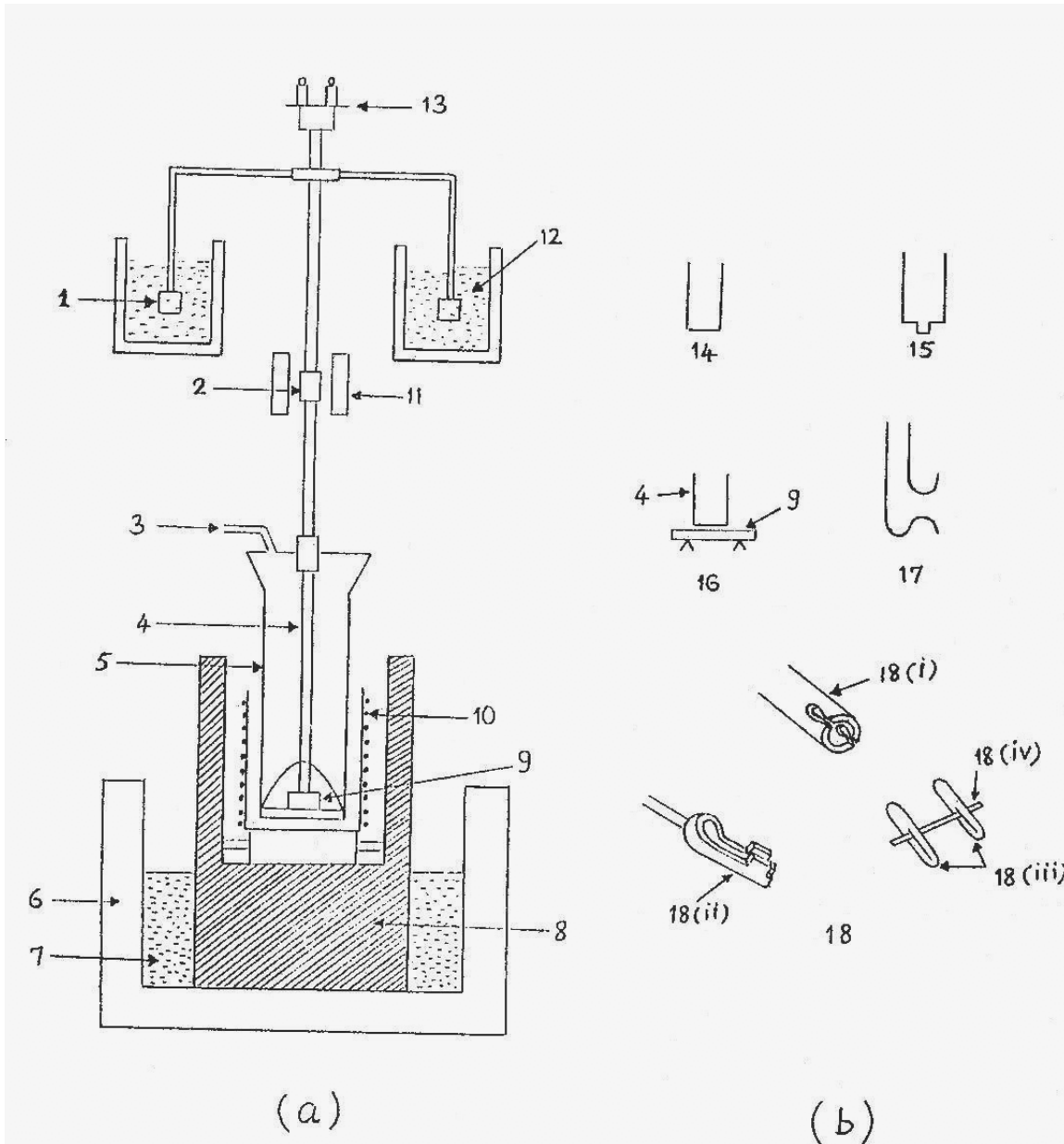
Fig. 3. Thermomechanical anlyser – schematic, a) Set-up, b) probe design
1 - float, 2 – ferritic core, 3 – purge gas, 4 – probe, 5 – sample tube, 6 – insulation, 7 – coolant, 8 – heat sink, 9 sample, 10 – furnace, 11 LVDT, 12 – high density liquid, 13 – weight tray, 14 – expansion mode, 15 - compression mode, 16 - flexure mode, 17 and 18 – extension modes, 18 (i) - sample tube, 18 (ii) – probe, 18 (iii) – sample clips, 18 (iv) - sample
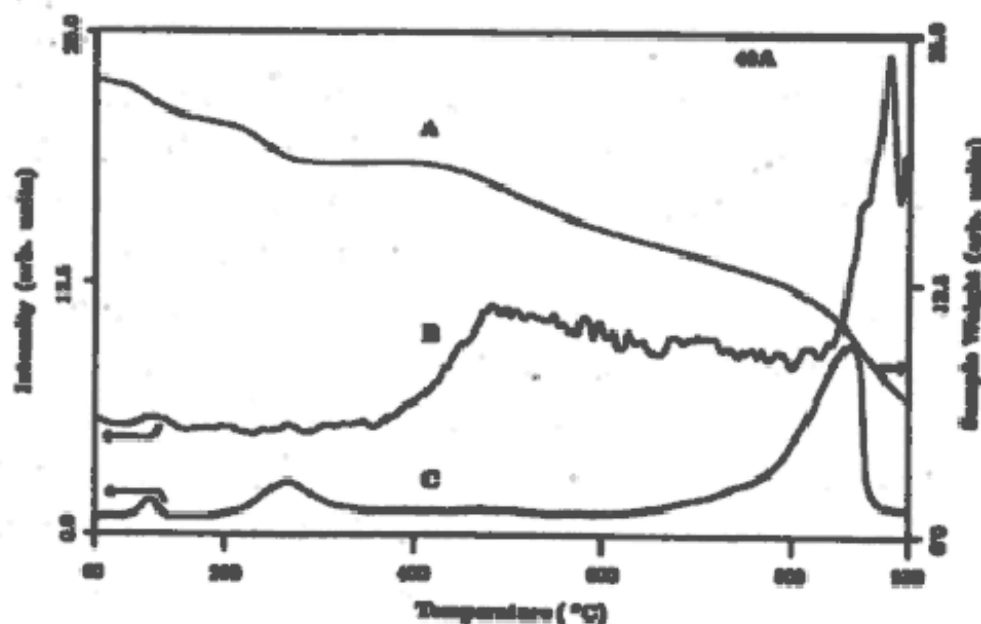
Fig. 4. Evolved gas analysis curves for a powder sample of $YBa_2Cu_3O_x$ (# 40A). Curve B shows the O_2 evolution while curve C depicts the CO_2 evolution. Accompanying changes in the weight of the sample are shown by curve A. Heating rate for the measurement was 5°C min^{-1}. Initial weight of the sample was 179 mg.

sample of yttrium oxide and a sample exposed to room air for a week were carried out. The result with the exposed sample of yttrium oxide presented in Fig. 5 clearly established that the low temperature release of carbon dioxide was from basic carbonate of yttrium. The study helped to conclude that exposure of yttrium-barium-copper oxide to ambient air leads to removal yttrium from it in the form of yttrium basic carbonate. It is noteworthy in this context that X-ray diffraction measurements could not provide such vital information on the nature of sample and the use of EGA helped in establishing the nature of impurity phase even at insignificant levels.

Quantitative Thermal Analysis

TG, DTA and DSC data have been used for quantitative interpretation of heat effects in the sample. The quantitative application of TG is evident in view of measurement of weight involved. However, when more than one active component is contributing to the weight change, such quantitative interpretations are not straightforward as evident from the example presented above. In cases where the removal or addition of active gaseous components are well resolved thermal events, the observed
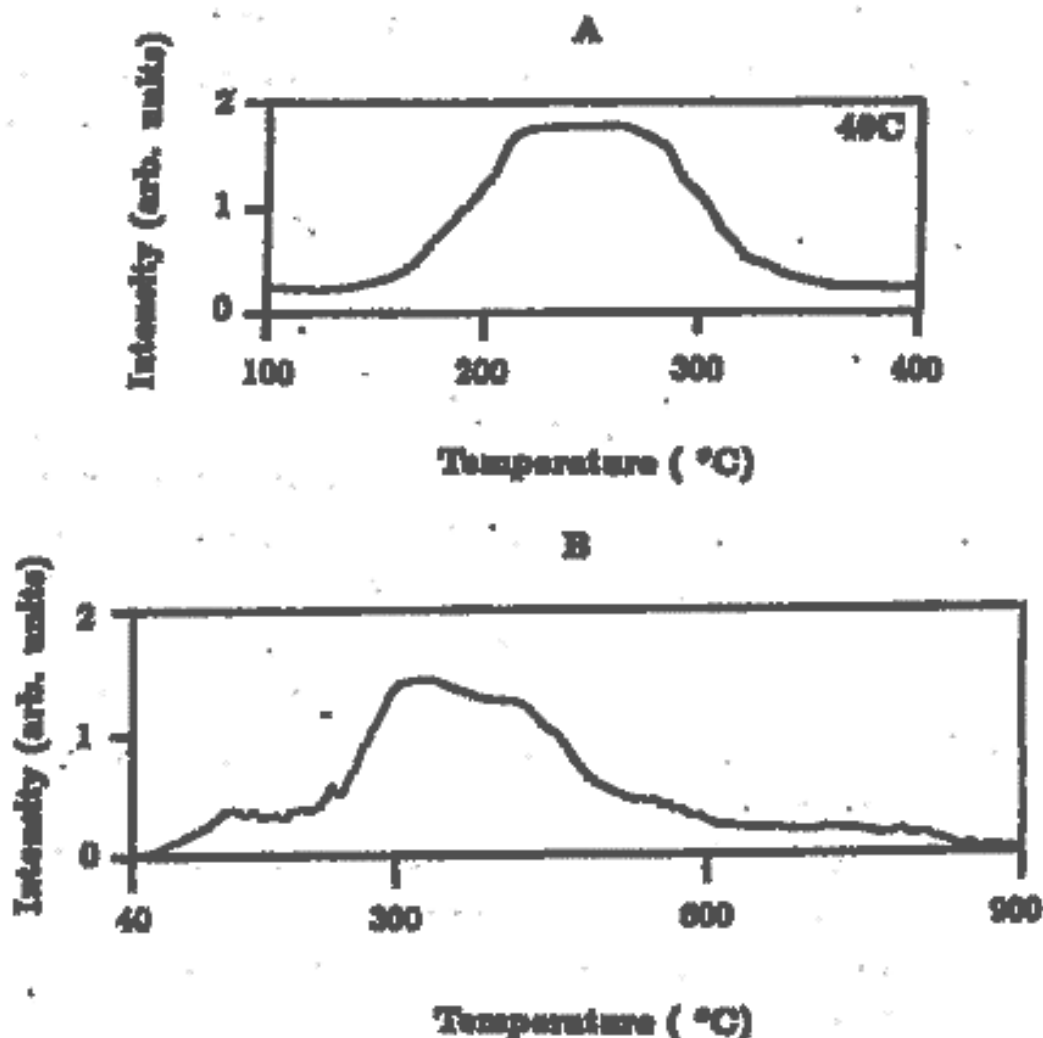
Fig. 5. CO_2 evolution from (A) $YBa_2Cu_3O_x$ (#40C) and (B) Y_2O_3, exposed to ambient for 6 days. The heating rate and the sample weight for measurement "A" were $5°C\,min^{-1}$ and 171 mg respectively, while those for measurement "B" were $10°C\,min^{-1}$ and 41 mg.

weight change is proportional to the extent of reaction. Knowing the composition of either the initial or final equilibrium phases, the stoichiometry of the reaction can be established from the weight change observed during the reaction step.

One of the widespread quantitative applications of Thermogravimetry has been for the elucidation of kinetic parameters of solid-gas reactions. The activation energy, Arrhenius pre-exponential factor and mechanistic model describing the rate determining step of the reaction have been determined using isothermal as well as non-isothermal

weight change data. Knowledge of these three factors together enables the prediction of reaction rate at any temperature in the interval of the reaction. Further, carefully determined mechanistic model is useful in fixing the variables for controlling the reaction. The basic equation used in such analyses is the rate equation represented as

$$\frac{d\alpha}{dt} = k \, f(\alpha) \quad \cdots\cdots\cdots\cdots\cdots\cdots\cdots\cdots\cdots\cdots\cdots\cdots\cdots\cdots\cdots \quad (9)$$

where α is the fraction transformed given in terms of the weights, W_o, W_t and W_f of the active component at the initial time, chosen time, t, and final time, respectively, as

$$\alpha = \frac{W_o - W_t}{W_o - W_f} \quad \cdots\cdots\cdots\cdots\cdots\cdots\cdots\cdots\cdots\cdots\cdots\cdots\cdots \quad (10)$$

The form of function $f(\alpha)$ is defined on the basis of the mechanistic model describing the rate-determining step. The constant k is the specific rate constant given by the Arrhenius equation as,

$$k = Z \exp(-E/RT) \quad \cdots\cdots\cdots\cdots\cdots\cdots\cdots\cdots\cdots\cdots\cdots \quad (11)$$

with Z as pre-exponential factor, E as activation energy, R as universal gas constant and T as absolute temperature.

The peak area of the DTA curve is approximately proportional to the heat of reaction and hence to the amount of reactant. However, the calibration factor, K', essentially a heat transfer coefficient, is temperature dependent and hence has to be evaluated at the temperature of reaction. It is determined as a function of temperature using calibrants with transitions at different temperatures (Table 2). The value at the required temperature determined from a plot of calibration factor versus temperature is then used to determine the unknown heat of reaction using the equation,

$$\Delta H = K' \, A \quad \cdots\cdots\cdots\cdots\cdots\cdots\cdots\cdots\cdots\cdots\cdots\cdots\cdots \quad (12)$$

where A is the total area (in units of ^{o}C.s) enclosed by the DTA peak and the baseline interpolated in the reaction interval.

Eq. (12) is also the basis for the application of DTA for the study of kinetics of solid-state reactions. The extent of reaction can be obtained as a function of temperature using the relation,

$$\alpha = \frac{a}{A} \quad \cdots\cdots\cdots\cdots\cdots\cdots\cdots\cdots\cdots\cdots\cdots\cdots \quad (13)$$

where α is the fraction decomposed and 'a' is the area swept by the DTA curve upto temperature, T. This can be combined with eq. (9) to determine the kinetic parameters. Similar treatments can also be carried out using eq. (8) in the case of DSC.

The effects of mass transfer and heat transfer on the shapes of thermoanalytical curves are not taken into account in the rate equation and hence significant variation of non-isothermally determined kinetic parameters with experimental variables, like, heating rate and sample weight has been observed. Such variations are most pronounced in the case of reversible reactions (e.g., dehydration processes). Hence caution must be exercised while interpreting the significance of the experimentally derived parameters

from a generalised perspective. In any case, it is preferable to work with samples of known particle size and lower weights under lower rates of heating and defined dynamic conditions of sample environment to minimize these effects.

Conclusion

A large number of techniques enabling measurement of changes in physical properties of substances as a function of temperature can be classified as thermoanalytical techniques. Though the measurement techniques involved are simple, the interpretation of the results necessitates careful consideration of several parameters affecting heat and mass transfer in the system studied. Hence, it is necessary to use multiple techniques, preferably in the simultaneous measurement mode, to arrive at unambiguous conclusions.

Calorimetric techniques

K. Nagarajan

Fuel Chemistry Division, Chemistry Group, Indira Gandhi Centre for Atomic Research, Kalpakkam 603102, Tamil Nadu, India.

Dr.K. Nagarajan joined the 18th batch of the BARC training school in 1974 after graduation and the Indira Gandhi Centre for Atomic Research (then Reactor Research Centre) after one year of training. In the initial years, he carried out studies on vaporisation behaviour of actinide halides. Since 1980 he has been working on high temperature calorimetry and has generated large amount of heat capacity and enthalpy of formation data on ceramic compounds and alloys of interest in nuclear technology. He obtained PhD from Madras University in 1992 and did his post-doctoral fellowship in Nagoya University under the JSPS programme. Earlier, he had been deputed to Max-Planck Institute for Metallforachung in Stuttgart, Germany. His current interests are pyrochemical reprocessing and sol-gel methods for nuclear fuel fabrication. He has more than 100 publications in journals and international conferences.

1. Introduction

Calorimetry involves measurement of thermal energy changes associated with the change in the state of the sample. The change of state may be brought in by change of temperature or pressure or a chemical reaction. Calorimetric methods that are used extensively in the experimental thermochemistry can be classified into two groups, namely, (i) reaction or thermochemical calorimetry wherein the sample undergoes a change in its chemical state and (ii) non-reaction calorimetry where there is only a change in the physical state of the sample such as change of temperature, phase transition etc. Measurements of the enthalpy increments, H_T^0-H_{298}^0 and heat capacities fall under the category of non-reaction calorimetry. Reaction calorimetric methods are used for the determination of the partial or integral enthalpies of mixing of liquid alloys and the enthalpies of formation of compounds including intermetallic compounds. In reaction calorimetry itself, two kinds of approaches are used. In the direct reaction calorimetry or single stage methods, the enthalpies of formation are directly measured in the calorimeter where the reaction occurs to form the alloy whereas in the indirect reaction calorimetry or two stage methods, the enthalpies of formation are derived from the measured values for the enthalpies of other reactions such as solution, combustion etc.. I would briefly discuss some of these methods.

2. Thermodynamic relations of relevance

Heat capacity of a system, C, is defined as C = (dq/dT) where the dq represents the amount of heat absorbed or released and dT, the associated temperature change. Heat capacity will depend on the conditions under which the experiment is being carried out such as constancy of pressure or volume. Accordingly, two heat capacities are known, namely, C_p and C_v, which correspond to the conditions of constant pressure and constant volume. In this article, the discussion will pertain to the calorimetric measurements on condensed phases, solid or liquid, only and under these conditions, the difference between C_p and C_v is very small. Enthalpy increment is the difference in enthalpies at two different temperatures. In general one of the temperatures is fixed as 298 and represented as H_T^0-H_{298}^0.   The following thermodynamic relations are well known:

$$C_p = (dq/dT)_p = (dH/dT)_p$$ ------------- (1)
$$C_v = (dq/dT)_v = (dE/dT)_v$$ ------------ (2)

$$H_T^0\text{-}H_{298}^0 = \int_{298}^{T} Cp \,.dT$$ ----------- (3)

3. Types of calorimeters

Calorimeters can be classified into three main types, based on the temperature of the calorimeter(Tc) and the temperature of the surroundings, (Ts), as shown in Fig.1.

A) Tc =Ts= Constant ; Isothermal

B) Tc =Ts both varying ; Adiabatic

C) Ts= Constant; Tc varies; Isoperibol
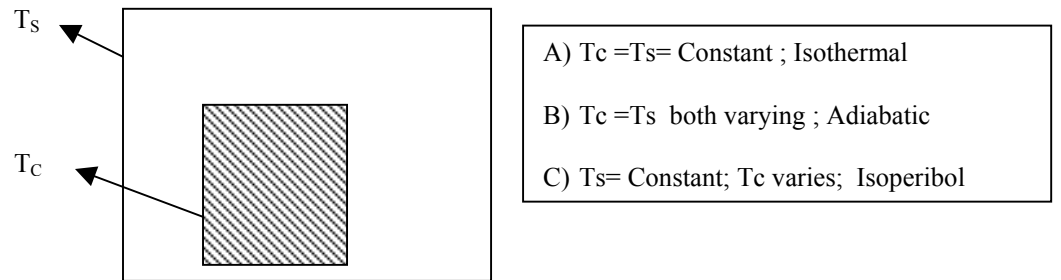
Fig. 1. Classification of calorimeters

It may be remembered that for an accurate calorimetric measurement, it is necessary to avoiding or minimize the heat leak from the calorimeter and, depending upon how this is done, the calorimeters are classified into various types. In the case of isothermal calorimeters, since both Tc and Ts remain constant and equal throughout the measurement, there is no heat leak. The heat energy is measured in terms of a phase change in a material like ice. In the case of adiabatic calorimeters, Ts is controlled in such a way as to be equal to Tc and thus heat leak is avoided. In isoperibol calorimeters, Ts is maintained at the same value, though Tc alone varies. The heat leak is minimized by packing the gap between the calorimeter and the surrounding with a

very good insulation material. Though there are other ways of classifying calorimeters, all the calorimeters can be considered to be one of the three main types described above.

3. Calorimetry of non- reacting systems

There are two ways to determine heat capacities. One is to measure the enthalpy increments, namely, H_T^0-H_{298}^0 and then derive heat capacity data as the derivative of the enthalpy increments. The other is to measure heat capacities directly.

Heat capacity measurements below 300 K down to 10 K are carried out using adiabatic calorimeters. As explained above, in an adiabatic calorimeter the temperatures of the calorimeter and the surrounding (in this case , a shield) are kept equal throughout the measurement, though both vary with time. The measurement of heat capacity is carried out by measuring the rise in temperature of the sample for a given amount of electrical energy. Since the temperature of the shield has to be controlled to be equal to that of the sample, the rate of heating is restricted to 1 K per minute. Measurements using adiabatic calorimeters are very precise and reproducibility of 0.01% have been reported. However, lower the measurement temperatures more tedious and more time consuming will be the measurements.

In the last four decades, Differential Scanning Calorimeters(DSC) have become more popular for heat capacity measurements. These are used , in general, for heat capacity measurements above 150 K up to 1100 K [1], though commercial models with extended temperatures above and below these values are also known. As its name implies, DSC involves a differential measurement and thus it has a reference pan and a sample pan. Differential measurements help to compensate for any disturbances such as temperature fluctuations variations in the environment. A characteristic feature of the DSC is its dynamic mode of operation [1]. In a DSC, the sample and reference pans, made of the same material (generally aluminium) are heated through a linear heating program, typically of the order of 5-10 K min^{-1}. There are two types of DSCs: (i) power compensation DSC and (ii) heat flux DSC. In the power compensation DSC, the reference and the sample are maintained at the same temperature, as they are heated by a linear heating profile. The measured quantity is the difference between the powers fed to the sample and the reference, which was required to maintain them at the same temperature. In a heat flux DSC, the difference between the sample and the reference temperatures is measured, as they are heated. In both the cases, the measured quantities are proportional to the heat flow rate and hence they are converted into heat flow rates using the conversion factors. In a DSC , heat capacity is measured using a three step procedure. In the first step of blank run, the heat flow rate (ϕ_0) is measured, as a function of temperature, between two empty pans on the sample and reference side. Then, a calibration substance like α-alumina is loaded onto the pan on the sample side and the heat flow rate(ϕ_{ref}) is measured between this and the empty pan on the reference side. In the third step, the heat flow rate(ϕ_s) between the pan containing the sample and

the empty pan on the reference side is measured. Heat capacity of the sample is given by the following equation:

$$C_s = [(\phi_s-\phi_0)/ (\phi_{ref}-\phi_0)]\ (m_{ref}/m_s)\ C_{ref} \quad \text{-----------} \quad (4)$$

Where the m_s = mass of the sample, m_{ref} = mass of calibrant , C_{ref} = heat capacity of the calibrant and C_s = heat capacity of the sample. If the temperature dependent calibration constant, $K_\phi (T)$ is fairly constant with time, then the second step of calibration can be avoided and the expression can be modified

$$C_s = [(\phi_s-\phi_0)/ (m_s)]\ [K_\phi (T)/ \beta] \quad \text{-----------} \quad (5)$$

where β is the heating rate. These are shown in Fig.2.
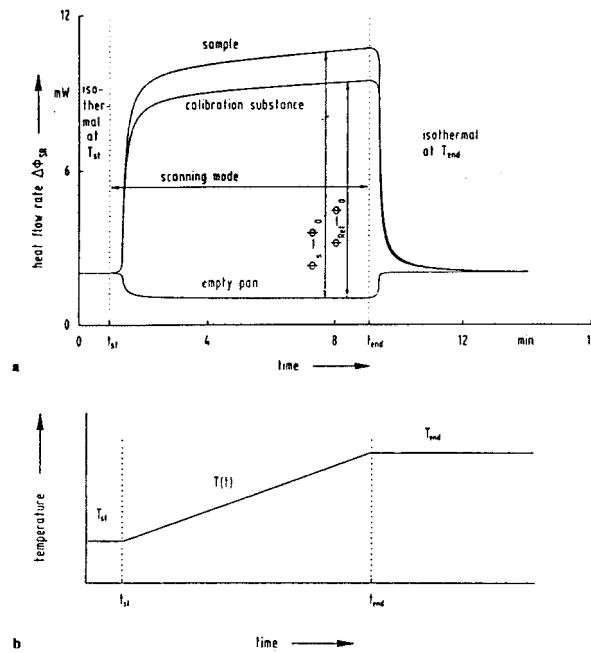
Fig.1. (a) Heat flow curves and (b) temperature profile during the DSC runs

The heating rate and the mass of the sample have to be optimized for getting the desired sensitivity and resolution. In the recent years, a new technique known as Temperature Modulated DSC(TMDSC) has been introduced [2]. In this technique, a sinusoidal or another periodic wave form is imposed over the basic linear heating profile, as given by the following equation:

$$T(t) = T_0 + \beta.t + A_T \sin\omega t \quad \text{------------} \quad (6)$$

where A_T= amplitude and ω = angular frequency. In this technique, it is possible to determine the heat capacity in a single run by using the sample and calibrant in the sample and reference pans, respectively, . It is possible to carry out measurements under quasi-isothermal conditions in this technique by keeping the temperature amplitude very small. It is claimed that heat capacities could be measured with an accuracy of 0.1% and there is intense debate on the efficacy of the method. However, the advantage of the technique is its ability to separate reversible and kinetic effects unlike the conventional DSC where the total heat flow is measured. The reversible heat flow is due to the intrinsic heat capacity of the sample and the irreversible heat flow is due to the kinetic effects. Hence it is argued that irreversible heat effects due to heat leaks etc. can be eliminated and using only the reversible heat flow, the heat capacity can be determined more accurately than conventional DSC measurements.

Drop calorimetry [3] is the technique used for measurements of heat capacities above 300 K, even though some adiabatic calorimetric measurements have been reported up to 800 K. In the conventional drop calorimetry, as shown in Fig.3, the sample is heated in a furnace to a constant temperature and then dropped into the calorimeter maintained at a lower temperature, generally, the ambient temperature. The calorimeter is known as the receiving calorimeter and isothermal and isoperibol calorimeters can be used for this purpose.
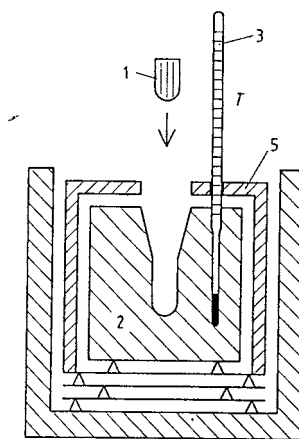
Fig.3. Schematic diagram of drop calorimetry (1- heated sample being dropped
;   2- calorimeter block; 3- temperature measuring device,5- heat shield)

The temperature of the calorimeter starts increasing as the sample is dropped and the sample gets cooled until thermal equilibrium is attained. The temperature increase of the calorimeter due to the drop is measured. The heat energy gained by the calorimeter, Q_c due to the drop of the sample is given by

$$Q_c = m_c \times C_{p,c} \times \Delta T_c \qquad \text{----------} \qquad (7)$$

where m_c is the mass of the calorimeter, $C_{p,c,}$ its heat capacity and ΔT_c the increase in temperature. Q_c is equal to the amount of heat energy released by the sample, Q_s, on cooling from the temperature, T_s, (to which it was heated in the furnace) to the temperature of the calorimeter, say, 298 K, thus,

$$Q_c = Q_s = (m_s/ M_s) \ x \ (H_T^0 \text{-} H_{298}^0)_s \qquad \text{-----------} \qquad (8)$$

where m_s = mass of the sample, M its molecular weight and $(H_T^0 \text{-} H_{298}^0)$ its enthalpy increment. Thus, since the mass of the sample, mass of the calorimeter and ΔT_c are known, if the heat capacity of the calorimeter is known the enthalpy increment can be calculated. The heat capacity of the calorimeter is determined in an indirect way. A reference sample, whose heat capacity is well known, is dropped from the same temperature, T_s into the calorimeter maintained at 298 K and the temperature increase, $\Delta T_{c'}$ is measured. Then, the heat energy gained by the calorimeter in this case, Q_c is given by :

$$Q_{c'} = m_c \ x \ C_{p,c} \ x \ \Delta T_{c'} \qquad \text{------------} \qquad (9)$$

which again is equal to Q_{ref}, the het enrgy released by the reference during the drop.

$$Q_{c'} = Q_{ref} = (m_{ref/} M_{ref}) \ x \ (H_T^0 \text{-} H_{298}^0)_{ref} \qquad \text{-----------} \qquad (10)$$

where m_{ref}, mass of the reference sample dropped, M_{ref}, molecular mass of reference and $(H_T^0 \text{-} H_{298}^0)_{ref}$, enthalpy increment of the reference are known and thus $Q_{c'}$ can be computed. Equation 9 can be rearranged to give

$$C_{p,c} = Q_{c'} / (m_c \ \Delta T_{c'}) \qquad \text{------------} \qquad (11)$$

$C_{p,c}$ derived from the above equation could then be used to compute the enthalpy increment of the sample from equation 8.

In drop calorimetry, enthalpy increments are measured at various temperatures and these values are generally fitted to a polynomial in temperature of the following form .

$$H_T^0 \text{-} H_{298}^0 = \ A.T + B. \ T^2 + C. \ T^{-1} + D \qquad \text{------------} \qquad (12)$$

where are A,B,C and D are empirical constants with no physical meaning. For least square fitting of the enthalpy increment data to the above expression, generally two constraints are used; (a) $H_T^0 \text{-} H_{298}^0 = 0$ at 298 K and (b) heat capacity at 298 K obtained from the above fit equation , $C_{p,298}$, is equal to the value reported in the literature.

Using the values for A,B,C and D obtained from fitting the measured enthalpy increment data , the enthalpy increment and heat capacity can be computed for any temperature.

$$C_p = A + 2.B \, T - CT^{-2} \hspace{4cm} \text{---- (13)}$$

In drop calorimetry, it is essential that the sample returns reproducibly to the same state, whenever dropped from high temperature, so that reproducible results are obtained. There could be problems in meeting this criterion in some systems for which drop calorimetry has to be used with caution. One is the "freezing-in" of the phase transitions. When the sample is cooled rapidly from a higher temperature to room temperature, any phase transition in the intermediate temperatures is likely to be incomplete leading to uncertainties in the state of the sample and hence uncertainties in the thermal quantities measured. The other is with respect to intermetallic compounds, which are not line compounds. There will be uncertainties in the composition of such compounds obtained by dropping them from liquid state and hence reproducible results will not be obtained. However, in the inverse drop calorimetry wherein the sample is dropped from a lower temperature into the calorimeter maintained at a higher temperature, the problem of freezing-in of phase transitions will not occur.

Besides the above techniques, there are other transient ones for measuring the heat capacity at high temperatures. One is the laser flash method, which is used for measurement of thermal diffusivity. In this method, the laser light is impinged on one surface of a thin disc sample and the temperature change at the rear side is followed as a function of time. From the temperature against time plot, $t_{0.5}$, the time required for the temperature to raise by half the maximum temperature is determined which in turn is used for the computation of thermal diffusivity. In the same equipment, if the front side of the sample on which the laser light is directed is coated with a suitable material so as to ensure that all the laser energy is absorbed and the temperature increase can be measured, then the heat capacity can be computed. There are other pulse heating techniques where the sample is taken in the form a thin wire through which high current is passed to increase the sample temperature by a few K and then from the known input energy and the temperature change, the heat capacity can be calculated.

Adiabatic calorimeter, DSC and TMDSC can also be used for the measurements of heats of phase transitions under non-isothermal conditions. The phase transition is recorded as a peak whose area is proportional the enthalpy of transition which is computed by using the calibration constant determined in another experiment.

3 Reaction Calorimetry
3.1. Aqueous solution calorimetry

Solution calorimetry has been used, since very long time, for the determination of the enthalpies of formation of the many inorganic compounds as well as intermetallic compounds In solution calorimetry, the enthalpy of dissolution of the compound whose enthalpy of formation is of interest , in a solvent is measured. In general, an acid is used as the solvent. Aqueous solution calorimeter is one of the simplest calorimeters

that can be constructed in a laboratory. The schematic of an aqueous solution calorimeter is shown in Fig. 4 .
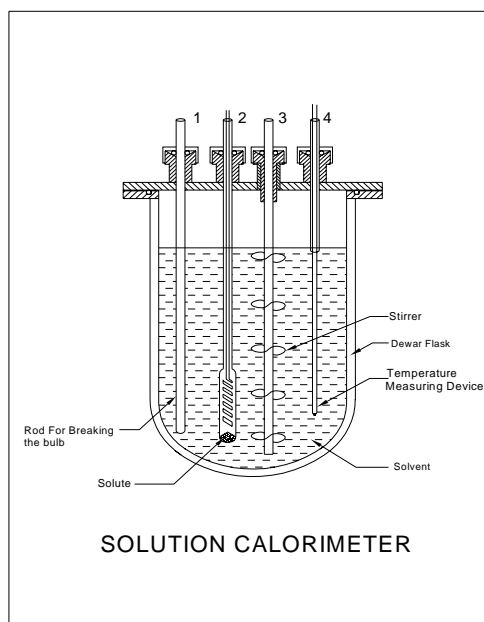
Fig.4. Schematic of an aqueous solution calorimeter

It consists of a Dewar flask closed with a lid. The lid has provisions for introducing a stirrer (3), a glass bulb containing sample(2), a rod fro breaking the sample bulb(1) and a temperature measuring device such as thermometer, thermistor etc.(4). The calorimeter is kept inside another container and the gap between the calorimeter and the container is packed with good insulating material. The calorimeter enables the measurement of the change in temperature, when a solute is added to a solvent. From the change in temperature and the heat capacity of the calorimeter, the amount of heat involved in the reaction that occurs in the calorimeter can be computed. As in the case of drop calorimetry, the need for the knowledge of the mass and heat capacity of the calorimeter can be obviated by carrying out measurements on standard substances whose enthalpies of solution are well established. It is generally used for the determination of the enthalpies of formation of inorganic compounds at 298 K. A typical determination of the enthalpy of formation of α- $Cs_2U_4O_{12}$ by aqueous solution calorimetry is shown below:

(soln) refers to 1.505 M H_2SO_4 + 0.0350 M $Ce(SO_4)_2$

$\Delta H_{11} = -\Delta H_1 + \Delta H_2 + \Delta H_3 + \Delta H_4 + \Delta H_5 + \Delta H_6 + \Delta H_7 - \Delta H_8 + \Delta H_9 + \Delta H_{10}$

				$(kcal \cdot mol^{-1})$
(1)	$\alpha\text{-}Cs_2U_4O_{12} + |4\ H_2SO_4 + 2\ Ce(SO_4)_2|_{(soln)}$	$\rightarrow$	$|Cs_2SO_4 + 4\ UO_2SO_4 + 4\ H_2O + Ce_2(SO_4)_3|_{(soln)}$	$-\ 114.70 \pm 0.43$
(2)	$UO_2(s) + 2\ Ce(SO_4)_{2(soln)}$	$\rightarrow$	$|UO_2SO_4 + Ce_2(SO_4)_3|_{(soln)}$	$-\ 53.92 \pm 0.06$
(3)	$3\ \gamma\text{-}UO_3(s) + 3\ H_2SO_{4(soln)}$	$\rightarrow$	$|3\ UO_2SO_4 + 3\ H_2O|_{(soln)}$	$-\ 60.69 \pm 0.27$
(4)	$3\ U_{(s)} + 4\tfrac{1}{2}\ O_2(g)$	$\rightarrow$	$3\ \gamma\text{-}UO_3(s)$	$-\ 877.5\ \pm 0.60$
(5)	$U(s) + O_2(g)$	$\rightarrow$	$UO_2(s)$	$-\ 259.3\ \pm 0.2$
(6)	$Cs_2SO_4(s)$	$\rightarrow$	$Cs_2SO_{4(soln)}$	$+\ 6.22 \pm 0.05$
(7)	$2\ Cs(s) + S(s) + 2\ O_2(g)$	$\rightarrow$	$Cs_2SO_4(s)$	$-\ 344.89 \pm 0.13$
(8)	$H_2(g) + S(g) + 2\ O_2(g)$	$\rightarrow$	$H_2SO_{4(soln)}$	$-\ 211.50 \pm 0.010$
(9)	$H_2(g) + \tfrac{1}{2}\ O_2(g)$	$\rightarrow$	$H_2O(\ell)$	$-\ 68.315 \pm 0.01$
(10)	$H_2O(\ell)$		$H_2O_{(soln)}$	$-\ 0.012$
(11)	$2\ Cs(s) + 4\ U(s) + 6\ O_2(g)$	$\rightarrow$	$\alpha\text{-}Cs_2U_4O_{12}(s)$	$-\ 1332.21 \pm 0.83$
	with $\Delta H_1 = -\ 114.72 \pm 0.55$:			$-\ 1332.19 \pm 0.89$
			average	$-\ 1332.20 \pm 0.85$

It is based on the Hess' law of heat summation. In this case, a mixture of 1.505 M sulphuric acid and 0.0350 M $Ce(SO_4)_2$ is used as the solvent. As shown in the table, the species formed during the dissolution (reaction 1) must be known and the enthalpies of formation of all these species should be either determined or taken from literature, as in the case of water. It must be ensured that the reaction goes to completion in all the measurements. The scheme of the all the measurements and the corresponding reactions should be planned in such a way that the algebraic sum of all the reactions leads to the formation reaction of the compound, $\alpha\text{-}Cs_2U_4O_{12}$ in this case.

3.2. Enthalpies of formation of intermetallic compounds

In the case of intermetallic compounds, aqueous solution calorimetry had been used in the earlier years. However, since the 1950's, after the innovative idea of Ticknor and Bever [4] who used molten tin as the solvent, high temperature dissolution calorimetry by using molten metals as solvents has gained currency. The reason for this is the fact that the enthalpies of solution of the intermetallic compounds in acids is very large and the enthalpy of formation obtained as the difference among the large values of enthalpies of dissolution results in large uncertainties.

As an example of the high temperature solution calorimetry, determination of the enthalpy of formation of $CeMg_3$ [5] is shown here. For these measurements, at first prepared the intermetallic compound, $CeMg_3$ was prepared and characterized by using X=ray diffraction. The schematic of the high temperature calorimeter used for these measurements is shown in Fig.5.

1.ISOTHERMAL METAL BLOCK
2.SAMPLE ADDITION TUBE
3.THERMOPILE
4.STIRRER
5.MOLTEN METAL/ALLOY
6.SAMPLE CONTAINER
7.THERMOCOUPLE
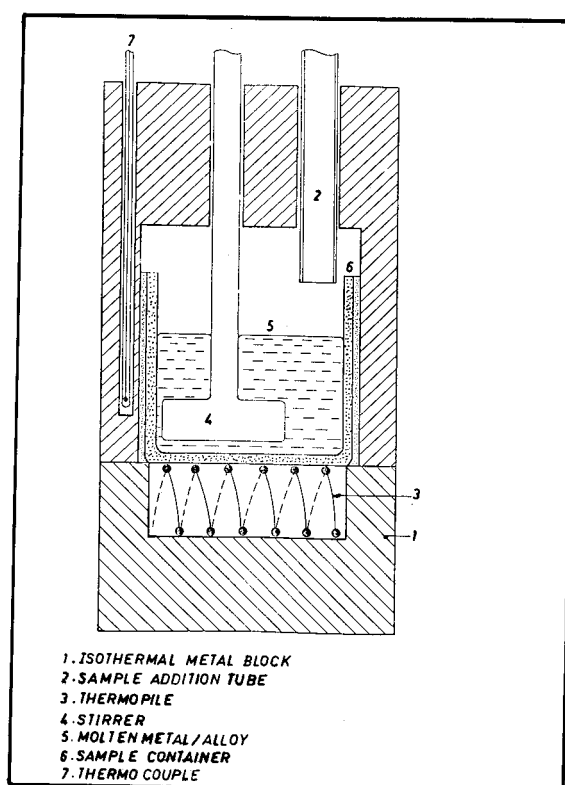
Fig.5. Schematic of the high temperature calorimeter

The calorimeter is based on the measurement of heat flow between the calorimeter and a constant temperature metal block, which is done in this case, using a thermopile. A thermopile is a set of thermocouples connected in series. In the above calorimeter, the solvent is kept at high temperature and the samples of solute are added from ambient

temperature. For the determination of the enthalpy of formation of $CeMg_3$, liquid Mg was chosen as the solvent . In the first experiment, magnesium was taken in the crucible of the calorimeter and heated above its melting temperature, say, 1000 K. Samples of cerium metal were added from ambient temperature into liquid magnesium. The measurement is represented as;

$$Ce(s,298) \rightarrow \{Ce\}_{Mg,T} \; ; Q_{Ce}\text{-----------} \tag{13}$$
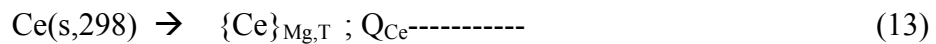
The heat energy involved in cerium going from 298 K into solution in liquid magnesium at T, Q_{Ce}, is measured which is less than the enthalpy of solution of Ce in Mg by the amount of heat absorbed by Ce for going to T from 298 K . In the experiment, Q_{Ce} is measured as a function of concentration of Ce and then the values are extrapolated to zero concentration of Ce to get the heat effect at infinite dilution, Q^{∞}_{Ce}. The measurements are restricted to a maximum cocntration of 5 at.% Ce to ensure that the measurements are in dilute solution region. Similarly, samples of $CeMg_3$ are dropped into liquid magnesium at the same temperature, T and the corresponding heat effect, Q_{CeMg3} is measured.

$$CeMg_3 \, (s,298) \rightarrow \{Ce + 3 \, Mg\}_{Mg,T} \; ; Q_{CeMg3} \quad \text{-----------} \tag{14}$$

From these measurements, the heat effect at infinite dilution, Q^{∞}_{CeMg3} , is derived. Then using Hess law of heat summation, the enthalpy of formation of $CeMg_3$ is derived as shown in the following figure:.
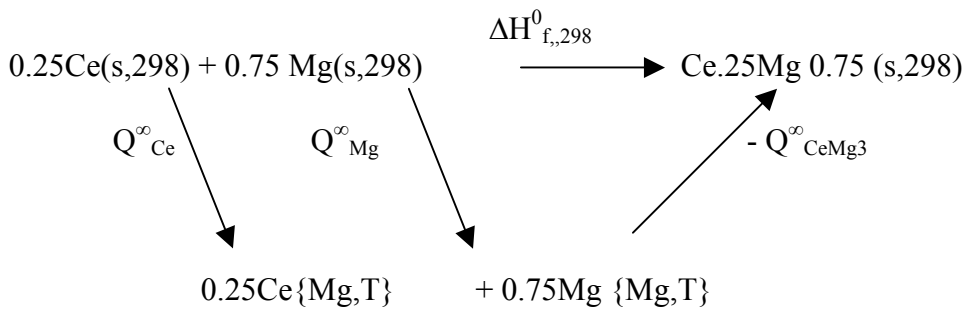
$$\Delta H^0_{f,298}(Ce.25Mg.75) = 0.25.Q^{\infty}_{Ce} + 0.75 \, Q^{\infty}_{Mg} - Q^{\infty}_{CeMg3} \quad \text{----------} \tag{15}$$

In the above example, Q^{∞}_{Mg} is not measured. Since enthalpy of solution of magnesium in liquid magnesium is zero, Q^{∞}_{Mg} can be computed from the enthalpy increment data of pure magnesium. The inherent advantage of the method is that one does not require the enthalpy increment data of the intermetallic compound for deducing its enthalpy of formation.

3.3. Combustion calorimetry

Combustion calorimetry using bomb calorimeters have been widely used for the determination of the enthalpies of formation of oxides. A typical bomb calorimeter is shown in Fig.6.
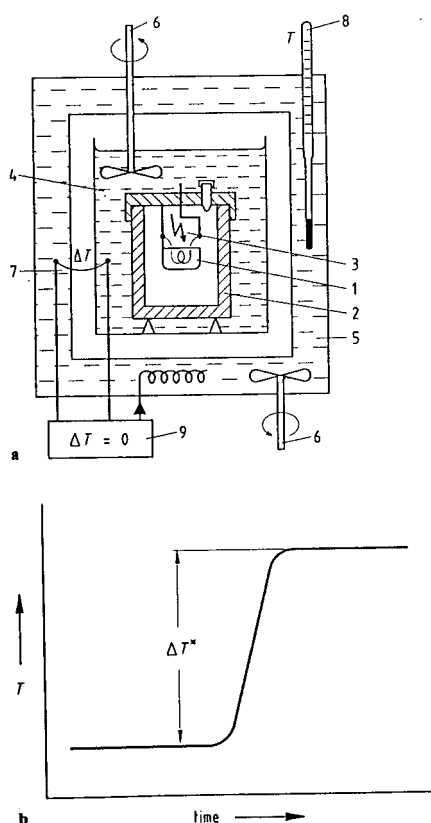
In the bomb calorimeter(2), the sample is contained in a vessel (1) and is ignited by passing a high current through a wire(3) in presence of oxygen gas at a high pressure. Since the vessel is designed to withstand high pressure, it is termed "bomb". The calorimeter shown above is operated on adiabatic calorimeter principle. The temperature change due to reaction of the sample with oxygen to form its oxide is measured from which the enthalpy of formation is derived. One should ensure that the reaction goes to completion. Or if the reaction is incomplete, then, one should analyse the samples to find out the extent of reaction. Bomb calorimeters can also be sued for the determination of the enthalpies formation of nitrides, by using nitrogen gas instead of oxygen.

5. References

1. B. Wunderlich , Thermochim. Acta 355 (2000) 43.
2. A. Boller, Y. Jin and Wunderlich, J. Thermal Analysis 42 (1994) 307.
3. R.A. Rapp, Physicochemical Measurements in Metals Research, Vol. 4, Part 1,
   Interscience Publishers, New York, 1970.
4. L.B. Ticknor and M.B. Bever, J. Met., 4 (1952) 941.
5. K. Nagarajan and F. Sommer, J. Less-Common. Met., 142 (1988) 319.

Glasses and Ceramics

V. Sudarsan

Chemistry Division, Bhabha Atomic Research Centre, Trombay,

Mumbai 400085, India

V. Sudarsan joined Chemistry Division of BARC in the year 1994 after graduating from the 37th batch of the training school. He received his Ph. D degree in Chemistry from Mumbai University in the year 2002 for his work on the structural aspects of inorganic glasses. Subsequently he worked for a period of two years with Prof. Frank C. J. M van Veggel at the University of Victoria, British Columbia, Canada in the area of structural aspects and luminescence of lanthanide ions doped in nanoparticles of inorganic hosts. Currently he is working on the optical properties of nanoparticles and glassy materials.

Introduction

Glass is one of the most ancient of all materials known and used by mankind. The mysterial physical, optical and aesthetic properties of glass have always intrigued man. Before people learned how to make glass, they had found two forms of natural glass known as fulgarites and obsidians. Fulgarites are produced by the fusing of sand caused when lightning touches the sand and the obsidians are produced from the immense heat of volcanic eruption, which fuses rocks and the sands. In olden days people shaped obsidians in to knives, arrow heads, jewels and money. Man made glass objects appear to be first reported in Egypt and Mesopotamian region as early as 3000 BC. There after glass science and technology have developed rapidly over the years [1]. With the discovery of newer machines, techniques and processes, variety of glasses with tailor made properties were made to help mankind to make life more convenient, safer, comfortable and more beautiful.

Definition of Glass

Glass is commonly defined as an amorphous product produced by the rapid quenching of a melt. However more generally glasses can be defined as an

amorphous material, which exhibits a phenomenon called glass transition. During glass transition an amorphous phase exhibits abrupt changes in the derivative thermodynamic properties (eg. Heat capacity, thermal expansion etc.) from crystal like to liquid like values with change of temperature [1]. The terms amorphous and non-crystalline are synonymous and can be used interchangeably. Unlike Crystalline materials the amorphous materials have non-periodic structures.

Glass preparation

Normally prepared by Melt and quench process. Quenching is usually done with water/liquid nitrogen/ metallic surfaces etc. However for certain glasses particularly for the metallic glasses, extremely fast quenching rates are required which is normally achieved through melt spinning technique. Sol-gel method is very widely employed for glass making. However the method is applicable only for few selected glass compositions/materials.

Conditions, which decide, glass formation.

Zacharaisen and Sun [1] based on their pioneering works on a number of glasses given few requirements for materials which are either as a glass former or modifier. They are summarized below.

1. Oxygen atoms should be linked (bonded) to not more than two atoms

2. Oxygen coordination around glass forming cations should be small, i.e. 3, 4

3. Cationic polyhedra should share corners and not edges or faces

4. At least three corners need to be shared

Sun's Bond Strength Model for glass forming materials

Bond strength is the main criteria for glass formation. Based on this concept following are the requirements of glass forming and glass modifying materials

1. Glass formers form strong bonds to oxygen – rigid network, high viscosity

2. Modifiers from weak bonds to oxygen – Disrupt, modify network

3. Intermediates form intermediate bonds to oxygen – can't form glasses   on their own, but aid with other oxides to form glasses

Typical bond energy values

>80 kcal/mole bond strength with oxygen: B_2O_3, SiO_2, GeO_2, P_2O_5, Al_2O_3

> 70 kcal/mol bond strength with oxygen: TiO_2, ZnO, PbO….

< 60 kcal/mole bond strength with oxygen: Li_2O, Na_2O, K_2O, MgO, CaO….

The glass transition phenomena

When a liquid is cooled either crystallisation may take place at the melting point T_m or the liquid will become super cooled for temperatures below T_m, increasing its viscosity and finally gets converted to glass. These changes are schematically represented in fig 1.
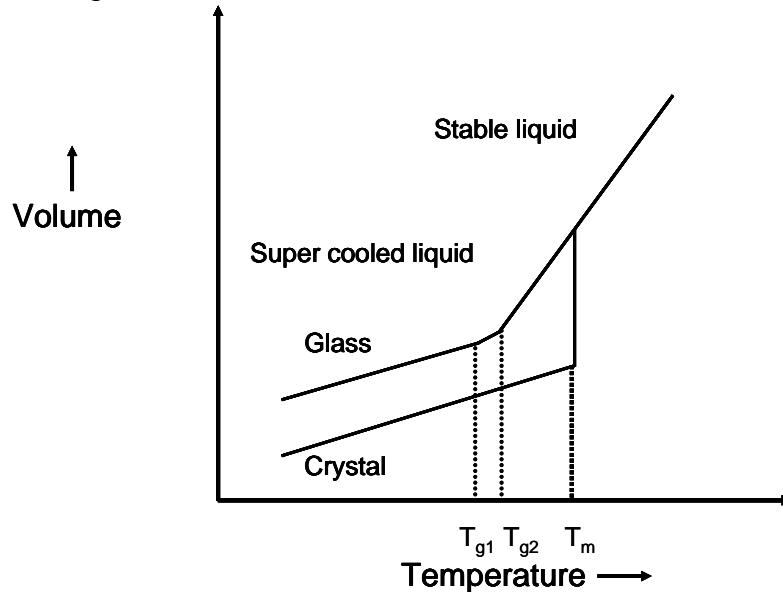
Figure 1. Temperature Vs Volume plots for glass forming and crystalline materials.

Glass transition temperature (T_g)

Glass transition temperature is defined as the temperature corresponding to the onset of structural relaxations. This can be obtained from dilatometry or DTA/DSC technique.

3
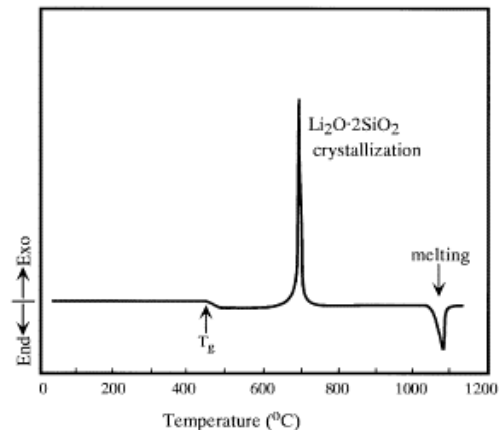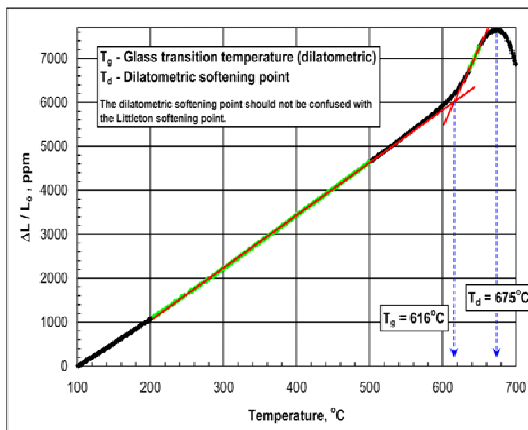
Figure 2. TMA and DTA pattern for Li_2O-$2SiO_2$ glass.

A representative TMA and DTA pattern corresponding to lithium silicate glass is shown above

Glass-ceramics

These materials are derived from glasses and obtained by the controlled crystallization of glasses. The process is schematically shown below
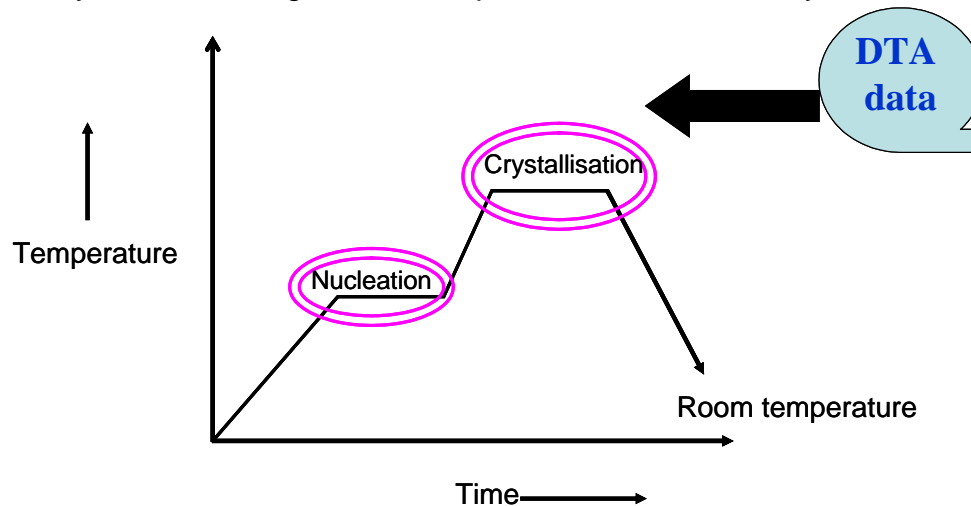
Figure 3. Time - Temperature variation used to convert a glass to glass-ceramic

They possess both the properties of the glass and crystalline materials.

Why do we study glass and glass ceramics.

Glasses and glass ceramics have got number of technological applications, which include

➢ Glass to metal seals (TEC values are relevant here)

➢ Optical fibers/transparency (E_{opt} values are relevant here)

➢ Nuclear waste immobilization (Thermal stability is the deciding factor)

➢Glass-ceramics: Machineable character

Understanding the structural aspects of the glasses and glass ceramics is essential for explaining their physico-chemical properties as well to develop materials with improved properties.

Probing the structure of glasses/glass-ceramics.

Structural aspects of glassy materials can be classified into mainly two regimes. They are

1. Short range order (less than 10 Å)

This regime is involved with the type of coordination polyhedra, bond lengths, bond angles etc around a central atom.

2. Intermediate range order (10- 20 Å) scale

Here one is concerned about the way in which the coordination polyhedra are interlinked.

For glass-ceramics in addition to the above structural parameters, nature of the crystalline phases and their distribution in glassy phase is a matter of interest.

Methods of characterizations

Diffraction techniques

➢ X-ray diffraction,

➢ Neutron diffraction,

➢ Extended X-ray absorption Fine Structure (EXAFS)

In all the diffraction techniques mentioned above Information is obtained through Radial Distribution Functions (RDFs)/pair correlations etc. Short and medium range order can be obtained by this technique. However it is complicated for multi component glasses

For glass-ceramics diffraction techniques are ideally used for identification of crystalline phases and their distribution, calculation of lattice parameters etc.
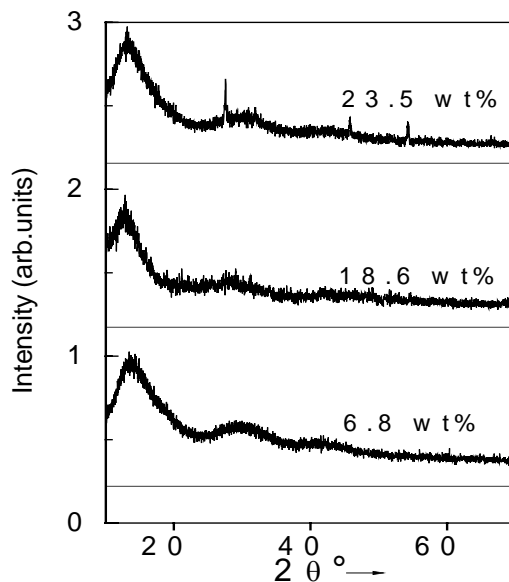
Figure 4. XRD patterns of barium borosilicate glasses containing different amounts of ThO_2

XRD patterns corresponding to barium borosilicate glass containing different amounts of ThO_2 is shown in Figure 4. Up to 18 wt%, glassy nature is maintained. Above 18 wt% ThO_2 incorporation, devitrification of the glass results. Sharp peaks are characteristic of crystalline ThO_2.

Vibrational Techniques

IR and Raman Spectroscopy.

Widely used to identify the different structural vibrations in glasses and glass-ceramics. Mostly gives short range order and in some cases medium range order can also be obtained.
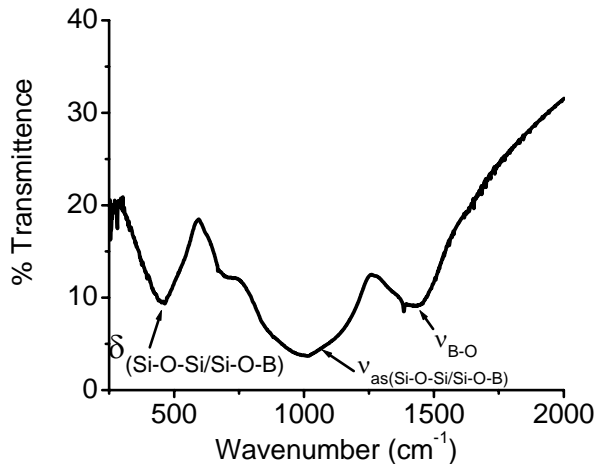
Figure 5 IR pattern of a representative borosilicate glass.

Broad peaks are characteristic of the glassy nature. The peak around 1400 cm^{-1} is characteristic of B-O stretching vibrations. Broad peaks around 1000 and 450 cm^{-1} are characteristic of Si-O-Si/Si-O-B stretching and bending vibrations respectively.

Structural studies using probe sensitive techniques

Probe sensitive techniques like nuclear magnetic resonance (NMR), nuclear quadrupole resonance (NQR) and Mossbauer spectroscopy can be very effectively used to understand the short range order existing in the glass.

Advantages of using solid state NMR for structural elucidation of glasses

- ➢ NMR-Nuclei/element selective technique
- ➢ Do not require long range ordering
- ➢ Sensitive to the local environment
- ➢ Very high interaction selectivity
- ➢ Tailor the internal interactions

Basic interactions in NMR

For spin ½ nuclei there are two major interactions [1]

1. Chemical shift interaction

$\nu(\theta) = \nu_0\{1 - \sigma_{iso} - 1/3\Delta \ \sigma(3\cos^2\theta - 1)\}$

2. Dipole-dipole interaction

$H_D = \gamma_1\gamma_2\hbar \ r^{-3}\{(1-3\cos^2\theta)I_{z1}I_{z2} - (1-3\cos^2\theta)[I_{+1}I_{-1}+I_{+2}I_{-1}]/4\}$ Figure 6
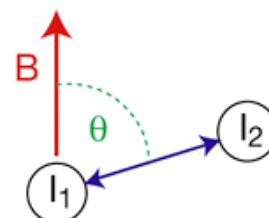
Figure 6 shows Schematic representation of dipole-dipole interaction.

Where σ_{iso} is the isotropic value of chemical shielding, $\gamma 1$ and $\gamma 2$ are gyromagnetic ratios of nuclei 1 and 2. ν_0 is the Larmor precessional frequency. I_{+1} and I_{-1} are raising and lowering operators of spin angular momentum quantum number. These expressions very clearly reveal that the angular term $3\cos^2\theta - 1$ decides the NMR line widths/shapes. Hence by reducing this term to a very small value, significant improvements in terms of the line width and resolution can be achieved. Angle at which $1-3Cos^2\theta$ becomes zero is called magic angle and its value is 54.74°. Schematic representation of magic angle spinning is shown in Fig. 7

Magic Angle Spinning (MAS) NMR

At $\theta = 54.74°$, $1 - 3\cos^2\theta = 0$
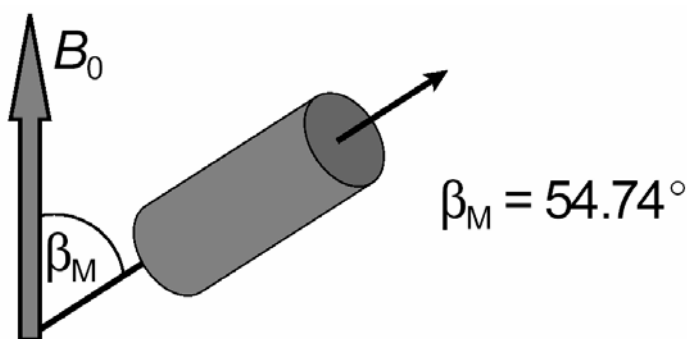
Figure 7. Schematic representation of magic angle spinning

Interactions gets averaged out at the magic angle and NMR lines get narrowed

Representative ^{31}P MAS NMR patterns from binary lead phosphate glasses are shown in Figure 8. The patterns essentially consist of peak around -10 and -24 ppm characteristic of Q^2 and Q^1 structural units of P.

Structural units in phosphate glasses

(a) (b)
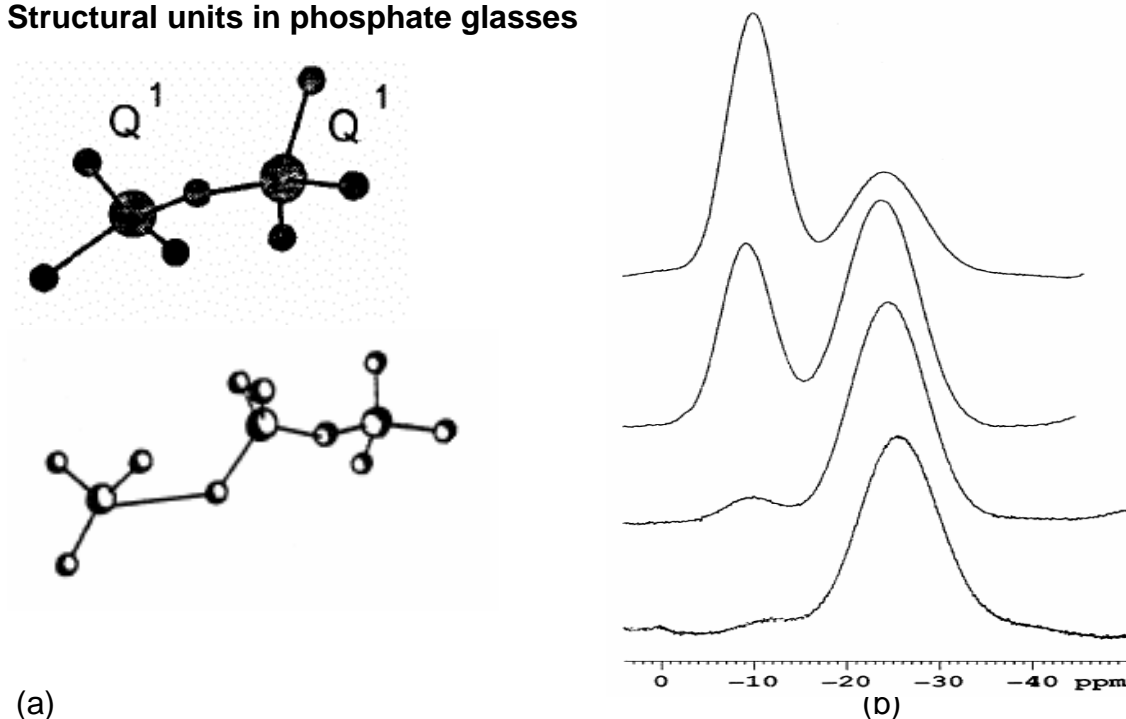
Figure 8: (a) Structural units in lead phosphate glasses, (b) ^{31}P MAS NMR patterns for binary lead phosphate glasses

^{11}B MAS NMR is very useful for identifying the structural units of boron. ^{11}B MAS NMR patterns from a representative zinc borosilicate glass recorded at two different magnetic fields is shown in Figure 9. Broad peak around 15 ppm has been attributed to BO_3 structural units and the sharp peak around 0 ppm to the BO_4 structural units. Unlike BO_4 structural units, BO_3 structural units lack cubic symmetry leading to the increased extent of quadrupolar interaction and thereby broadening the NMR line shape corresponding to BO_3 structural units.
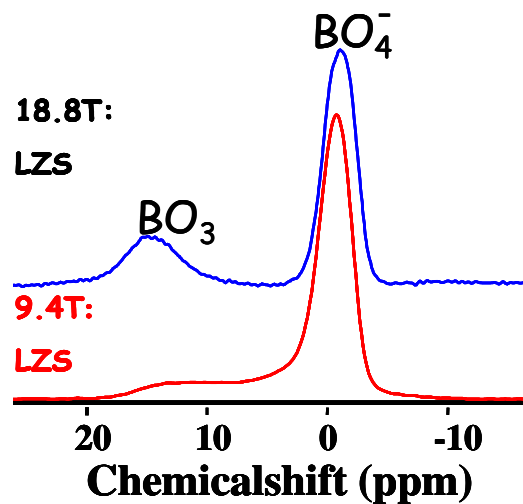
Figure 9, ^{11}B MAS NMR pattern of Lithium zinc borosilica glasses at two different magnetic fields.

Structural studies on Glass-ceramics

Magnesium Alumino Silicate glasses

Magnesium alumino silicate based glass ceramics are examples of machineable glass ceramics and the machineability arises due to the presence of Potassium fluorophlogopite phase. This phase has got tile like structure.
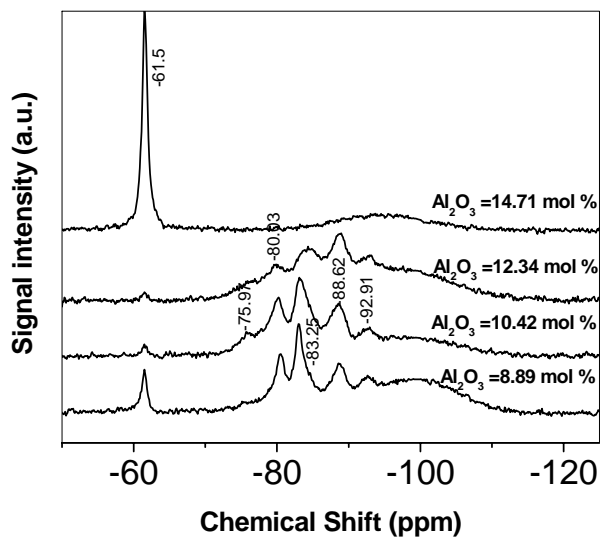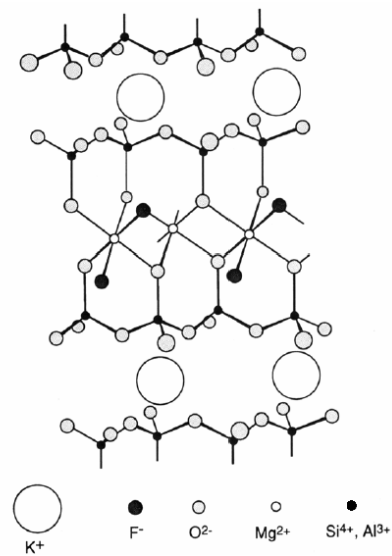
(a)   (b)

Figure 10: ^{29}SI MAS NMR pattern (b) structure of potassium fluorophlogopite phase

Examples of technologically important glasses / glass-ceramics

Following section deals with examples of few technologically important glasses.

1. Heavy metal oxide glasses

Examples: PbO, Bi_2O_3, CdO etc. one of the constituents with P_2O_5 and SiO_2 as other components. They have got applications as

•Scintillating glasses,

•High non-linear refractive index materials,

•High thermal expansion coefficient materials.
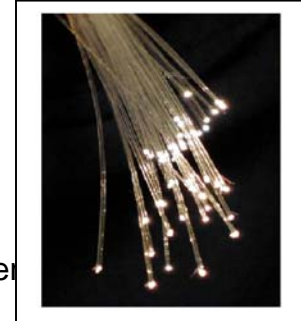
Figure 11. Example of heavy metal oxide phosphate glass fiber

Figure 12. Lead silicate based Glass to metal seals

$SiO_2/PbO = 6.9$ and containing alkali and alkaline earth metal oxides

Compression type seals, withstand highly corrosive environments
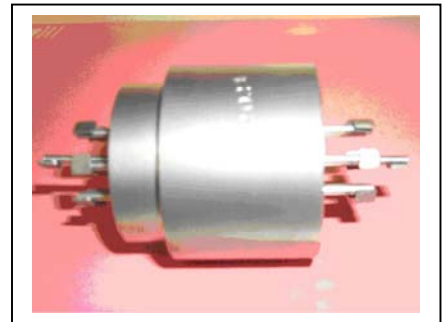
Glass-Ceramics

Some examples of technologically important glass-ceramics are given below.

(b)

Figure 13**:** Highly machineable Magnesium Alumino Silicate Glass ceramic
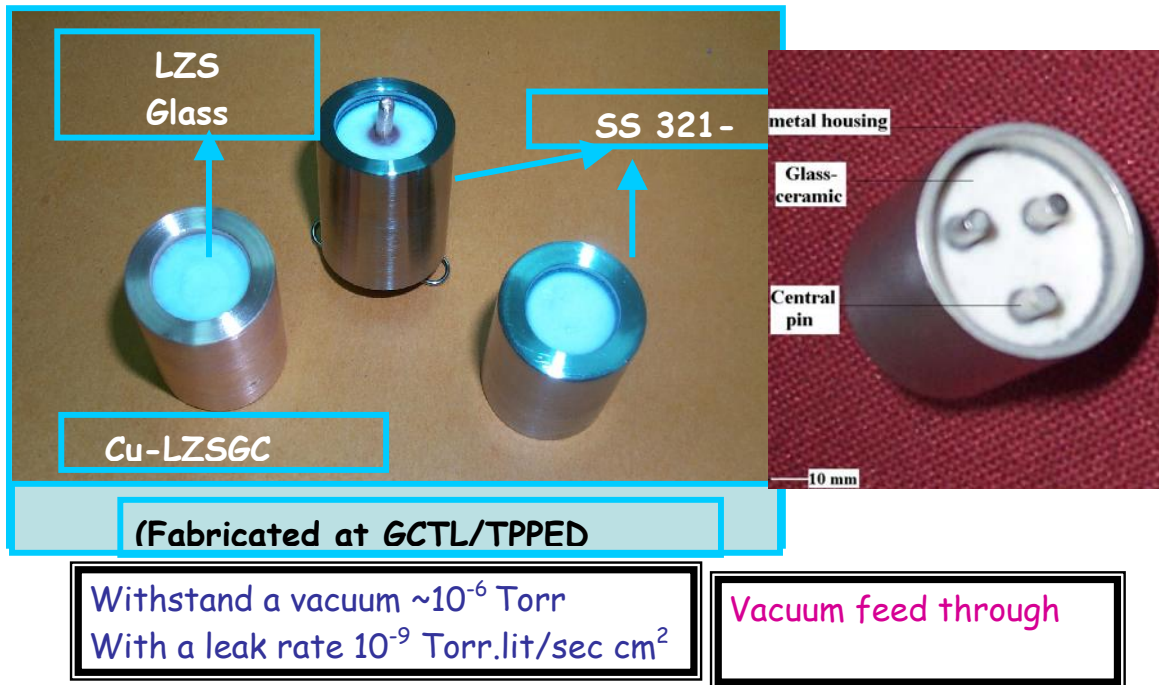
Figure 14. Lithium zinc silicate glass ceramics and glass-to-metal seals.

Conclusions

Understanding the structure of glasses and glass ceramics is essential for predicting and explaining their physico-chemical properties. Techniques like NMR, IR etc. are very useful for understanding the short range order in glasses and glass ceramics. X-ray diffraction techniques though complicated for multi component glasses, can be used to understand both short and medium range order in glasses and glass ceramics

References

1. J. Zarzycki in : R. W. Cahn, P. Haasen, E. J. Kramer (Eds.), Materials Science and Technology, vol. 9, VCH, Weinheim, 1991.

2. R.K. Mishra, V. Sudarsan, A.K. Tyagi, C.P. Kaushik, Kanwar Raj , S.K. Kulshreshtha, Journal of Non-Crystalline Solids 352 (2006) 2952.

3. V. Sudarsan and S. K. Kulshreshtha, J. Non-Cryst. Solids 286 (2001) 99.

4. M. Goswami, G. P. Kothiyal, V. Sudarsan and S. K. Kulshreshtha
Glass Technol. 46 (2005) 341.

Vapour Pressure Measurements

Ziley Singh

Product Development Section, RC & I Group,

Bhabha Atomic Research Centre, Trombay, Mumbai – 400085

Email: zsingh@barc.gov.in

Dr. Ziley Singh joined BARC in 1969. He did his PhD from Mumbai University. He has been engaged in the field of research in high temperature thermodynamics. He has contributed significantly in the alloy fuel development and compatibility studies of FBTR fuels, carbon potential of Mark-I fuel and stainless steel clad. He has more than 100 publications in national and international journals. Presently, he is heading High Temperature Chemistry Section and his field of interest is the thermodynamic studies of the compounds formed due to fuel-clad and fuel-coolant interactions.

All substances evaporate. They do so by different types of reactions and at vastly different pressures. The temperature required may be very high but ultimately all evaporate. Vaporization is a reaction that involves condensed and vapour phases. The condensed phase may be a solid or a liquid, an element or a compound or a mixture of them. Similarly, the vapour phase may also contain one or more species. The complexity of the vaporization process increases with increase of number of species and the temperature.

Vaporization is a chemical reaction and hence it can be represented by a balanced chemical equation showing the species present and their state of aggregation. Generally, vaporizations are equilibrium process and the equations written represent the reactions that occur in the equilibrium system. In high temperature system, there are more interactions between sample and container materials and thus the vaporization reactions may involve unknown compositions and even unsuspected phases. However, reactions that are possible for stoichiometric compounds may not be possible for actual phases or vice versa.

There are many reasons for the study of the evaporation process. Such a study serves very well to establish the nature and energetics of chemical bonding, particularly in the gaseous state, to establish the nature of high temperature reactions and to measure the thermodynamic properties of solids, liquids and gases. The evaporation process is also useful

for the study of the kinetics of high temperature reaction and they are necessary for any study of vapour pressure measurement.

Congruent Vaporization

A substance may evaporate in several different ways. The processes may be either congruent or incongruent. A system is said to be congruently vaporizing if the condensed phase and the vapour phase arising from it have the same composition. The simplest congruent vaporizing system in case of an element can be represented as:

$$H_2O \text{ (l)} \rightarrow H_2O \text{ (g)} \tag{1}$$

or,

$$A_2B_3 \text{ (s)} \rightarrow AB(g) + AB_2(g). \tag{2}$$

The process in which the composition of the vapours is different than that of the condensed phase is called incongruent vaporization. Such systems can be represented as;

$$2 NaO_2 \text{ (s)} = Na_2O_2(s) + O_2(g) \tag{3}$$

or,

$$3 MoO_2(s) = Mo(s) + 2 MoO_3(g) \tag{4}$$

During the evaporation, in general, association, dissociation or disproportionation reactions may take place. The congruency of the vaporization process can be established by examining the residue after successive experiments with the same sample. If the residue always has the same composition, the process is a congruent one. But if the overall composition of the residue changes the process is an incongruent one.

Chemical interaction of the sample under investigation with the container material or residual gases etc. may give erroneous results. A study of these aspects is therefore essential in a vaporization experiment. A chemical or x-ray analysis of the residue or sublimate can be used to reveal contamination of the sample. The occurrence of fusion at temperature below the known melting temperatures or the unexpected destruction of the container material is indicative of interactions. The lack of mass balance may also indicate interaction. One of the simplest ways of discovering reactions with container material is to study vaporization behavior using a variety of container materials.

Thermodynamic Treatment of Vapour Pressure Data

For thermodynamic determinations, the activities of the species in the vapour are related to their partial pressures. Equilibrium constants of reactions of interest are obtained from appropriate ratios and product of these activities, and heats and entropies can be obtained from the variation of the equilibrium constant with temperature.

For vapour pressure less than one atmosphere, and certainly for pressure in the range studied by means of Knudsen cells, vapour species may be considered ideal and equilibrium constants K_p may be calculated from partial pressures, P. For reactions such as:

A(s or l) = A(g) $\qquad\qquad$ ($K_p = P_A$) $\qquad\qquad\qquad\qquad\qquad$ (5)

or AB(g) = A(g) + B(g) $\qquad$ ($K_p = P_A P_B / P_{AB}$). $\qquad\qquad\qquad\qquad$ (6)
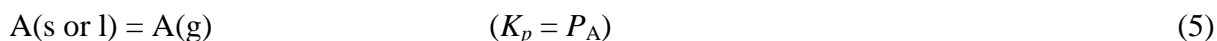
The standard free energy change at temperature T is:

$$\Delta G^o(T) = - RT \ln K_p \qquad\qquad\qquad\qquad\qquad\qquad\qquad\qquad (7)$$

One obtains heats and entropies of reaction from equilibrium constants by two different approaches. In the so-called "second law" method one plots $\ln K_p$ vs. $(1 / T)$, and since

$$\Delta G^o(T) = \Delta H^o(T) - T\Delta S^o(T) \qquad\qquad\qquad\qquad\qquad\qquad (8)$$

$$\ln K_p = \frac{-\Delta H^o(T)}{RT} + \frac{\Delta S^o(T)}{R} \qquad\qquad\qquad\qquad\qquad\qquad (9)$$

Then, one obtains the heat and entropy of reaction from the slope and intercept of the best straight line through the experimental points. In the so-called "third law" method one calculates ΔH^o at some reference temperature, generally 298.15 K from each experimental point by computing the change in free energy functions (*fef*) based on 298.15 K. Thus

$$\Delta fef = -\frac{\Delta G^o(T) - \Delta H^o(298.15)}{T} \qquad\qquad\qquad\qquad\qquad (10)$$

where Δfef is the sum of fef's of the products minus that of the reactants.

$$\Delta H^o(298.15) = -RT \ln K + T\Delta fef \qquad\qquad\qquad\qquad\qquad (11)$$

Measurement of Vapour Pressure

Every substance has a definite vapour pressure at any temperature, but the degree of vaporization varies with the type of substances. The mode of the vaporization is determined by the properties of the condensed and the vapour phases. Meaningful vapour pressures can be obtained if the degree of freedom of the system is one. Thus by fixing temperature,

pressure of the system is fixed automatically. So, there exists a close relationship between the phase diagram and vapour pressure measurements.

If a condensed phase is in thermal, mechanical and chemical equilibrium with the vapour phase, then the chemical potential of a species in the condensed and the vapour phase are equal and related by the following equation:

$$\mu(s,l) = \mu^0(g) + RT \ln(p/p^0) \tag{12}$$

where μ (s, l) and μ^0(g), are the chemical potentials and p^0 and p are vapour pressures of the pure condensed phase and partial pressure of the species respectively. The (p/p^0) ratio represents activity of the species under ideal condition. Thus one can get partial, integral and excess thermodynamic quantities using standard calculations.

The vapour pressure measurement methods can be categorized as:

1) Absolute methods

    a) Static method

    b) Boiling point method

2) Relative methods

    a) Transpiration

    b) Effusion methods

    c) Isopiestic method

In the absolute methods, knowledge of molar mass of the vapour species is not required whereas in a non-absolute method a prior knowledge of molar mass of the vapour species is required.

Generally, static and boiling temperature methods are used for more volatile systems and effusion and transpiration techniques are used for less volatile systems. Some of the important techniques for vapour pressure measurements are discussed here.

Static Method

In static methods, the vapour is held in a closed vessel at a constant temperature to allow equilibrium to be established between the condensed phase and the vapour. Pressure is then measured either directly, using a manometer or indirectly, by measuring the quantity of the vapour in a known volume. Although many of the static methods are simple, direct and

applicable to a wide variety of elements, alloys and salts, however, these methods require thorough removal of absorbed gases and impurities, which is difficult to ensure in all cases. Furthermore, refractory materials suitable for construction of high temperature apparatus are not easily available and static measurements much above 1250 K are usually difficult. Various types of manometers are available for direct pressure measurement, of these mercury manometers are widely used.

Manometric Techniques

These instruments are used mainly for measuring relatively high pressures ranging from 100 Pa to 100 kPa. Generally, this is a U-shaped glass tube filled with mercury with one of its arm connected to the vessel containing vapour, the pressure of which is to be measured and the other arm is opened to the atmosphere or evacuated. A typical experimental setup is shown in Fig. 1.
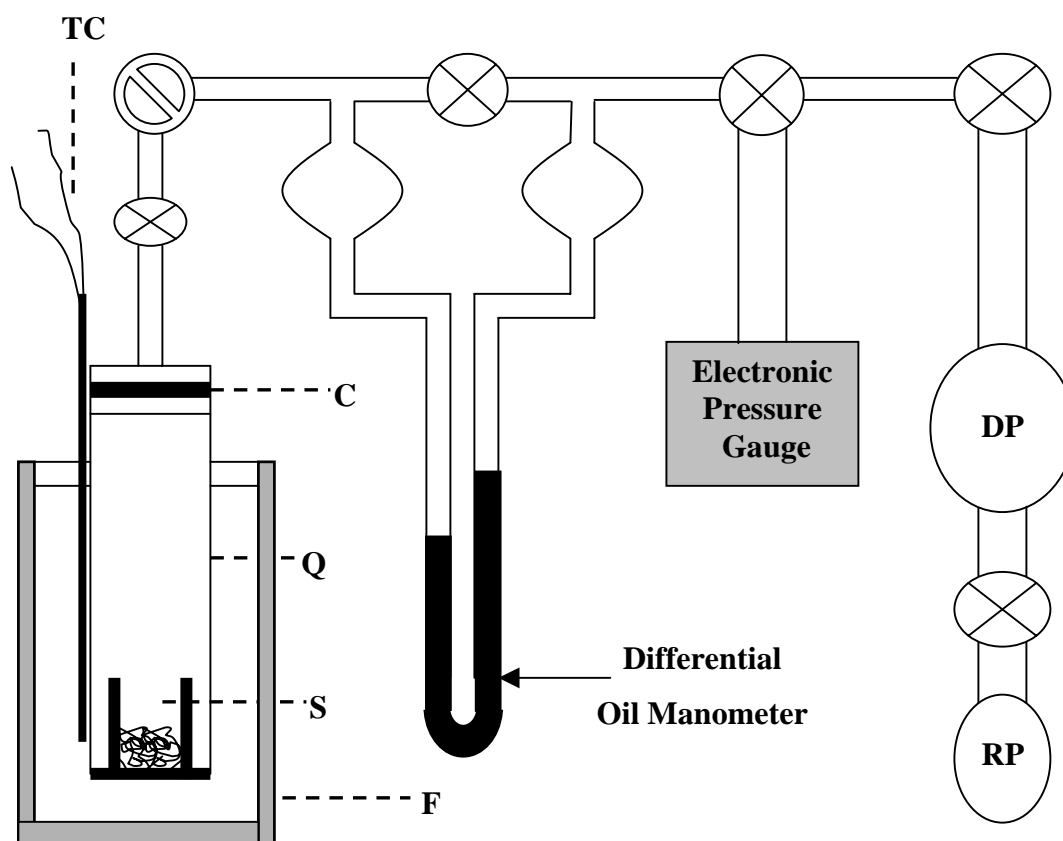
Fig. 1. Schematic diagram of Manometric apparatus 5

TC - Thermocouple, ⊗ - bellows-sealed CF flange VAT valves, **RP** - rotary pump,

DP- diffusion pump, **Q**- quartz reaction tube, **S** – sample in alumina crucible,

The mercury level is measured either by a graduated scale or with the help of a cathetometer. The sensitivity of the measurements can be increased using manometric liquid of low density or the modified manometers such as Rayleigh's [1] differential manometer and Sharder and Ryder's [2] lever manometer with a lamp and scale arrangement. McLeod [3] developed a simple manometer, known as McLeod gauge for measuring pressures as low as 5×10^{-3} Pa. This gauge is used for measuring the pressures of permanent gases (O_2, N_2, CO, H_2, inert gases etc.) but it is not suitable for measuring the vapour pressure of liquids and solids. It is used most extensively as a standard for calibrating other instruments designed for measurement of pressure of residual gases in vacuum systems.

Quasi-static Method

Static methods, though used for a large number of systems are limited by two fundamental points: a) the difficulty and uncertainty of removing all absorbed gases before sealing off the sample and b) difficulty in finding suitable refractory material for high temperature use. Rodebush and Dixon [4] have overcome the difficulty related to residual gases by developing a quasi-static technique, in which the sample is not sealed off. The sample is placed in a shallow vessel connected with two narrow tubes. One tube is connected to inert gas supply and a manometer and the other to a high vacuum system. Above the furnace both these tubes are connected to the opposite side of a differential manometer. The system is first evacuated and flushed with inert gas. Inert gas pressure over the sample is kept slightly more than the sample pressure at a specified temperature. The sample is allowed to vaporize and cause a reflux in the lower portion of the tubes. As the system temperature becomes constant, the gas pressure is reduced gradually at a constant rate until the pressure of the sample is equal to the inert gas pressure as indicated by a differential manometer. As soon as the pressure of the inert gas falls below the vapour pressure, the sample vapour acts as a valve to cut off any further flow of gas from the reservoir tube to the pump and a permanent difference is created in the level of the differential manometer limbs. This action depends on the fact that as long as the pressure in the manometer tube is greater than the vapour pressure, gas will flow through the system to equalize any pressure differences but as the pressure in the manometer tube becomes less than the vapour pressure, the flow of the gas is blocked by

the streaming vapours. This method is liable to give low results on account of the slow but finite flow of gas through the system.

Transpiration Method

The transpiration method, also called the transport or the entrainment method is one of the oldest and most versatile ways of studying vapour pressure and heterogeneous equilibria involving gases. It can be used in making measurements of vapour pressures up to less than 100 kPa, and its use is practically limited to pressures above 0.1 Pa. However, when radioactive tracers are used, this lower limit may sometimes be considerably exceeded. Regnault [5], the French chemist and physicist, was the first to use this method as early as 1845. It is used primarily for vapour pressure and dissociation pressure measurements but it may be applied to gas-solid or gas-liquid equilibria. It is one of the methods that can be used to measure the pressure of vapour in the presence of large concentrations of other gases.

In the transpiration method, a carrier gas is employed. The gas may be inert, or partially or wholly composed of chemically reactive gases. The applicable temperature range is limited only by the experimental system and chemical kinetics. Vapour-laden gas passes through a capillary, the vapour condenses down-stream in the cooler portion of the system and the total volume of the carrier gas passed is monitored. The amount of condensate is determined by chemical analysis, by mass gain of the condenser or by the mass loss of the sample.

Argon, nitrogen and hydrogen are the most frequently used carrier gases. Since, hydrogen gives a reducing atmosphere it has often been used in measuring vapour pressure of metals and alloys. Reactive carrier gases are often used to form species or to prevent the dissociation of the species being studied. Ackermann et al. [6] studied the vapour pressure of the oxides of uranium, molybdenum and tungsten using oxygen as carrier gas.

Principle and method of measurement

In this method the sample is kept in a boat in the constant temperature zone of the furnace. The carrier gas which may be pure or a mixture of gases, inert or reactive is introduced from one end of the reaction tube. It passes over the sample at a predetermined flow rate. Under carefully optimized experimental conditions, the carrier gas gets saturated

with sample vapour at the temperature of measurement. Then it enters the condensation region through a capillary. In the condensation region, the vapour gets condensed and the carrier gas escapes out. A schematic diagram of the apparatus is shown in the Fig. 2. The amount of vapour thus transported is dependent on the total volume of the carrier gas passed, the temperature of the sample, the flow rates of the carrier gas and the vapour pressure of the sample; hence, from the experimentally determined amount of condensate and the total volume of the carrier gas passed the vapour pressure at the experimental temperature can be computed as follows;

By the Dalton's law of partial pressures and assuming that the vapour behaves as an ideal gas under the conditions of low pressure and high temperature,

$$P_v = \frac{n_v}{n_v + n_g} \cdot P \tag{13}$$

where P_v is the vapour pressure of the sample, n_v is the number of moles of sample vapours, n_g is number of moles of carrier gas passed and P is the total pressure ($P_v + P_g$) of the system, usually one atmosphere. A prior knowledge of molar mass of the vapour is essential for this technique.
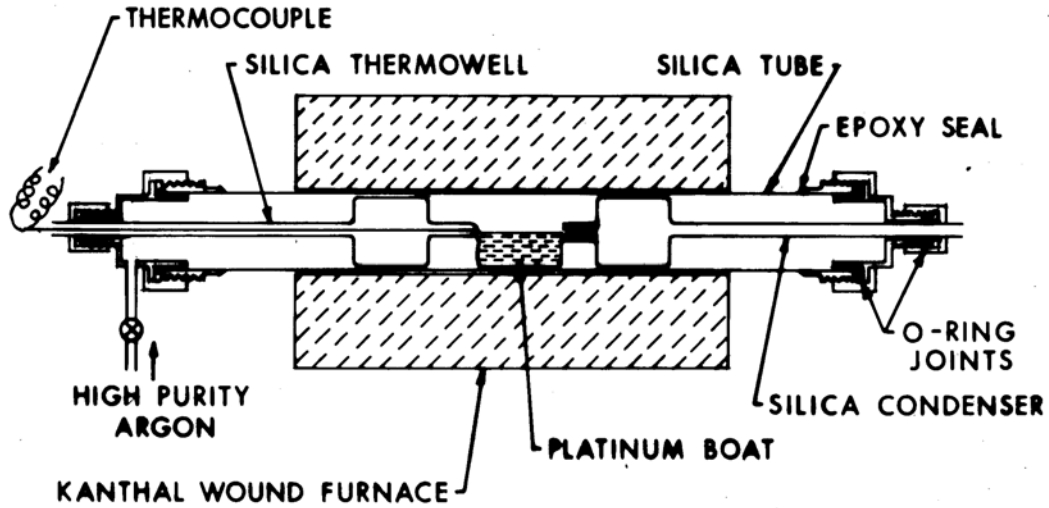
Fig. 2: Schematic diagram of transpiration apparatus

Transpiration measurements are basically dynamic in nature but are aimed at obtaining equilibrium data. It is therefore essential to control the experimental parameters in order to obtain meaningful data. Important parameters in this respect are:

a) Availability of a zone saturated with sample vapour,

b) The carrier gas flow rate and

c) Uniformity of temperature in the zone containing the sample, thermocouple and the condenser inlet.

Saturation zone

In order to ensure saturation of the carrier gas with sample vapour it is essential to have a wide enough zone in the vicinity of the sample which is saturated with the sample vapour. This is achieved by having a large surface area of the sample, small diameter of the reaction tube and by incorporating radiation shields on either side of the sample boat.

Effect of flow rate

This is one of the most important parameters in the transpiration technique. The gas flow rates are controlled within what is known as the 'plateau region'. This is obtained by studying the variation of the mass of the condensate per unit volume of the carrier gas as a function of carrier gas flow rates. The result of a typical study is shown in Fig. 3.
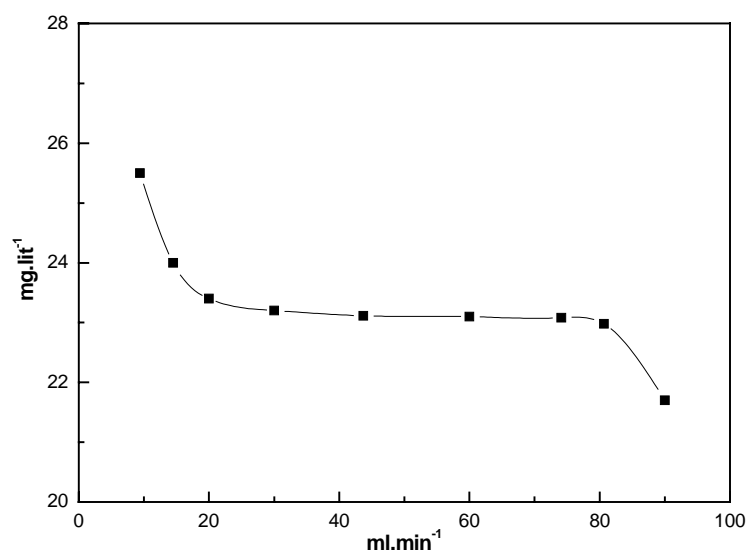
Fig.3. A typical flow rate Plataeau in transpiration technique

There are three different regions in this plot, namely,

a) Low flow rate region or diffusion controlled region,

b) Plateau region where the mass of the condensate per unit volume of the carrier gas is independent of the carrier gas flow rates, and

c) High flow rate region or un-saturation region.

Low flow rate region

In this region the fraction $n_v / (n_v + n_g)$ becomes larger compared to the equilibrium values since the vapour is transported to the condenser region not only by the carrier gas but also by self diffusion. In fact, the vapour diffuses in both directions of the sample chamber. Diffusion in the upstream direction may give a higher value of vapour pressure if mass loss of the sample is taken for the calculation of vapour pressure. Diffusion in the downstream condenser region complicates the vapour pressure measurements more seriously than does the upstream diffusion.

Plateau region

In this region the flow rates are high enough to nearly eliminate the problems related to the diffusion effect, but at the same time low enough so as not to cause any un-saturation effects due to the kinetics of the evaporation process. This region is insensitive to small variations in flow rate and represents the equilibrium values of vapour pressure. Since, the plateau region changes with the geometry of the experimental assembly and with the kinetics of the evaporation process, it is necessary to find out the plateau region with each experimental arrangement and with each sample whose vapour pressure is to be measured. To determine the region a series of experiments are carried out at a constant temperature using different flow rates. The temperature chosen for this purpose is normally the mean temperature of the range of interest.

High flow rate or un-saturation region

At high flow rates the saturation of carrier gas may be prevented by poor gas mixing or inadequate sample evaporation rate. These kinetics effects may be minimized by the proper

experimental setup design to provide intimate contact between the sample and the carrier gas. A sample should provide an evaporating surface that is as large as possible.

In addition to the problem arising from diffusion and kinetics, vapour pressure data can also be affected by non-uniformity of temperature. Temperature gradient in the saturation chamber may result in redistribution of sample vapour to the coldest part of the chamber. If there is no condensation of the gaseous components on reaching the cold region, there may be a diffusive flow caused by temperature gradient in the exit portion of the apparatus. If a mixed carrier gas is employed, it may separate in the thermal gradient. While designing the apparatus, care must be taken to avoid any temperature gradient in the sample chamber and also the capillary end should not be the coldest portion of the system.

Boiling Temperature Method

This method is based on the ability of the liquids to boil freely when their saturated vapour pressure is equal to the external pressure. The schematic diagram of the apparatus is shown in Fig. 4.
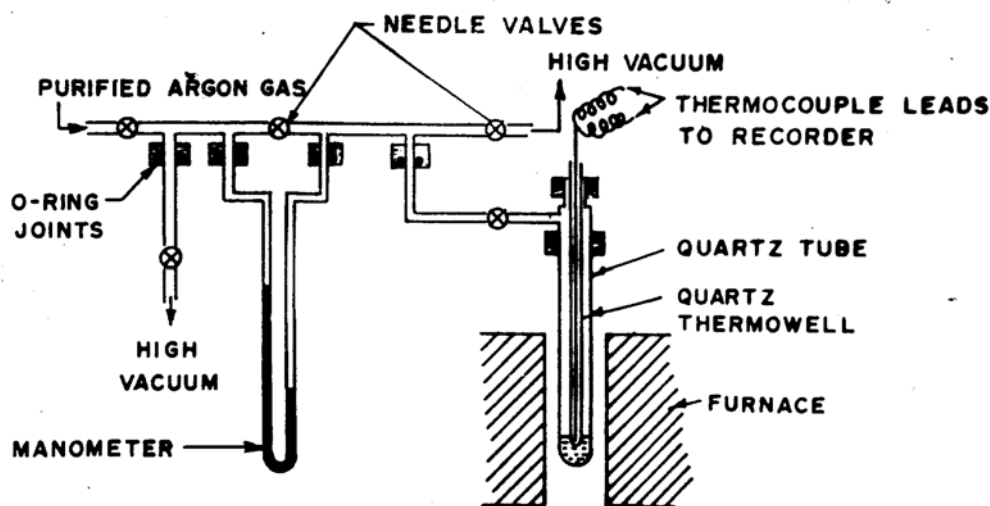
Fig. 4. Schematic diagram of boiling temperature apparatus

Principle and method of measurement

When the external pressure above the condensed phase is equal to its saturated vapour pressure the condensed phase begins to boil. The method consists of letting a condensed phase boil under a definite pressure and measuring the temperature of the vapour in equilibrium

with the boiling condensed phase. This method is simple, very useful and reliable to carry out vapour pressure measurements over a wide range of pressures provided that boiling is accurately identified. Two possible approaches to boiling temperature determination are:

a) Maintaining a constant external pressure and varying the temperature till boiling is observed or conversely,

b) Keeping the temperature constant and continuously varying the pressure.

The instant of boiling is indicated by the discontinuity in one of the properties of the system. For this either mass or the temperature of the sample is monitored.

The limiting sensitivity of the method is sometimes set by the output of the thermocouple or the manometric measurements. The main source of error in this method is the interaction of the cover gas with sample vapour and hence gradual loss of the buffer gas and the interaction of sample vapour with containment material and this can be overcome by proper selection of the cover gas and the container for the sample. Since temperature change involved at the instant of boiling is small (1 or 2 K) precise control of temperature is necessary and to detect this small change a high precision millivolt recorder is required. Sensitivity of the Manometric reading can be increased by the use of a cathetometer and further reduced by using a manometric fluid of low density such as 'Apiezon-B' oil.

Knudsen effusion technique

In this method, the rate of vaporization of the molecules from a small orifice is measured. It is used for the measurement of vapour pressure less than 1 kPa. In this pressure range the mean free path of molecules become larger and the vapour pressure determination are based on kinetic theory of gases by which the molecular flux at a boundary can be calculated for a gas at equilibrium. The vapour composed of a single species in equilibrium with its congruently evaporating condensed phase is allowed to flow from an isothermal container through a small thin edged orifice into an evacuated space. If the orifice is small enough such that the equilibrium inside the cell is not disturbed and the edge of the orifice is so thin that the chance of molecular collisions with the edge of the orifice are small and if the pressures are low enough that intermolecular collisions are absent within the orifice, then the rate of effusion per unit area per unit time can be given by:

$$\Phi = \frac{dn}{dt} \cdot \left(\frac{1}{A}\right) \cdot \left(\frac{1}{M}\right) = \left(\frac{1}{4}\right) \cdot v \cdot n \tag{14}$$

where v is average molecular velocity $\{= (8RT/\pi M)^{1/2}\}$, t is time and n is the number density of the molecule ($= P / RT$), R is the universal gas constant, T is the temperature, M is the molecular mass and P is the pressure. Then Φ will become:

$$\Phi = \left(\frac{1}{4}\right) \cdot \left(\frac{P}{RT}\right) \cdot \left(\frac{8RT}{\pi M}\right)^{1/2} = P \cdot \left(\frac{1}{2\pi RTM}\right)^{1/2} \tag{15}$$

$$P = \left(\frac{dw}{dt}\right) \cdot \left(\frac{1}{A}\right) \cdot \left(\frac{2\pi RT}{M}\right)^{1/2}. \tag{16}$$

These equations are known as Knudsen equations or sometimes the Hertz-Knudsen equations. Thus by knowing the temperature (T), molecular mass (M) of the vaporizing species and the rate of effusion mass loss (dw/dt), the vapour pressure (P) of the system can easily be calculated. In equation (16) molecular speed is assumed to be independent of direction, so that molecules can strike a given area of the wall from all the directions of approach in equal probability. Also the equation is valid for infinitely thin walled orifice. But if the orifice has the form of a channel of finite length, then some molecules will not escape but will strike the wall of the orifice and be reflected diffusively from it. These molecules have a finite probability to return to the cell after one or more reflections. The result is such that the net flux from the cell is decreased. For this, Clausing [7] has introduced a correction factor (K_c), which can be given as:

$$K_c = [1 + 0.4 \cdot (L/r)] \ / \ [1 + 0.95 \cdot (L/r) + 0.015 \cdot (L/r)^2] \tag{17}$$

where L is the length and r is the radius of the of the orifice. Claussing factor calculated from equation (17) agrees within 1% for L/r between 0 and 4 and within 3% for L/r between 4 and 100. The value of K_c may be found in Clausing's tabulation [7] or calculated by means of Kanard's [8] empirical formula. Considering the Clausing factor, equation (16) becomes:

$$P = \left(\frac{dw}{dt}\right) \cdot \left(\frac{1}{A}\right) \cdot \left(\frac{1}{K_c}\right) \cdot \left(\frac{2\pi RT}{M}\right)^{1/2}. \tag{18}$$

The Clausing factor varies with the Knudsen cell dimensions. Hence, it is to be determined for different types of cells by measuring the vapour pressure of substances such as magnesium metal whose vapour pressure is well known.

Upper pressure limit

The low pressure limit depends on the detection limit of the measuring instrument. However, pressures down up to 10^{-6} kPa can be easily measured using a microbalance. The upper limit of pressure measurement depends on the following factors:

i)   Free molecular flow is necessary, that means the collision between gaseous molecules does not occur in the vicinity of the orifice,

ii)   When mean free path approaches the orifice diameter, molecular interactions become important and as the pressure increases further, molecular flow goes over to a transitional type and that is ultimately replaced by viscous flow and the bulk gas flows out at a higher rate than that given by the Knudsen equation for a given pressure and

iii)   The upper limit to true molecular effusion through an ideal orifice is set at approximately, $\lambda/d = 10$, where $\lambda = [(N/V)\sqrt{2}\pi\delta^2]^{-1}$, where δ is the collision diameter, N/V is the molecular density. δ is a difficult quantity to define accurately and its limit varies from 1 to 10 A°.

At higher pressures the mean free path of the vapour reduces, thus the diameter of the orifice has to be very small which is difficult to manufacture.

Conditions of equilibrium pressure measurements

Because of the continuous loss of vapour through the orifice, the Knudsen cell is not a perfectly equilibrium system. Thus the vapour pressure calculated from rate of effusion may be less than the equilibrium vapour pressure, which a substance would exhibit in a completely closed system. This is serious if:

i)   There is some kinetic barrier to evaporation at sample surface such that the rate of evaporation is less than the rate of effusion,

ii)   The molecular form of vapour species is different from that in the solid (e.g. AlO above Al_2O_3) and

iii)   The molecular size and packing hinder evaporation process.

Cell geometry

The geometry of the cell body and the location and area of the sample within it affect the rate of the flow of the molecule. For the cell to be saturated with isotropic vapour, following conditions should be maintained:

i)   Wall collision density must be constant and

ii)   Ratio of radius of the orifice to radius of the cell should be 0.1.

Surface diffusion and creep

The molecule may migrate appreciable distance along the surface and re-evaporate from a different location. This process is called surface diffusion. It is a molecular or atomic phenomenon and

i)   It increases as orifice diameter and length decreases,

ii)   Lid is hotter than the body of the crucible and

iii)   It also increases as the pressure decreases.

Surface diffusion could be detected by measuring vapour pressures using cells of different geometry and different material of construction.

When the molecule condenses near the orifice, it may migrate along the wall of the orifice and re-evaporate from the external surface thus significantly altering the measured pressure and distribution of effusion beam. This process is known as creep. It is a bulk phenomenon (e.g. Pu in Ta cell and U in Ta / W cell etc.).

Effect of orifice area

If the orifice area is large, then the radiant energy is not reflected back from the orifice into the cell but is lost. The cell cavity and orifice do not behave as a black body and a cold spot may develop on the floor of the effusion cell immediately below the orifice.

Experimental apparatus

The description of experimental apparatus and procedure for vapour pressure measurements by this technique has been discussed in detail in a number of review articles [9-13]. The experimental set-up generally used in this study for vapour pressure measurements by Knudsen effusion mass loss method is given in Fig. 5. The sample whose vapour pressures is required to be measured is placed in a suitable Knudsen cell. The Knudsen cell is hanged from one arm of the microbalance using a fine hang down wire in such a way that the cell was
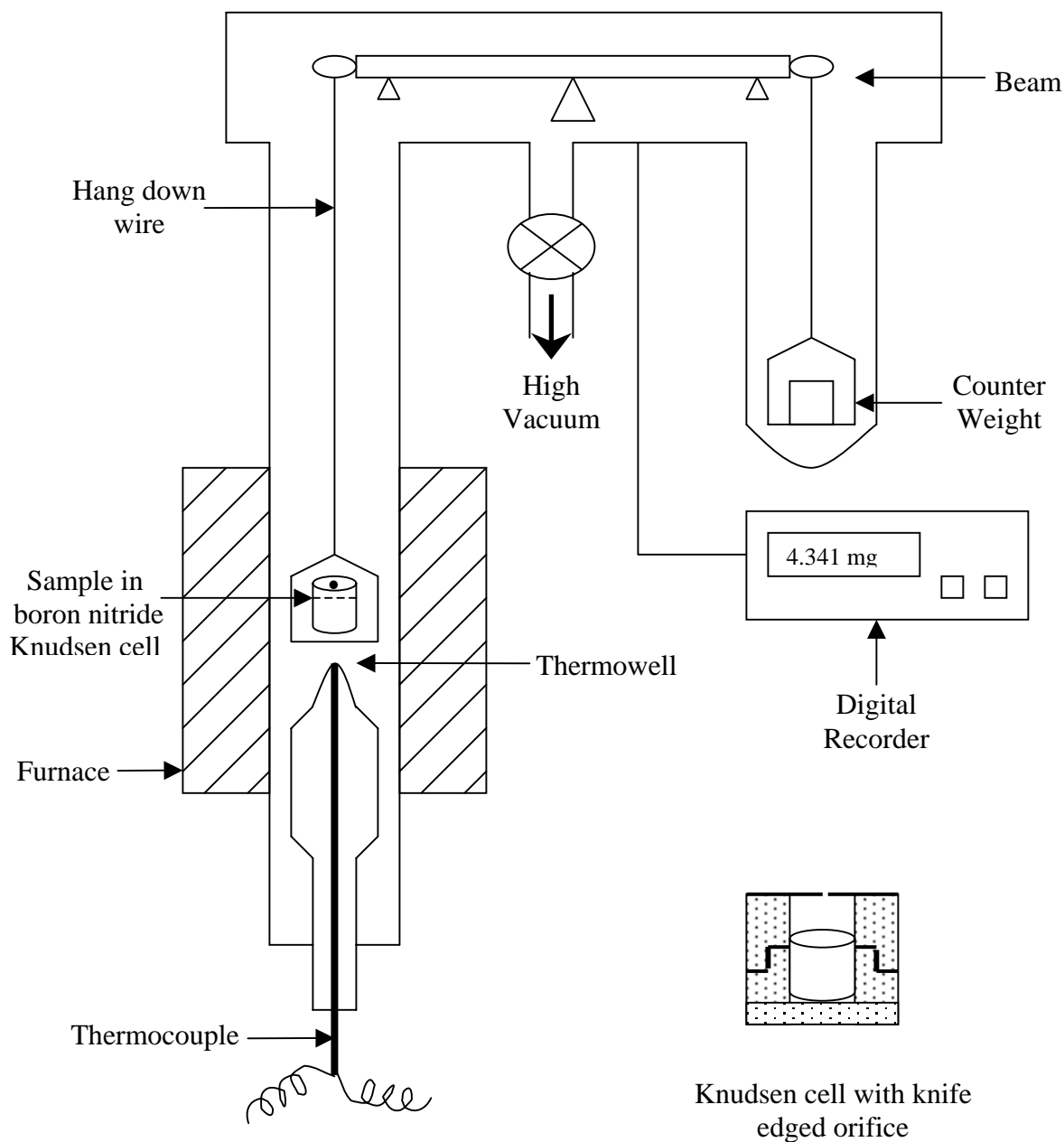
Fig. 5. Schematic Diagram of Knudsen Effusion Mass-Loss Technique

within the constant temperature zone of a furnace. The experimental assembly is evacuated to a high vacuum ($\sim 10^{-7}$ kPa) using an oil diffusion pump or turbo molecular pump backed by a direct driven rotary pump. The sample is heated to a known constant temperature using a PID temperature controller. The temperature of the Knudsen cell is measured by a pre-calibrated

thermocouple placed below the Knudsen cell in the isothermal zone. Once the temperature became constant, the mass loss for a known period of time is measured by using a highly sensitive microbalance capable of detecting 1 μg mass change. This rate of mass loss was used to calculate the vapour pressure.

Target collection technique

A schematic diagram of the apparatus is shown in Fig. 6. Rather than weighing the sample with the effusion cell itself, it is often preferable to collect a known fraction of the effusate on a target. The amount collected can be subsequently determined by chemical, electrochemical, spectroscopic, X-ray fluorescence or radiochemical techniques, often to greater accuracy than is possible by weighing.
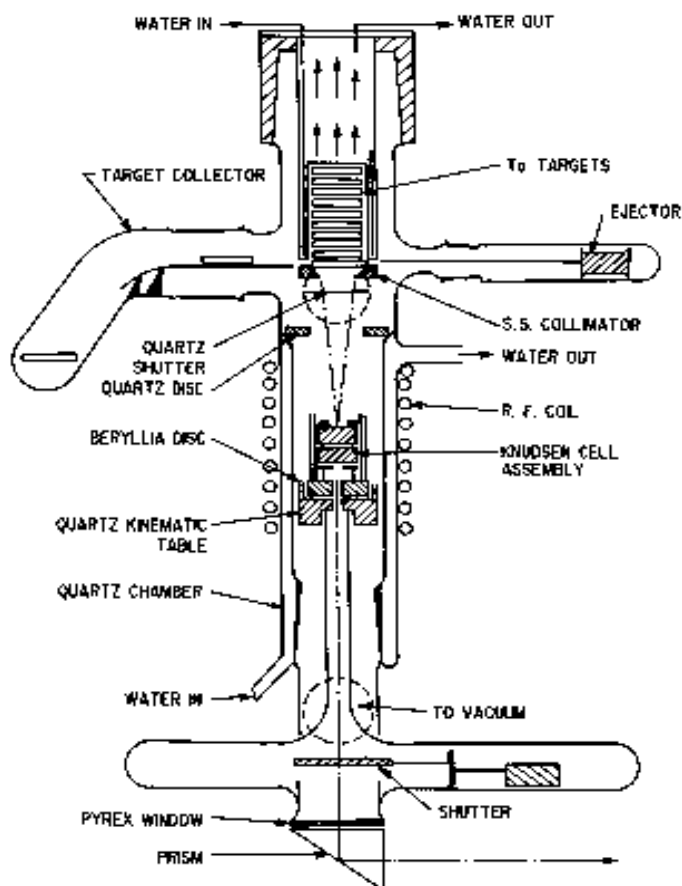
Fig. 6. Schematic diagram of target collection apparatus

In some cases the total effusate is collected on a cooled surface and analyzed. For a circular target of radius 's' placed coaxially with the orifice but a distance 'S' from it, and for an

orifice very small compared to the target, so that it constitutes a point source. The pressure can be represented as:

$$P = \frac{w}{A \cdot t} \left(\frac{2\pi RT}{M} \right)^{1/2} \left(\frac{s^2 + S^2}{s^2} \right)$$ (19)

where 'w' is the weight of vapour of molecular weight 'M' collected on the target. An advantage of the target method is that corrections for non-ideality of the orifice are generally negligible, since for wide ranges of orifice dimensions the molecular beam intensity is constant for θ near zero. It may be possible to analyze for various elements separately on the targets and so learn something about the molecular makeup of the vapour. This should be particularly useful when studying the activities of the components of binary alloys. The main disadvantage is that one cannot follow in details the progress of the experiment, because the analyses are performed following the completion of the series of actual vaporizations. In using targets one must determine whether all the vapour condenses upon striking the target, that is, whether the condensation coefficients is unity.

The Isopiestic method

One of the most accurate methods for determining comparative vapour pressure is the isopiestic method. In this method samples are partially equilibrated through the vapour state so that they display a common vapour pressure of a particular component. Analyses of these samples then provide the necessary compositional information to describe the systems. Isopiestic studies have value in the determination of comparative vapour pressures of non-stoichiometric materials, i.e., solid or liquid solutions. Absolute pressures can be realized only through a comparison with known vapour pressure systems with which a sample is isopiestic. The isopiestic method has been widely used in aqueous solution chemistry to establish systems with equal vapour pressures (activities). Isopiestic equilibrium, of course, is accomplished under isothermal conditions. However, studies made under non isothermal conditions have been found to be very useful and are given the name "pseudo-isopiestic" studies. It is in the field of high temperature studies that this method has been reported.

Methods

The principle involves the establishment of an equilibrium vapour pressure between an

alloy specimen held at high temperature end of a sealed tube and the pure volatile component of the alloy held at low temperature end. In this technique the temperature of the hot and cold ends of the tube are fixed and the equilibrium composition of the alloy is determined. The activity of the volatile component of the alloy at the temperature of the hot end can then be calculated provided the vapour pressure/temperature relation of the volatile component is known. As a time saving device the hot end may be supplied with a row of several alloy specimen held at the temperature gradient rather than constant temperature. Since, the activity of the volatile component in the alloy varies with the temperature, subsequent analysis of the alloy specimens produces a number of results per run. A schematic diagram used by Krachler et al. [16] is shown in Fig. 7.
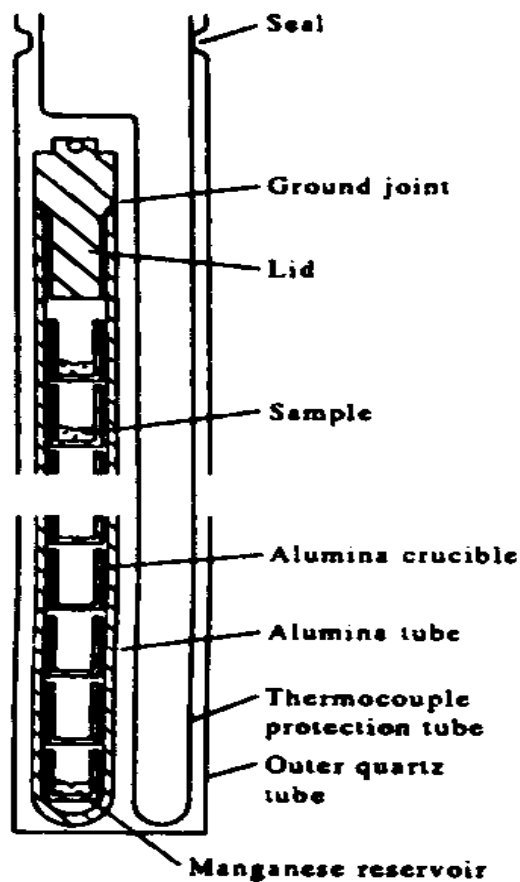
Fig. 7. Schematic diagram of isopiestic apparatus with multi sample arrangement

Since, vapour transport can be limiting factor in determining the duration of the experiment, equilibrium is usually accomplished in a vacuum. The results of these studies are usually determined after quenching of the samples. *In situ* determination of results of the experiment is made possible by use of radioisotopes and it affords much higher degree of sensitivity than conventional means.

Conclusions

Determination of the vapour pressure of a given material may be undertaken for many purposes. The rate of vaporization may be the factor limiting the usefulness of the material at elevated temperatures. Vapour pressure data is of interest to know the activities of the components in an alloy. Even chemical purification or synthesis may involve vaporization processes. Heats and free energies of formation and entropies of gaseous and condensed species can be determined using vapour pressure data.

References

[1] L Rayleigh, Phil. Trans. A196 (1901) 205.

[2] J.C. Sharder, H.N. Ryder, Phys. Rev. 13 (1919) 321.

[3] H. McLeod, Phil. Mag. 48 (1874) 110.

[4] W.H. Rodebush, A.L. Dixon, Phys. Rev. 26 (1925) 851.

[5] H.V. Regnault, Ann. Chim. 15 (1845) 129.

[6] N.J. Ackermann, R.J. Thorn, C. Alexander, N. Tetenboum, J. Phys. Chem. 64 (1960) 350.

[7] P. Clausing, Ann. Physik, 12 (1932) 961

[8] E. H. Kennard, Kinetic Theory of Gases, McGraw Hill, New York, 1938.

[9] A. N. Nesmeyanov, Vapour Pressure of the Elements, Translated by J. I. Carasso, Academic Press, New York and London (1963).

[10] W. C. Demaruus, The Problems of Knudsen flow, Report-K-1302, Part-III, Union Carbide Corporation, Oak Ridge Gaseous Diffusion Plant, Oak Ridge, Tenn., 1957.

[11] R. P. Iczkowski, J. L. Margrave, S. M. Robinson, J. Phys. Chem., 67 (1963) 229.

[12] J. L. Margrave, editor, The Characterization of High Temperature Vapours, John Wiley, New York, 1967.

[13] J. C. Edwards, P. W. Gilles, J. Chem. Phys., 44 (1966) 4426.

[14] J. L. Margarve, in: Physico-chemical Measurements at High Temperatures, J. O. M.

Bockris, J. L. White, J. D. Mackenzie (editors), Ch.10, Butterworths, London, 1959.

[15] E. D. Carter, "The effusion methods at age 69; Current State of the Art", NBS Spl. Pub., 561, Proceedings of 10th Materials Research Symposium on Characterization of High Temperature Vapours and Gases, held at NBS, Gaithersburg, Maryland, Sept., 18-22, 1978.

[16] R. Krachler, H. Ipser, K.L. Komarek, Z. Metallkunde 73 (1982) 731.

ELECTRICAL CONDUCTIVITY STUDIES OF ION CONDUCTING MATERIALS

By

Prof. N. Satyanarayana

Department of Physics, Pondicherry University, Puducherry - 605014

Prof. N. Satyanarayana completed his graduation (1977) graduation and postgraduate (1979) from Osmania University and obtained his Ph.D from IIT, Madras in the year 1984. At present he is professor in the Department of Physics, University of Pondicherry. His research interests include developing various types of nano-crystalline and nano composite materials by wet chemical methods, development of fast ion conducting lithium and silverbased electrolysts for solid state battery application etc. He has carried out several projects under DRDO, CSIR and DST schemes. He has more than sixty publications in referred journals and more than seventy publications in conferences /symposia. He has guided several students for their M.Sc., M.Phil and Ph.D degrees and carried out several projects under DST, CSIR, UGC and DAE schemes. Prof. Satyararayana also holds several collaborative projects with foreign universities and companies.

1. ATOMIC TRANSPORT:

In crystalline or amorphous / glassy solids, conduction of electric current is due to charge transport, either purely electronic or ionic or both (mixed). Electronic conduction is due to the flow of electrons/holes, called electronic conductivity (σ_e). Ionic conduction is due to the flow of Cations/anions, called ionic conductivity (σ_i). Also, it is possible to have both σ_e & σ_i (mixed) simultaneously and in this case, the total conductivity (σ_t) is [1,2]

$$\sigma_t \ = \ \sigma_i \ + \sigma_e \ \textbf{..........} \ \ (1)$$

The transference number ($t_{x \ (e \ or \ i)}$) can be expressed as

$$t_{x \ (e \ or \ i)} = \sigma_{x \ (\ e \ or \ i)} / \ \sigma_t \ldots\ldots\ldots(2)$$
$$t_i \ \ + \ \ t_e \ = \ 1.0 \ldots\ldots\ldots(3)$$

If t_i = 0.9 means that the 90% of the charge is by ionic transport and 10% is electronic, since $t_i + t_e = 1.0$. The transference number of cation t_i^+, anion t_i^- and electrons t_e^- and holes t_e^+ (or $t_{e,h}$) in several compounds is given table. 1.

Table. 1.

Compound	Temp (deg)	t_i^+	t_i^-	t_e^- & t_e^+ (or $t_{e, h}$)
NaCl	400	1.00	0.00	-
NaCl	600	0.95	0.05	-
Kcl	435	0.96	0.04	-
Kcl	600	0.88	0.12	-
Kcl+.02cacl$_2$	430	0.99	0.01	-
Agcl	20-350	1.00	-	-
AgBr	20-300	1.00	-	-
BaF$_2$	500	-	1.0	-
PbF$_2$	200	-	1.0	-
CuCl	20	-	-	1.00
CuCl	366	1.0	-	0.00
ZeO$_2$ + 18%CeO$_2$	1500	-	0.52	0.48
ZeO$_2$ + 50%Ce$_2$O	1500	-	0.15	0.85

2. ELECTRICAL CONDUCTIVITY (σ):

The electrical conductivity (σ) is defined as the ratio of current density (J) to the electric field (E) [2].

$$\sigma = J/E \qquad \text{...............} \qquad (4)$$

J is the electric charge (q) crossing a unit area (A) per second and $q = ze$, z is the valence e is the unit charge. If the velocity of carrier is v and there are n identical carriers per unit volume, then the current density (J) will be

$$J = nqv \qquad \text{.................} \qquad (5)$$

v is related to field E. The velocity of carrier at any time 't' will be changed from its initial random value Vo by an amount (Δv). Then, an average velocity [$<v>$] of carrier is given by (from classical free electron model)

$$<v> = qe(\tau)/2m \qquad \text{......} \quad (6)$$

Where, m is the mass of the electron (or m* effective mass) and τ is the mean time between collisions. Combining eq (4), (5) and (6), will get,

$$\sigma = nq^2\tau/2m \quad \text{or} \quad \sigma = n\mu q \quad \text{............} \quad (7)$$

Where, μ is the mobility defined by $\mu = q\tau/2m$ .... $\qquad$ (8)

In the case of ions, which hope from site to site, a relation between the diffusion constant (D_i) and the mobility (μ) can be derived from the Boltzmann transport equation.

$$\mu = eD_i/KT \qquad \text{........} \quad (9)$$

$$D_i = Do \exp\{-Q_d/KT\} \qquad \text{.......} \quad (10)$$

Where, $D_0 = zd^2v/6$ (crystalline solids), v is the attempt frequency, d is the distance between sites and z is the valence. Using eq. (7), (9) & (10), the general expression for ionic conduction will be

$$\sigma = (nqe/KT) \, (zd^2v/6) \, exp[-Q_d/KT] \qquad or$$

$$\sigma = \sigma_0/T \, exp[-Q_d/KT] \qquad \text{.......} \quad (11)$$

Where $\sigma_0 = (nz^2e^2d^2v/6K)$. Another equation for conductivity (σ_{exp})

$$\sigma_{exp} = (t/a) \, x \, (1/R) \qquad \text{.....} \qquad (12)$$

Where t is the thickness of sample, a is the area of the sample and R is the resistance of the sample [$R \propto t$, $R \propto 1/a$, $R = \rho t/a$, $\rho = 1/\sigma$ and $\sigma_{exp} = (t/a) \, x \, (1/R)$], ρ is the resistivity].

3. THEORY OF IONIC CONDUCTIVITY:

Ionic Conductivity involves the long-range migration of ionic charge carriers through the material under the deriving force of an applied field (E). The electric force (F) on the ion perturb its random thermal motion and increases the probability of a transition in the direction of the applied field. This can be described easily by considering the schematic two potential energy wells as shown in fig.1. Solid lines indicate energy without field and dashed lines indicate energy with field. V is the potential barrier height and b is the distance between two wells [2]. Consider the ions move in 1-d parallel to the X-axis jumping over the potential. The probability that an ion will move to either the right or left is

$$P = \alpha \, KT/h \, exp[-V/KT]\ldots\ldots\ldots(13)$$

Where, α is an accommodation coefficient, KT/h is the vibrational frequency of the ions in the well, K is the Boltzmann constant and T is absolute temperature. When a field E is applied, the ion coordination is slightly distorted and correspondingly, the potential barrier to the ion motion is slightly shifted by an amount 1/2zeEb=1/2Fb, as shown in fig.1. Therefore, the probability of motion to the right is

$$P^+ = 1/2 \, \alpha KT/h \, exp\{-(V-1/2Fb)/KT\} \qquad Or$$

Using (16) we get $\quad P^+ = 1/2 \, P \, exp\{+Fb/2KT\} \qquad \text{.........} \quad (14)$

The probability of the motion to the left is

$$P^- = \tfrac{1}{2} \, \alpha \, KT/h \, exp\{-\{V+1/2Fb/KT)\} \qquad Or$$

$$P^- = \tfrac{1}{2} \, P \, exp\{-Fb/2KT\} \qquad \text{.........}(15)$$

There will be an average drift velocity to the right in the direction of the field, since

the +ve transitions will be more frequent than the -ve. The mean velocity of the drift motion is

$$V = b \, (P^+ - P^-) = \tfrac{1}{2} \, bP\{exp(Fb/2KT)-exp(Fb/2KT)\} \qquad Or$$

$$V = bP \, sinh \, Fb/2KT \qquad \text{..........}(16)$$

As long as the field strength is much smaller than KT ($1/2Fb \ll KT$), then the drift velocity can be expressed as

$$V \sim b^2 PF/2KT \ldots\ldots(17)$$

For large field strengths, the first term in sinh of eq (16) will dominate and

$$V \cong \text{constant} \; X \; \exp[bF/2kT] \ldots\ldots(18)$$

At RT, bF is small compared with KT up to field strengths of 10V/cm. Using eq(17) and eq(5), we get;

$$J = nzeb^2 PF/2KT = nz^2 e^2 b^2 PE/2KT \ldots\ldots(19)$$

Substituting $V = \Delta F_{dc}/N$ in equ(13)

$$P = \alpha \; KT/h \; \exp[-\Delta F_{dc}/N \; KT] \quad \ldots\ldots\ldots \quad (20)$$

where ΔF_{dc} is the change in free energy for dc conduction in units of kilocalories/mole and N is Avogadro's number. $N = 6.023*10^{23}$ atoms/mole. Substituting eq(20) in eq(19), we get

$$J = (n\alpha z^2 e^2 b^2 E)/2h \; \exp\{-\Delta F_{dc}/RT\} \ldots\ldots (21)$$

Where R is the gas constant (R=8.31 J/mole°K). Therefore electrical resistance is

$$R_{ohm} = E/J = 2h/n\alpha z^2 e^2 b^2 \; \exp[\Delta F_{dc}/RT] \; \text{Or} \; \log R_{ohm} = \log. \; 2h/n\alpha z^2 e^2 b^2 + \Delta F_{dc}/RT \ldots (22)$$

$$G_{ohm}^{-1} = n\alpha z^2 e^2 b^2/2h \; \exp[-\Delta F_{dc}/RT] \quad \text{Or} \; \log G_{ohm}^{-1} = \log n\alpha z^2 e^2 b^2/2h - \Delta F_{dc}/RT \ldots(23)$$

Eq(22) & (23) are similar to the **R-H (ROSCH-HINLICHSEN) law** of **electrical resistivity of glass, discovered empirically many years ago.**

$$\text{Log } \rho = A+B/T \quad \ldots\ldots \quad (24)$$

Many glass compositions behave according to eq(23), as shown in fig.2. The ionic conductivity of crystalline oxide ceramics is also described by eq(23) & (24), as shown in fig.3. It is also possible to distinguish between enthalpy and entropy changes involved in the dc conduction by using II law of thermodynamics.

$$\Delta F_{dc} = \Delta H_{dc} - T\Delta S_{dc} \ldots\ldots\ldots(25)$$

Which yields to final expression for electrical conductance.

$$\text{Log } G = \log [n\alpha z^2 e^2 b^2/2h \; \exp(\Delta S_{dc}/R)] - \Delta H_{dc}/RT \ldots\ldots(26)$$

Therefore the enthalpy and entropy can be calculated respectively from the slope and intercept of the logG vs 1/T plot.

4. SOLID ELECTROLYTES (SES):

The conductivity of solid electrolytes (SEs) is several order of magnitude higher ($> 10^{-6}$ $\Omega^{-1}cm^{-1}$) than normal ionic compounds. They are often called as Fast ion conductors (FICs), superionic conductors (SICs), or High Ion Conductors (HICs) or optimized ionic conductors (OICs).

4.1. Criterion for fast ion conduction:

In normal ionic conductors (NICs), the number of charge carriers are arising from the frenkel or schottky defects, which are determined by thermal generation. So, in eq (35), $\Delta H_{dc} = \Delta H_f + \Delta H_m$ and $\Delta S_{dc} = \Delta S_f + \Delta S_m$. Where, ΔS_m and ΔHm are the entropy and enthalpy respectively for the ion motion under an applied field. ΔS_f and ΔH_f are the entropy and enthalpy respectively for the formation of the charge carriers associated with motion. The conductivity of eq (26) thus becomes

$$LogG = log(n\alpha z^2 e^2 b^2/2h)exp[\Delta S_m + \Delta S_f/R]-[\Delta H_m + \Delta H_f/RT]$$
.... (27)

The characteristic of fast ion conduction arises from the large value of N, the concentration of the charge carriers, with respect to n, the total number of potentially mobile ions, which is due to inherent vacant sites in the lattice (called built in defects). Since lattice vacancies are structurally inherent, their conduction is not thermally dependent. Therefore, for FICs, $\Delta S_f = 0$, $\Delta H_f = 0$ and hence, the eq(27) becomes

$$LogG = log[\alpha\beta n_0 z^2 e^2 b^2/2h]exp(\Delta S_m/R) - (\Delta H_m/RT)$$
…..………. (28)

Where, β is the fraction ($\beta = N/n$) of mobile charge carriers. Eq (27) & (28) are the temperature dependent of conductivity equations for NICs and FICs respectively.

5. ELECTRICAL CONDUCTIVITY MEASUREMENTS:

5.1. General a.c. theory:

Dc measurement cannot yield the exact resistance of the sample, since no sample is purely due to resistive. Thus, an electrical behavior of any sample can be represented as a combination of various individual circuit elements such as resistance (R), capacitance (C), inductance (L) and the contribution of any given component being dependent on the frequency of measurement. Consider the A.C. theory concerned with simultaneously carrying currents and voltages in resistance (R), capacitance (C) and inductance (L) of the form [3,4].

$$E = E_0(cos\omega t + jsin\omega t)………..(29)$$
$$I = I_0(cos\omega t + jsin\omega t)………… (30)$$

1.   For a pure resistance (R), the current at any time simply equals to

$$I = 1/R\ E_0(cos\omega t + jsin\omega t) ……….(31)$$

2.   For a pure capacitance (C)
$$I = (-\omega C E_0 \sin\omega t + j\omega C E_0 \cos\omega t) \ldots\ldots\ldots (32)$$

3.   For a pure inductive load (L)

$$I = (E_0/\omega L)\sin\omega t - j(E_0/\omega L)\cos\omega t \ldots\ldots\ldots\ldots(33)$$

Eq (31), (32) and (33) may be written respectively as

$$I = E/R, \quad I = -j\omega CE \text{ and } I = E/\omega jL \ldots\ldots\ldots\ldots (34)$$

Equations (34) have the form, $I = E/Z$, where $Z = R$, $1/j\omega C$ and $j\omega L$ for R,C,and L respectively. Z is known as the electrical impedance and expressed in unit of ohms. The impedance behaves mathematically in a similar manner to resistance. Hence, for series circuit, $Z_s = \sum Z_i$ and for parallel circuits, $Z_p^{-1} = \sum Z_i^{-1}$.

Experimentally measured impedance data at a given frequency contain R and C in series or parallel two component configuration. The complex plane analysis (CPA) is a mathematical technique, which allows the determination of the individual component values from the reduced data obtained over a range of f. Hence, the complex plane analysis technique has become a basic tool in the study of any materials (including solid electrolytes). A small amplitude of sinusoidal (a.c) signal is applied to perturb the system and the frequency response is recorded as impedance (Z*) and phase angle (ϕ). The applied potential is given by
$$E = E_o \exp (j\omega t) \ldots\ldots\ldots(35)$$
Where, $\omega = 2\pi f$. The output current of the system is also a sinusoidal and it is given by
$$I = I_o \exp (j\omega t + \phi) \ldots\ldots\ldots (36)$$

Complex impedance (Z*) of the circuit at any frequency can be represented by

$$Z^* = E/I = (E_o / I_o) \exp (-j\phi) = Z^* = Z_o\cos \phi - j Z_o\sin \phi =$$
$$Z^* = Z' - j Z'' \ldots\ldots\ldots (37)$$

where, $Z' = Z \cos \phi$ and $Z'' = Z \sin \phi$ are respectively real and imaginary parts of the impedance and $j = \sqrt{-1}$. Similarly, other related complex quantities are defined as.

Complex admittance $Y^* = 1/Z^* = Y' + jY'' \ldots\ldots\ldots\ldots.. (37a)$
Complex permitivity $E^* = 1/j\omega Z^* = E' - E'' \ldots\ldots\ldots\ldots... (37b)$
Complex modulus $M^* = j\omega Z^* = M' + M'' \ldots\ldots\ldots\ldots.. (37c)$

The above equations form the basis for the complex plane analytical (CPA) techniques

5. 2. Equivalent circuit representation

5.2. 1. Series combination of R and C

Circuit containing a resistance and a capacitance in series are shown in Fig. 4a. The total impedance of the circuit is given by [3,4]

$$Z^* = R + (1/ j \omega C) = R - (j / \omega C) \quad (or) \quad Z^* = Z' - J Z'' \quad \ldots\ldots\ldots \quad (38)$$

Where, $Z' = R$, $Z'' = 1/ \omega C$ and $\omega = 2\pi f$, f is frequency. The resultant impedance plot for R and C in series is represented by a vertical line parallel to the imaginary axis intersecting the real axis at R, as shown in Fig 4a, and the corresponding admittance plot gives the semicircle intersecting the real axis at a point 1/R, as shown in Fig.4b.

5.2.2. Parallel combination of R and C

Circuit containing a resistance and a capacitance in parallel are shown in Fig 4c and the total impedance of the circuit is given by

$$Z^* = (1 / R + j \omega C)^{-1} = R / (1 + j \omega R^2 C)$$
$$= \{R / (1 + (\omega R C)^2)\} - \{j \omega R^2 C / (1+(\omega R C)^2)\} \; or \; Z^* = Z' - J Z'' \ldots\ldots (39)$$

Where, $Z' = R / (1 + (\omega R C)^2$ and $Z'' = \omega R C / (1+ (\omega R C)^2)$. The complex impedance plot for the circuit containing a resistance and a capacitance in parallel represents a semicircle as shown in Fig 4c, and the corresponding admittance plot gives the vertical straight line as shown in Fig 4d. Intersection of the semicircle with the real axis at a point R gives the bulk resistance of the material. The equation of the semicircle with radius R/2 and center at R/2, 0 is

$$(Z'- R/2)^2 + Z''^2 = R^2/4 \ldots\ldots\ldots (40)$$

5.3. Electrical conductivity through Impedance studies:

Fig.5, shows the impedance (Z'' verses Z') plots of all the different former compositions of SAT samples [5]. The bulk resistance for each composition of the SAT glass was obtained from the intercept of the each inclined straight line on the real axis. Bulk conductivity of all glasses was calculated using bulk resistance, obtained from impedance analysis, and sample dimensions. The conductivity verses former compositions of plot for SAT glasses is shown in Fig.6 and the highest conducting composition of the system fixed from log σ verses former composition plot.

Fig.7, shows the impedance (Z'' verses Z') plots obtained at different temperatures for highest conducting former composition of SAT sample. Bulk conductivity was calculated by analyzing impedance plots obtained at different temperatures. Fig. 8, shows the log (σT) vs. $10^3/T$ plots for all SAT glasses and were fitted to the Arrhenius equation

$$\sigma = \sigma_0 \exp (-E_a/K_T) \ldots\ldots\ldots \quad (41)$$

where, σ_0 is the pre-exponential factor, E_a is the activation energy, k is the Boltzman constant and T is the absolute temperature. The activation energy was estimated from the slope of log (σT) vs. 10^3/T plots. Fig. 6, also shows the activation energy vs. former compositions of the SAT glasses. From Fig. 6, it is found that the highest conducting former composition shows the lowest activation energy in the SAT glass.

5.3.1. Low Temperature Studies

Fig 9(a-d) show the imaginary (Z″) versus real (Z′) parts of complex impedance plots for the high conducting former composition of x = 0.5 for SAT glass measured at low temperatures (104 -180 K). The various types of open symbols and '∗' respectively show respectively the measured and the fitted impedance data of the SAT glass. From Fig. 9a and b, within the measured frequency window, the inclined straight line is found to disappear and the formation of complete depressed semicircle is observed with decrease in temperature. On further decrease in temperature, the partially formed semicircle are observed as shown in Fig. 9 (c & d). The depressed semicircle corresponds to the parallel combination of bulk resistance and constant phase elements (CPE) [4] in series with another CPE, from the inclined straight line, assigned to the double layer capacitance, for SAT glass. The equivalent circuit is shown in inset of Fig. 9a. Bulk conductivity σ is calculated using pellet dimensions and bulk resistance (R_b) obtained from the analyzed impedance data, measured at low temperatures, for the high conducting former composition of x = 0.5 for SAT glass. The temperature dependent of d.c conductivity for SAT glass is fitted to Arrhenius equation. Fig. 10, shows the plot of log σT vs. 1000/T for the high conducting former composition of x = 0.5 for SAT glass in the temperature range of 104 -180 K, where symbols represent measured conductivity data and the line represents Arrhenius fit. From the slopes of log (σT) vs. 1000/T plot, the activation energy (E_a) for Ag^+ ion migration is calculated and it is found to be 0.27 eV for SAT glass.

6. TRANSPORT NUMBER:

6.1. Electronic conductivity: D. C. Wagner polarization method

Under steady state condition, the total current due to non-ionic (I $_{(non-ionic)}$) passing through the cell is given by

I $_{(non-ionic)}$ = I_e (electrons) + I_e (holes)

I $_{(non-ionic)}$ = (RTa/lF) [σ_e {1- exp (-EF/RT)} + σ_h { exp (EF/RT) -1}]……… (42)

where, a is area of cross section, l is thickness of sample, E is applied potential, R is gas constant, F is Faraday constant, T is absolute temperature, σ_e and σ_h are the conductivities respectively due to electronic and holes. The type of non-ionic current due to electrons or holes can be obtained from the shape of the current vs. voltage plots. If the

non-ionic current is due to electrons, from eq(44), the expression for non-ionic current ($\approx I_e$) is given by [1]

$$I_{\text{(non-ionic)}} \approx I_e \approx (RTa/lF)\ \sigma_e\ [1\text{-exp}\ (\text{-EF/RT})] \ldots\ldots\ldots \quad (43)$$

If the non-ionic current is due to holes, from eq(44), the expression for non-ionic current ($\approx I_h$) is given by [1]

$$I_{\text{(non-ionic)}} \approx I_h \approx (RTa/lF)\ \sigma_h\ [\text{exp}\ (\text{EF/RT})\ \text{-1}] \ldots\ldots\ldots (44)$$

According to eq (42) to eq(44), the type non-ionic current, is due to electrons or holes, can be obtained from the shape of the current verses voltage plots.

Using the circuit shown in Fig 11, the steady state current as a function of voltage can be measured for a given material. If the plot of current vs. voltage indicates that the non-ionic current is due to electrons and hence, the expression for electronic current (I_e) is given by eq (43). The non-ionic conductivity due to electrons (σ_e) can be calculated from the slope of the measured I_e (the non-ionic current is due to electrons) verses [1-exp (-EF/RT)] plot. Similarly, the non-ionic conductivity due to holes (σ_h) can be calculated. Hence, Transport numbers due to ionic (t_i) and also due to electronic (t_e) can be calculated using eq(1) and eq(2). Similarly, transport numbers due to ionic (t_i) and also due to electronic (t_e) can be calculated by measuring the resultant current as a function of time under d.c potential using mobility method and also by measuring cell potential using electrochemical potential method. [Electronic (t_e) or Ionic (t_i) transport number is: $t_{x\ (e\ or\ i)} = i_{x\ (e\ or\ i)}\ /\ i_t$, Where, i_t is the total current, i_i is the ionic current and i_e is the electronic current (i_e); ($i_t = i_i + i_e$) and $t_i = V/\ V_0$ Where, V is the emf developed across the cell and V_0 is the theoretical emf].

REFERENCES:

[1]. Suresh Chandra, "Super ionic Solids: Principles and applications", North –Holland Publishing Company, Amsterdam (1981)
[2]. L. L. Hench. J. K. West, 'Principles and Electronic Ceramics', John Wiley Sons, Inc. Singapore. (1990)

[3]. A. Hooper, "Application of a.c measurement and analysis techniques to materials research", AERE- R9757, (1980)
[4]. Ross Macdonald, (ed.) 'Impedance Spectroscopy', John Wiley &Sons, New York, (1987)
[5]. S. Jayaseelan's Ph.D. thesis, Pondicherry University, Puducherry, INDIA, (2005)
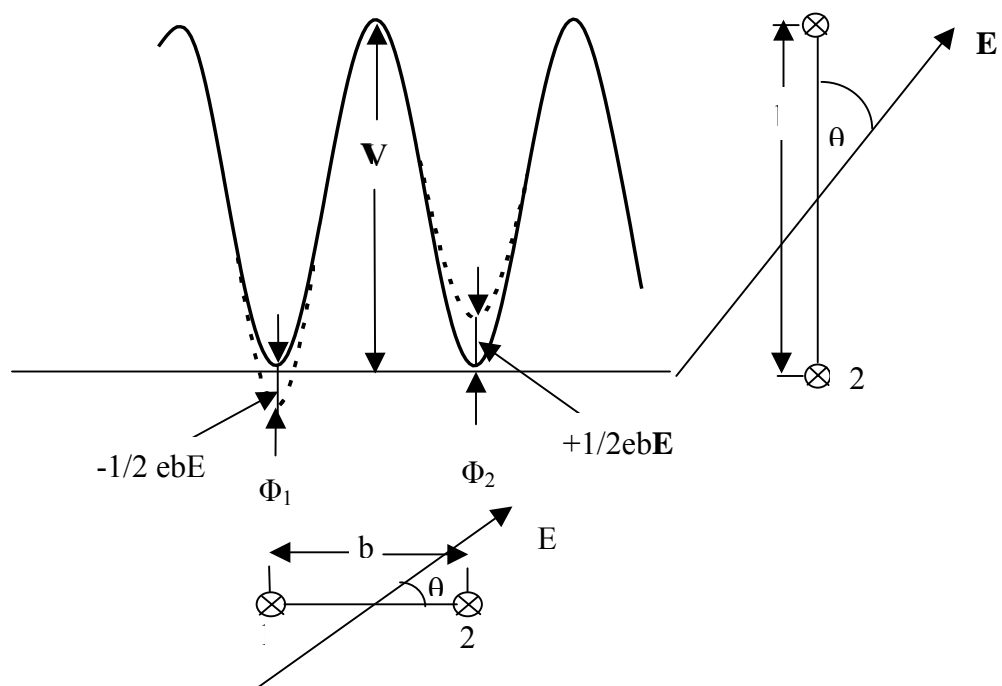
Fig. 1. potential well configuration
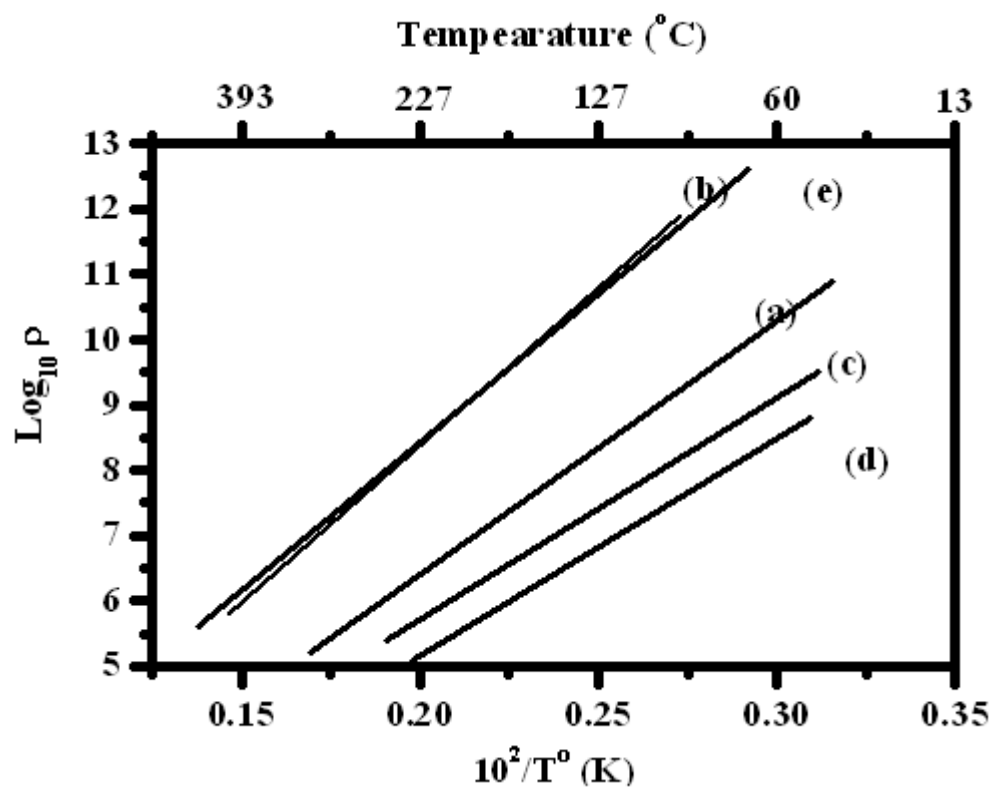
Fig. 2. Resistivity of some ionic glasses
a) $18Na_2O . 10CaO . 72SiO_2$ b) $10Na_2O . 20CaO . 70SiO_2$
c) $12Na_2O . 88SiO_2$, d) $24Na_2O . 76SiO_2$
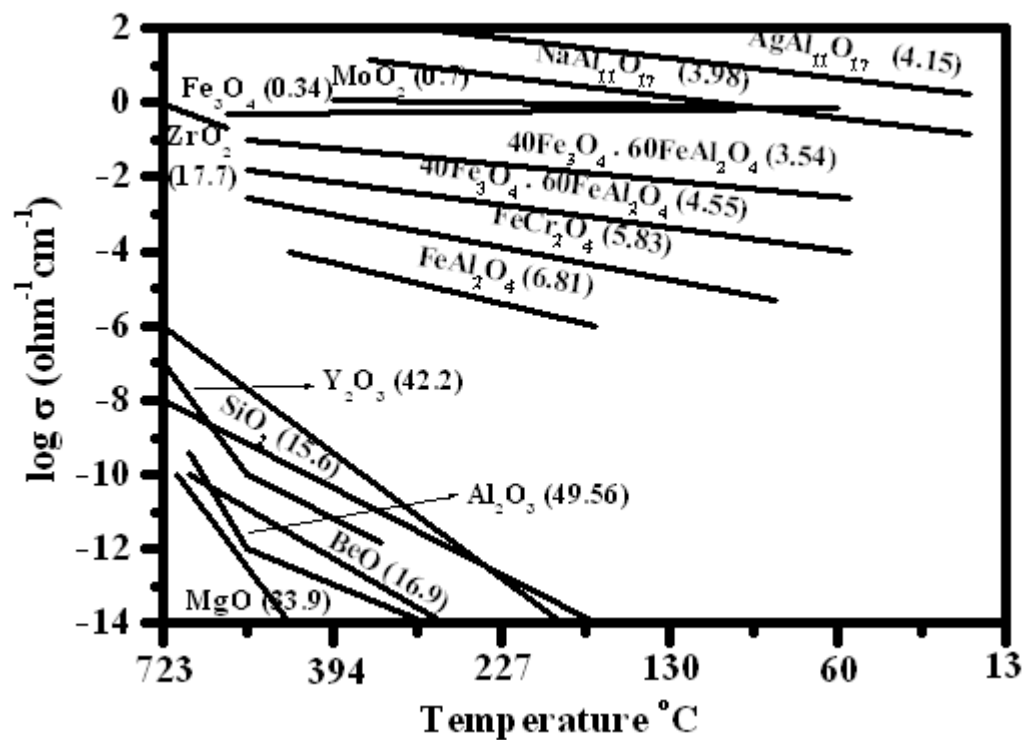
Fig.3.Temperature dependence of conductivity for various oxides
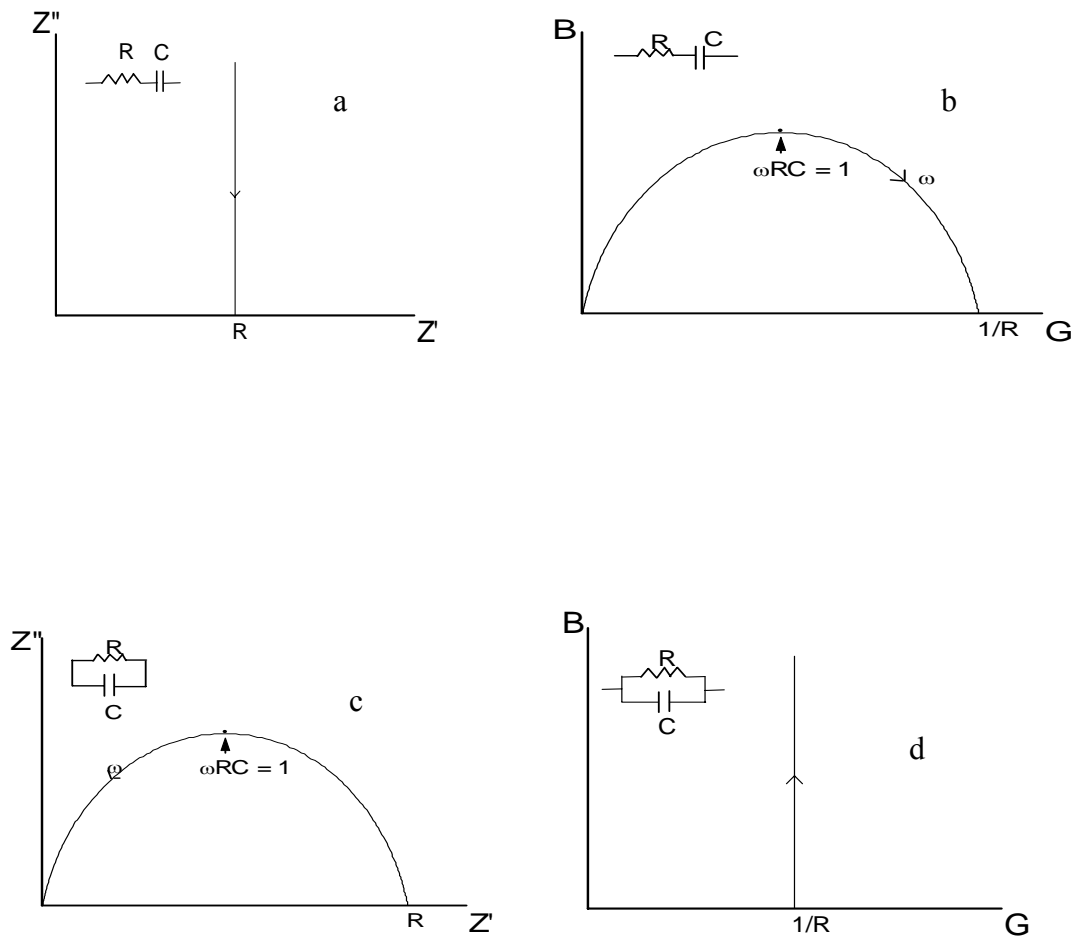
Fig.4.a) $Z^{''}$ Vs. $Z^{'}$ & b) B Vs G for series and c) $Z^{''}$ Vs. $Z^{'}$ &
d) B Vs G for parallel combinations of RC Circuits

Fig.6. Log(σ) and E_a verses former compositions of plots for SAT glasses
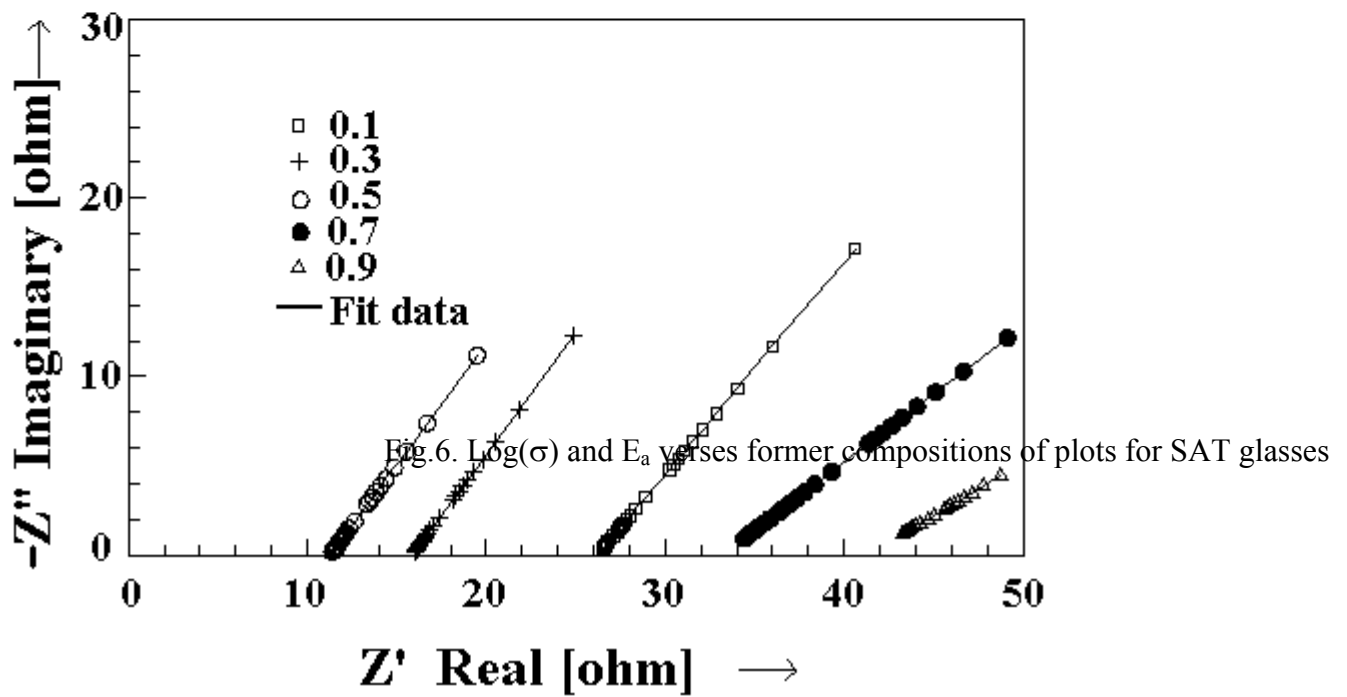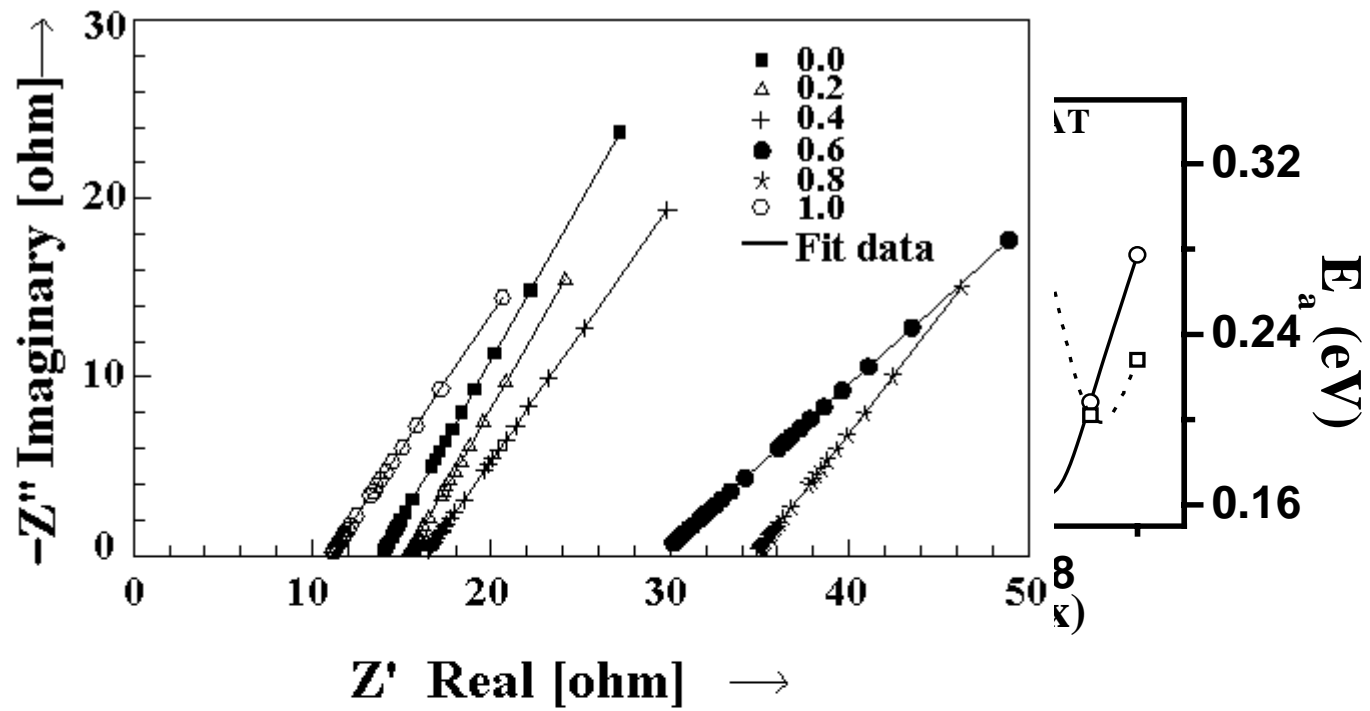
Fig.5. Impedance (Z" verses Z') plots of different former compositions of SAT samples
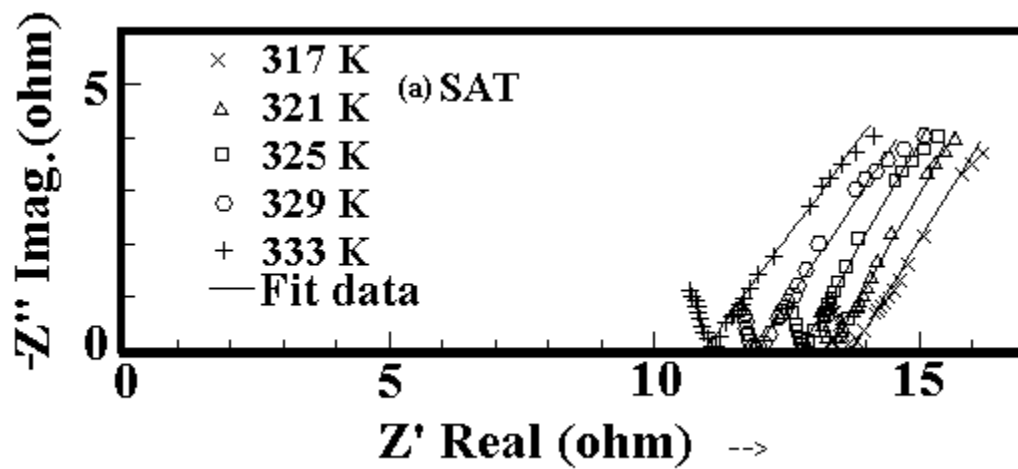
Fig.7. Impedance (Z" verses Z') plots obtained at different temperatures for highest conducting former composition of SAT sample
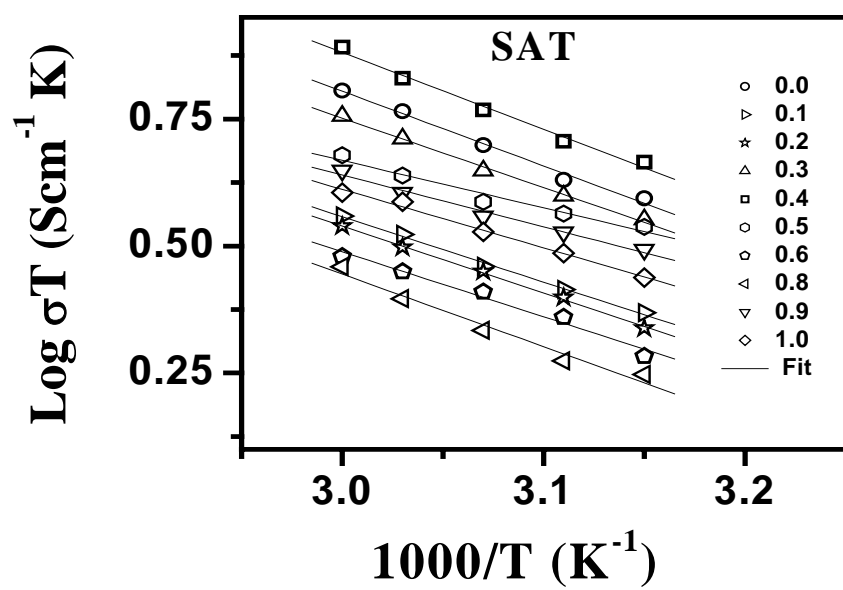
Fig. 8. log (σT) vs. 10^3/T plots for all formers compositions of SAT glasses
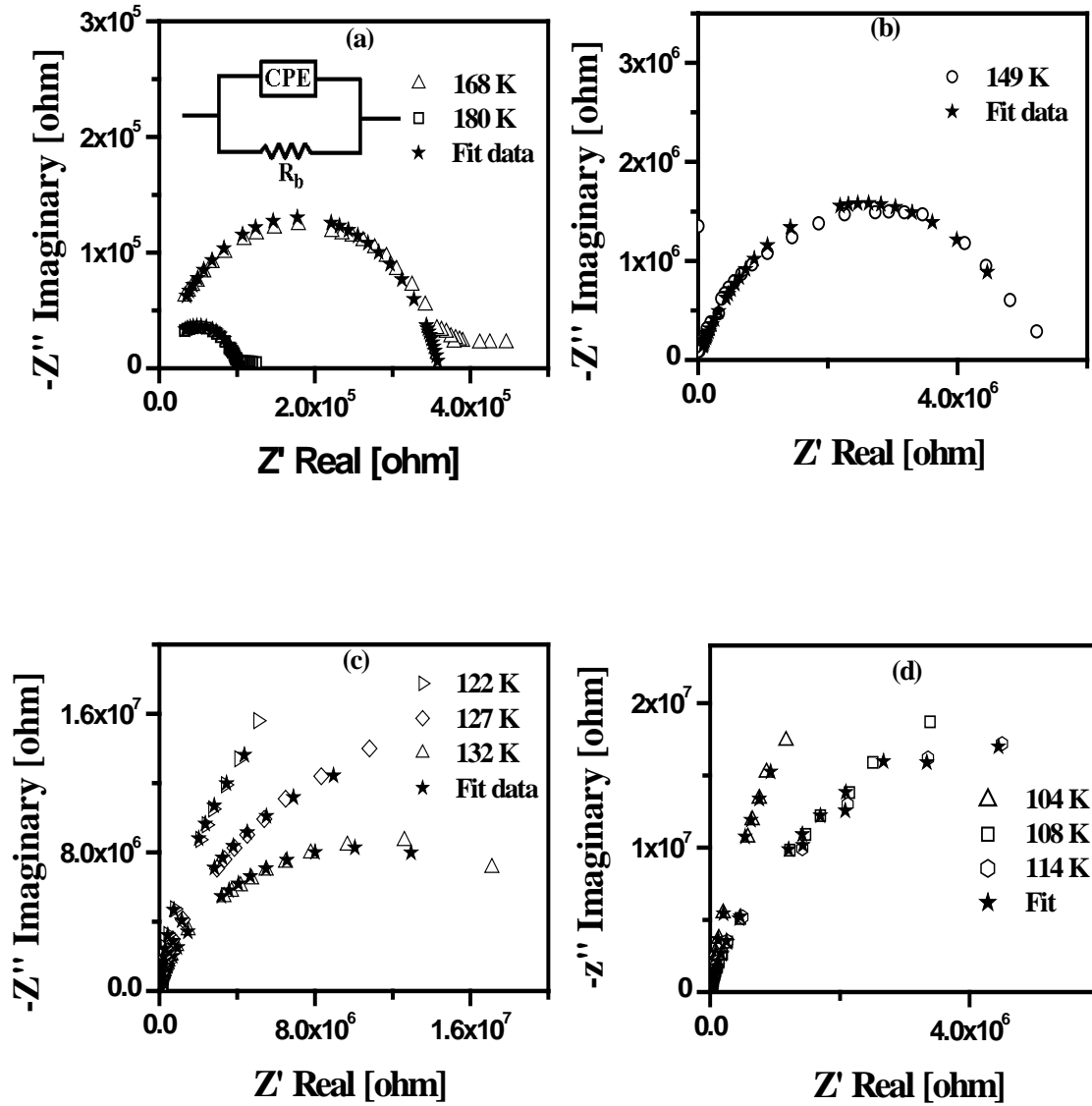
Fig 9(a-d). Imaginary (Z″) versus real (Z′) parts of complex impedance plots for the high conducting former composition of x = 0.5 for SAT glass measured at low temperatures (104 -180 K).
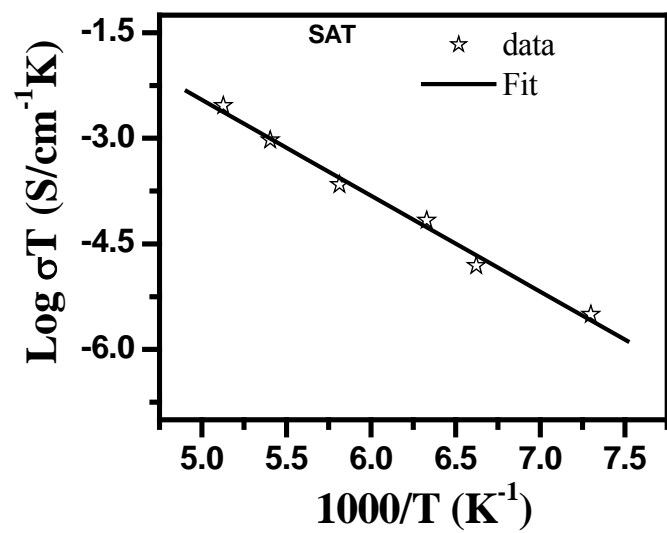
Fig. 10. Plot of log σT vs. 1000/T for the high conducting former composition of x = 0.5 for SAT glass in the temperature range of 104 -180 K
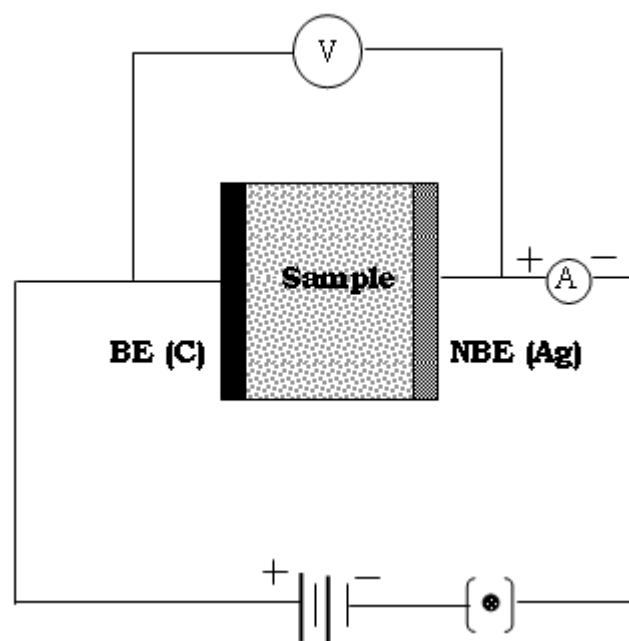
Fig. 11. Schematic diagram for D. C. Wagner polarization method

Thermal Conductivity measurment Techniques

M. V. Krishnaiah,
Liquid Metals and Structural Chemistry Division, Chemistry Group, IGCAR Kalpakkam.

Sri. M.V.Krishnaiah, is an M.Sc., from S.V. University. He is from 22nd batch of training school. He worked in the field of thermo physical properties for the last 20 years. He is responsible for the setting up of the laser flash thermal diffusivity measurement system in his laboratory. Using this system, thermal diffusivity of (U,Pu) O_2 , (U,Pu)C, (U,Pu)N was measured.

Introduction:

Heat is a form of energy, which mankind has known for a very long time. This particular form of energy is the most widely used. Normally flow of any form of energy is associated with the difference in potential (height for mechanical, voltage for electrical ..). In the case of heat it is the temperature, which is responsible for the flow of heat energy.

It is known that heat energy is exchanged with the surroundings in 3 modes, conduction, convection and radiation. Conduction process is observed in solids, where as convection is normally observed in liquids and gases, where movement of medium is observed due to density variation associated with the temperature of the medium The other mode of transmission is radiation. This mode of heat transfer is significant only at high temperatures.

Conduction of heat:-

It is defined as the quantity of heat, ΔQ, transmitted during time Δt through a thickness L, in a direction normal to a surface of area A, due to a temperature difference ΔT, under steady state conditions and when the heat transfer is dependent only on the temperature gradient.

thermal conductivity = heat flow rate × distance / (area × temperature difference)

$$K = \frac{\Delta Q}{\Delta t} \, x \, \frac{L}{A \Delta Tt} \qquad \text{-----------(1)}$$

Alternately, it can be thought of as a flux of heat (energy per unit area per unit time) divided by a temperature gradient (temperature difference per unit length)

$$K = \frac{\Delta Q}{A \Delta T} \, x \, \frac{L}{\Delta t} \qquad \text{------------(2)}$$

This is the general for of the Fourier equation, and the minus sign arises from the fact that heat always flows from the hottest to the colder region.

units are SI units -- W/(m·K) and in British units, Btu·ft/(h·ft²·°F). To convert between the two[1], use

the relation 1 Btu·ft/(h·ft²·°F) = 1.730735 W/(m·K).

In metals thermal conductivity approximately follows electrical conductivity according to the Wiedemann-Franz law, as freely moving electrons are responsible for both the types of conduction. However such correlation always does not exist for materials, where the conduction is due to phonons, (quantized lattice vibrations). Examples for materials where the conduction is due to phonons are ceramics, diamond, etc.,

Normally, for isotropic solids, the K is independent of direction. For materials which are ansiotropic, like alumina, graphite and the like, this property depends on the direction of heat flow in the medium. Diamond-- (Isotropoc), Sapphire(Anisotropic) ,Graphite (Anisotropic).

From the conservation of energy, and from the first principles, the continuity equation can be derived having the form

------ (3)

$$k \nabla^2 T \quad = \quad \frac{dT}{dt}$$

where k is known as thermal diffusivity. Depending on the sample geometry, the above equation can be solved for one dimensional samples, two dimensional sample, and so on.

$$k = \frac{\lambda}{C_p \, \rho} ,$$

------(4)

Where K or λ is thermal conductivity, C_p is specific heat ,and ρ is the density.

Based on the solutions to the equation (3), we have two types of measurements
Steady State methods and transient methods.

Steady state methods are based on solutions $\frac{dT}{dt} = 0,$ and the transient methods are based on

$\frac{dT}{dt} \neq 0 \ or \ f(t).$

In the present talk some of the methods for measurement of thermal conductivity / diffusivity will be discussed

2.0   Experimental methods:-

2.1   Steady state methods.

Among the steady state methods, most widely used are, axial heat flow method, comparator method, guareded hot plate method and the radial heat flow method.

2.1.1   Axial method

The method of measurement based on the one dimensional equation is the simplest of all the methods.

And is known as linear axial heat flow method. Typical experimental set up is shown in fig. 1..
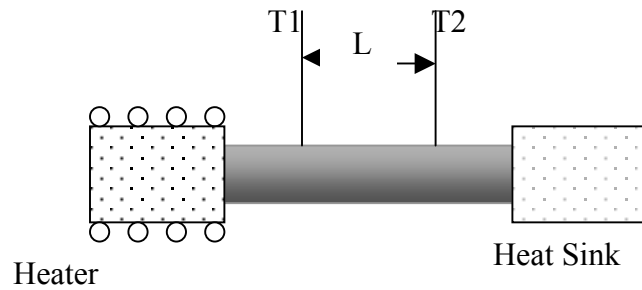
Fig. 1 Axial heat flow method Schematic

$$\lambda = \frac{\phi}{A}\frac{dL}{dT}$$

------(5)

if one knows the L , the heater power, and the steady state temperature, one can evaluate the thermal conductivity. This type of measurements are known as steady state measurements.

$$\lambda = \frac{\phi}{A}\frac{dL}{dT} = \frac{\phi}{A}\frac{L}{\Delta T} = \frac{\phi}{A}\frac{L}{(T_1 - T_2)}$$

- - - - -(6)

This assumes that the heat losses from the periphery of the sample and along the temperature sensors are negligible. In order to ensure that the heat flow is linear between the thermometers, they should not be closer to the heater or the heat sink than a length equal to the sample diameter.

2.1.2   Comparator method. (ASTM E1225 Test Method).

Another variant of the linear heat flow method is comparative method. It is not always possible
 to obtain samples sufficiently long for the guarded system, particularly when studying single crystals of new materials. Measurements can be made on samples with smaller L/A ratio by making a composite bar consisting of the disc under test sandwiched between two discs of a material of known conductivity, similar in magnitude to that of the test material. The temperature gradient in the unknown disc and in the two standards is then measured. This method has the advantage that one need not know the exact ϕ value to evaluate the thermal conductivity λ of the specimen. This method has the disadvantage, that it assumes that there is no thermal resistance between the contacts. Using this method, Mirkovich (1965) measured thermal conductivity of ceramics. Laubitz (1969) has briefly analyzed some of its defects. This method needs little instrumentation and is suitable for measurements on discs a few millimeters thick. The presence of a standard on either side of the unknown sample helps in controlling heat losses. This method can yield good results especially when the thermal conductivities of the sample and the standard material are in close to each other.
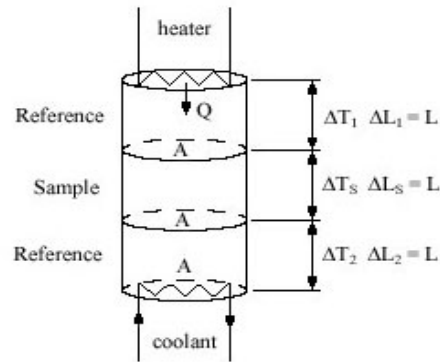
Fig. 2 Comparator method Schematic

$$\frac{Q}{A} = K_S \frac{\Delta T_S}{L} = K_R \frac{\Delta T_1 + \Delta T_2}{2} \frac{1}{L}$$

The main assumption is that heat flows from reference into the sample,and the heat out to the sample to the reference is assumed to be same. Based on the assumption the Q is eliminated from the equation. Only the sample thickness and reference thicknesses need to be known, for the thermal conductivity of the sample to be evaluated.which can be measured with reasonable accuracy.

Though this method is yields reasonably accurate results, the heat flow through lateral surfaces of the sample and references will be significant at higher temperataures. Hence this method was modified to include corrections for the lateral heat heat transfer by a method known as guarded hot plate method.

2.1.3   Guarded Hot plate method:

Specifications for this method are given in BS874(1965) and ASTM C177(1963) and the principle is illustrated in figure 3. The apparatus consists of two similar samples sandwiched between heat sinks and separated by a transverse heater. This heater has a central section separated from an annular guard by a small gap. The whole assembly surrounded by material of low conductivity. The two sections of the heater are supplied from independent stabilized power supplies, which are adjusted until the temperature of the guard, and the central section is the same, there by eliminating radial heat losses from the central heater. The thermal conductivity is then found from equation where ϕ is the power supplied to the central heater, A is the cross-sectional area of the heater plus half that of the gap, L is the total thickness of the two samples and (T_1-T_2) is the temperature difference across each sample.
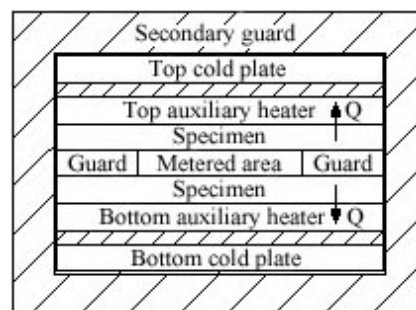
3. Guarded hot plate method Schematic

At higher temperatures, heated plates are inserted between the heat sinks and the samples. In order to maintain axial flow over the measured area through the samples, these must not be too thick and the guard must be sufficiently wide. A ratio of diameter of the central heater to sample thickness of about three was recommended by the British Standard. Analysis of edge losses by Woodside(1957) indicates that this value is too small and that the ASTM requirement of a limiting ratio of 1.5 or more realistic if an accuracy of 1% is to be achieved. For measurements above room temperature the gap between the central and guard sections of the heater should be filled with loose insulation and an additional cylindrical guard heater must be provided in order to control the edge temperature conditions.

2.1.4   Radial Heat flow method.

The radial heat flow methods are for measuring λ directly and are suited for higher temperatures since the longitudinal methods are well suited for measurements at low temperatures. In radial heat flow method, the flow of heat is radial and, in accordance with equation, grad T represents the temperature gradient along the normal to the isothermal surface. The most common geometry used consists of a right circular cylindrical sample with the heat source along the axis, as shown in figure 4.. If its length is sufficient to be assumed to infinite, then the solution to the Fourier equation is

$$\frac{\phi}{L} = \frac{2\pi\lambda(T_1 - T_2)}{\ln\left(r_2 / r_1\right)}$$

Where ϕ/L is the heat flow per unit time per unit sample length, and T_1, T_2 are the temperatures at radii r_1 and r_2 respectively. An optimum of L/d ratio of 12 is used by Kingery (1954)[2]. in measurements on alumina . Measurements up to 2600^0C have been achieved by this technique with an apparatus designed by Rasor and McClelland (1960).[3] .The heat flow was radially inward and was measured by a water calorimeter on the specimen axis.
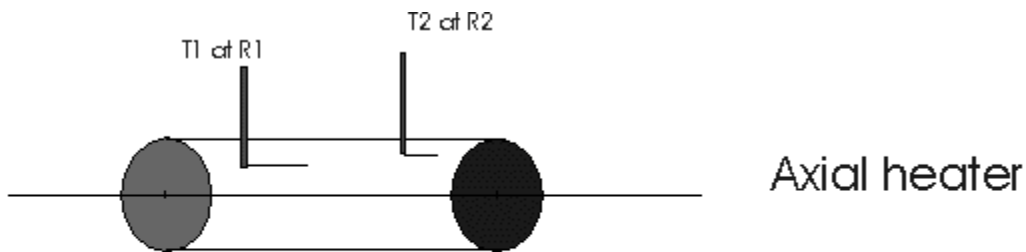
Fig. 4. Radial heat flow method arrangement.

Most of the steady state methods need reasonably large samples, and unusually long recording times, to achieve stability of the temperature. It is normally difficult to maintain the ambient at a constant temperature for such long times. This gives scope for expermental errors to creep in to the measurements very easily. To overcome the difficulties associated with steady state methods, transient

methods were developed.

2.2 Transient methods.

In transient methods, we monitor the temperature as a function time, and derive thermal diffusivity.

The thermal diffusivity, κ, of a medium is the thermophysical property that determines the speed of heat propagation by conduction during changes of temperature with time. The higher the thermal diffusivity, the faster the heat propagation. The thermal diffusivity is related to the thermal conductivity λ, specific heat C_p and density ρ as follows. All the transient methods yied thermal diffusivity. These

methods are based on the solution to the equation (3), where $\dfrac{dT}{dt} \neq 0 \ or \ f(t)$

all these techniques give us thermal diffusivity.

Amonng transient methods, Hotwire/linear Heat source method, modulated electron beam method, and laser flash method are the most popular

2.2.1 Hotwire method or Linear Heat Source Method.

The **hot wire method** is a standard transient dynamic technique based on the measurement of the temperature rise in a defined distance from a linear heat source (hot wire) embedded in the test material. If the heat source is assumed to have a constant and uniform output along the length of test sample, the thermal conductivity can be derived directly from the resulting change in the temperature over a known time interval [4]. The **hot wire probe method** utilizes the principle of the transient hot wire method. Here the heating wire as well as the temperature sensor (thermocouple) is encapsulated in a probe that electrically insulates the hot wire and the temperature sensor from the test material [5].

The ideal mathematical model of the method is based on the assumption that the hot wire is an ideal, infinite thin and long line heat source, which is in an infinite surrounding from homogeneous and isotropic material with constant initial temperature. If q is the constant quantity of heat production per unit time and per unit length of the heating wire (W.m^{-1}), initiated at the time t=0, the radial heat flow around the wire occurs. Then the temperature rise $\Delta T(r,t)$ at radial position r (see Fig. 5) from the heat source conforms to the simplified formula

$$\Delta T(r,t) = \frac{q}{4\pi k} \, x \ln\left[\frac{4\,a\,t}{r^2} \, C \right] \qquad\qquad \dots 5$$

where k is the thermal conductivity (W.m^{-1}.K^{-1}), a thermal diffusivity (m^2.s^{-1}) ($a=k/\rho c_p$, with ρ is the density (kg.m^{-3}) and c_p the heat capacity (J.kg^{-1}.K^{-1}) of the test material and C=exp(γ), γ=0,5772157 is the Euler's constant.
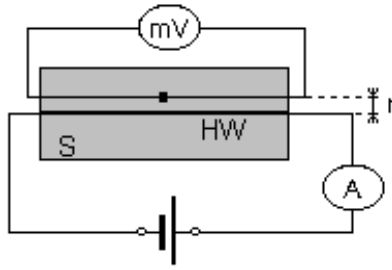
Fig. 5 Hotwire method arrangement

The equation (5) is valid only when $r^2/4at<<1$ is fulfilled, i.e. for a sufficiently long time t larger than certain minimum time t_{min} and for a small distance r. Thus the measurement of temperature rise $\Delta T(r,t)$ as a function of time is be employed to determine of the thermal conductivity k, calculating of the slope K of the linear portion of temperature rise $\Delta T(r,t)$ vs. natural logarithm of the time ($\ln t$) evolution from

The hot wire temperature rise reaches usually up to 10ºC and its time evolution has typically the form as shown in the Fig. 6.
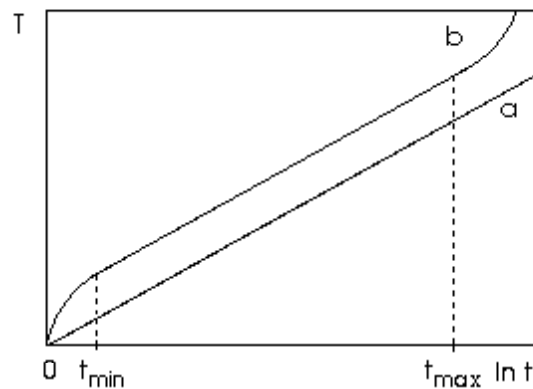
Fig. 6 Typical temperature rise curve (a - ideal, b – non-ideal case)

The hot wire method can be applied in several experimental modifications. In the **standard cross technique** the wire cross is embedded in ground grooves between two equally sized specimens. The cross consists of a heating wire and the legs of a thermocouple, which acts as the temperature sensor. The hot spot of the thermocouple is in direct contact with the heating wire. In the **resistance technique** the heating wire acts also as the temperature sensor. Here the temperature is measured by the change in resistance caused by the heating-up of the hot wire. In the measurement of electrically conducting materials the heating wire and thermocouple wires, or potential leads, are insulated from the sample. This is done either by making of a non-conducting coating on the wires, or to enclose the heater and temperature sensor in a thin sheath or needle probe, which is inserted into the test material, respectively. The second approach is called as the **hot-wire-probe** method.

Measurement:

Three measuring techniques are there available: standard cross wire technique, resistance - potential lead method, that is based on the four point principle and the probe modification of the hot wire method. In the cross wire technique the platinum (Heraeus) or kanthal (Bulten Kanthal AB) wires, with various diameter (0,1 – 0,4 mm), depending on the measured material and the measurement temperature act as the linear heat source. The temperature rise vs. time evolution is measured by the spot welded K type thermocouple, made from Ni-NiCr wires (Heraeus), or S type – Pt/PtRh 90/10% (Heraeus). The hot spot of the thermocouple is in direct contact with the heating wire and is placed in the center of sample. The reference junction is immersed in the Dewar cup at 0°C. In the resistance technique the platinum wire acts as the heating wire as well as the temperature sensor. Potential leads consist of thin platinum wires, fixed to the heating wire at about 1,5 cm from the end of the sample. The probe method uses home-made cylindrical probe original construction, consisting of the heating wire and the temperature sensor, both placed in the ceramic microcapilary (Degussa).

The apparatus currently allows performing *in-situ* measurements of solid materials in the temperature range 20 – 1200 ºC. Details concerning the apparatus can be found in [6]
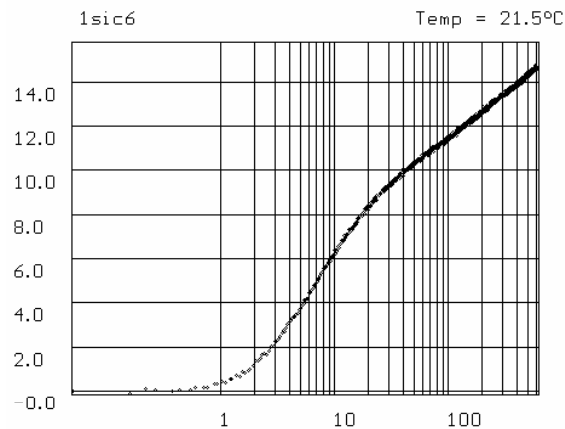
Fig. 7 Typical experimental temperature rise vs. time evolution

Sample dimensions.

The solid samples consist either of two cuboids, or of two cylinder halves, respectively. They dimensions are up to 100x100x50 mm or the cylinder should be up to 10 mm in diameter with length 100 mm, all depending on the thermal diffusivity of the measured material.

The sand, powder and granular materials are usually put into cube container of 100x100x100 mm.

2.2.3   Modulated Electron beam method.

The electron beam is amplitude modulated to vary sinusoidally with time and the phase difference between the resulting temperature fluctuations of the two faces of the slab yields the thermal diffusivity of the sample. [7]

$$\Delta\theta = \frac{2.9l^2\,\omega}{2\pi\,k}$$

where l is the thickness of the sample ω is the frequency, k is thermal diffusivity, $\Delta\theta$ is the shift in the phase of the electron beam to that of the temperature at the rear surface.

2.2.4   Laser Flash Method.

The most popular method used for measuring thermal diffusivity is the flash method and was developed by Parker etal [8]. It has the advantage of being fast while providing values with excellent accuracy and reproducibility. After the sample has been stabilized at a desired temperature T0, a nearly instantaneous pulse of energy (usually laser or other discharge source) is deposited on its front face, and the temperature increase DT(t) on the rear face of the sample is recorded as a function of time (Fig. 8). The thermal diffusivity is then determined from this thermogram.
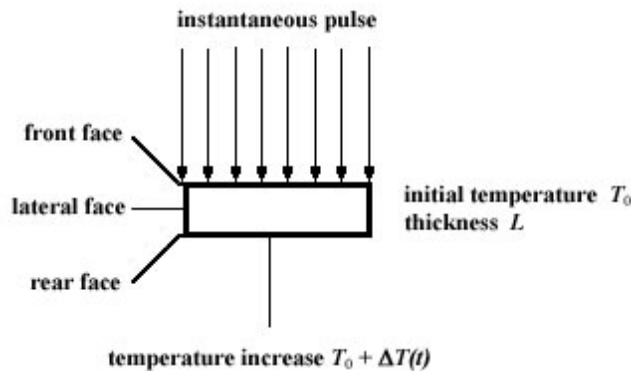
Figure 8: Schematic of the flash method

The characteristic shapes of the temperature increase curves are depicted in Fig. 9. If no heat loss is involved, the temperature of the rear face will rise to a maximum and remain at that level indefinitely (curve A). However, with increasing heat losses, the temperature on the rear face decreases after reaching a maximal value (curves B and C).

Figure 9 : Temperature increase for various experimental conditions
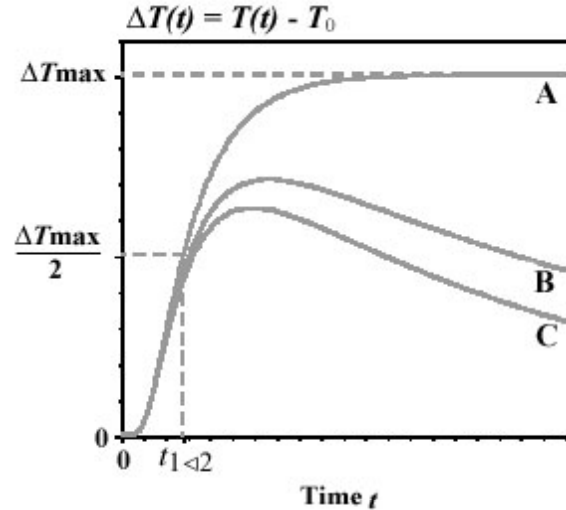
The original method proposed by PARKER assumes an isotropic and adiabatic sample (no heat loss). The thermal diffusivity is determined from the thickness, L, of the sample and the time, $t^{1/2}$, the thermogram takes to reach half of the maximal temperature increase:

$$\alpha = 0.1388\, x \frac{L^2}{t_{1/2}}$$

The factor 0.1388 is corrected based on the heat losses from the surfaces. (9)

Since this method assumes ideal conditions of adiabatic sample and instantaneous pulse heating, it is somewhat limited in applicability. To make it more suitable to experimental conditions, other methods have been introduced over the years, which account for heat losses, finite pulse duration, non-uniform pulse heating, and composite (non-homogeneous) structures.

Major advantages of the method are:

- it requires a very small sample, usually 12 mm diameter and few millimeters thick;
- it is very fast, the actual measurement takes few seconds;
- the same instrument can be made to test a very broad range of thermal diffusivities (10^{-3} to 10 cm²/s), while usual thermal conductivity test instruments barely cover 10:1 ratio range;
- it can be used, with proper precautions, to also measure other thermophysical properties (specific heat, thermal conductivity, etc.)

it can be used to test samples up to much higher temperatures than steady state methods, even through the melt in some cases.

Major disadvantages of the flash method are that:

- the equipment is usually expensive due to the heat pulse generation, the optical detection and the high speed data acquisition;
- porous and non-homogeneous materials require special care to properly process the thermogram.

3.0   References

[1].   Perry's Chemical Engineers' Handbook, 7th Edition, Table 1-4

[2].   Kingery, W.D., 1954, *J. Am. Ceramic. Soc.,* 37, 88

[3].   Rasor,N.S., McClelland, J.D., 1960, *Rev. Sci. Instrum.*, 31, p 595

[4]. Davis W R, Hot-Wire Method for the Measurement of the Thermal Conductivity of Refractory Materials, in Maglić K D, Cezairliyan A, Peletsky V E, (Eds.) *Compendium of Thermophysical Property Measurement Methods*, Vol. 1 *Survey of Measurement Techniques,* 1984, New York, London, Plenum Press, p. 161

[5]. Wechsler A E, The Probe Method for Measurement of Thermal Conductivity in Maglić K D, Cezairliyan A, Peletsky V E, (Eds.) *Compendium of Thermophysical Property Measurement Methods*, Vol. 2 *Recommended Measurement Techniques and Practices, 1992, New York, London, Plenum Press, p. 281*

[6] Vozár L, A Computer-Controlled Apparatus for Thermal Conductivity Measurement by the Transient Hot Wire Method, 1996, *Journal of Thermal Analysis*, **46**, 495-505

[7] M. J. WHEELE R, Thermal diffusivity at incandescent temperatures by a modulated electron beam technique, in BRIT. J. APPL. PHYS., 1965, VOL. 16.

[8]   Parker,W.J., Jenkins, R.J., Butler,C.P., Abbott, G.L., 1961, *J. Applied. Physics* ., 32, p1679.

[9] .Cowan, R.D (1963), *J. Applied Physics* , 34, p926.

Knudsen Effusion Mass Spectrometry

A Powerful Tool for Inorganic Gas Phase Analysis and Thermodynamic Studies

Dietmar Kobertz

Forschungszentrum Jülich, IEF, 52459 Jülich, Germany

Abstract

"Look into my vapor phase and you will know what I am" could be a modified version of a famos proverb. The knowledge of the vaporization behaviour is an important property in materials research either under kinetic or under equilibrium conditions. Kinetic orientated vaporization is strongly dependent on material conditions like surface structure, atmosphere sorroundings et. al. while vaporization in equilibrium conditions really allows to describe the material at different states. Only in equilibrium it is possible to see the difference between a start-state and an end-state on changing the energy situation in a system and that the way to go from one to the other state is arbitrary; that is exactly the characteristic of a state-function in thermodynamics.

On the way to obtain these information, one needs a tool that allows to produce an equilibrium state of the material with its sorrounding, to change the energy state of this system from one state to another, and one must have a possibility to analyse all the given species in the vapor phase over this material. Excactly these specifications can be fullfilled in a Knudsen Effusion Mass Spectrometer (KEMS)

This article describes the fundamentals of the method and gives examples of thermodynamic properties for the gaseous phase of its application. The materials considered are salts, alloys and graphitic materials that are of interest for metal halide lamps, superalloys, and nuclear reactors. More details will be given in the presentation.

Introduction

All materials show vaporization and under equilibrium conditions the gaseous species will define the thermodynamic state of the system. The chemical structures of these species can be different from that given in the condensed phase.

Mass spectrometry is the most versatile method for the analysis of such vapors because it enables the identification of the species present in the gaseous phase and the determination of their partial pressures. If the vapors are generated under equilibrium conditions, thermodynamic data can be evaluated from the partial pressures and the temperatures s. Refs. [1 – 9].

The mass spectrometric method used for the determination of thermodynamic data of high-temperature vapors is a so-called Knudsen effusion mass spectrometry (KEMS). This method offers the highest potential for equilibrium vaporization studies and is used whenever it is possible. By use of this technique numerous gaseous halides, oxides, carbides, hydroxides, and metallic and intermetallic molecules, have been identified for the first time.

The inherent limitation of the method is the restriction of the upper Knudsen condition that is given by the maximum total pressure in the Knudsen cell of about 10 Pa. Further limits lie in the Knudsen cell material at high temperatures and its possible chemical interactions with the sample to be investigated (container problem). The maximum investigation temperatures are thereby practically between 2500 K and 3000 K.

Instrument

The principle setup of a KEMS is seen in Fig. 1. It consists of a single-focusing magnetic type sector-field mass spectrometer, an electron impact ion source, a Knudsen cell and a collector arrangement of multiplier and Faraday cup. A cryogenic pump filled with liquid nitrogen reduces the background in the ion source. Ion pumps generate the ultrahigh vacuum in the mass spectrometer; and a turbomolecular pump is used for the Knudsen cell chamber. This chamber can be separated from the mass seperator by a valve, a so-called shutter, that is further used as a beam suppressor.

A fast and precise mass adjustment is possible by the use of a Hall probe supported magnetic field controller and a mass programmer. The mass peak scan is done by sampling the accelerating voltage in a small range sufficient enough to cover some peak widths in the mass range of interest.
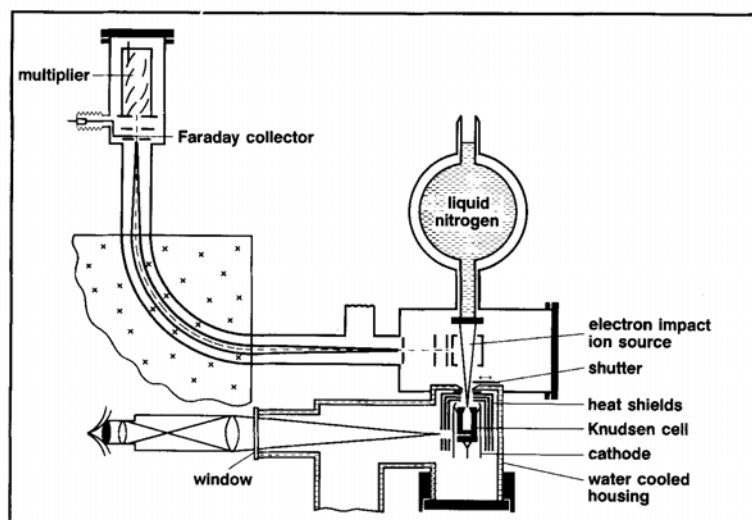
Figure 1. Schematic representation of the Knudsen cell-mass spectrometer system using a single-focusing magnetic type sector-field instrument.

The important part of the instrument is the Knudsen cell that is, for example, made of tungsten and contains the sample to be investigated (Fig. 2). It can be heated by heat radiation and electron bombardment and temperatures up to 3000 K can be reached. The temperature is measured either with an optical pyrometer or a thermocouple, respectively, depending on the temperature range of interest. For the set-up shown in Fig. 1, the pyrometer is sighted on the blackbody cavity laterally positioned, and close to and below the bottom of the cell.
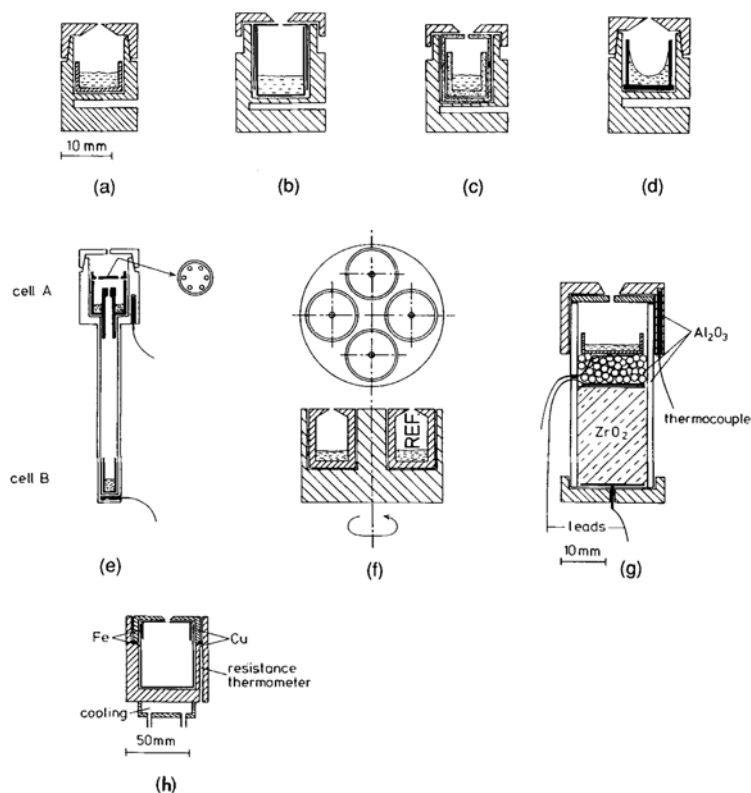
Figure 2. Standard Knudsen cell (a), with lining made of metal (b), and of ceramics (c). 'anti-creep' Knudsen cell (d), two-compartment cell (e), multiple cell (f), electrochemical Knudsen cell for oxygen injection from non-stoichiometric zirconia (g), and low-temperature Knudsen cell with cooling (h).

More details of the instruments are given in Refs [1] and [2] and will be given in the presentation. The mass spectrometer type used in our labs have been modified substantially by us with things like installing an ion counting arrangement or a computer controlled heating and mass scanning.

Principle of the method

Real thermodynamic equilibrium can only be fulfilled in a closed system. The Knudsen cell is a quasi closed system since it has a very small effusion orifice (typical diameter: 0.1-1 mm) through which a small fraction of molecules effuse practically without disturbing the equilibrium in the cell and since the mean-free path of the molecules is much longer than the dimension of the orifice. Fundamentals are given in Refs. [10 - 14].

A molecular beam representing the equilibrium vapour in the cell is formed by the effusing species. This molecular beam crosses the electron ionization source where ions are formed by electron impact in principle after equation (1)

$$A(g) + e^- = A(g)^+ + 2\ e^- \tag{1}$$

Different other impact reactions producing molecule ions and fragments of molecules will give helpful fingerprints to understand the gaseous phase. The ions are accelerated and than monoenergetically entering the mass analyser where they are separated by their mass to charge ratio (m/e). After separation the collectors register the ion and the obtained intensities are proportional to the quantity of atoms or molecules present in the vapor. From the ion intensities partial pressures can be determined with equation (2)

$$p(i) = k\ I(i)\ T \tag{2}$$

with k as an instrument constant, I(i) as ion intensity, T as absolute temperature

The equilibrium state of the system allows to formulate a constant related to the pressures (equ. (3))

$$K_p = \Pi\ [p(i)/p°]^{x(i)} \tag{3}$$

with p(i) is partial pressure of species *i*, p° is standard pressure, and x(i) is the stoichiometric coefficient of species *i*, that describes vaporization reactions such as:

A(s) λ A(g)   with the equilibrium constant $K_p = p(A)$ or

AB(s)λA(g) + B(s)   with $K_p = p(A)$
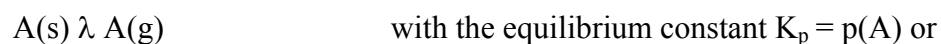
or the dissociation reaction:

$$AB(g) \lambda A(g) + B(g) \qquad \text{with } K_p = p(A) \, p(B)/p(AB)$$

or the dimerisation:

$$2A(g) \lambda A_2(g) \qquad \text{with } K_p = p(A_2)/(p(A))^2$$
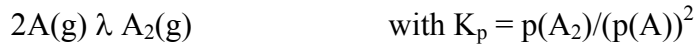
are often studied. Enthalpy and entropy changes of these reactions are determined, in accordance with second and third law methods, from the equations:

$$\Delta H°_{(T)} = - R \, d \, \ln K_{p(T)}/d(1/T) \qquad\qquad (3)$$

$$\Delta H°_{(298)} = -T \, [R \, \ln K_{p(T)} + \Delta \, (G°_{(T)} - H°_{(298)})/T] \qquad\qquad (4)$$

$$\Delta S°_{(T)} = \Delta H°_{(T)} /T + R \, T \, \ln K_{p(T)} \qquad\qquad (5)$$

Equation (3) is based on the Clausius-Clapeyron equation and its rearrangement leads to a linear form that can be used in an Arrhenius plot ($\ln Kp$ versus $1/T$) like shown in Fig. 3 to determine the reaction enthalpy in a small temperatur range (ΔT) as the slope ($- \Delta H°_{(T)}/R$) of the linear plot.

$$\Delta \ln Kp_{(T)} = - \Delta H°_{(T)}/R \, \Delta(1/T) \qquad\qquad (6)$$
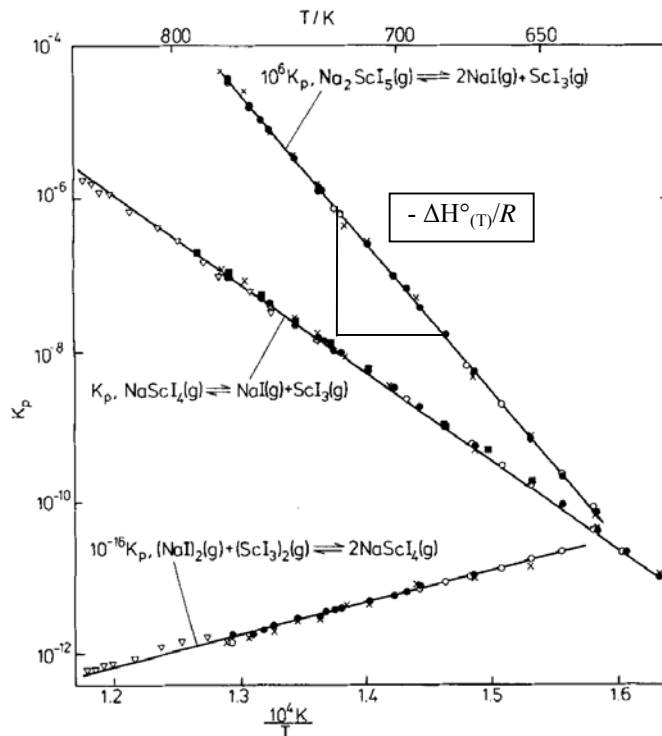
Figure 3. Temperature dependence of the equilibrium constant of selected reactions of the NaI – ScI$_3$ system

This way to obtain reaction enthalpies has the advantage that there is no need to calculate the absolut partial pressures after equation (3) and k can be neglected. The proportional factor k is taken always from calibration measurements with all its possible errors and the ionisation cross-section, also include in the faktor, is not always confirmed.

The Gibbs energy of reaction is obtained from the equilibrium constant according to the relationship:

$\Delta G°_{(T)} = -R\, T\, \ln K_{p(T)} = \Delta H°_{(T)} - T\, \Delta S°_{(T)}$ or to avoid the independently known $\Delta S°_{(T)}$

$$= \Delta H°_{(\Theta)} - T\, \Delta[(G°_{(T)} - H°_{(\Theta)})/T] \qquad\qquad (6)$$

$(G°_{(T)} - H_{(\Theta)})/T$ is the free energy function (fef) and Θ is the reference temperature normally 0 or 298.15 K depending on the data base.

Fundamentally, data treatment with the Second and Third Laws of Thermodynamics is equivalent, but the resulting error estimates may be quite different. Other important informations about the condensed phase in a system are the thermodynamic activity $a_{(i)}$ of its components and the chemical potentials $\mu_{(i)}$ related to these activities.

$$\mu_{(i)} = \mu°_{(i)} + R\, T\, \ln a_{(i)} = \mu°_{(i)} + R\, T\, \ln (p_{(i)}/p°_{(i)}) \qquad\qquad (7)$$

p(i) is the partial pressure of species i in a system and p°(i) the partial pressure of the same species over the pure compound. Different methods to obtain the activity $a_{(i)}$ like the monomer/dimer relation or heterogeneous reactions with one condensen phase or the Gibbs-Duhem integration can be used depending on the matchable measurement conditions. More about this in the presentation.

Applications

The following materials have been studied so far by high-temperature mass spectrometry in our laboratory for different applications (selected list):

1. Metal halides, predominantly iodides and their quasi-binary systems with their complex mass spectra for metal halide discharge lamps [15, 16, 17, 18].

2. Amalgam systems, e.g., Mg/Hg, Ca/Hg for fluorescent mercury lamps [19, 20, 21, 22].

3. Multicomponent Ni-base alloys for high-temperature applications [23, 24].

4. Alloys of the Al/Ni and AI/Ni/Hf system for materials developed on the basis of intermetallic phases [25].

5. Graphitic materials for the sorption of fission products Cs and Sr for the safety analysis of nuclear high-temperature gas-cooled reactors [26, 27].

6. Oxides, e.g., $CsA1Si_2O_6$ $CsAlSiO_4$, $BaZrO_3$ for nuclear technology [28, 29, 30].

7. B_2O_3/SiO_2 system for industrial glasses [31].

8. Oxide systems like lanthanum gallate, lanthanum chromates for Solid Oxid Fuel Cells (SOFC) [32, 33, 34].

Conlusion

The potential of the high-temperature mass spectrometric method is summarized as follows:

- Identification of the gaseous molecules forming the equilibrium vapour in the Knudsen cell.

- Determination of their partial pressures between 10 to 10^{-9} Pa and up to temperatures of 3000 K.

- Computation of thermodynamic functions from the measured partial pressure and their temperature dependences as, for example, enthalpies and entropies of vaporization, of dissociation, and of formation.

References

1. Hilpert, K., HIGH-TEMPERATURE MASS-SPECTROMETRY IN MATERIALS RESEARCH, in Rapid Communications in Mass Spectrometry, (1991). 175-187.

2. Hilpert, K., Chemistry of Inorganic Vapors. Structure and Bonding, 73 (1990) 97-198

3. Drowart, J. and P. Goldfinger, "Investigation of Inorganic Systems at High Temperature by Mass Spectrometry", Angewandte Chemie, 6 (7) (1967) 581 - 648.

4. J. Drowart, C. Chatillon, J. Hastie, D. Bonnell, in Pure And Applied Chemistry, 77 (2005). 683.

5. W. A. Chupka and M. G. Inghram. J. Chem. Phys., 21 (1953) 371–372

6. Drowart, J.; Chatillon, C.; Hastie, J.; Bonnell, D. "High-temperature mass spectrometry: Instrumental techniques, ionization cross-sections, pressure measurements, and thermodynamic data - (IUPAC technical report)", In Pure And Applied Chemistry, 77 (2005) 683.

7. Ipser, H., "Vapor pressure methods: A source of experimental thermodynamic data", Berichte Der Bunsen-Gesellschaft-Physical Chemistry Chemical Physics, 102 (9) (1998) 1217-1224.

8. Chatillon C, Senillou C, Allibert M, Pattoret A. "High-Temperature Thermodynamical Studies by a Mass-Spectrometry Device for Measurements Using Multiple Effusion Cells", Rev. Sci. Instrum. 47 (1976) 334-340

9. Gilles, P.W., High Temperature Chemistry. Annual Review of Physical Chemistry, 12 (1) (1961) 355-380.

10. Clausing, P., „Über eine Messung der molekularen Geschwindigkeit und eine Prüfung des Kosinusgesetzes". Annalen Der Physik, 7 (5) (1930) 569-578.

11. Clausing, P., „Über die Strömung sehr verdünnter Gase durch Röhren von beliebiger Länge", Annalen Der Physik, 12 (8) (1932) 961-989.

12. Gokcen, N.A., „Diffusional Processes in Knudsen Cells", J. Phys. Chem., 69 (10) (1965) 3538-3541.

13. Knudsen, M., "The laws of the molecular current and the internal friction current of gases by channels", Annalen Der Physik, 29 (1) (1909) 75-130.

14. Knudsen, M., "The molecular current of gases through openings and the effusion". Annalen Der Physik, 29 (5) (1909) 999-1016.

15. K. Hilpert, J. Electrochem. Soc., 13 (1989). 2099

16. D. Kobertz, K. M. Miller, U. Niemann, L. Singheiser, K. Hilpert, Thermochimica Acta, 430 (2005) 73

17. D. Kobertz, K. Hilpert, J. Kapala, and M. Miller, Calphad-Computer Coupling of Phase Diagrams and Thermochemistry, 28 (2) (2004) 203.

18. Ohnesorge, M., Thesis, Forschungszentrum Jülich, (2005)

19. K. Hilpert, Ber. Bunsenges. Phys. Chem., 84 (1980) 494

20. K. Hilpert, Z. Metallkunde, 75 (1984) 70

21. K. Hilpert, Ber. Bunsenges. Phys. Chem., 88 (1984) 37

22. K. Hilpert, in Advances in Mass Spectrometry, Vol. 8A, ed. by A. Quayle, p. 383. Heyden, London (1980).

23. K. Hilpert and I. Ali-Khan, J. Nucl. Mat., 78 (1978) 265

24. K. Hilpert, H. Gerads and D. F. Lupton, J. Nucl. Mat., 80 (1979) 126

25. K. Hilpert, D. Kobertz, V. Venugopal, M. Miller, H. Gerads, F. J. Bremer and H. Nickel, Z. Naturforsch., 42a (1987) 1327

26. K. Hilpert, H. Gerads and D. Kobertz, Ber. Bunsenges. Phys Chem., 89 (1985) 43.

27. K. Hilpert, H. Gerads, D. Kath and D. Kobertz, High Temp.-High Pressures, 20 (1988) 157

28. R. Odoj and K. Hilpert, High Temp.-High Pressures, 12 (1980) 93

29. R. Odoj and K. Hilpert, Z. Naturforsch., 35a (1980) 9

30. R. Odoj and K. Hilpert, Z. Phys. Chem. Neue Folge, 102 (1976) 191

31. Boike, M. Chemisch thermodynamische Untersuchungen der Systeme SiO_2 - B_2O_3 und SiO_2 - Al_2O_3 durch die Knudsen Effusionsmassenspektrometrie, Thesis, Technische Hochschule Aachen, (1991)

32. W. Kuncewicz-Kupczyk, D. Kobertz, M. Miller, C. Chatillon, L. Singheiser, and K. Hilpert, J. Am. Ceram. Soc., 85 (9) (2002) 2299

33. A. Matraszek, L. Singheiser, D. Kobertz, K. Hilpert, M. Miller, O. Schulz, and M. Martin, Solid State Ionics, 166 (3-4) (2004) 343

34. Peck D.H, Hilpert K, Miller M, Kobertz D, Nickel H. „Vaporization of LaCrO3: Partial and integral thermodynamic properties", Journal of the American Ceramic Society, 79 (1996) 3266

Experimental aspects of emf measurements using liquid electrolytes for thermodynamic studies on alloys

Adolf Mikula

University of Vienna

Institute of Inorganic/Material Chemistry

Waehringerstrasse 42

A-1090 Vienna / Austria

Prof. Dr. Adolf Mikula began his career in 1974 as a teaching assistant at Univ. of Vienna. Between 1976 and 1978 he visited University of Wisconsin-Milwaukee (USA) as a postdoctoral fellow. Since then he has held several positions such as research scientist at the Institute of Mineral Dressing and Metallurgy, Tohoku Univ. Sendai, Japan (1983), research scientist at the Max Pplanck Institute für Metallforschung, Stuttgart, Germany (1989), Univ. Dozent for inorganic chemistry at the University of Vienna (1993). At present he is Professor at University of Vienna and Vice Chairman of the Department of Inorganic Chemistry/ Materials Chemistry. He is a specialist in short range order in liquid alloys (from experimental activities and gibbs energies; from neutron diffraction); lead-free solder materials (phase equilibria, thermochemical properties, surface and interface properties; currently bi-sn, bi-cu-sn, al-sn-zn). In 2006, he was awarded the N. S. Kurnakov memorial medal of the Russian Academy of Science.

Introduction:

The aim of thermodynamic studies of metallic systems is the determination of the partial and integral thermodynamic properties in dependence of temperature, concentration and pressure. To measure the partial Gibbs energies directly and derive the Gibbs energy of formation three different experimental methods are available: the electromotive force (emf) -measurements, various vapour pressure techniques and gas equilibria methods.

The measurement of the emf of a suitable galvanic cell is one of the most accurate methods of obtaining thermodynamic properties of alloys at elevated temperatures. At such experiments the negative electrode of such a cell is formed by the more electronegative of the metals and its positive electrode consists of the alloy itself. The cation of the electrolyte is the ionised form of the anodic metal. The cell can be presented schematically by

$$- \text{Me}^{\text{I}} \mid \text{M}^{\text{I}} \text{ (cation)} \mid \text{Me}^{\text{I,II}} \text{ (alloy)} \ +$$
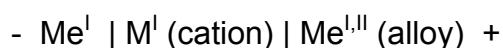
When the cell is in operation the metal M^I is transferred into the alloy $Me^{I,II}$. If the potentiometric method is used to measure the emf, it involves no transfer of M^I, so in practice there should be no change of composition of the alloy.

The principal problem of an experimentalist who would like to apply the galvanic cell technique to measure thermochemical quantities is to find a suitable electrolyte for the cell. For many metallic systems the temperature range of the measurements will be above 700K. In this case, both solid and liquid electrolytes can be used depending on the problems and the systems to be studied.

The second aspect for correct results is: the cell must operate reversible i.e. the emf should show no drift or polarization effects. At constant temperature the ems should be independent of time (at least for several minutes) and has to be reproducible regardless from which side, from lower or higher temperature, the equilibrium temperature is approached. The emf should return to the same value after a small current is passed through the electrodes from one or the other direction.

Other important conditions for accurate emf measurements are:

1.) The charge of the electropositive ion Me^{I+} has to be known exactly and should be

$$Me \leftrightarrow Me^{I+} + Ie^-$$

the only charge transfer through the electrolyte and the only reaction on the surface of the electrodes.

2.) The electronic conduction through the electrolyte should be purely ionic. There should be no reaction of the electrodes and the electrolyte with the material used to construct the cell.

3.) The temperature gradient in the cell should be negligible and no reaction between the lead wire and the electrodes and electrolyte should occur. If two different materials for the lead wire are used the thermoelectric voltage between the two wires must be determined separately. So, if possible, only lead wires of the same material should be used.

4.) Concentration changes of the electrodes or the electrolyte must be taken into account.

5.) The furnace in which the measurements are carried out must be wired noninductively in order to avoid any electrical interference with the emf measurements.

6.) The emf measurements must be carried out without the passage of electricity through the cell. This can be achieved by using a voltmeter with an input impedance of more than 10^{10} Ω (ohms).

If all these conditions are fulfilled the relationship between the reversible cell potential E and the Gibbs energy change ΔG for the cell reaction is described by the following equation.

$$A_{(s,l)} / A^{z+}, \text{ ionic electrolyte/ AxBy }_{(s,l)} \text{(alloy)}$$
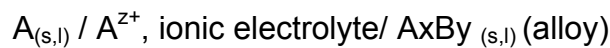
$$\overline{G}_A = -nFE = RT \ln a_A$$

,F the Faraday constant (96 486 coulomb/mole), n is the equivalent of charges passed through the circuit, F the Faraday constant (96 486 coulomb/mole), R the universal gas constant (8.31434 J/mole.degree in K), a_A the thermodynamic activity of the component A in the alloy, and T the absolute temperature.

From the temperature dependence of E, the molar enthalpy ΔH and molar entropy ΔS are calculated with the use of the Gibbs-Helmholtz relation.

$$\overline{\Delta S}_{Zn} = zF \left(\frac{\partial E}{\partial T} \right)_{x,P}$$

$$\overline{\Delta H}_{Zn} = \Delta \overline{G}_{Zn} + T \Delta \overline{S}_{Zn} = -zF \left[E - T \left(\frac{\partial E}{\partial T} \right)_{x,P} \right]$$

With the help of the Gbbs-Duham equation, given by Elliott and Chipman [1] the integral thermodynamic quantities can be calculated.

Electrolytes:

Solid electrolytes:

With the improvement of their performance, the use of solid electrolytes has steadily increased. The basic requirements for such electrolytes are the thermal stability, ionic conduction and an electrical conductivity of not less than 10^{-6} $\Omega^{-1}cm^{-1}$ to establish a stable potential in the galvanic cell.

The most widely used solid electrolytes are the zirconia based electrolytes. The high temperature form of ZrO_2 has a cubic fluorite structure and this form must be stabilized. This is achieved by the addition of 10-15 mole% of CaO, Y_2O_3 or MgO. This doping produces vacancies in the oxygen lattice which are responsible for the ionic conduction of these materials.

Advantages of solid oxide electrolytes are:
They can be used at higher temperatures above 1273K and can be used several times (the oxid electrolytes can be cleaned with acids and after rinsing with water for a longer period of time and drying they can be used again)
The charge transfer through the electrolyte is done by oxygen ions and we don´t have to worry about the charge of the electropositive ion as in liquid electrolytes.

Disadvantages and possible errors:
Since the diffusion of the Oxygen ions is slow through the solid it takes some time until the equilibrium and therefore a stable emf is reached.
Principal sources of error are the following factores cited by Anthony, Baumard and Corish [2]:
Microcracks or open porosity of the ceramic material can cause electrical conductivity.
Because of the poor thermal shock resistance of ceramic materials zirconia tubes should not be cooled faster than 150K/h.
Uncertainty in the cell temperature, cell voltage and evaluation of the reference partial pressure of oxygen can cause some errors.
Nonuniform cell temperature can cause thermoelectric voltage.
Other solid electrolytes are β-alumina ($NaAl_{11}O_{17}$) and β´´- alumina ($NaAl_5O_8$).
In recent years many sodium alloys have been investigated.
A very extensive and excellent summary of different investigations with solid electrolytes is given by Pratt [3].

Fluoride electrolytes:
Fluoride electrolytes are useful under reducing conditions, in which solid oxide electrolytes become electronic conductors. They offer the possibility to determine the activity of strongly electropositive metals such as Na and Mg. Serious problems with fluorides as electrolytes are their chemical activity at higher temperatures. The

electrolyte can easily oxidise and hydrolyse and the fluoride can form intermediate compounds with metals or metal fluorides. Purification and drying of the protective atmosphere is necessary for ionic conduction. Since grain boundary diffusion of electrode cations tends to limit the lifetime of such an electrolyte it is useful to use high purity CaF_2 single crystals in form of polished plates or crucibles.

A review on CaF_2 galvanic cells is given By Azad and Sreedharan [4]. Iwao Katayama of the Osaka University has done extensive research on alloy systems using solid electrolytes [5].

Liquid electrolytes:

Since most of our emf measurements at the University of Vienna is done with liquid electrolytes. So I will concentrate on it. The use of liquid electrolytes for thermodynamic investigations at higher temperature has some advantages and some disadvantages compared with solid electrolytes.

Advantages are:

1.) At the measurements the thermodynamic equilibrium is reached much faster than by solid electrolytes, where the diffusion of the ions is much slower through the solid than through the liquid.

2.) The liquid electrolyte covers the electrodes and hinders the evaporation of the metals

3.) Molten salt electrolytes can be used at lower temperatures.

4.) No cracks and porosity can occur in the liquid salt.

Some limitations are:

1.) The electrolytes must be prepared very carefully and can be used only for one experiment.

2.) At higher temperatures, for KCl-LiCl at approx. 1123 K, the electrolyte can get some electronic conductivity.

3.) The reaction of the lead wires and the containers with the liquid salt mixture must be taken into account.

4.) The whole container material and the thermocouple protection tube should not react with the sometimes aggressive liquid salt mixture.

The liquid electrolyte frequently used for emf measurements consists of alkali chlorides in which a small amount of the halide salt of the electronegative metal is added. The most commonly used salt electrolyte is the eutectic mixture of LiCl-KCl with 46 wt.% LiCl and 54 wt.% KCl. The melting temperature is 625 K according to Vassiliev et al. [6]

Preparation of the electrolyte:

The two halide salts are weight and put into a beaker and this beaker is put in a furnace at 400K for two days. The alkali-halides attract water during storage and part of it should be removed by drying the salts. The salts and 0.5% of the halide salt of the electronegative metal is put into the reaction tube which is shown in Fig. 1.This halide salt can only be added if there is only one stable valence state for instance $ZnCl_2$ with Zn^{+2}. If the reaction with chlorine gas would oxidise the cation in the salt mixture like from Sn^{+2} to Sn^{+4} or Bi^{+3} to Bi^{+5}.this salts must be added after the purification of the eutectic mixture.

In such salts as the alkali-halide mixtures the major impurities are water and hydroxides. A preferred method to dry and clean the halides is to pass a stream of dry gas (e.g. nitrogen or argon) through the powdered salt. After this the temperature is slowly raised until the salt mixture is molten. Through the melt hydrogen chloride or in our case chlorine gas is passed through followed by a stream of nitrogen or argon. We prefer chlorine gas over hydrogen chloride because it gives us a lower residual water and hydroxide content. The following reaction can occur:

$$OH^- + Cl_2 \rightarrow Cl^- + HCl + \tfrac{1}{2}O_2$$

$$O^{2-} + Cl_2 \rightarrow \tfrac{1}{2}O_2 + 2Cl^-$$

$$H_2 + Cl_2 \rightarrow \tfrac{1}{2}O_2 + 2HCl$$
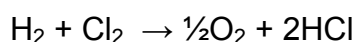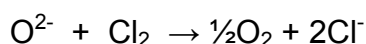
For our measurements we prepared the LiK-KCl electrolyte with the equipment shown in Fig.1 and given in [7].
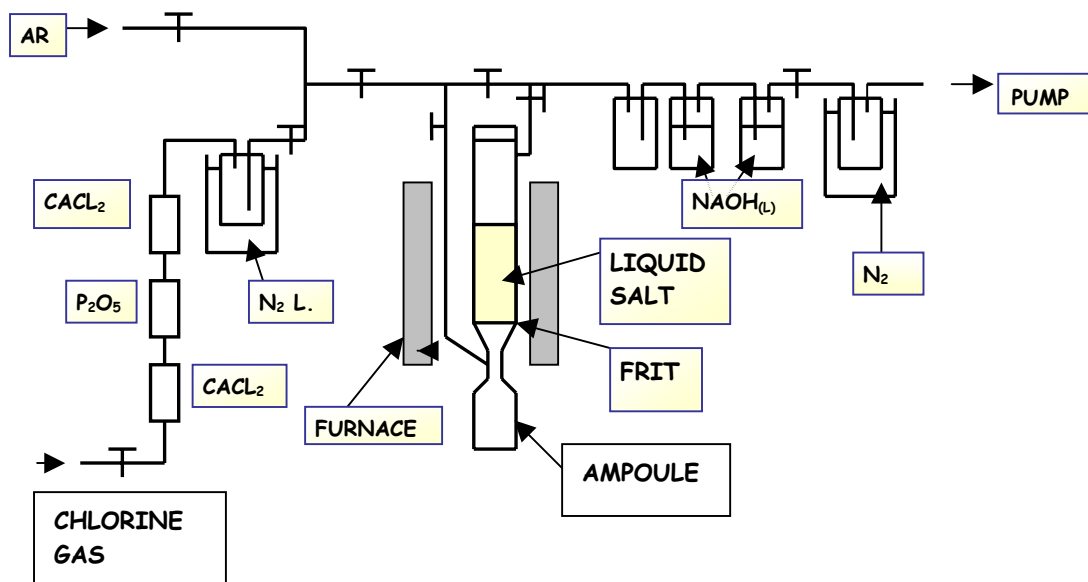
Fig.1. Equipment for cleaning the KCl-LiCl electrolyte

The whole apparatus is made of pyrex (higher melting) glass.

First argon is passed through the fine powdered salt mixture which is above the frit. Be careful with the gas flow because the powder will "explode" if the gas comes too fast. After a few minutes the furnace is turned on and the salt is slowly heated until it is molten. The liquid salt is kept above the melting point all the time. If it would cool down the glass tubes would break.

In the mean time chlorine gas is taken out of a pressure bottle and filled in a container which has two stopcocks. The container is in liquid nitrogen and the chlorine gas is condensed in this container until we have approx. 2ml of gas. The container is connected to the apparatus. It would be in the drawing where Cl_2 is shown. After the connection is gas-tight the chlorine gas is slowly heated and it vaporises. The gas is passed through $CaCl_2$ and P_4O_{10} and then condensed again in liquid nitrogen. After we have all the chlorine in the second cool trap we evaporate the gas again and pass it slowly through the molten salt mixture. The mixture which was colourless at the beginning turns slowly yellow-green. The chlorine gas is passed for one hour through the mixture. Since the gas pressure is coming from bottom side of the frit the salt stays above the frit. We have to be very careful that there is always gas coming from the bottom otherwise the salt would run down through the frit. The excess chlorine gas will be collected in the NaOH solution, which will slowly turn green if the chlorine get there. After all the chlorine gas has passed through the molten salt, argon is bubbled through for four hours because there

should be no chlorine left in the electrolyte. A very good indication that all chlorine gas has left the electrolyte is: the salt mixture must be completely colourless again. After the reaction is finished the gas flow is turned around and the liquid salt is filtered through the frit into the ampoule. The ampoule is then sealed under vacuum with a torch. The electrolyte in the ampoule can be stored for several months prior to its use. Sometimes there is a black residue on the frit. This is some carbon which is left in the salts during the production process.

emf measurements:

The arrangement of the apparatus is shown in Fig. 2. All the components are of quartz. The electrolyte is put into the quartz tube and when Sn or Bi-systems are measured the salt of the electronegative element is added, as already explained previously. The four electrodes, one of the pure element and the three others are filled with the alloys are arranged around the thermocouple protection tube (See Fig. 2). The top of the quartz tube was sealed with a brass head (see Fig.2). Four electrodes were used in one experiment. These and the thermocouple protection tube could be raised and lowered through O-ring seals. The tube is evacuated and
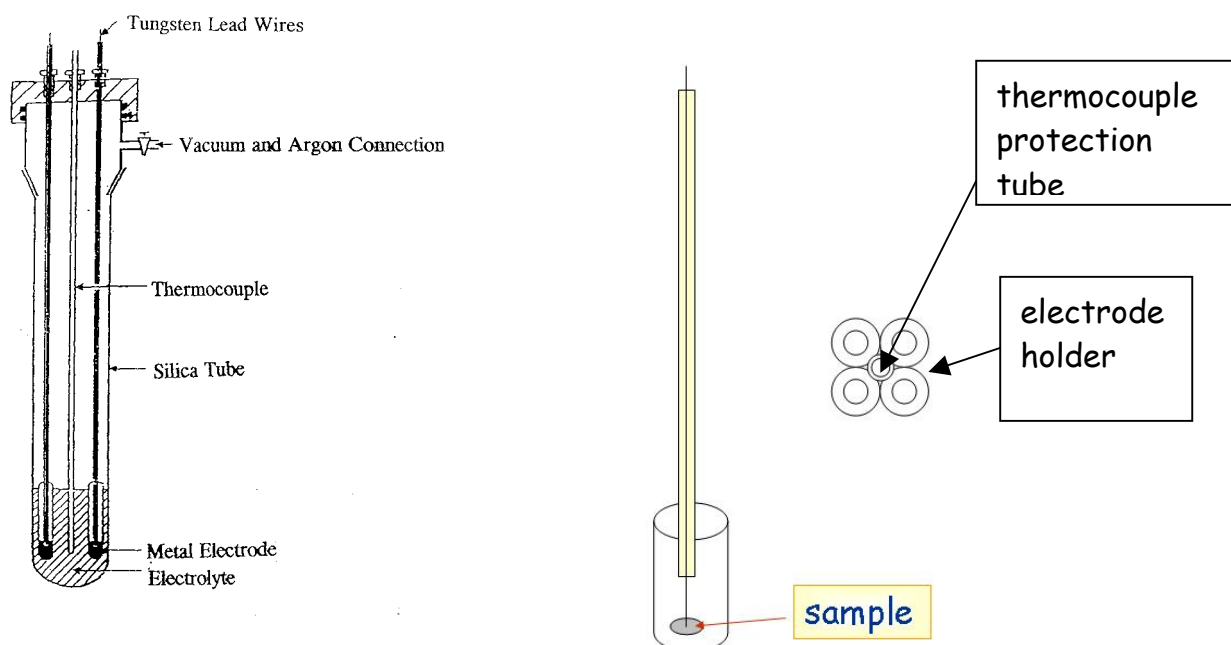
Fig.2 The cell to measure the emf, electrode container with the lead wire and the arrangement of the electrode holder and the thermocouple protection tube

After flushing with argon several times, the tube is filled with argon, so that the pressure inside at 1000K is approx. one bar. The apparatus is put into a vertical furnace and heated until the electrolyte is molten. Now the electrodes and the thermocouple tube are lowered in the molten electrolyte and the lead wires which are enclosed in quartz tubes are also lowered to the electrodes. For the thermocouple we use Ni/NiCr.

Now we can start the measurement. One electrode is the pure electrode and the three others are the electrodes of different alloy compositions. The thermocouple and the electrodes are connected to a voltmeter with a scanner and the voltmeter is connected to a computer. Every fife minutes the computer takes a reading of the temperature and the emf of the three electrodes. Electrode 1 is measured against the pure electrode, then electrode 2 against the pure one and after this electrode 3. So we get the emf of the three electrodes and can calculate the activity of the electro-negative element.

The measurements of the emf are carried out on heating and cooling, the heating and cooling rate being 10K/h. Several times the temperature is kept constant for a period of time to check the stability of the emf. For the evaluation of the data we usually take the results of the first cooling curve. If there is a slight evaporation of the metals, in most cases it is the pure metal, a very thin metallic film can be detected on the cooler part of the cell.

Results of our measurements:

Ag-Bi-Sn system [8].

The ternary alloys were prepared from high purity metals. The metals were weighed and sealed in a quartz tube and melted at 873K for fife days. Afterwards the samples were quenched and 2g of each alloy was used for the measurements. To the liquid LiCl-KCl electrolyte 0.5 mole% of potential forming Sn^{+2} ion salt - dehydrated $SnCl_2$ was added directly to the mixture because the chlorine gas would have oxidized the Sn^{+2} to Sn^{+4}. Tungsten wire was used for the leads because no reaction was found between W and the alloys.

The measurements were carried out at three cross sections with constant ratios of Ag:Bi = 2:1,1:1 and 1:2. At all cross sections the emf versus temperature curves were

straight lines. Using the least-square fit, the emf was expressed by the following equation:

$$E(mV) = a + bT(K)$$

The activity of Sn shows a positive deviation from Raoult´s law. The activity of Sn at 900K for the cross section Ag:Bi = 1:2 is shown in Fig.3.
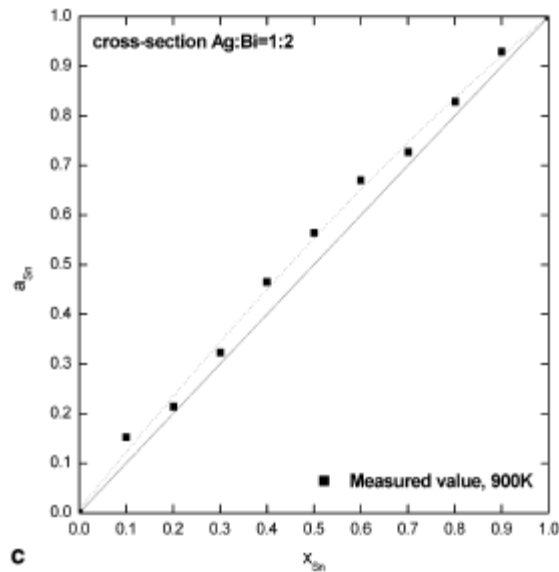
Fig.3: Activity of Sn at 900K in the Ag-Bi-Sn system

The integral Gibbs free energy and the enthalpy of mixing for the ternary Ag-Bi-Sn system were calculated using an equation given by Elliott and Chipman [1]. The integration was carried out along the line of the constant Ag to Bi ratios, and for the integration constant $G^{xs}_{binary}(Ag-Bi)$, the values of Hultgren et al.[9] were used. The emf measurements of the ternary Ag-Bi-Sn system yield a consistent set of thermodynamic data of the liquid alloys.

That the emf vs. temperature curves are not always straight lines is shown in the next experiment.

Cd-As system [10]

In this case the electrolyte was also a eutectic mixture of KCl-LiCl with 0.5 mole% $CdCl_2$. The cell arrangement was:

$$Cd(l)/Cd^{2+} (KCl-LiCl)(l)/CdAs(l)$$

Two cooling curves were recorded during each experiment. Between the two cooling curves the potential decreased 50 to 300µV depending on composition (the decrease was less for cadmium-rich alloys.

Between pure Cd and 75%Cd, and at ≈55at% Cd and at 35At% Cd the emf-T curves are straight lines with a constant slope. All other plots exhibit a distinct curvature, which is positive for alloys with more than 55at% Cd and negative for alloys with less than 55at% Cd. In Fig. 4 several emf plots are shown as examples. The isothermal points are indicated by solid squares. Such results are only possible with the use of liquid electrolytes because the equilibrium is reached much faster and we could get data points at nearly every degree. Therefore it was possible to detect the slight curvature.

From the emf data the integral molar excess entropy of mixing was calculated (Fig. 5). It has appointed depression with a minimum at approx. 52 at% Cd. With increasing temperature the minimum gradually shifts towards more positive values.

From our results we concluded that there is a strong indication from the thermodynamic data that there might be some sort of Chemical Short Range Order (CSRO) in the liquid Cd-As system. With increasing temperature the "compounds" tend to dissociate in the melt and approach to a more statistical distribution of atoms in the liquid state.
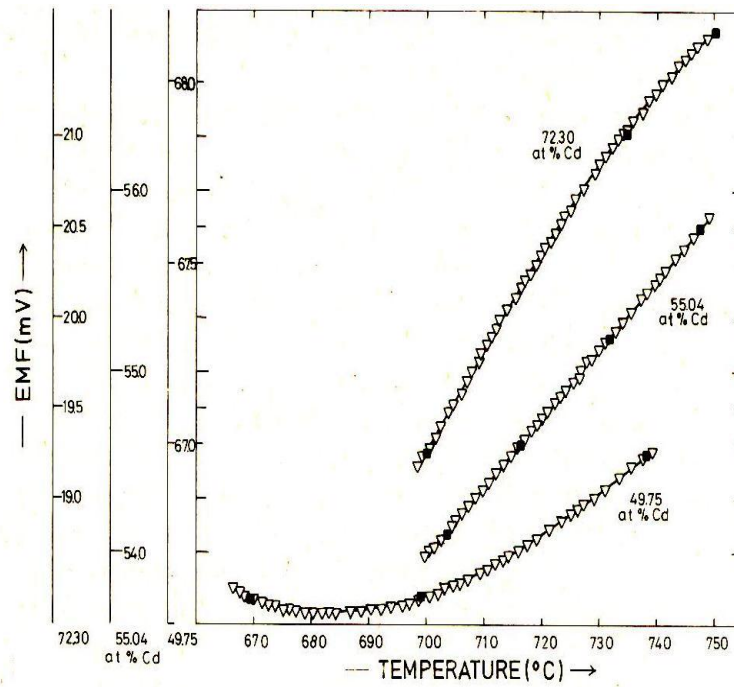
Fig. 4: Some emf vs. temperature curves in the As-Cd system
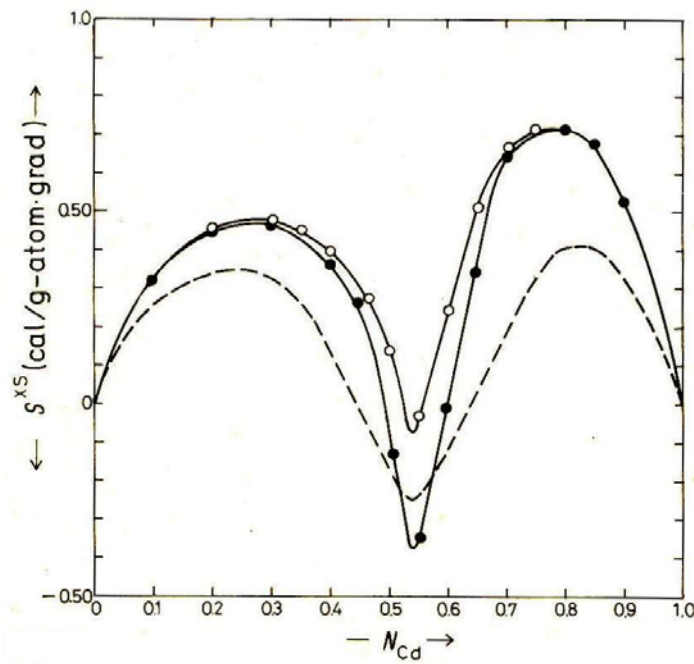
Fig. 5: Integral excessentropy of mixing of liquid -AsCd alloys, dashed line the results of Scheil and Kalkuhl [15]

There is always an argument in the scientific community which integral enthalpy data are more reliable, the results obtained by calorimetric measurements or the enthalpy data derived from emf experiments. In general I would agree that the calorimetric results are more accurate since the values are directly obtained from the experiment.

When the emf data are used the slope of the emf vs. temperature has to be determined and after this an integration has to be carried out. But in some cases it all depends on the system which results are to be trusted a little more. I would like to present an example where we carried out both measuremens emf and calorimetric.

The Au-Sn-Zn system.
The following cell arrangement was used:

$$Zn(l)/Zn^{2+} \text{ (KCl-LiCl) (l)/ Au-Sn-Zn alloys(l)}$$
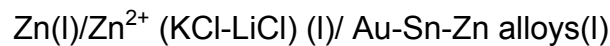
Under reversible conditions, the partial Gibbs energy change of the Zn component was directly obtained from the emf of the cell. From the temperature dependence of E the partial molar enthalpy ΔH_{Zn} was derived. The Gibbs-Duhem equation was applied to calculate the integral enthalpy of mixing.
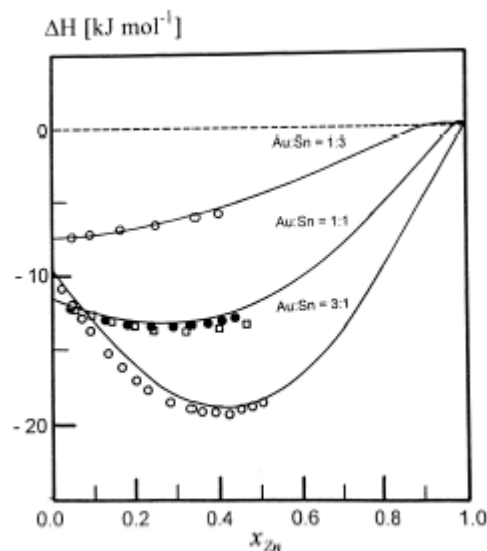
Fig. 6: Comparison of the ΔH values from the emf data with calorimetric measurements in the Au-Sn-Zn system.

For the calorimetric measurements a high-temperature calorimeter was used to measure the integral enthalpy of mixing. In our case solid Zn was added to liquid Au-Sn alloys.
The comparison of the ΔH values from the emf data with the calorimetric measurements of the Au-Sn-Zn system is shown in Fig.6. The solid lines are the emf

results and the circles and squares are the calorimetric data. In this case the agreement of both experiments is very good.

The Bi-Zn system [12]

The last example should demonstrate a method to determine the concentration fluctuation, Sxx(0), which is a long wavelength limit (q→0) of the concentration-concentration partial structure factors [13] are found to exhibit a strong temperature dependence for demixing liquid alloys [14]. Sxx can be determined experimentally either from small angle scattering experiments on extrapolating the scatter intensity of the neutron or X-ray radiation, or from measured thermodynamic data. Due to uncertainties in the extrapolation or in the numerical differentiation we tried to measure the composition gradient of the emf (i.e. (ΔE)/(Δx) and hence the concentration fluctuations of liquid Bi-Zn alloys above the miscibility gap.
For this experiment the following cell arrangement was used.

$$- \mid Bi_{1-x} - Zn_x \mid Zn^{2+} (KCl-LiCl) \mid Bi_{1-(x+\Delta x)}Zn_{x+\Delta x} \mid +$$
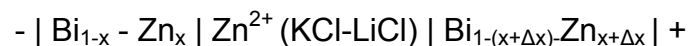
In this case we did not have a pure electrode but measured the emf of one electrode with 60 at%Zn against the second electrode with 65 at% Zn. All measured ΔE values are very small and the relevant values around the critical composition are less than 0.3 mV. The scatter in our experiment was less than 0.02 mV.
The second advantage of this experiment was the possibility to prevent a demixing of the alloy during the experiment, because the alloys were stirred several times by moving the lead wire up and down.
With this experiment we could determine Sxx(0) directly from the emf measurements.

Conclusion:

In this report I wanted to show the use of emf measurements to determine the activity or Gibbs energy. It depends on the type of investigations, systems and temperature range, which system and which electrolyte should or can be used. The biggest advantage of liquid to solid electrolyte lies in the much faster established equilibrium. The examples of some of our experiments, presented in this report should prove this. All the presented measurements would not have been possible without the use of

liquid electrolytes. It should also show how easy it is to carry our emf investigations with liquid electrolytes if the electrolyte is prepared very careful.

References:

[1] J.F. Elliott and J. Chipman, J.Am.Chem.Soc., 73 (1951), 2682.

[2] A.M. Anthony, J.F. Baumard and J. Corish, J.Pure Appl. Chem., 56 (1984), 1069.

[3] J.N. Pratt, Metall. Trans., 21A (1990), 1223.

[4] A.M. Azad and O.M. Sreedharan, J. Electrochem. Soc. 142 (1989), 17.

[5] I. Katayama and H. Yamashita, Koon Gakkaishi, 32 (2006), 80.

[6] V. Vassiliev, M. Azzaoui and J. Hertz, Z. Metallkd., 86 (1995), 545.

[7] S. Karlhuber, Master Thesis Univ. of Vienna. (1993).

[8] Z. Li, S. Knott and A. Mikula, J.of Electronic Materials 36 (2006) 40.

 [9] R. Hultgren, P.D. Desai, D.T. Hawkins, M. Gleiser and K.K. Kelley, eds., Selected Values of the Thermodynamic Properties of Binary Alloys (Metals Park, OH: ASM 1973).

[10] K.L. Komarek, A.Mikula and E. Hayer, Ber.Bunsenges.., 80, (1976), 765.

[11] S. Karlhuber, A. Mikula and F. Sommer, Met.Trans. 27B, (1996), 921.

[12] S. Karlhuber, A. Mikula, R.N. Singh and F.Sommer, J.Alloys and Compounds 283 (1999), 198.

[13] A.B. Bathia and D.E. Thornton, Phys.Rev. B2 (1979), 3004.

[14] R.N. Singh and F. Sommer, Rep.Prog.Phys. 60 (1997) 57.

[15] E. Scheil and A. Kalkuhl, Z. Metallkd. 52 (1961) 557.

Phase diagrams –Experimental Techniques

Dr R. Sridharan
Liquid Metals & Structural Chemistry Division,Chemistry Group
Indira Gandhi Centre for Atomic Research, Kalpakkam

Dr.R.Sridharan obtained his M.Sc and Ph.D. from Indian Institute of Technology, Chennai. He graduated from the 23rd batch of the BARC Training School and joined IGCAR in 1980. Since joining IGCAR, Dr.Sridharan has been involved in investigation of thermochemical and electrical properties of material systems for use in liquid sodium coolant circuits of Fast Breeder Reactor. He has established several binary and ternary phase diagrams of relevance to liquid sodium coolant systems and also for developing electrochemical sensors. He has investigated the electrical properties of different hydride ion conducting solid electrolyte systems and based on these studies, he has developed an electrochemical hydrogen sensor for measuring very low levels of hydrogen in liquid sodium circuits.

What is a phase diagram? It is a graphical representation of properties of phases present in a system in equilibrium under given conditions of variable parameters such as Temperature (T), Pressure (P) and Composition (C). The phase diagrams are primarily categorized by the number of components of the systems under investigation, the simplest being that of one component system such as water(of fixed composition). A 'phase' means the definite region in the physical system within the boundaries of which, the properties are found uniformly constant. Thus, an intimate mixture of two solids, namely, sugar and sodium chloride
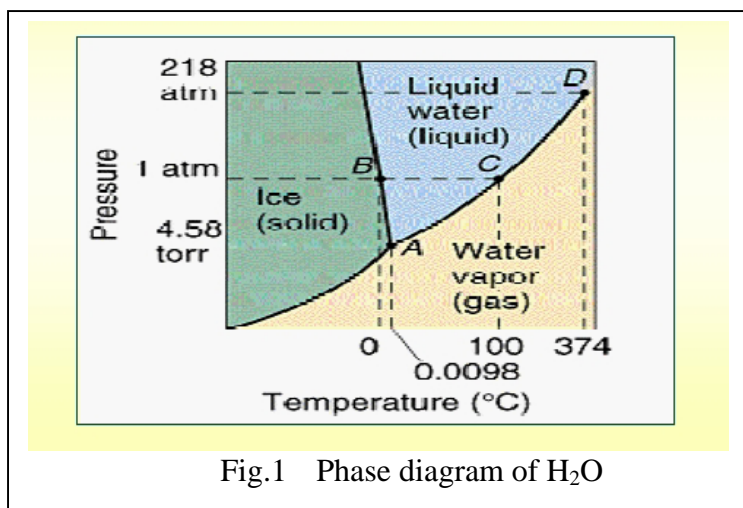
Fig.1 Phase diagram of H_2O

consists of two 'phases' because, in the mixture we have matter with two distinctly identifiable properties each exhibiting a distinct X-ray pattern, density, electrical conductivity,
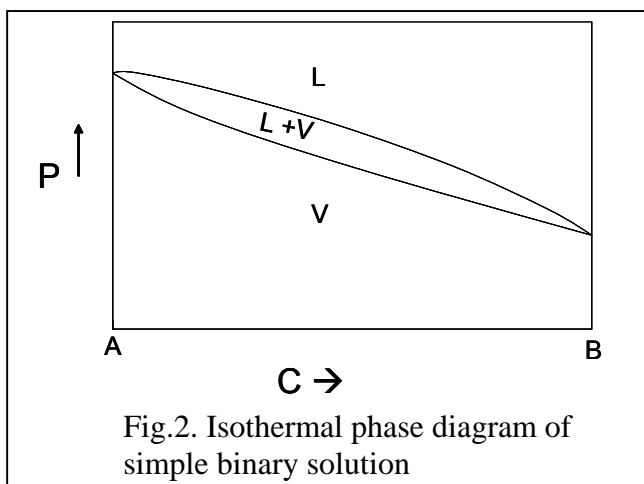
Fig.2. Isothermal phase diagram of simple binary solution

refractive index etc. In a one-component system, the phase diagram graphically represents the dependence of the equilibrium state of existence of the systems on two independently variable parameters P and T. The schematic phase diagram of H_2O is shown in Fig.1. The phase diagram shows three single phase regions of T and P where ice, water and water vapour exist. The T and P regions over which two phases co-exist at equilibrium, namely between ice-water vapour, liquid water- water vapour and ice-liquid water are represented by curves. Gibbs phase rule, which dictates the degree of freedom allowed by considering the conditions of equilibrium relationships between all the phases, is applicable at all the points in the phase diagram. Gibbs phase rule is : F = C –P +2 where F is the degree of freedom, P- the number of phases and C is the number of components whose composition needs to be fixed to define the properties of all the phases present in the system. Thus, at point A, where solid, liquid and the vapour phases exist in equilibrium, P=3, C=1 and F =3-1+2 =0. The point A where degree of freedom is zero is called the invariant point which is unique (T and P) to the system. For two component systems, phase diagrams are constructed either as T vs X or P vs X where X is the composition represented as mol fraction. Phase diagram of a binary system with complete solubility of components in each other is shown in Fig 2. Typical phase diagram of a simple eutectic system is also shown in Fig.3. While in the former the phase diagram shows equilibrium phases that co-exist as pressure is varied over composition, in the latter, phase diagram shows the co-existing phases as temperature is varied over composition. The complexity of phase diagram increases as number of components increases beyond two. In Fig.3, the phases that co-exist in equilibrium as a function of temperature and composition is shown. For this system, condensed phase rule is applied to the phase diagram since the effect of the independent variable, pressure (P), is negligible on the composition of solid and liquid phases. Thus, at point E, where solid A, solid B and the liquid are in equilibrium, degree of freedom, F = 2-3+1 =0 implying the uniqueness of point E, which is fixed by the system properties. This point is called the eutectic point and the corresponding composition and temperature are called the eutectic composition and the eutectic temperature respectively. The eutectic temperature is independent of composition and the eutectic reaction involves disappearance of one of the solid phases and appearance of a liquid phase of eutectic

Fig 3. Simple eutectic system

composition. Phase diagrams of binary and other multi component systems are often constructed in terms of their temperature-composition relationships.

From the above consideration, it is clear that experimental techniques needed for determination of phase diagram must be sensitive to the thermal energy changes accompanying processes such as crystallization, melting, vapourisation, solubility of one phase into the other and mixing. Thus, it is obvious that thermal analysis techniques such as DTA and DSC are very convenient techniques for experimental determination of phase diagram of condensed phase systems. Apart from recording the thermal changes accompanying the phase changes, characterization of phases under equilibrium conditions is essential to determine the phase fields. X-ray Diffraction(XRD) is widely used to characterize the solid compounds. Hence, DTA or DSC experiments and XRD analysis are complementary analytical tools to determine the phase diagrams of solid-liquid and solid-vapour systems. Characterization of the phases in liquid and vapour state need proper sampling of equilibrated samples and compositional analysis of phases by suitable chemical methods and/or spectroscopic techniques such as IR,UV spectroscopy, mass spectrometry, quadrupole mass spectrometry etc.

Other methods such as dilatometry and electrical conductivity measurements are also used to detect phase changes wherever is applicable. In fact a variety of methods based on detecting changes in physical and chemical properties have been used to detect phase changes.

For construction P-T phase diagrams, pressure and temperature measurements are needed. Pressure measurements are of two types – direct and indirect. In the range 10^{-1} to 760 torr, transpiration and Bourdon gauge methods or some variant of the latter are used. Above atmospheric pressure, the Bourdon gauge method alone of considerable utility. Capacitance manometers are available for use from 1torr to 5000 torr. While these methods are direct, vapour pressures below approximately 10^{-1} torr are mostly determined by Knudsen effusion method or some variant of it or by the transpiration method. These methods are indirect in the sense, ideal behaviour of gases is necessary to calculate the pressures. The limitation on the use of manometers and barometers is due to the fact that vapour being measured comes into contact with either mercury or oil. Temperature measurements are made using resistance thermometer at very low temperatures. Thermocouples or used from RT to 2200°C Optical pyrometry is also used to measure temperatures beyond 800°C.

Principles involved in Thermal analysis techniques – DTA and DSC

Thermal analytical techniques such as DTA and DSC are useful tools to detect phase changes in single as well as multicomponent systems and in the construction of phase diagrams.

Differential Thermal Analysis(DTA)

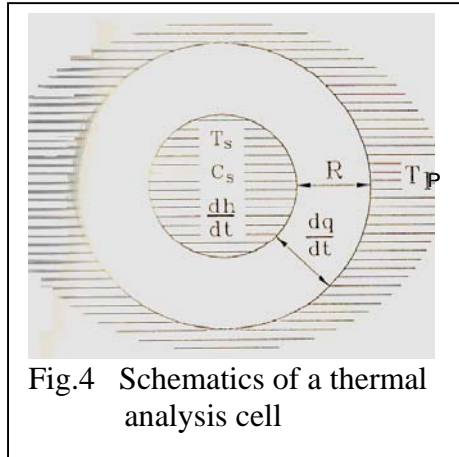A DTA apparatus is one in which a sample cell and a thermally inert reference cell are heated at a constant scanning rate and the difference in the temperature between the sample and the reference cell is recorded as a function of temperature. The essential parts of a thermal analysis cell are shown schematically in Fig. 4. They consist of the sample and its container at a temperature T_s; a source of thermal energy at temperature T_p(furnace) and a path having a certain thermal resistance, R, through which the thermal energy flows to or from the sample at a rate, dq/dt. C_s is the heat capacity of the sample plus container. A similar arrangement exists for the reference cell. The change in heat energy of the sample at any instant, dh/dt, is used up either to change the sample temperature or is lost to the surroundings. As energy must be conserved, the sum of these two effects must be equal.

Fig.4 Schematics of a thermal analysis cell

Therefore, $dh/dt = C_s (dT_s/dt) - dq/dt$ ....(1)

The rate of heat loss to the surroundings is given by Newton's Law:

$- dq/dt = k (T_p-T_s)/R$, where k is a constant.

Substituting this expression in equation (1) we get,

$dh/dt = C_s (dT_s/dt) + k (T_s-T_p)/R$ ....(2)

A similar expression for the reference cell is:

$dh/dt = C_r (dT_r/dt) + k (T_r-T_p\_)/R$ ....(3)

Since no heat is released or absorbed (other than the heat capacity) in the reference cell, L.H.S of the above equation is zero. In DTA one measures a difference in temperature between a sample cell and a reference cell and records this difference versus time or temperature. Substracting equation (3) from (2) and rearranging, the instantaneous rate of heat generation (dh/dt) by the sample can be expressed as:

$R \, dh/dt = k(T_s-T_r\_)+R(C_s-C_r)dT_r/dt + RC_s \, d(T_s-T_r)/dt$ ……(4)

where, k = a constant,

C_r - heat capacity of the reference,

Tr - temperature of the reference,
dTr/dt - scanning rate.

The DTA curve obtained thus reflects the three terms in the R.H.S of equation (4). A typical DTA curve obtained for a thermal event in the sample is shown in Fig.(5). The first

Fig.5 Typical DTA curve for a thermal event
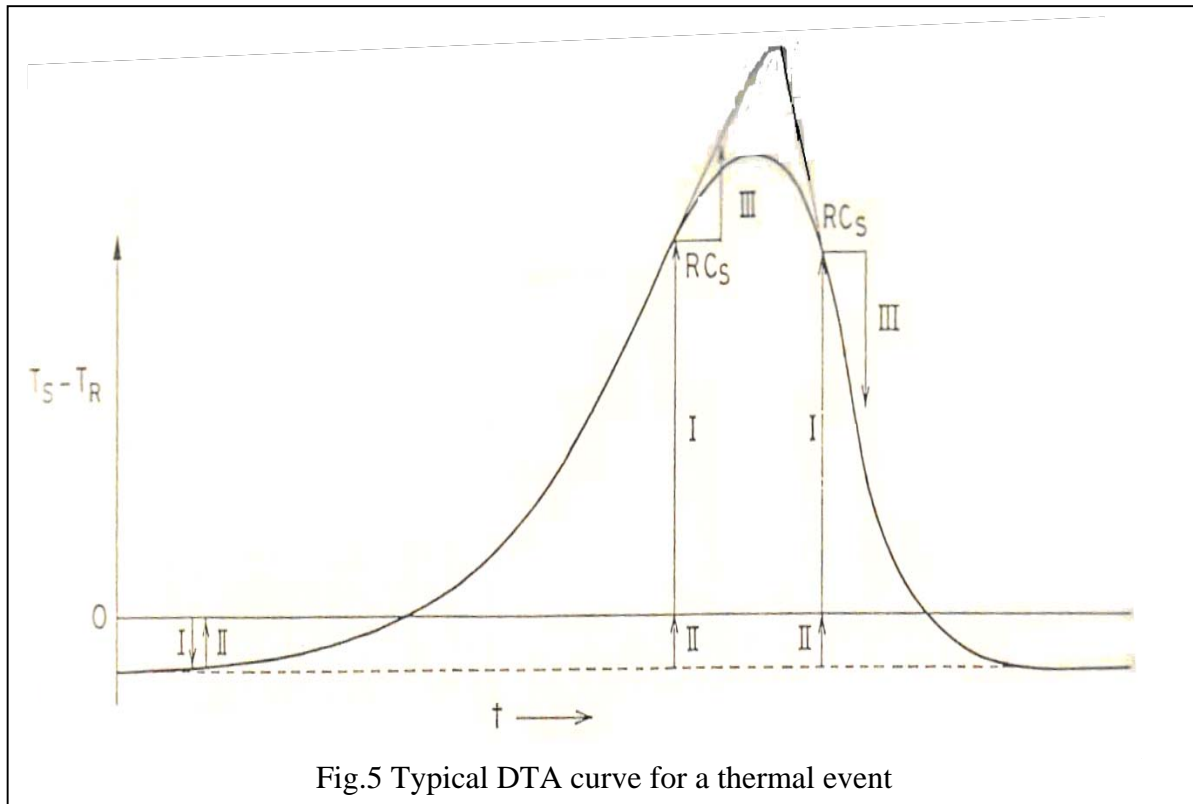
term $(T_s - T_r)$, is the differential temperature continuously recorded by the instrument. In the steady state, after the instrument has reached scanning thermal equilibrium, but when, dh/dt, is effectively zero, the third term also is zero because the difference between the temperatures of the sample and reference remains constant with respect to time. The signal, which is the first term is then equal to the second term in equation (4) but with opposite sign. The distance II thus represents the baseline displacement from the zero signal level. When a thermal event occurs in the sample, the slope of the signal changes continuously until the event is complete. The third term is the slope of the curve at any point of interest multiplied by a constant, RCs. The magnitude of the third term is represented graphically in Fig. 5. A tangent is drawn to the curve at any point of interest. From that point a horizontal distance, RCs is laid off in the direction of increasing time and a vertical line is drawn through the terminus. The vertical line cuts the tangent at some point to form a right-angled triangle whose hypotenuse is the tangent of slope and base is RCs. The height of the triangle is equivalent to the magnitude of the third term of the equation 4. At any

point on the curve, R dh/dt is equal to I+II+III. The displacement from the baseline at any time (or temperature) is proportional to the reaction rate at that time and the fraction of the total area swept out up to that time will be the fractional amount of the sample which has reacted. It is obviously advantageous in any instrumental design to make RCs as small as possible to minimise the thermal lag. Thus whenever two thermal events occur closeby, then, for better accuracy or resolution, RCs must be small. From equation 4, it is clear that the signal, Ts-Tr, is proportional to R. Hence, small R leads to loss of sensitivity. Thus in DTA, the sensitivity demands a compromise with the resolution or accuracy of the signal and is

$$\frac{dh}{dt} = \frac{dq}{dt} + (C_s - C_r)\frac{dTp}{dt} - RC_s\frac{d^2q}{dt^2}$$

Fig.2.9 : A typical DSC curve
[Factors influencing the shape of the curve are labelled]

R : Thermal resistance
C_s, C_r : Heat capacity of sample and reference
dq/dt : Rate of heat flow to sample and sample holder.
T_s, T_r : Temp. of sample and and reference
dh/dt : Rate of enthalpy change in sample.

Fig.6 Typical DSC curve for a thermal event
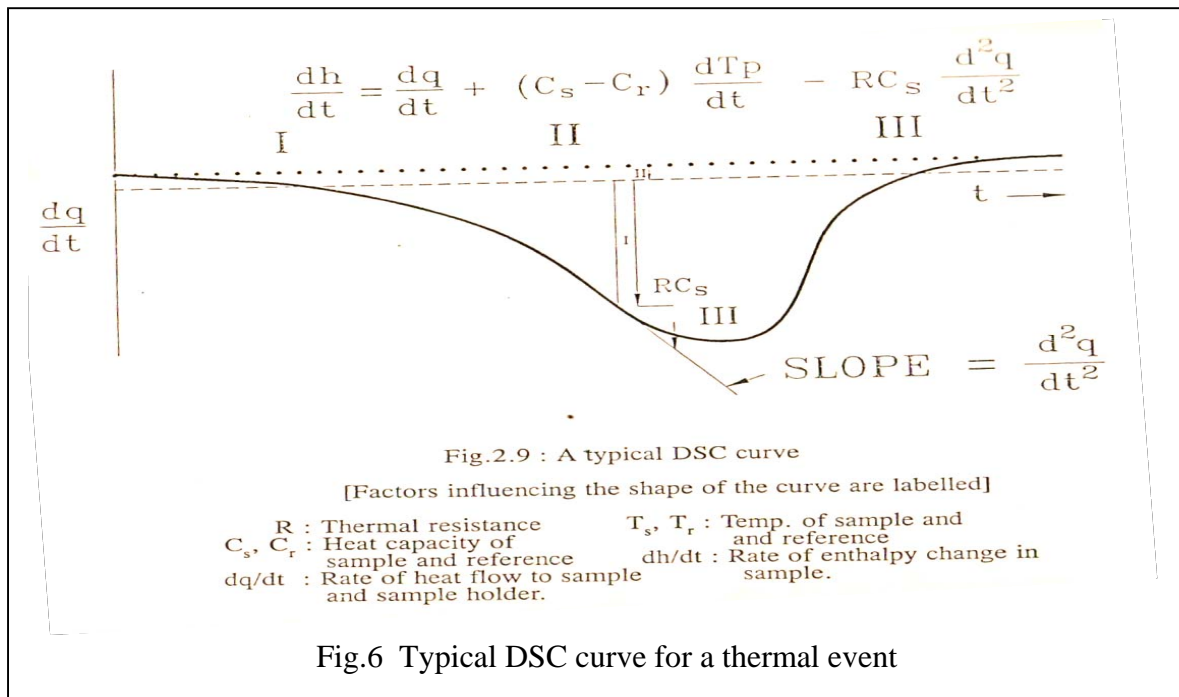
dependent on the instrumental design.

Differential Scanning Calorimetry (dsc)_

A differential scanning calorimeter consists of sample and reference holders which are insulated from each other. These are always maintained at the same temperature by a closed loop control of the electrical power that is supplied to the heaters in each of the holders. In order to maintain this condition of temperature equality, the energy per unit time, which the sample absorbs from or provides to the sample holder, must be exactly compensated by a corresponding variation in the differential electrical power provided to the heaters; measurement of this electrical power is equivalent to measuring dq/dt, defined

earlier. The basic equation relating dh/dt to the measured quantities is given by (the derivation is similar to that used for DTA technique):

$$dh/dt = -dq/dt + (Cs - Cr) \, dTp/dt - RCs \, d^2q/dt^2 \quad ...(5)$$

The first term on the R.H.S is the signal measured from the zero baseline, the second is the baseline displacement due to heat capacity mismatch between sample and reference, and the third being the slope of the recorded curve multiplied by the constant, RCs. Fig. 6 shows a typical DSC curve. The thermal lag of the DSC curve represented by the third term of equation 5, is shown in Fig.6 by means of graphical construction as was done previously for DTA. Although a DSC curve is analogous in many respects to those obtained in DTA, there are two important differences between the two. As the thermal resistance R, occurs only in the third term in equation 5, the thermal lag due to the term RCs can be reduced, unlike in DTA, without sacrificing the sensitivity. The second major difference is that the area under a DSC peak directly equals q = -h. Insofar as calorimetric measurements are concerned, the value of R need not be known nor need it be constant. The calibration of a DSC is therefore not dependent on the temperature, and a single point calibration applies over the whole range. The calibration constant " required to convert area to joules in DSC is a constant electrical conversion factor, whereas in quantitative DTA it is a thermal "constant" which in practice varies with the temperature. This is due to the fact that a DTA apparatus is basically a temperature measuring device and energy information is obtained through secondary relationships. A DSC apparatus, on the other hand, is basically an energy measuring
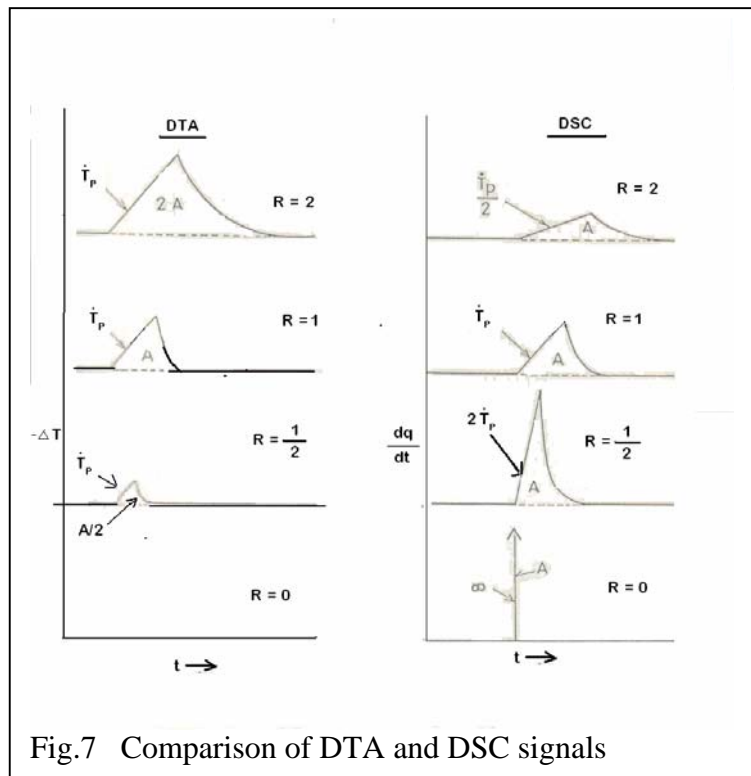
Fig.7   Comparison of DTA and DSC signals

device and temperature information is obtained through secondary relationships. In DSC the sample holder temperature is monitored and maintained equal to the program temperature Tp; the sample temperature, Ts, is not measured directly but is computed from the Newton's Law equation:

dq/dt = (Tp_-Ts)/R

Hence thermal lag is minimised and temperature accuracy and sensitivity maximised by reducing R to the smallest possible value in DSC. A distinctive difference between DSC and DTA is illustrated in Fig.7, which shows the effect of a change in R on the peak area and shape of a sharp transition. The DSC area is invariant with R and the resolution improves as R decreases. In DTA, resolution also improves as R decreases, but the peak area decreases proportionately and goes to zero as R goes to zero.

Determination of Phase Diagrams

The phase transitions in pure substances are simple as they are isothermal in nature. But the thermal behaviour of two-component systems show more variety and complexity than those of pure substances because of the occurrence of both isothermal and non-isothermal thermal events

Fig: 8 Typical DTA trace showing an endothermic peak and exothermic peak

in such systems [Chernik]. The non-isothermal events correspond to the appearance or disappearance of one of the coexisting phases in a wide temperature interval. e.g., change of composition of the liquid phase above the eutectic temperature upto the liquidus point. The shape of the DTA and DSC trace obtained for such non-isothermal events
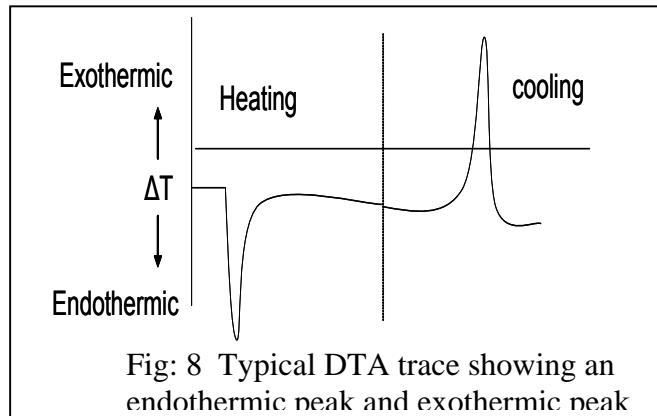
DTA trace of a simple eutectic system

Fig 9. Typical DTA curve for sample of composition 'x'

Fig. 10 Typical DTA signals in a complex binary system
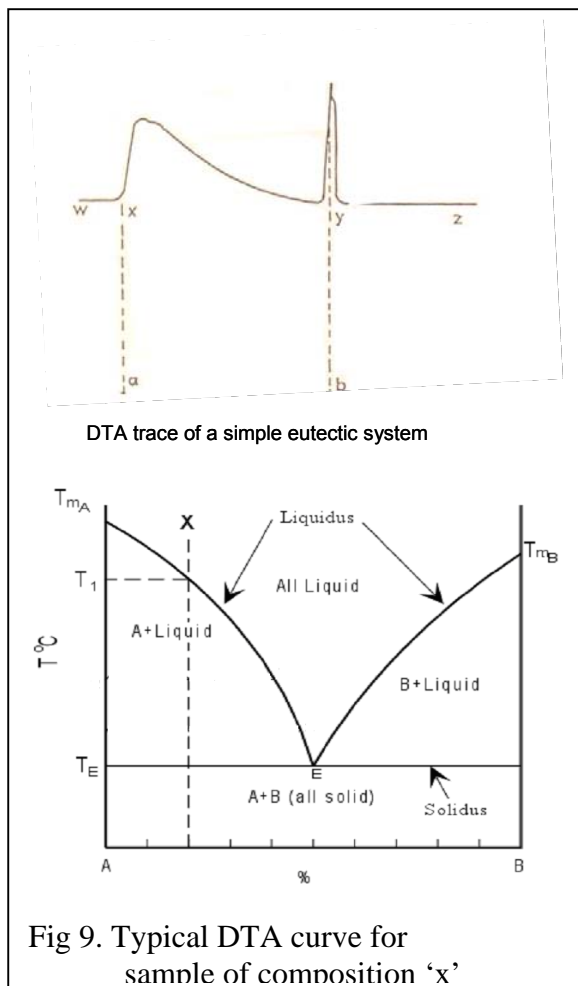
depend on the change in heat capacity and thermal conductivity of the sample as transformation takes place. Hence, the interpretation of the results must take into account these factors. In the determination of phase diagrams, the shape of the DTA or DSC peak is of great importance and yields useful information. Hence the response of these techniques to the analysis of some hypothetical phase diagrams are considered. A simple two-component phase diagram is shown in Fig. 9.

The components are completely miscible in the liquid state and the solid phases consist of pure components. The DTA or DSC trace of a sample of composition 'x' represented by the vertical dotted line during cooling would be as shown in Fig. 9. From w to x in the DTA curve, the sample will cool at the same rate as the reference material. There may well be a pronounced slope of the base-line due to the difference between the heat capacity of the molten sample and a solid reference. At point x, deposition of solid B commences and this results in the liberation of the heat of fusion. The temperature of the sample will therefore fall slowly relative to that of the reference and an exotherm will appear on the trace. This exotherm will, however, not be a single sharp peak (as shown in Fig.8), but will be initially sharp and will tail off as complete crystallization occurs. Its overall size will be dependent on the amount of compound B present in the mixture. As the eutectic temperature is approached, the trace will once again approach a stable base-line, as the temperature differences between sample and reference approach zero. At the eutectic temperature, solid A begins to crystallize and the temperature of the sample remains constant until all of component A has solidified. Since, the reference material will still be cooling at the programmed rate, the eutectic temperature is marked by a sharp exotherm. After all of A has solidified, further cooling of the sample occurs and the trace re-attains a stable base line. If the composition w were chosen to be that of the eutectic composition, the trace would only show a single sharp exotherm. For the simple system, the temperatures which should be plotted are the onset of the broad exotherm and the peak maximum in order to construct the phase diagram from the DTA or DSC trace. However, in many cases, it would be preferable to use the heating curve rather than the cooling curve in order to eliminate problems of supercooling. The trace obtained would be a mirror image of Fig.9. A more complex example of the use of DTA is shown in Fig.9. The system considered is a binary system exhibiting incongruently and congruently melting compounds and solid solution, eutectic and liquidus reactions. The first step in constructing the binary phase diagram from the information given by the DTA/DSC traces is to draw a curve through the temperatures of the highest temperature peaks on the traces; this will represent the liquidus curve. Having obtained the liquidus curve, then one should look for evidence of the presence of any isotherms, indicated by sharp peaks at the same temperature in different traces. From the shape and size of the peaks in different traces it is possible to designate the peaks for the eutectic and peritectic reactions as shown in Fig. 10.

Temperature calibration of the DTA or DSC instrument in the range of investigation using standard metals must be carried out as a function of heating rate to ensure accuracy of

the temperatures being determined. In the study of phase transformations which are sluggish, reversibility of transformation is to be ascertained by recording preliminary heating and cooling runs. In such cases, the samples must be temperature annealed for sufficient time insitu at temperatures closer to the transformation temperature and then start the heating runs. The reproducibility of the transformation temperature must be checked by this procedure.

References:

1. A. Reisman, Phase equilibria, Academic Press, New York, 1970

2. A.P. Gray, Perin-Elmer Corporation, Technical note.

3. B. Wunderlich, Differential Thermal analysis, Academic Press, New York, 1990

4. A. R. West, Solid State Chemistry and its Applications, John Wiley & Sons, New York, 1984

5. G.G. Chernik, Thermochimica Acta, 220 (1993) p. 37

6. S.Glasstone, Physical Chemistry Text Book

X-Ray Diffraction Technique for the Measurement of Thermal Expansion

K.V. Govindan Kutty and R. Asuvathraman

Liquid Metals & Structural Chemistry Division, Chemistry Group,
Indira Gandhi Centre for Atomic Research, Kalpakkam – 603 102,
Tamil Nadu, INDIA

Dr. K.V. Govindan Kutty took his M.Sc. and Ph.D degrees in Chemistry from Indian Institute of Technology, Madras. He graduated from the 21st Batch of the BARC Training School and joined IGCAR in 1978. He has been working in the area of materials synthesis and characterizarion. He is presently the Head of Solid State Chemistry Section of the Liquid Metals and Structural Chemistry Division. His research interests are novel synthesis of materials, ceramic matrices for radioactive waste immobilization, and thermophysical properties of materials.

Shri. R. Asuvathraman obtained his M.Sc. degree in Chemistry from University of Madras and M.Sc.(Engg.) degree in Metallurgy from Indian Institute of Science, Bangalore. He graduated from the 29th Batch of the BARC Training School and joined IGCAR in 1986. He has been working in the area of materials characterizarion using high temperature X-ray diffraction. His research interests are x-ray Rietveld analysis, novel synthesis of materials, ceramic matrices for radioactive waste immobilization and thermophysical properties of materials.

Introduction

Powder X-ray diffraction (XRD) is the most powerful technique for the identification of different materials (phases) present in a sample. It is based on the fact that each (crystalline) material crystallizes in a particular crystal structure characteristic of that phase, giving rise to a unique x-ray diffraction pattern. Thus, identification of materials by XRD is like identification of individuals by finger-print. XRD technique has the additional advantage that it requires only very little (< 50 mg) sample and is a non-destructive technique. Excellent books are available on this technique[1,2] and only a brief description is given below. High-temperature XRD is a convenient method for the measurement of thermal expansion of materials, by measuring the lattice constants at different temperatures. This is illustrated with examples in the following sections, and at the end, this technique is compared with the dilatometric method of measuring thermal expansion in the case of bulk solids.

Principle of XRD

In crystalline solids atoms of the constituent elements are present in periodic arrangements in three dimensions (3D) called crystal lattice. This 3D arrangement can be represented by the smallest repeating unit called unit cell. The unit cell is characterized by the six lattice parameters, viz., three axial repeat lengths and three inter-axial angles. Fig.1 gives the crystal structure of sodium chloride (common salt, NaCl). It is basically a cubic close packed structure wherein sodium ions are present at all the corners and face centres and chloride ion is present at all the edge centres and body centre. Thus each sodium ion is

surrounded by six chloride ions as the nearest neighbour forming an octahedran and similarly each chloride ion is surrounded by six sodium ions. There are four NaCl formula units in each unit cell. Several such unit cells are stacked together along the three axes **a**, **b** and **c** to form the grain (powder particle) of common salt.

The periodic arrangement of atoms in the crystal is represented by a set of crystallographic planes in the crystal which are identified by their Miller indices (hkl). The Miller indices of a plane is the inverse of the intercept at the three crystallographic axes expressed in whole numbers. In Fig.1 the crystallographic planes (111) and (200) are shown. The (111) plane intercepts the a, b and c axes at 1 where as the (200) plane incepts the a axis at ½ and is parallel to b and c axes i.e., intercept is infinity. Planes with same Miller indices in each unit cell of a crystal will be pararell. X-ray diffraction occurs by the scattering of x-rays from these sets of planes under certain conditions that leads to constructive interference of the scattered x-rays from each atom. Fig.2 describes the condition for x-ray diffraction from all the parallel planes in the crystal with a particular Miller index. The inter-planar distance d is the perpendicular distance between adjacent planes. The scattered x-rays from the planes will interfere constructively only when the path difference is an integral multiple of the x-ray wavelength. This condition leads to the Bragg's law for x-ray diffraction namely

$$n \lambda = 2 \, d_{hkl} \, Sin\theta_{hkl}$$

Fig.1 The crystal structure of sodium chloride (NaCl)

$\theta, 2\theta$ – Bragg angles

$2\Delta = 2d_{hkl} \sin\theta$ – path difference

$2\Delta = n\lambda$ – constructive interference
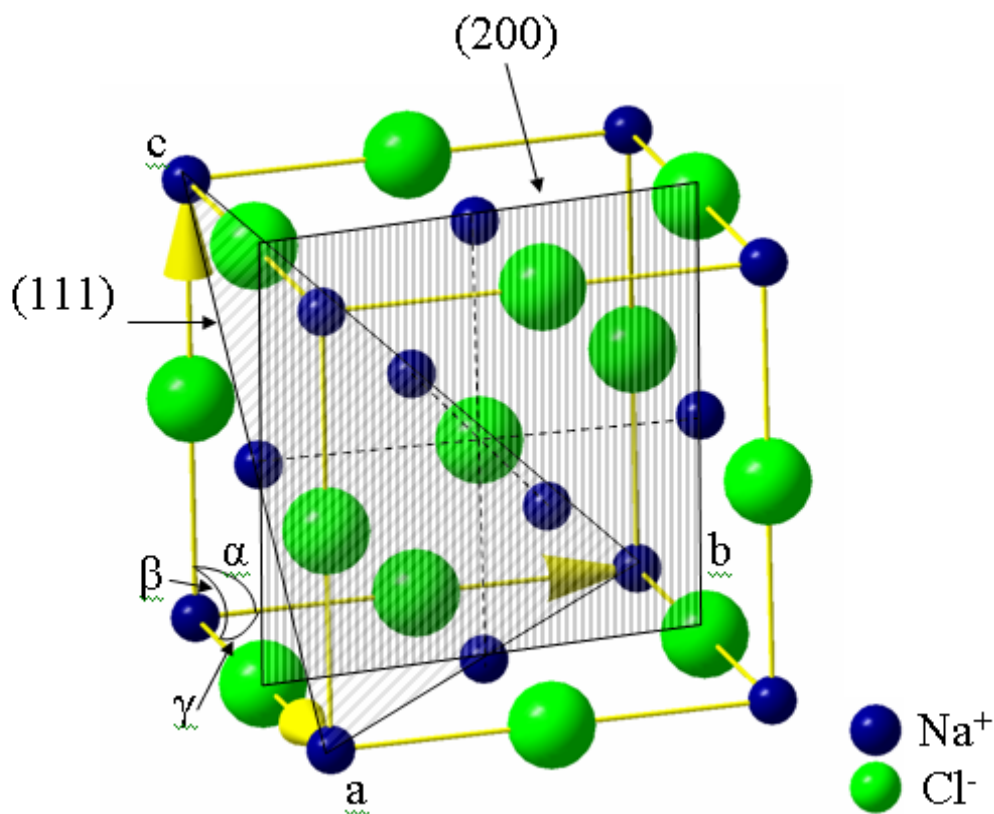
Braggs' law: $n\lambda = 2d_{hkl} \sin\theta_{hkl}$
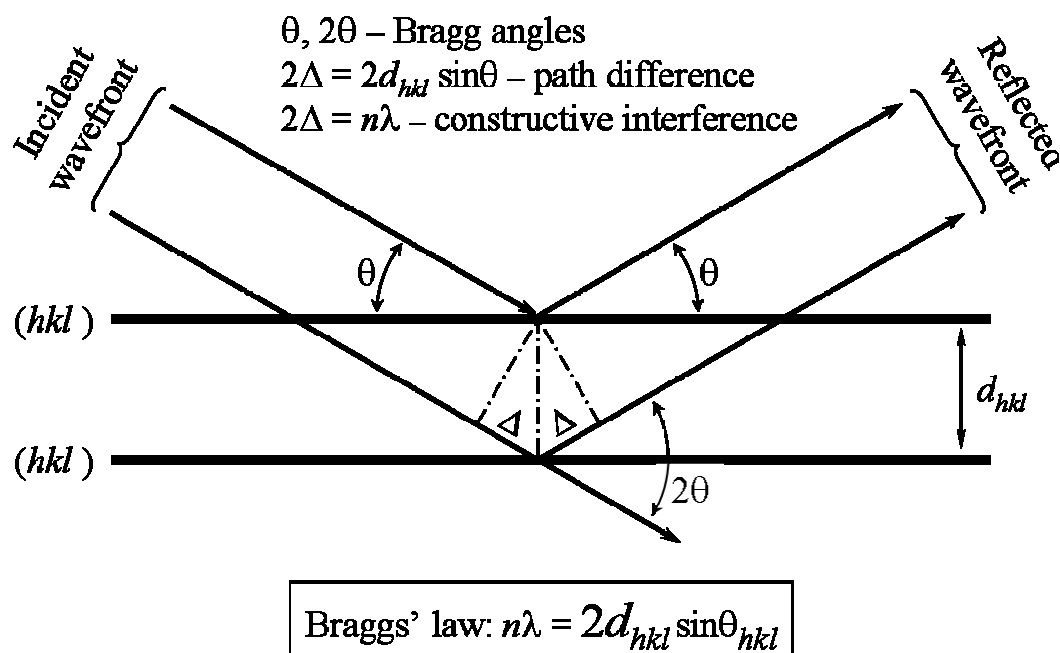
Fig.2 Bragg condition for x-ray diffraction by the crystallographic planes of Miller indices (hkl)

where n is the order of diffraction, λ is the wavelength of the x-ray used d_{hkl} is the inter-planar distance for the set of parallel planes with Miller index (hkl) and θ_{hkl} is the glancing angle also called the Bragg angle of diffraction. Thus each (hkl) plane will give a diffraction peak at a particular Bragg angle. It can be seen from the Bragg equation that the wavelength of x-ray used should be of the order of the inter-planar distances. The inter-planar distances in inorganic compounds are of the order of few Å and therefore Cu Kα radiation having a wavelength of 1.5418 Å is mostly used for powder diffraction analysis.

The x-ray powder diffractometer

Fig.3 gives the schematic of a modern powder diffractometer used for recording x-ray diffractograms of powder samples. In the modern diffractometers the sample is kept stationary at the centre of the goniometer with its top surface coinciding with goniometer axis. The focus of the x-ray tube and the receiving slit lie on the circumference of the measuring circle as shown in Fig.3. The x-ray tube and the detector are moved along the circumference of the measuring circle in such a way that they make equal angles with respect to the sample surface and this is called a $\theta - \theta$ diffractometer. Alternately, in some diffractometers, the x-ray tube will be stationary, and the sample carrier and detector will be rotating at a speed of 1:2 respectively (θ - 2θ diffractometer). The x-ray from the tube focus (F) before reaching the sample passes through a soller slit (SoS) and a divergence slit (DS). The soller slit, a set of equidistant parallel plates, limits the axial (perpendicular to the plane of the paper) divergence and the divergence slit (DS), an aperture, limits the in-plane divergence of the x-rays. The diffracted x-rays from the sample converges at the receiving slit after passing through a scatter slit (ScS). After the receiving slit the diffracted beam passes through a soller slit and falls on the monochromater (M) and then reaches the detector. The monochromater is a single crystal with constant d spacing and oriented at a particular angle to select x-rays of a particular wavelength used, mostly Cu Kα. The monochromater at the diffracted beam side also avoids any fluorescence radiation from the sample and there by reduces the background intensity. Mostly NaI(Tl) detector is used for detecting x-rays. In

the diffractometers generally the 2θ angle, the angle between the direct incident x-ray beam and the diffracted beam, is measured as shown in Fig.2.
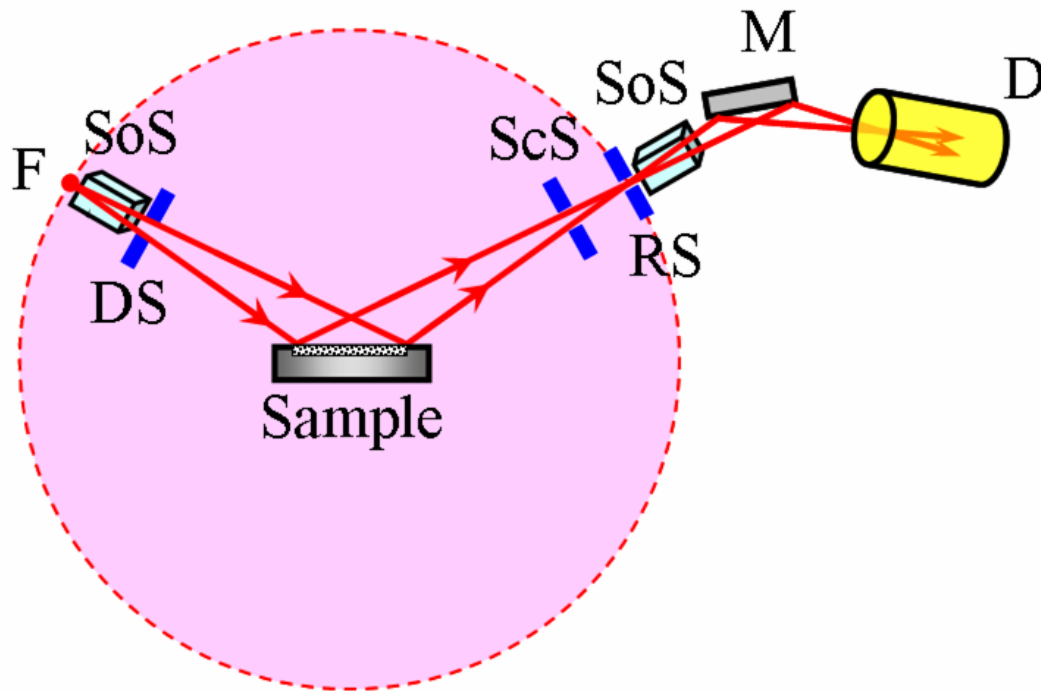

Fig.3 Schematic of a modern x-ray powder diffractometer

The x-ray powder diffraction pattern

To get good diffraction pattern the powders of the sample specimen should be ground in a pestle and mortar to a particle size of 10 μm to 50 μm. A small amount (~ 50 mg) of the powder is placed on a zero background quartz plate (specially prepared single crystal quartz plate) and spread into a thin layer using a few drops of volatile binder liquid. Digitized x-ray diffraction patterns are recorded in the step scanning mode in the range of say, 10 to 80° 2θ with a step size of 0.05° 2θ and 1 s counting time at each step. The data is processed using computer programs to get peak positions and intensities. In most cases, this powder diffraction pattern is enough to identify the material.

The peak positions (2θ) give information about the shape and size of the crystal unit cell (a, b, c, α, β, γ), the intensity gives information on the crystal structure (the way the atoms are arranged in the unit cell) and the peak shape (width) gives information about the grain size and strain. Lattice parameters are derived from the peak positions after indexing the peaks for their respective (hkl) Miller indices using computer programs. The equations connecting the interplanar spacing to the lattice parameters through the Miller indices in the case of different crystal systems can be found in standard texts on XRD.[1,2] The x-ray powder diffraction pattern of NaCl is given in Fig.4 along with the Miller indices for the peaks.
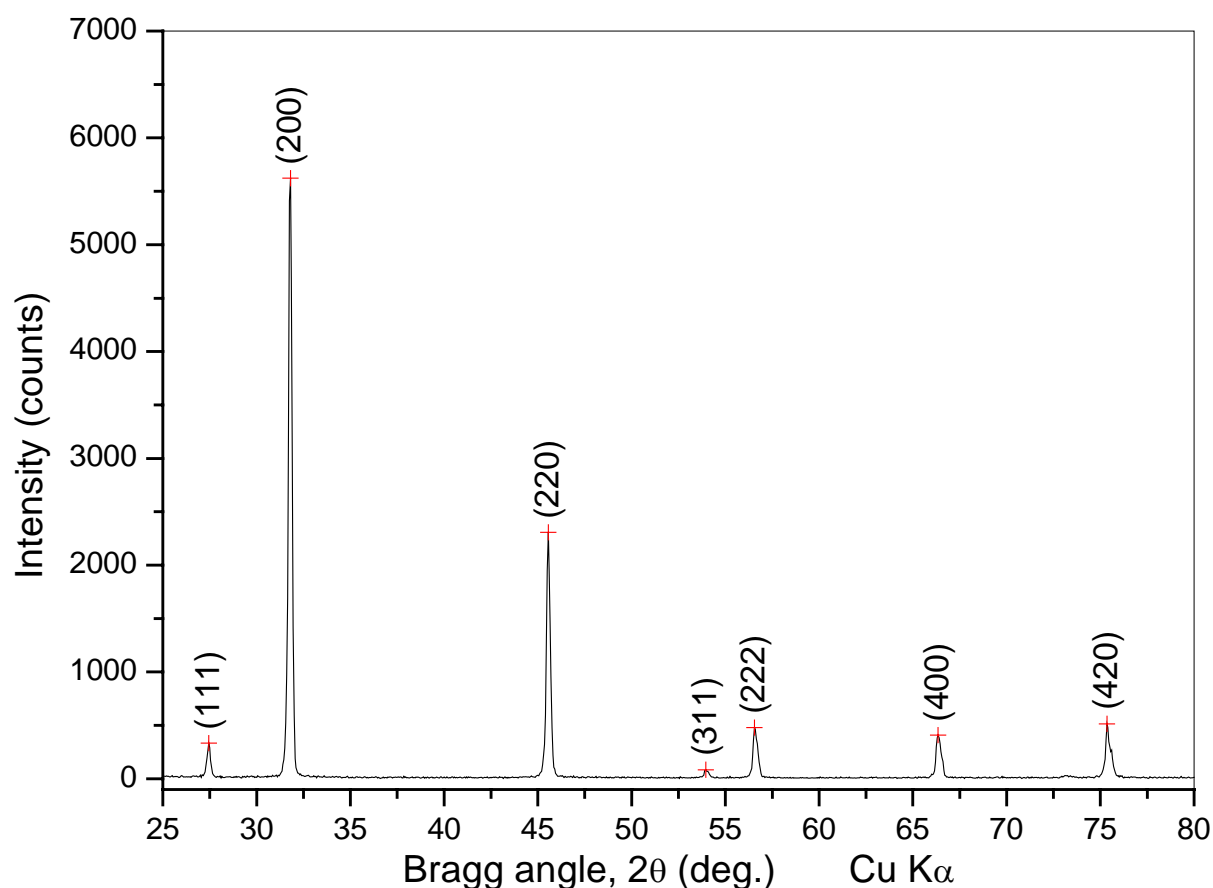
Fig.4 XRD pattern of sodium chloride (NaCl) powder

In Fig.5 the XRD pattern of platinum at room temperature (25°C) and at high temperature (1000°C) are compared. Three observations can be inferred from the figure: (i) the 2θ positions of the high temperature XRD pattern have shifted to lower angles, (ii) the intensity of the diffraction peaks at high temperature has decreased and the decrease in intensity is relatively higher at higher angles and (iii) the background is high for the high temperature XRD pattern and is distinctly high at higher angles (this is clearly shown in the inset of Fig.5). These differences are due to the fact that atoms in the crystal undergo thermal vibration about their mean position. The amplitude of this vibration increases as the temperature increases. Due to this increased thermal vibration the unit cell expands, causing changes in d spacing and therefore in the diffraction angles. Further the increased thermal vibrations have the effect of smearing out the lattice planes resulting in the imperfect reinforcement of the scattered x-rays and thereby reducing the intensity of the diffracted beam. This imperfect reinforcement also causes some general coherent scattering in all directions, called the thermal diffuse scattering, which increases the general background and its intensity increases with 2θ.
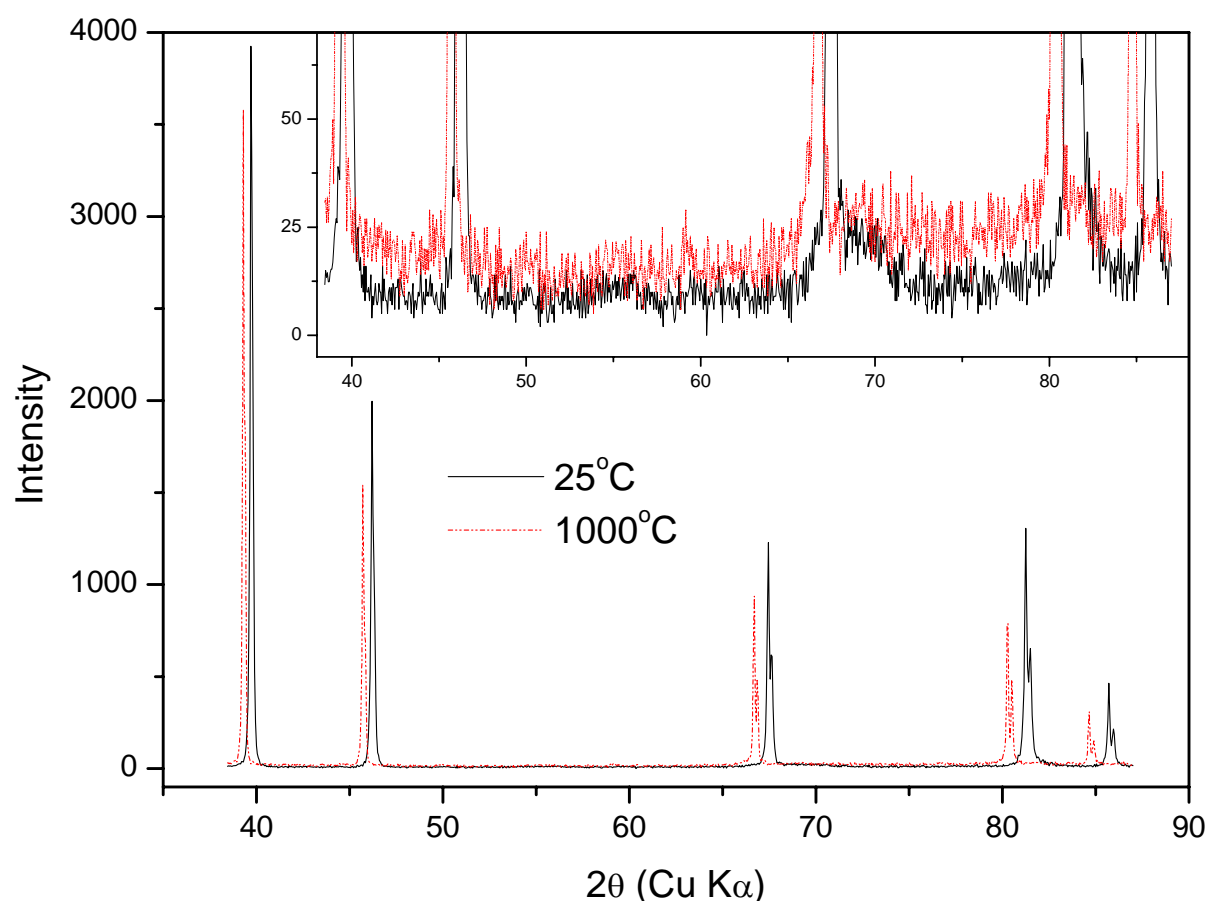
Fig.5 XRD pattern of platinum at room temperature (25°C) and at 1000°C. In the inset the background region is expanded.

Thermal expansion

The coefficient of thermal expansion, or thermal expansivity, is an important thermophysical property of materials. It is defined as the fractional change in length per unit rise in temperature. It governs the suitability of materials for many applications in research and industry. The theory and measurement methods of thermal expansion of solids have been discussed in detail in the literature.[3-5] Briefly, thermal expansion originates from the asymmetric nature of the potential energy curve against interatomic separation as given in Fig.6. Thus an increase in temperature increases the energy of longitudinal vibrations which results in an increase of the equilibrium distance, x, by an amount, Δx, as shown in Fig.6. Thus, the anhormonic vibrations of the atoms in the solid causes thermal expansion.
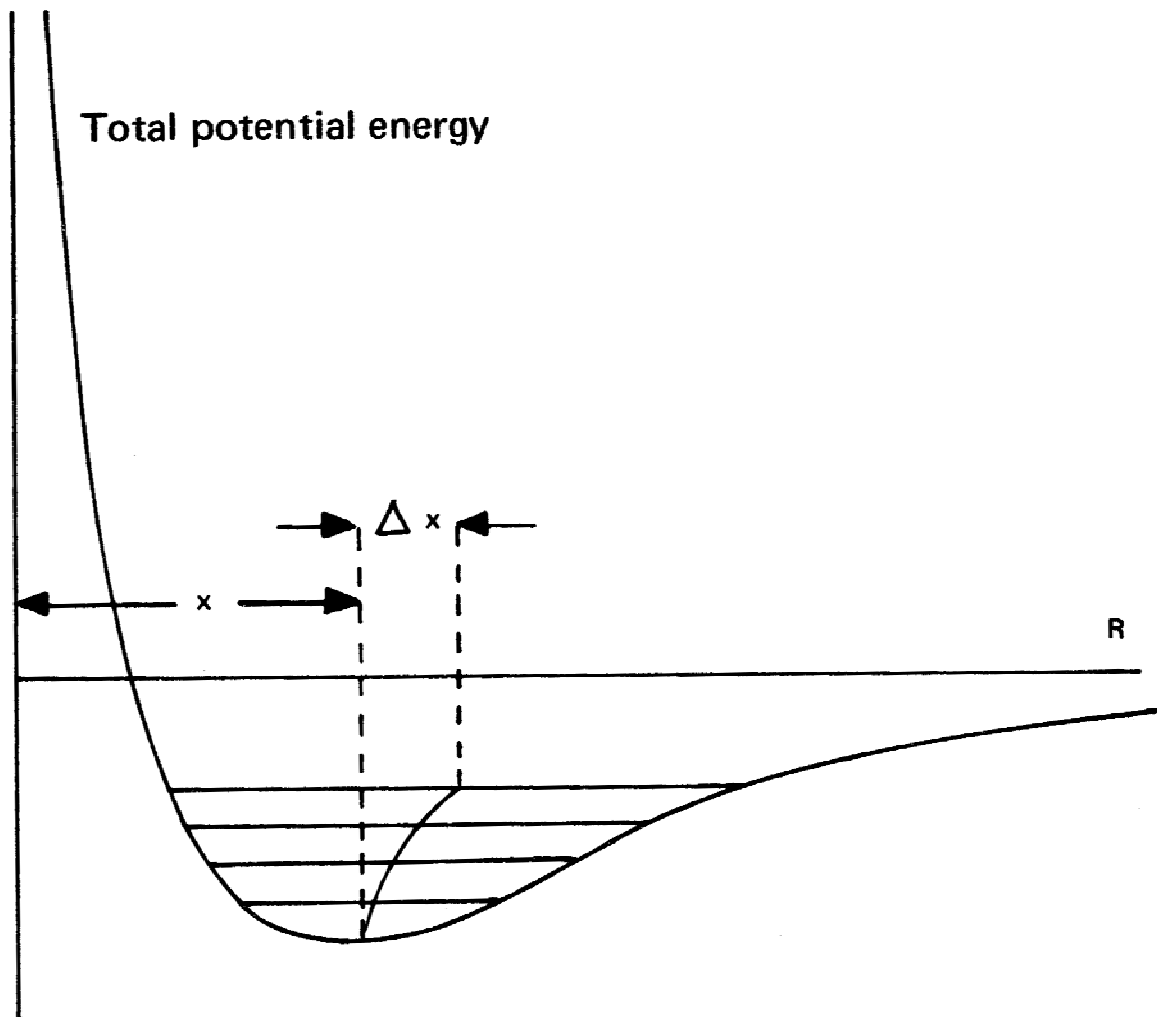
Fig.6 A typical potential energy curve for solids

The thermal expansion of crystals is related to their crystal structure and bonding strength of the atoms.[6] In layer type structures the expansion normal to the layer is relatively higher. For many cubic elements and binary compounds the thermal expansion has correlation with the melting point. The expansion along covalent bonds is small. The expansion of ionic and metallic bonds is relatively large and the expansion along van der Waals forces is even larger.

Thermal expansion is related to other thermophysical properties by the Gruneisen equation

$$\beta V = \gamma \chi C_p$$

where β is the volume expansion coefficient, V is the volume, γ is the Gruneisen constant, χ is the compressibility and C_p is the heat capacity. The Gruneisen constant is defined as

$$\gamma = -dln\nu / dlnV$$

where ν is the vibrational frequency. The Gruneisen constant is related to the anharmonicity of the pair potential; it is a measure of the strength of the anhormonic forces in the crystal.

High Temperature XRD

High temperature x-ray powder diffraction (HTXRD) is a convenient method for studying the thermal expansion behaviour of materials[3-5,7]. It is a micro-method of measurement, as opposed to macro-methods such as dilatometry on bulk solids. The expansion of the unit cell dimensions is measured here. The occurrence of thermally generated vacancies in the crystal at elevated temperatures does not, therefore, affect the expansion measurements. Only a small amount of material, often less than 50 mg, is enough for carrying out the experiment; or the specimen can be a small strip in the case of metal and alloy samples. The presence of small amounts of extraneous phases generally does not interfere with the measurements on the desired major phase. Additionally, thermal expansion measurements can be carried out along the different crystallographic axes in non-cubic systems. This enables an assessment of the thermal expansion anisotropy of the material; such anisotropy, in extreme cases, can lead to microcracking due to internal thermal stresses in the material, thus impairing its mechanical strength. The critical grain size before micro-cracking takes place in a material, has an inverse relationship with its thermal expansion anisotropy.[8,9]

HTXRD equipment

Fig.7 shows the schematic diagram of a typical HTXRD system. It shows the high temperature (HT) chamber attached to the goniometer of a vertical diffractometer. The HT attachment consists of a cylindrical, double-walled brass chamber provided with a gas-tight lid. A metallic strip held tight between two electrodes passing through the lid is situated at the centre of the chamber, and serves as the sample carrier. The powder sample is applied as a thin layer on the flat strip which is then electrically heated. The temperature is measured by means of a thermocouple spot-welded at the rear of the sample-carrying strip. The output of the thermocouple is also used to control the heating and cooling at programmed rates by means of a temperature controller. A beryllium window provided on the body of the cylindrical chamber allows the passage of the incident and diffracted x-ray beams. Through the annular space between the walls of the chamber, cooling water is circulated when the system is at high temperature. The chamber can be maintained at a vacuum or an inert atmosphere during experiments.

Measurement of thermal expansion from HTXRD experiments

In order to carry out thermal expansion measurements, the lattice parameters at different temperatures are calculated by determining the exact positions of high-angle reflections by step-scanning. The linear thermal expansion between the temperatures T_2 and a reference temperature T_1 (commonly the room temperature or 273 K) is then calculated as:

Thermal expansion (%) = 100 x $[a_2 - a_1] / a_1$

where a_2 is the lattice parameter at T_2 and a_1 that at T_1. The corresponding average linear thermal expansion coefficient (α) can be obtained by the expression:

$\alpha = [a_2 - a_1] / [a_1(T_2 - T_1)]$.

An instantaneous thermal expansion coefficient at a temperature T can also be defined as follows:

Instantaneous thermal expansion coefficient at T = $[1 / a_T] [da / dT]_T$

1. Detector
2. Detector slit
3. Focusing circle
4. Antiscatter slit
5. Beryllium window
6. Sample on resistor
7. High temp. chamber
8. Divergence slit
9. X-ray tube
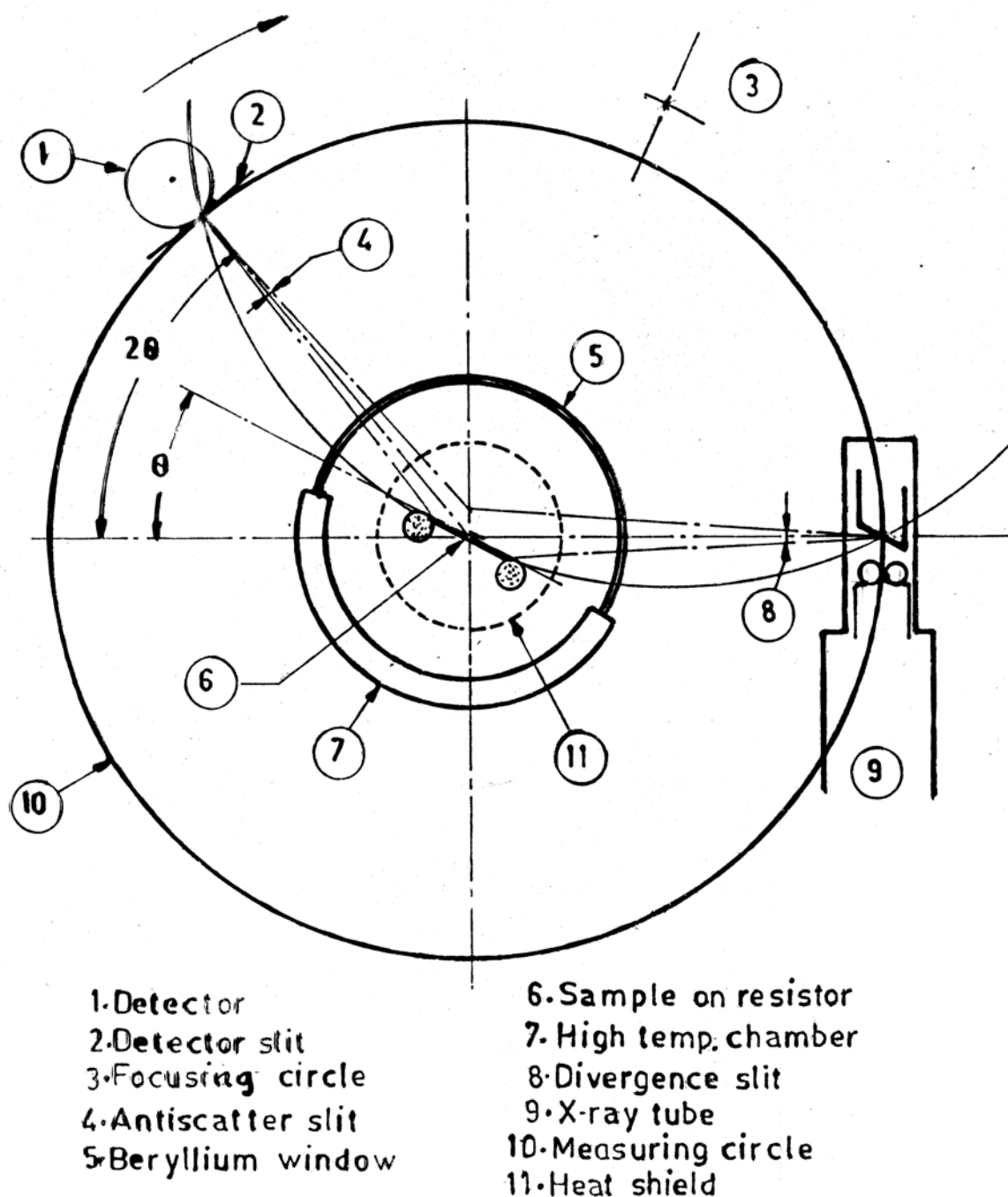10. Measuring circle
11. Heat shield

Fig.7 Schematic diagram of a High Temperature X-Ray Powder Diffractometer.

Thermal expansion studies on different materials by HTXRD: some examples

Thorium oxide:

Thorium dioxide, thoria (ThO_2), is one of the standards used in thermal expansion measurement. It has a face centred cubic structure with space group $Fm\overline{3}m$ and lattice constant a = 5.597 Å. The thermal expansion of ThO_2 measured in our lab using HTXRD (Panalytical X'Pert Pro MPD system with Anton Paar HTK16 high temperature attachment) is given in Fig.8. In Fig.8a the lattice parameter variation as a function of temperature is given and in Fig.8b the percentage of linear thermal expansion is plotted against temperature along with that measured (using HTXRD) by Belle and Berman.[10] The lattice parameter

varies from 5.601 Å at room temperature (RT) to 5.649 Å at 1200 K. The precision on the measurement of lattice parameter is ± 0.0005 Å. Between RT and 1200 K, the linear thermal expansion is about 0.842%. This corresponds to an expansion coefficient of 9.33×10^{-6} K^{-1}.
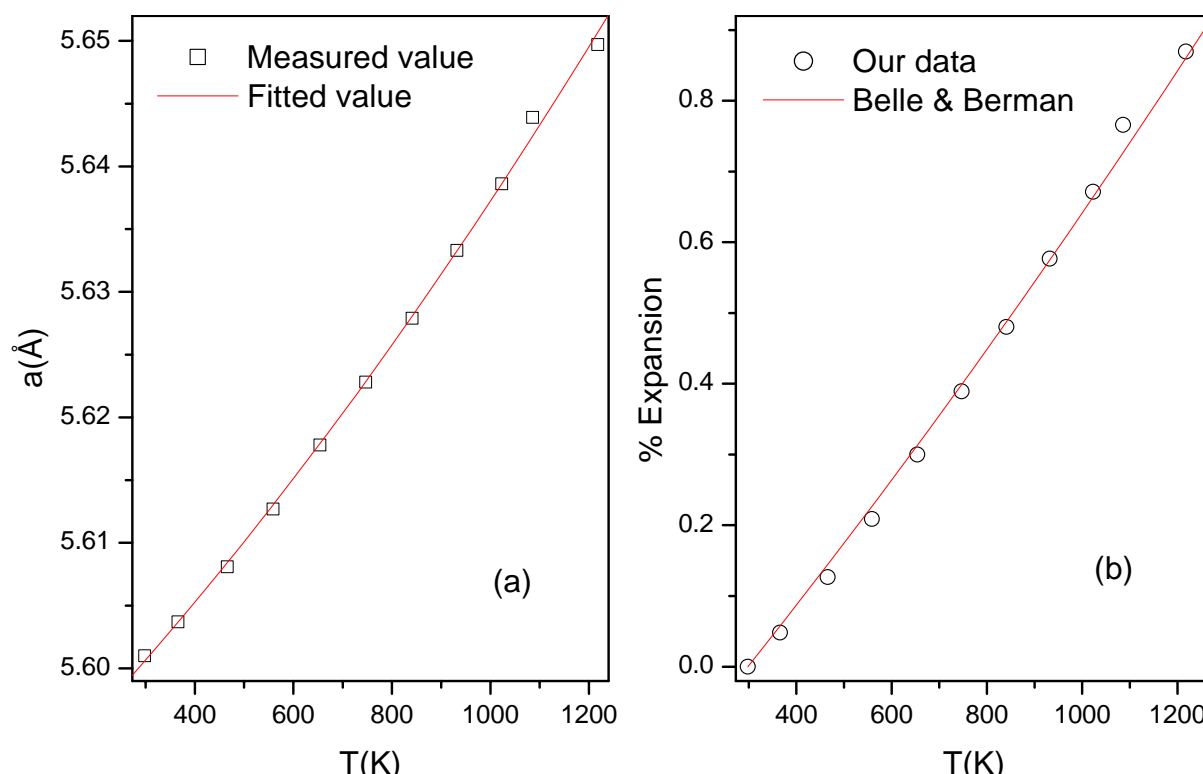
Fig.8 Linear thermal expansion of ThO_2, (a) lattice parameter versus temperature, (b) percent expansion versus temperature.

NZP compounds:

Sodium zirconium phosphate [$NaZr_2(PO_4)_3$, NZP] is the typical member of a family of isostructural compounds crystallizing with a rhombohedral - hexagonal structure (space group $R\bar{3}c$), built up of a flexible framework of corner-sharing ZrO_6 octahedra and PO_4 tetrahedra.[11] The three-dimensionally linked interstitial space so created is partially occupied by sodium. The compounds are characterized by low and controllable thermal expansivity and sodium ion conductivity. The phase is amenable to a wide variety of chemical substitutions, and is thus a potential crystalline matrix for nuclear waste immobilization. Under thermal stresses, the crystal expands anisotropically; it expands along the hexagonal c-axis and contracts along the a-axis. The average expansivity, as per the formula given below, becomes very low because one of the terms is negative.

Average linear expansivity $(\alpha) = -(2/3)\ \alpha_a + (1/3)\ \alpha_c$

This kind of axial expansion is brought about by bond angle distortions in the crystalline framework; the ZrO_6 and PO_4 polyhedra undergo coupled rotation under the stress created by the large thermal expansion of the Na – O bond[12]. The bonds within the polyhedra exhibit nigligible expansion[13]. Fig.9 depicts the axial expansion behaviour of $Na_2Hf_2(PO_4)_3$.[14] Between the room temperature and 1273 K, the expansion coefficient along the crystallographic a-axis is $- 6.5 \times 10^{-6}$ K^{-1} and that along the c-axis is $+ 18.3 \times 10^{-6}$ K^{-1}; the average expansivity of a polycrystalline sample thus works out to be $+ 1.8 \times 10^{-6}$ K^{-1}. This is the typical expansion behaviour of an NZP compound. It is controlled by the concentration,

size, and the crystallographic site occupancy of the interstitial ion. However, in some compounds, the framework ions play a dominant role, an example of which is $NbSn(PO_4)_3$. The d electron subshell of the tetravalent tin ion is fully filled, and it becomes easy to bend and distort the Sn – O – P bonds, so much so that the room temperature space group of the compound is $R\bar{3}$ (against $R\bar{3}c$ of a typical NZP compound); this structure is a little more close-packed than the NZP structure. Fig.10 displays the axial expansion of this compound. Expansion along the a-axis is the predominant thermal effect at temperatures up to 650 K; under this stress, a contraction takes place along the c-axis. At about this temperature, thermal agitations open up the structure and the space group transforms to $R\bar{3}c$, typical of NZP; thereafter, the crystal expands along the hexagonal c-axis and contracts along the a-axis.
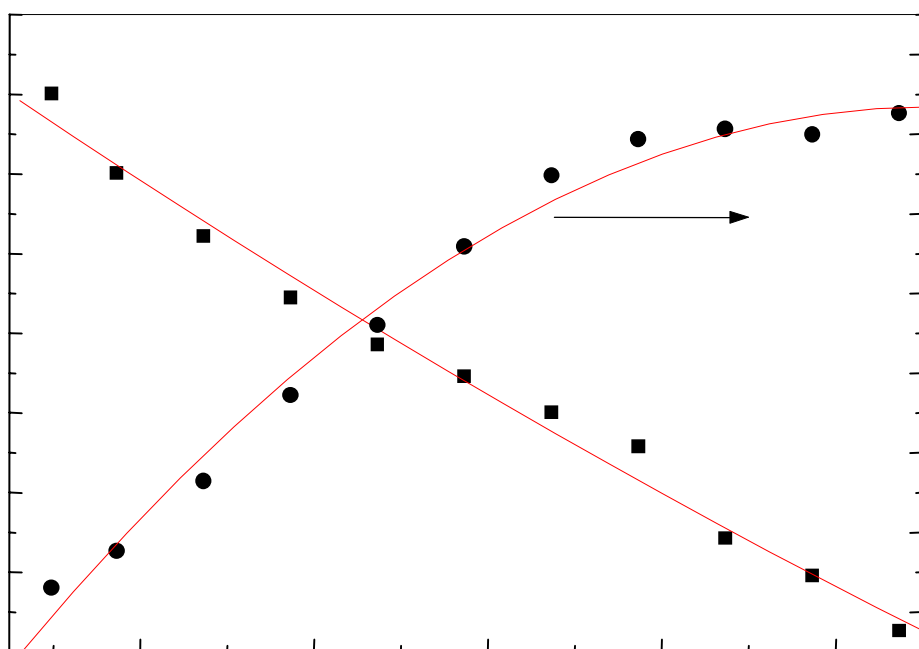
Fig.9 Axial expansion behaviour of $NaHf_2(PO_4)_3$.

The axial thermal expansion of NZP compounds can be controlled by altering the framework and interstitial composition of the ions. This also enables us to control the axial thermal expansion anisotropy (maximum difference in the axial expansivities) of the materials. Table 2 illustrate this with a series of NZP compounds. It shows that $Ca_{1/2}Zr_2(PO_4)_3$ and $Ca_{1/2}Hf_2(PO_4)_3$ have low average thermal expansivities between room temperature and 1273 K[15], but they are also characterized by high expansion anisotropy; whereas $Sr_{1/2}Zr_2(PO_4)_3$ and $Sr_{1/2}Hf_2(PO_4)_3$ are characterized by low expansivity and low anisotropy.

Metal and alloy samples:

Metals and alloy samples in the form of thin flat strips can be directly connected to the electrodes of the high temperature XRD chamber and heated. The thermal expansion of the alloy permandur (49Fe – 49C0 – 2V) measured by this method is shown in Fig.11. The sample exhibits the XRD pattern of α - iron (BCC). Table 3 lists the measured lattice

parameters of the material at different temperatures. At 873 K, the thermal expansion with respect to the room temperature is about 0.6 %; this amounts to a linear thermal expansion coefficient of 10.6 x 10^{-6} K^{-1} in this temperature interval.[16]

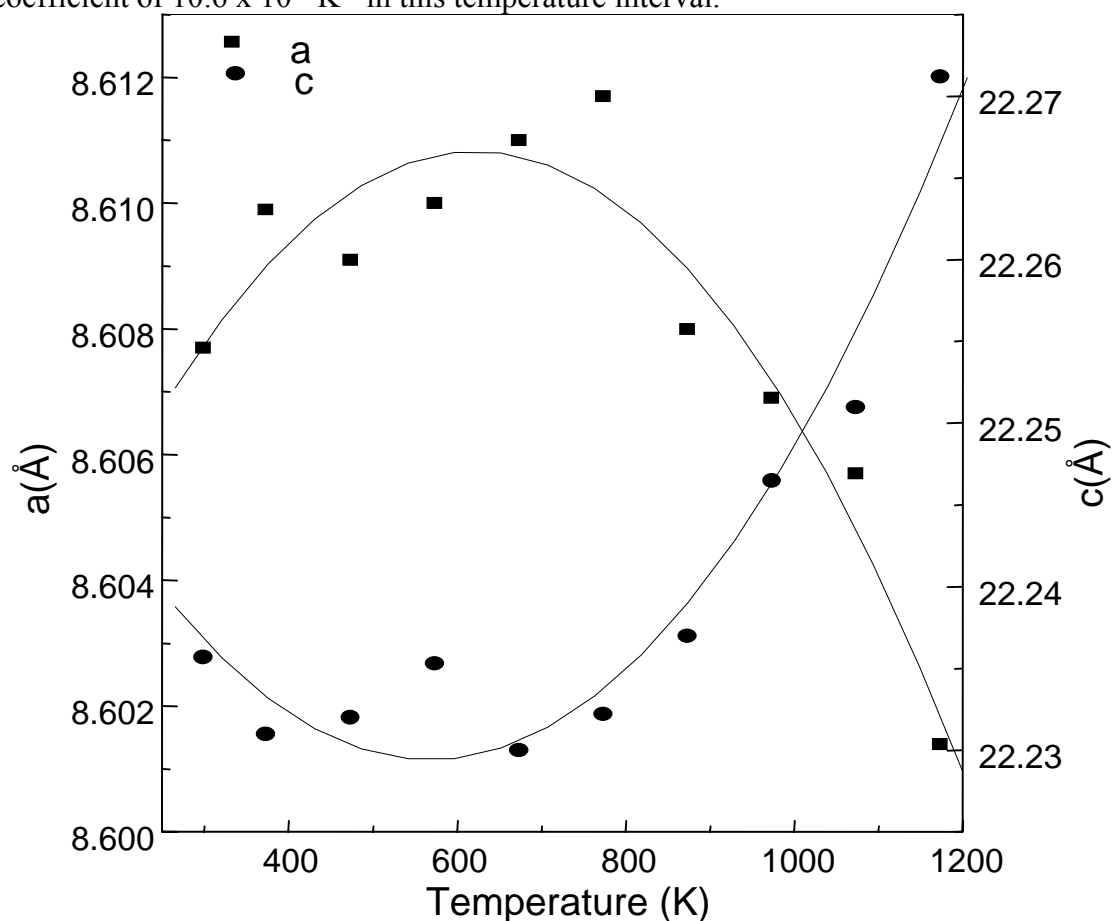**Fig.10** Axial expansion behaviour of $NbSn(PO_4)_3$.

Table 2 Axial expansion behaviour of $A_{1/2}M_2(PO_4)_3$ [A = Ca, Sr; M = Ti, Zr, Hf, Sn] in the temperature range 298 – 1273 K

Compound	α_a x 10^{-6} K^{-1}	α_c x 10^{-6} K^{-1}	α_{vol} x 10^{-6} K^{-1}	$\alpha_{av} = \alpha_{vol}/3$ x 10^{-6} K^{-1}	$\lvert \alpha_a - \alpha_c \rvert$ x 10^{-6} K^{-1} Anisotropy
CaZrP	-2.57	7.74	2.55	0.85	10.31
SrZrP	2.24	2.28	6.65	2.22	0.04
CaHfP	-3.29	7.52	0.92	0.31	10.81
SrHfP	1.66	1.67	5.01	1.67	0.01
CaTiP	6.99	1.31	15.41	5.14	5.68
SrTiP	9.88	-0.14	19.73	6.58	9.74
CaSnP	8.95	2.05	20.05	6.68	6.90

SrSnP	8.07	0.50	16.88	5.63	7.57
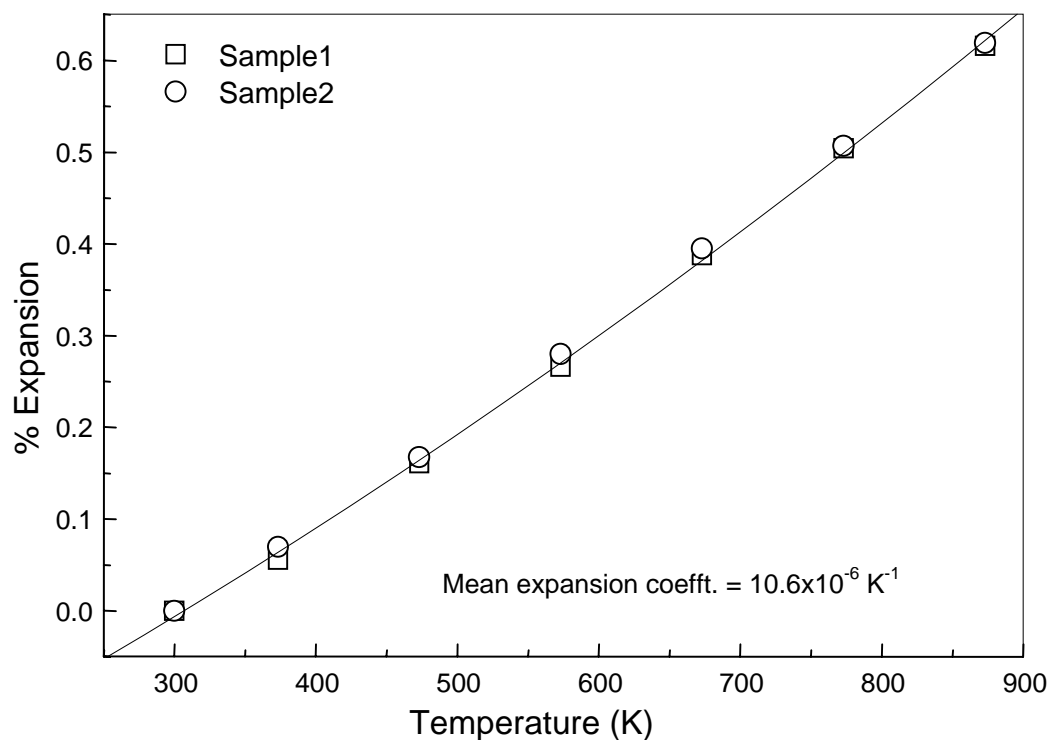
Fig.11 Thermal expansion behaviour of permandur alloy.

Table 3 Lattice thermal expansion of permandur

Temperature (K)	Lattice Parameter (Å) ± 0.0005 Å
298	2.8593
373	2.8609
473	2.8639
573	2.8669
673	2.8704
773	2.8739
873	2.8769

The lattice expansion of nickel[17] about its ferromagnetic-to-paramagnetic transition at ~ 630 K as measured by HTXRD is given in Fig.12. The λ-type anomaly marking this transition could be seen clearly in the variation of the linear thermal expansion coefficient with temperature.

Experimental Limitations in HTXRD

The main experimental difficulties in HTXRD are sample displacement from the focussing circle, accuracy of the measured sample temperature owing to heat losses, and temperature gradients through the sample.[18,19] Due to the thermal expansion of the thin heater strip (which also carries the sample), sample displacement from the x-ray para-focussing geometry can occur. This would alter the reflection angles and lead to erroneous lattice parameter values. This problem can be avoided by first going to a higher temperature and then coming down to the desired temperature. In some equipment, we will be able to rotate the electrodes slightly and make the strip taut after reaching the required temperature. Temperature gradients across and through the sample can be minimized by employing a very thin sample layer. To avoid heat losses from the heater strip, some high temperature XRD chambers will be equipped with a surroundings heater around the sample. This is very effective in minimizing the temperature gradients in the sample. When the surroundings heater is not provided, the heat losses can be significant. In such cases, a temperature calibration can be made by measuring the thermal expansion of standard substances like MgO with the equipment.
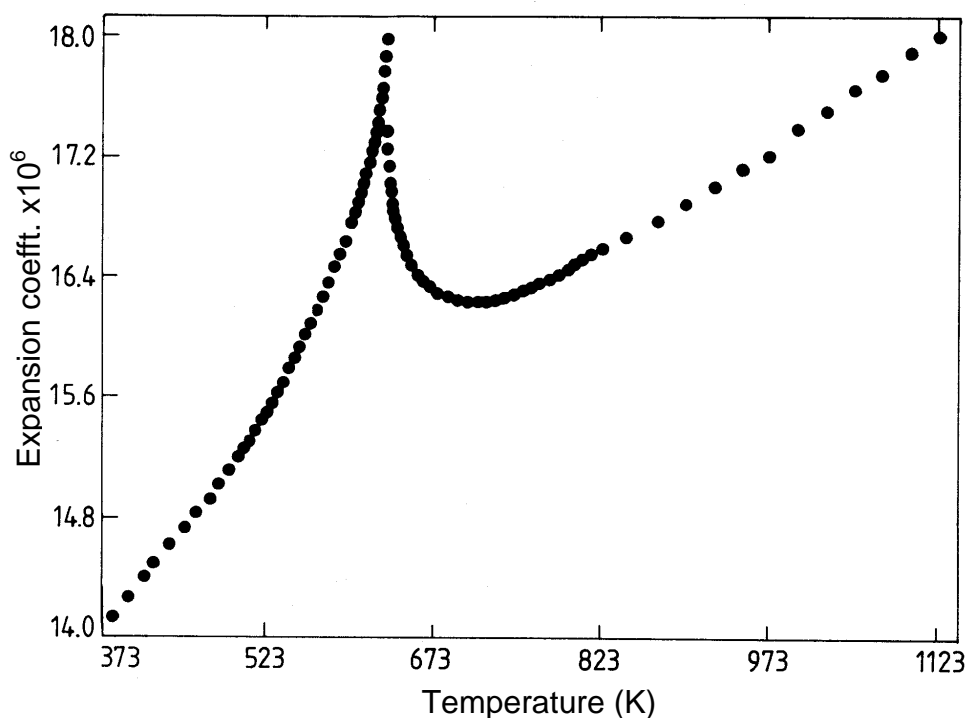
Fig.12 Thermal expansion of nickel about the Curie magnetic transition.

The errors in thermal expansion measurement mainly depend on the precision of the lattice parameter values and the magnitude of the thermal expansion coefficient.[20] Since the change in the unit cell dimension is a difference between two nearly equal quantities, it can be known accurately only if the individual lattice dimensions are measured with high precision. Depending on the expansion coefficient of the material, the change in length also varies. McKinstry et al. have worked out the expected error in the measured thermal expansion coefficients of various ranges by assuming a typical precision of 0.0001 Å in lattice parameter measurement; for a material of initial lattice parameter 5 Å and having a thermal expansion coefficient of 10×10^{-6} K^{-1}, the error is 4 % if the temperature difference is 100 K. The error is a few % for high expansivities, but it is higher for low expansivity

systems. In general, the method of high temperature XRD is sufficiently accurate for meaningful thermal expansion measurements on materials in research and industry.

Comparison of thermal expansion measurement by HTXRD and bulk dilatometry

The other technique that is widely used for the measurement of thermal expansion of solids is the push rod dilatometer. This method is simple, sensitive and reliable for practical use and academic research. In this method a rod or tube made of low expansion material is used to convey the change in length of a specimen (pellet or compact body) at high temperature to the displacement sensor kept at or near room temperature. The schematic and photograph of such a dilatometer system[21] is shown in Fig.13.

Dilatometry is a macroscopic technique as it probes the overall dimension of the specimen, whereas HTXRD is a microscopic technique as it probes the unit cell dimensions. High-density pellet of at least 10 mm length is required for dilatometry. Presence of phase impurities will interfere with the thermal expansion of the major phase.
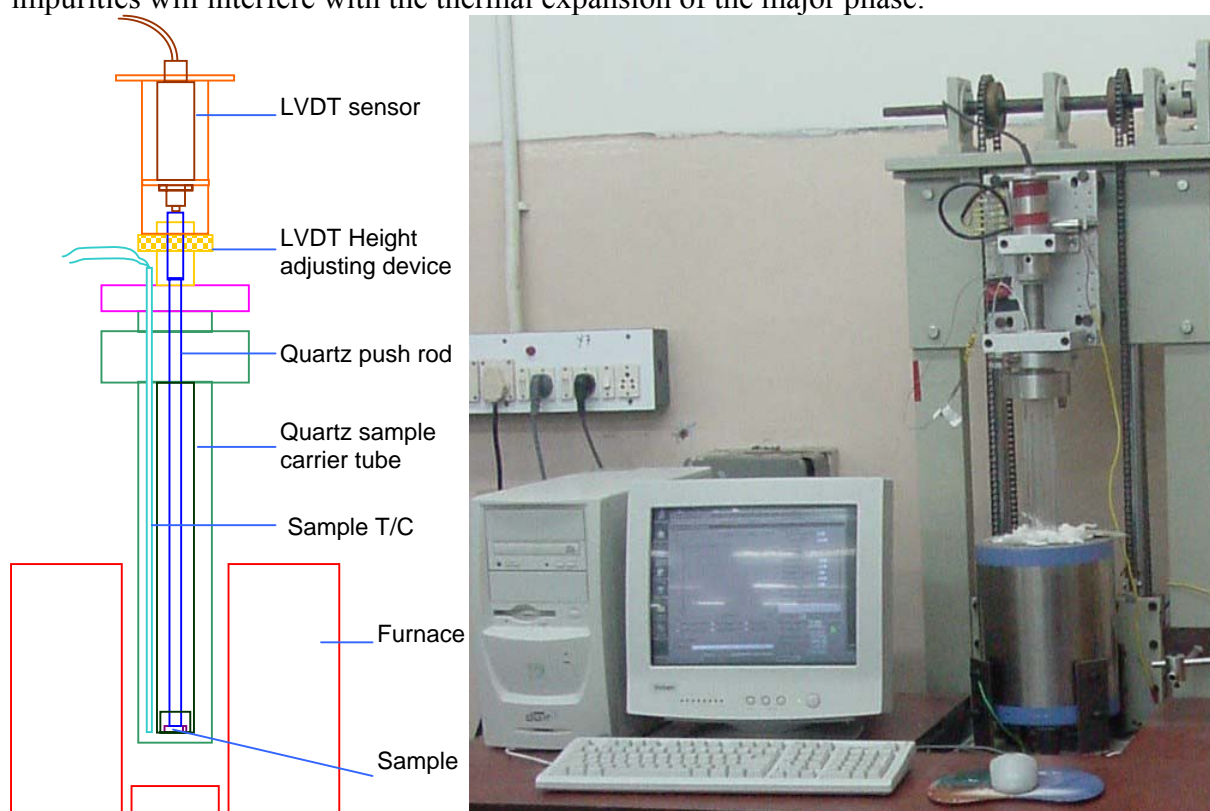
Fig.13 Schematic and photograph of a push rod dilatometer system.

In Fig.14 the thermal expansion of a high density thoria pellet (12 mm diameter and 10 mm long) measured in our lab using a quartz push rod dilatometer built in-house is compared with that measured using HTXRD. In this temperature range no appreciable difference is seen between the two measurements. But at high temperatures, near the melting point, the thermal expansion value measured by dilatometer will be higher than that measured by HTXRD. This is so, because at high temperatures the thermally created vacancy concentration will be high. These thermally created vacancies will have influence on the overall dimension, but not on the unit cell dimension. One such example of platinum thermal expansion measured by HTXRD and dilatometry is given in Fig.15.[22] The difference

between the measurements is clearly seen in the inset of Fig.15. From this thermal expansion difference the vacancy concentration can be estimated and from which the entropy and enthalpy of vacancy formation can be determined.
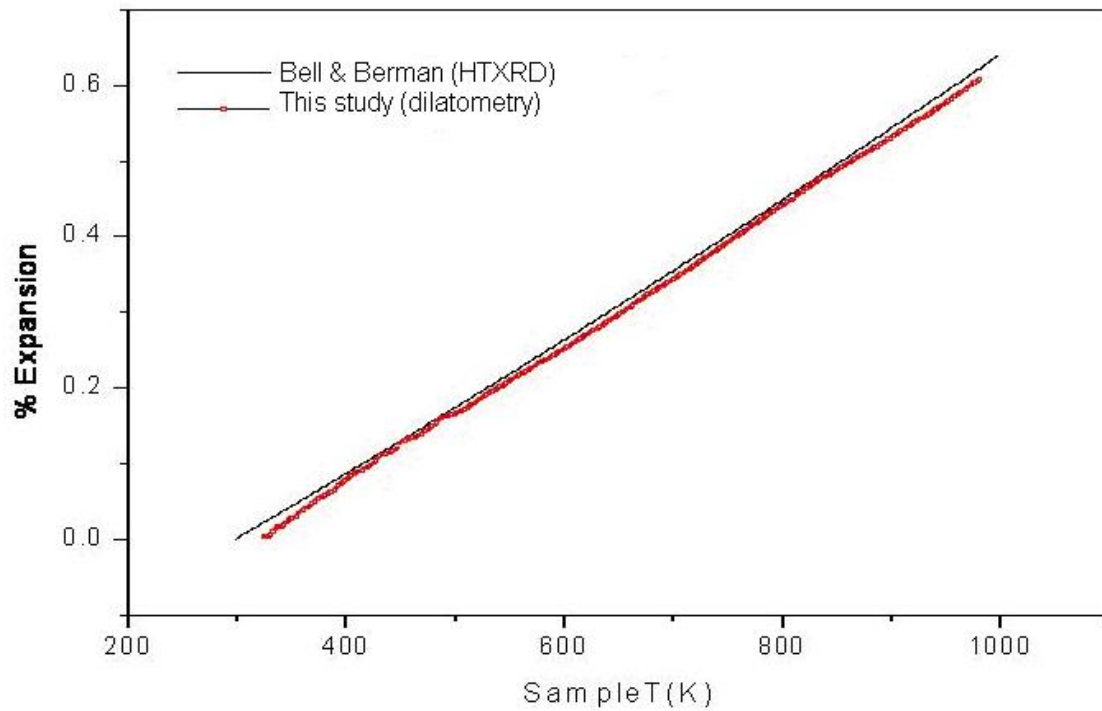

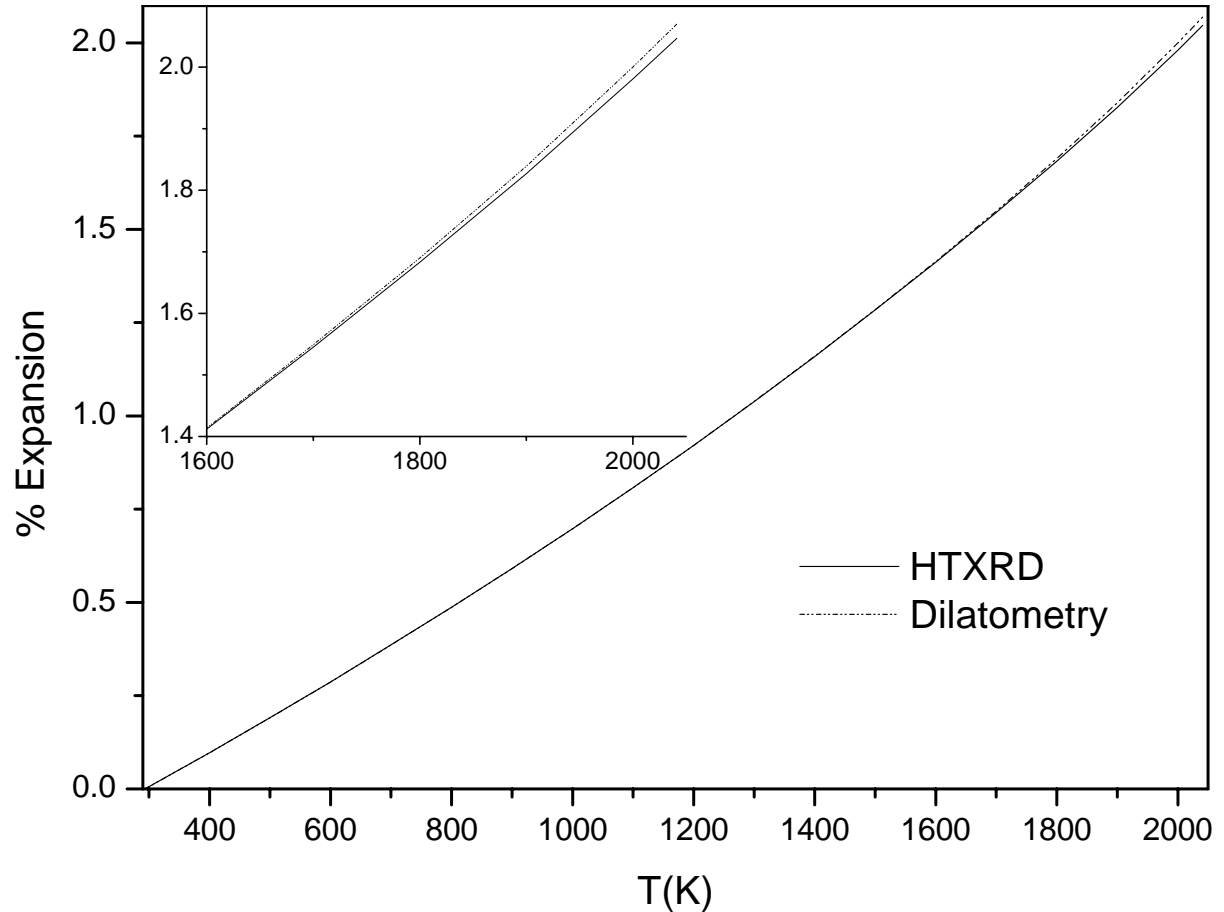**Fig.14** Linear thermal expansion of thoria (ThO$_2$) measured using dilatometer.

Fig.15 Thermal expansion of platinum measured by HTXRD and dilatometry. The inset shows the region of very high temperature.

References

1 V.K. Pecharsky and P.Y. Zavalij, Fundamentals of Powder Diffraction and Structural Characterization of Materials, Kluwer Academic Publishers, 2003.

2 B.D. Cullity, Elements of X-ray Diffraction, Second Edition, Addison-Wesley, 1978.

3 C.Y. Ho (ed.), Thermal Expansion of Solids, ASM International, Materials Park (1998).

4 R.S. Krishnan, R. Srinivasan and S. Devanarayanan, Thermal Expansion of Crystals, Pergamon Press, Oxford (1979).

5 B.Yates, Thermal expansion, Plenum Press, New York, (1972).

6 C.H. Macgillavry and G.D. Rieck, International tables for x-ray crystallography Vol. III: Physical chemical tables, 2nd edition, International Union for Crystallography, (1968)125.

7 R.K. Kirby, in Compendium of Thermophysical Property Measurement Methods, Vol. 2. Recommended Measurement Techniques and Practices, ed. K.D. Maglic, A. Cezairliyan and V.E. Peletsky, Plenum Press, New York, (1992)549.

8 I. Yamai and T. Ota, J. Am. Ceram. Soc. 76(1993)487.

9 S. Senbhagaraman and A.M. Umarji, J. Solid State Chem. 85(1990)169.

10 J. Belle, in Thorium Dioxide: Properties and Nuclear Applications, ed. J. Belle and R.M. Berman, Govt Printing Office, Washington, D.C. (1984)167.

11 T. Oota and I. Yamai, J. Am. Ceram. Soc. 69(1986)1.

12 G.E. Lenain, H.A. McKinstry, J. Alamo and D.K. Agrawal, J. Mater. Sci. 22(1987)17.

13 R.M. Hazen, L.W. Finger, D.K. Agrawal, H.A. McKinstry and A.J. Perrotta, J. Mater. Res. 2(1987)329.

14 K.V. Govindan Kutty, R. Asuvathraman, C.K. Mathews and U.V. Varadaraju, Mater. Res. Bull. 29(1994)1009.

15 K.V. Govindan Kutty, R. Asuvathraman and R. Sridharan, J. Mater. Sci. 33(1998)4007.

16 K.V. Govindan Kutty, S. Rajagopalan and C.K. Mathews, unpublished results.

17 Mohammad Yousuf, P.Ch. Sahoo, H.K. Jajoo, S. Rajagopalan and K. Govinda Rajan, J. Phys. F: Met. Phys. 16 (1986)373.

18 S. Rajagopalan, K.V.G. Kutty, H.K. Jajoo, S.K. Ananthakrishnan and R. Asuvathraman, Thermal expansion and phase transformation studies on some materials by high temperature x-ray powder diffractometry, IGC-96, Indira Gandhi Centre for Atomic Research, Kalpakkam (1988).

19 D.D.L. Chung, P.W. DeHaven, H. Arnold and Debashis Ghosh, X-ray Diffraction at Elevated Temperatures: a method for in situ process analysis, VCH Publishers, New York (1993).

20 H.A. McKinstry, C.Y. Huang and H.T. McKinstry, in Thermal Expansion of Solids, ed C.Y. Ho, ASM International, Materials Park (1998)193.

21 K.V. Govindan Kutty, R. Asuvathraman, M.V. Krishnaiah, V. Ganesan, R. Parthasarathy, D. Sai Subalakshmi, B. Suhasini, K.C. Srinivas, K.A Gopal and P.V. Kumar, Design, fabrication and commissioning of a push rod dilatometer for thermal expansion studies on solids, IGC-283 , Indira Gandhi Centre for Atomic Research, Kalpakkam (2006).

22 J.W. Arblaster, Platinum Metals Rev. 41(1997)12.

The role of Thermal Techniques in Microwave Processing of Technical Ceramics

S. R. Dharwadkar

Department of Chemistry
University of Mumbai
Kalina Campus, Mumbai 400098

Dr. S.R. Dharwadkar graduated from Mumbai University and joined the BARC Training School in the year 1961. Since then for nearly thirty seven years he worked extensively in problems connected with the chemistry related problems of nuclear fuel. The other major area of his work is related to the development of processes for the safe disposal of high level nuclear work. After retirement from BARC, Dr. Dharwadkar joined the Institue of Science of Mumbai Universi+ty as Honorary Professor of Physical Chemistry and continued his teaching and research activities. Dr. Dharwadkar received the Netzsch-ITAS Award for his outstanding work in Thermal Analysis. More than 160 papers based on his work along with his associates have been published in international peer reviewed journals.

ABSTRACT

The paper discusses the role of microwave heating in combination with suitable precursor chemistry in the low temperature solid state synthesis of important technical ceramics. The importance of thermal techniques in optimization of microwave processing temperatures is highlighted with the examples from the work done in the author's laboratory and the published literature.

INTRODUCTION

Microwave processing of materials has opened new vistas in the field of material science. Several, different types of materials difficult to synthesize and sinter employing the conventional chemical routes and sintering procedures have been synthesized and sintered much more rapidly at remarkably lower temperatures, following the microwave

processing techniques[1-5]. The present article highlights the role of microwave processing in materials technology including the discussion on some of the basic principles leading to the explanation of enhanced reactivity of the materials in presence of microwave radiation.

General Methods for the Enhancement of the Reactivity of Solids

The Precursor Approach

Solid state synthesis of large number of materials including some of the important technical ceramics involves heating of the reactant components to very high temperatures (>1200 to 1300C) for prolonged periods, ranging from several hours to days, with intermittent grinding. Attempts have been made during the last several years to reduce the reaction temperatures and increase the reaction rates. These include formation of the reaction components from their precursors, prior to reaction, 'in situ' either from the individual precursors or the precursor containing all the components participating in the reaction. This approach facilitates the intimate contact between the reactant components. Mixed hydroxides ,carbonates and carboxylates have, for instance, often been employed to produce the oxides in the "active " form 'in-situ', which subsequently react to form the product at much lower temperatures than those needed, if the two or more oxides are taken separately and mixed together prior to the reaction[6-14]. The role of precursors and 'in situ' generated reactants in enhancing the solid state reactivity is presented in an excellent monograph by Hedvall[15] .

Sol-gel Process

Sol-gel process is yet another approach that has often been employed to obtain uniform distribution of the reaction components prior to the formation of the product. [16-19] .The product which is generally obtained at lower temperatures is often amorphous and needs much higher temperature treatment for crystallization [18].

Self Propagating High Temperature Synthesis

In another approach known as self propagating high temperature synthesis(SHS), the reactants are chosen in such a way that there is fuel as well as oxidant in the reactants

and the overall reaction is highly exothermic which facilitates very rapid rise of local temperature and hence the reaction rate. The product formed in this reaction is often amorphous or poorly crystalline and needs higher temperature heat treatment for its crystallization. Moreover, the fuel to reactant ratio utilized in such reactions is often very high and the combustion reaction results in the formation of voluminous gaseous products and porous carbon, which has to be removed from the product by heating it in air or oxidizing atmosphere at high temperatures. Several important ceramics have been synthesized following this approach [20-22] .

The Role of Defects in the Enhancement of the Solid State Reactivity

In the methods mentioned above the in situ generated reactants are metastable and have structures, replete with different types of defects, and high surface activity. Further, the particle to particle contact between the reactants is more intimate which results in considerable enhancement of the reaction rate. The presence of defects such as vacancies, interstitials etc. provides the driving force for the reaction and assists in the enhancement of the reaction rate.

The role of defects in the reactivity of the solids is well known. Several investigators have reported the enhancement of the reaction rate in the systems in which the defects have been created by subjecting the reactants to various treatments, including the nuclear radiations such as alpha rays, neutrons etc [23,24] . The defects introduced in the structure of the reactants by different means could be responsible for the changes in their numerous properties, which include electrical, mechanical, optical, magnetic and several others. Such defects can also alter the reactivity of solids and speed up the rates of reaction by several orders of magnitude.

Enhancement of the Solid State Reactivity by Microwave Radiation

A remarkable break through leading to the increased reactivity of the solid state reactions has resulted from "microwave heating" of the reaction mixture. It has been reported that several ceramics requiring very high temperatures for their synthesis by

conventional methods can be prepared at much faster rates at lower temperatures if the microwave heating is employed in place of conventional heating [1-4].

Interaction of Microwaves with Matter

The clear understanding of the enhanced reactivity of the materials in the presence of microwave radiation necessitates the knowledge of the interaction of the microwave radiation with the matter. Microwaves are coherent electromagnetic radiations
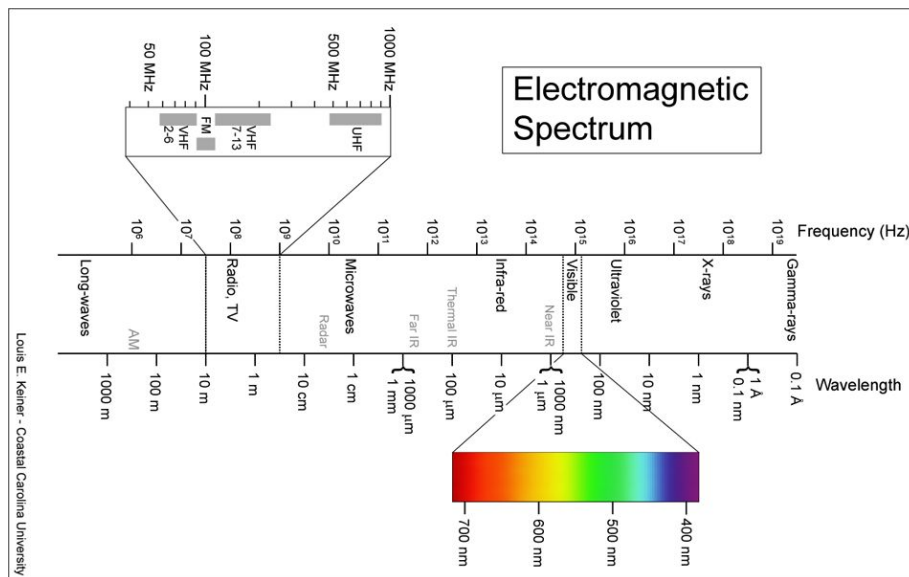

Figure 1: Different regions of electromagnetic spectrum

in the range 300MHz to 300GHz(Figure.1). These waves are either reflected by materials like metals, absorbed by certain types of materials (having high dielectric constants) or transmitted [Figure 2].
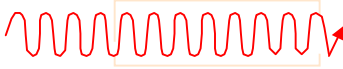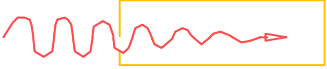
Material type	Penetration
TRANSPARENT **(Low loss insulator)**	**Total**
OPAQUE **(Conductor)**	**None** **(Reflected)**
ABSORBER **(Lossy insulator)**	**Partial to total**
ABSORBER **(Mixed)** **(Low loss insulator + absorbing materials)**	**Partial to total**

Figure 2:Different types of interaction of microwaves with materials

The materials subjected to microwave radiation, unlike in other heating, get heated in the bulk(volumetric heating) due to its inherent properties like high dielectric loss[1] . The interaction of microwaves with such materials results in the conversion of microwave energy into heat energy. The mode of bulk heating resulting from such interaction heats the material uniformly and the product obtained has a uniform microstructure and grain size due to uniform heating. The heat transfer in this case is from the bulk of the sample to the surrounding i.e. reverse compared to that in conventional heating. The mode of heating of the material by microwave radiation is shown schematically in Fig.3.
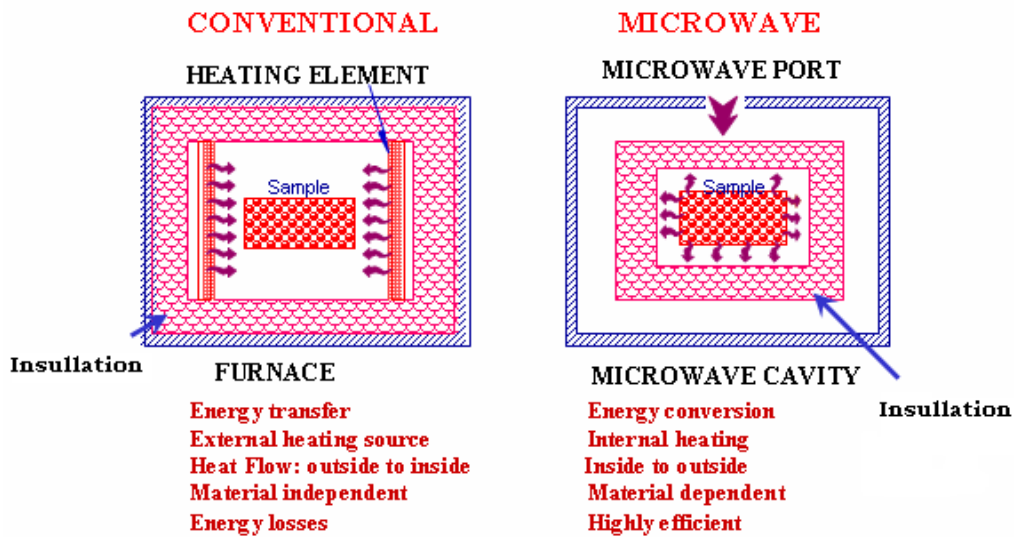
Figure 3: The modes of heat transfer in conventional and microwave heating

The heating in this case is much more rapid compared to that in conventional heating. The comparative rate of heating in the two cases is brought out in Fig.4
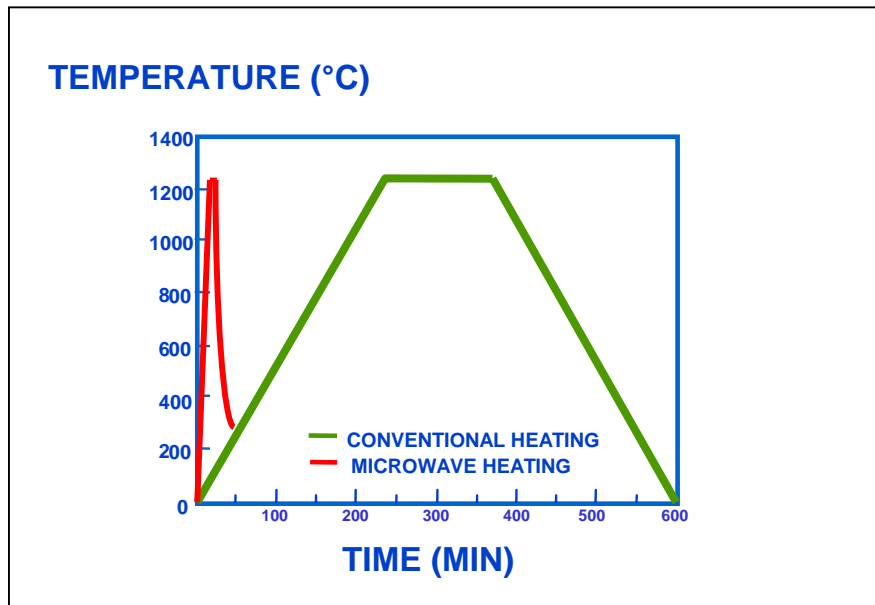

Figure 4: Comparative rates of heating in conventional and microwave heating

The enhanced reactivity of the reactants in the presence of the microwave field is not due to the type of defects introduced in solids by high energy radiation such as neutrons, alpha rays, gamma rays etc. but is related to the dielectric and magnetic properties of the reacting materials. The energy associated with the microwave radiation is much too smaller compared to that of the radiations such as gamma- rays. According to Roy and co-investigators [26-28] different reactants interact with the microwaves to different extent. The reactants interacting strongly with the microwaves heat up much faster than the materials which are non-interacting. The sharp temperature gradients between the various reaction components (microwave active and non-active or poorly active), interacting with the microwaves to different extent, is assumed to provide the driving force for the reaction and bring down the average temperature of the reaction. In conventional heating, on the contrary, all the reaction components in the mixture are heated to the same extent. The difference in the two modes of heating is schematically shown in Figure 5. Roy et.al [27] supported their hypothesis by studying a model reaction of Fe_3O_4 with Y_2O_3 to form yttrium iron garnet (YIG).
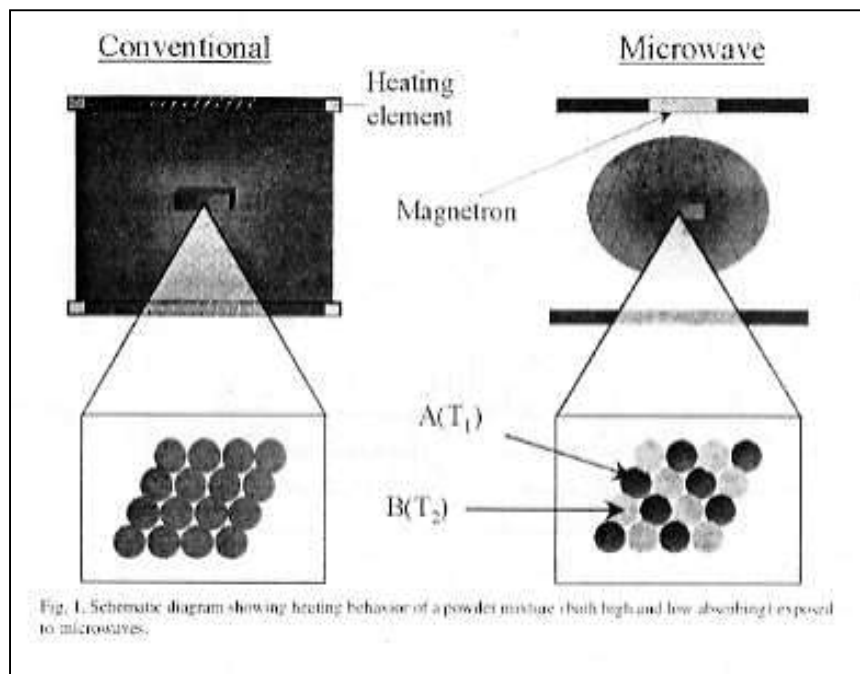

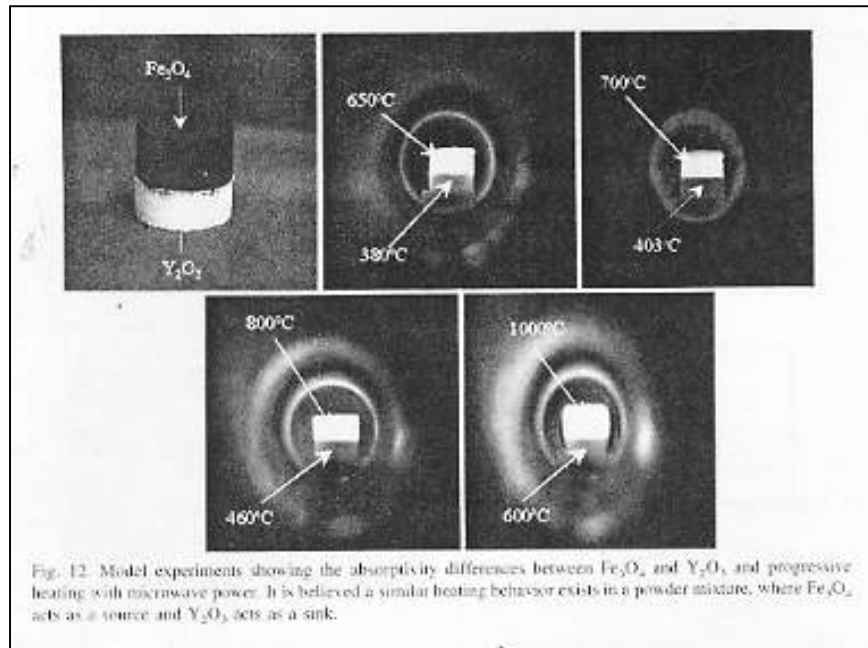Figure 5: Schematic representation of the difference in the conventional and Microwave heating

Fig. 12. Model experiments showing the absorptivity differences between Fe₃O₄ and Y₂O₃ and progressive heating with microwave power. It is believed a similar heating behavior exists in a powder mixture, where Fe₃O₄ acts as a source and Y₂O₃ acts as a sink.

Figure 6: Photographs of the Fe_3O_4 and Y_2O_3 pellets heated in contact in the microwave field

The photograph in Figure 6 shows the difference in the heating characteristics between Fe_3O_4 and Y_2O_3. It can be seen from this Figure that Fe_3O_4 heats up much faster than Y_2O_3 and the temperature rise of Y_2O_3 at least in the initial stages is by a heat transfer from Fe_3O_4 to Y_2O_3. The huge temperature gradient between these two phases provides the driving force for the diffusion of iron oxide species in Y_2O_3 which subsequently results in the formation of YIG.

The difference in the interaction of the reactants with the microwaves could mainly be due the intrinsic difference in the properties of these substances, mainly the difference in their dielectric property which is thought to be the key parameter involved in the interaction of the microwaves with the materials and their subsequent heating. The microwaves are low energy radiations and their interaction of matter is not similar to that of nuclear radiations like gamma-rays or neutrons, but results from the interaction of the microwave radiation with the electric and magnetic dipoles of the material to be heated

and inhibition of the charge transport in the material in the presence of the fluctuating electric field vector of the applied microwave field.

It has been recently reported that the substances containing the lattice defects such as vacancies in hypo-stoichiometric oxides can affect favorably their interaction with the microwave radiation [3], particularly its electric component. More recently, Agrawal and co-workers [28], in their experiments performed in a single mode microwave set up demonstrated that the magnetic properties of the components involved in the heating experiments, in addition to the dielectric properties could be equally important for the interaction of the microwave radiation with the materials and their subsequent heating. They observed that the ferritic materials such as Fe_3O_4 and other materials containing unpaired d-electrons decrystallized on heating in the magnetic component of the microwave radiation. The collapse of structure results in the formation of an amorphous phase which could augment the reactivity by orders of magnitude. The collapse of the crystal structure of partially reduced and manganese doped TiO_2 is shown subjected to magnetic component of microwave radiation is shown in Figure.7
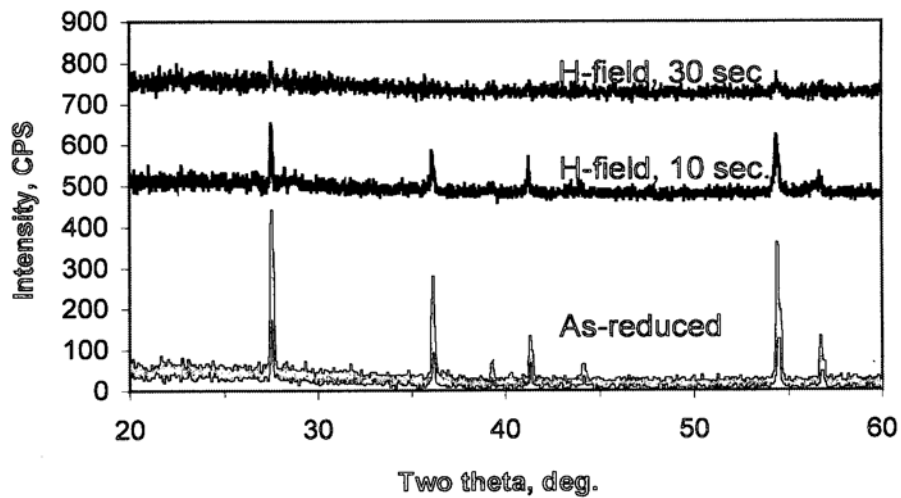
(A)
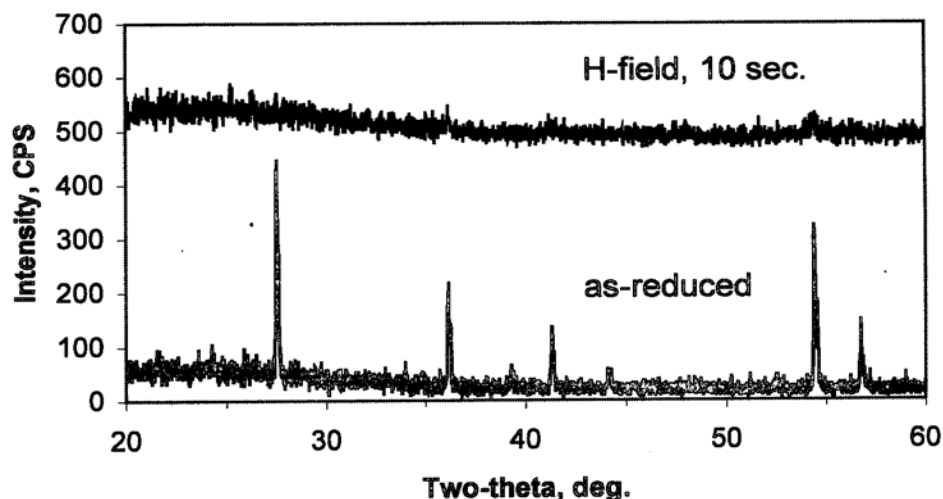
(B)

Figure 7. Behaviour of pure(A) and manganese doped partially reduced TiO2 in magnetic component of microwave radiation.

As stated earlier, the dielectric property of the material depends on the defect structure of the material which will decide the ease with which the dipoles can reorient in the presence of the applied microwave field. Agarwal and co-workers [3,26,27] in fact, observed considerable difference in the reaction rate involving the formation of BaTiO3 from BaCO3 and TiO2 when the stoichiometric TiO2 in the mixture was replaced partially by reduced TiO2 prior to the reaction, In the case of reduced TiO2 the reaction initiated at much lower temperature and progressed much more rapidly. Agarwal [3] attributed this dramatic change to the oxygen vacancies in hypostoichiometric TiO2, which interacted much more strongly with the microwave field.

Microwaves are electromagnetic radiations and comprise of both electric as well as magnetic components mutually perpendicular to each other. Microwave heating was initially attributed mainly to the interaction of the electric field vector with the material to be heated [1]. However, in more recent investigations it has been demonstrated that the magnetic vector of the microwave radiation also interacts much more strongly with the materials to be processed and contributes substantially to its overall heating [4,5] .

Typical examples of the difference in heating of materials in electric and magnetic components of the microwave radiation for Fe powder and ZnO are presented in Figure 7.
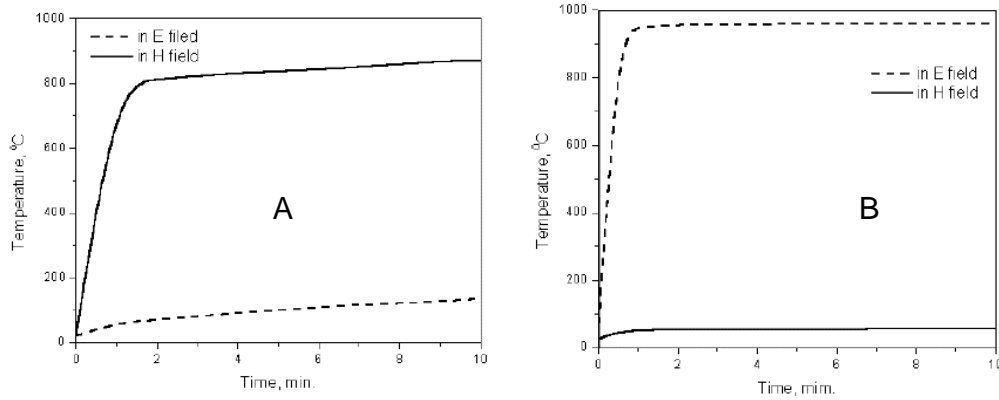
Figure 7: Difference in the heating of Fe (A) and ZnO (B) in electric and magnetic components of microwave radiation

Careful evaluation of some of the recent experiments of Agrawal and co-workers, involving the sintering of the materials [5], suggests that the materials having the atoms with one or more unpaired electrons(particularly in 'd' block elements) interact strongly with the microwaves, which subsequently leads to very rapid heating.

The experimental observations made on the enhancement of the rate of synthesis of materials and sintering in microwave field finds support in the equation proposed for the absorption of the microwave power by the materials and their relationship with the dielectric and magnetic properties.

The pov   microwave radiation can be expressed by the equation

$$P = w(e_0 e'' E^2 + \mu_0 \mu'' H^2)$$

Where

P = power absorbed

w = frequency

e_0 = permittivity of free space

e'' = dielectric loss factor

E = intensity of electric field

$\tilde{\mu}$=permeability of free space

μ'' = magnetic loss factor

H = intensity of magnetic field

It is clear from this equation that the rate of reaction in the microwave field will depend on the **dielectric** as well as the **magnetic** properties of the materials participating in the reaction.

The first and second term in the equation represent the interaction of the microwave with the **dielectric & magnetic** properties respectively of the components participating in the chemical reaction.

It is obvious from the above equation that **the rate of reaction between the reaction components will be enhanced phenomenally, due to strong interaction with the microwaves if the reacting materials have favorable dielectric as well as magnetic properties**. Solid state synthesis of several compounds was carried out in our laboratory, keeping this principle in mind.

Microwave Processing of Materials

The basic understanding of the factors governing the rate of solid state reactions is necessary for the effective use of microwave radiation in solid state synthesis.

Some of the important criteria are listed below.

- In solid state reactions the rate of reaction, in addition to the concentration of the reactants (mole fractions) depends strongly on the interfacial area between the reacting phases and the product formed.

- The progress of the reaction is dictated by the rate of transport of the reacting species through the product layer.

- Larger surface area of the reactant components increases the probability of the particle to particle contact and considerably enhances the reaction rate.

The general methods adopted for increasing the effective surface area of the reactants and particle to particle contact of the components to enhance the rate of the reaction are:

- Ball Milling
- Homogeneous precipitation
- Sol Gel Process
- Hydrothermal Process
- Combustion Process
- Precursor Chemistry

The reaction components in most of the cases are however, generated 'in situ' from the precursors and allowed to combine prior to agglomeration and reduction in their effective surface area.

STRATEGY FOR THE SOLID STATE SYNTHESIS ADOPTED IN THE PRESENT WORK

To increase the effectiveness of microwave heating, only those reactions were selected in which the reaction rates could, a priori, be increased even in the absence of microwave radiation by modifying the conventional ceramic methods. It was felt that the microwave heating would further enhance the rates of such reactions. This involved generation of the reactants 'in situ' from suitable precursors which subsequently reacted chemically, to yield the products at temperatures much lower than those required in normal ceramic methods. The reactions were carried out by conventional electrical heating.

The same reactions under identical conditions were carried out by microwave heating of the reaction mixture, which was found to further augment the rate of the reaction and lower the average reaction temperature by several hundred degrees.

Choice of the precursors

The choice of the precursor was based on the following factors:

1. On thermal decomposition, the precursor produced the reaction components ' in situ' which reacted rapidly to yield the product.
2. During the thermal decomposition of the precursor one or more reducing gaseous species were formed which provided reducing ambient environment around the sample.
3. The gases liberated during the decomposition reaction reacted exothermically among themselves or with the ambient atmosphere to produce local heating, which could result in the increase in the reaction rate (SHS).
4. At least one of the reaction components generated 'in situ' had unpaired'd' electrons.

The above criteria are based on the following premises:

1. It is known that the mixture of reactants generated 'in situ' from the precursors is far more reactive than the mixture of the same components prepared externally [15],probably due to the ' nascent' surface, finer particle size and more uniform dispersion in the reaction mixture, which is responsible for the enhancement of the reaction rate.
2. The reducing environment around the reaction mixture could facilitate reduction of some of the cations in reactant components to the lower oxidation state and produce oxygen vacancies in the reactants which interact strongly with microwaves and provide most efficient heating.
3. The presence of unpaired'd' electron/s in the reaction components could facilitate strong interaction with the magnetic component of the microwave radiation, thereby considerably enhancing the reaction rate, due to the formation of the amorphous phases[28].
4. The local heating of the reaction mixture due to exothermicity of the reaction could further augment the rate of reaction in the microwave field, by creating thermally induced dipoles in materials in which the intrinsic dipoles are absent

Compounds synthesized

Following compounds were synthesized in the author's laboratory via the reactions carried out by microwave heating:

1. TiO_2 (Anatase and the mixture of Anatase and Rutile)
2. Lanthanum Cobaltite ($LaCoO_3$) and Chromite($LaCrO_3$) – the components of Solid Oxide Fuel Cells.
3. Sodium Zirconium Phosphate (NZP)
4. $CaTiO_3$, $CaZrO_3$ and $BaTiO_3$
5. Calcia Stabilized Zirconia (CSZ)

 Thermoanalytical information derived from TG and DTA for the completion of the reaction under normal experimental conditions, in the absence of the microwave field, was used for the optimization the temperature of heat treatment of the precursors in microwave system.

Preparation of TiO_2 (Anatase &the mixture of Anatase and Rutile)

TiO_2 was prepared by heating Ti $(OH)_4$ precursor in microwave oven at 350^oC. The precursor was obtained from titanium chloride solution by controlled precipitation using urea or by controlled dilution of $TiOCl_2$ solution.

The XRD patterns of TiO2 produced by heating Ti(OH)$_4$ precursor by these methods are presented in figures 8 and 9 respectively.
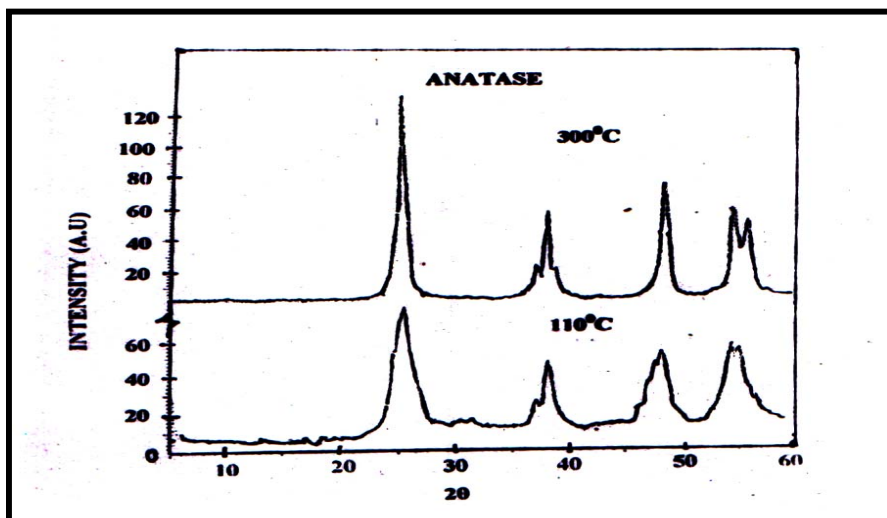
Figure 8. XRD patterns of TiO_2 obtained by heating hydroxide precursor prepared by controlled precipitation method at two temperatures 110^0C and 300^0C
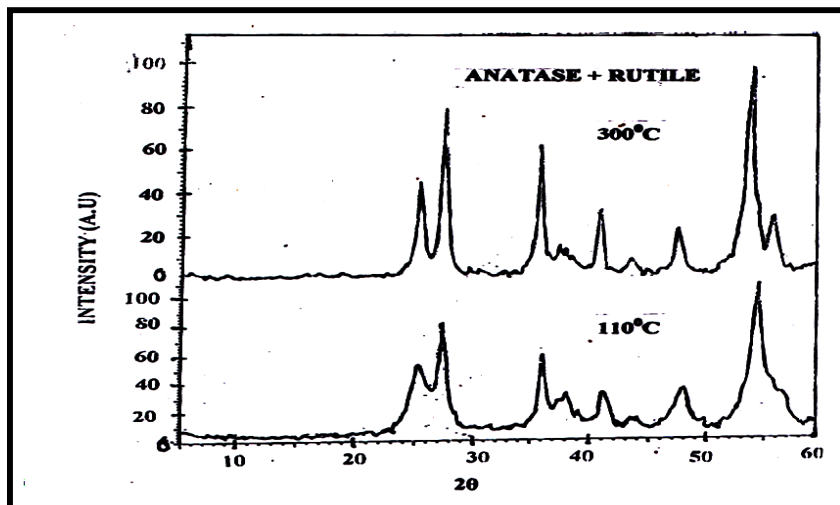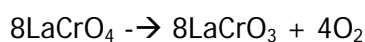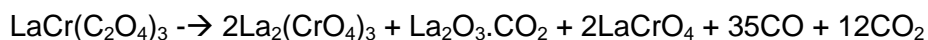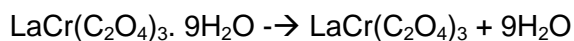

Figure 9. XRD patterns of TiO_2 obtained by heating hydroxide precursor prepared by controlled hydrolysis method at two temperatures 110 and 300C.

Formation of TiO_2 at lower temperatures in the present case could be mainly due to the strong interaction of the electric component of the microwave with the dipoles in the hydroxide precursor. The product obtained in this study has high specific surface area and minimum crystallite size.[29]

Solid State Synthesis of Lanthanum Chromite(LaCrO3) and cobaltite (LaCoO3) – The components of Solid Oxide Fuel Cells

These compounds were prepared from their co-precipitated mixed oxalates by microwave heating. $LaCoO_3$ (cathode material for SOFC) could be prepared at lower temperatures[30] compared to that needed for the preparation of $LaCrO_3$ (interconnect material for SOFC)[31]. Both the compounds however, could be prepared in the microwave system below 500^oC.

LaCrO$_3$ could be prepared by heating the mixed oxalate of La and Cr in resistance heated furnace, in air, at 900°C, at which temperature LaCoO$_3$ was not formed. The co-precipitated mixed oxalate hydrates of lanthanum and chromium on heating ,lost their water of hydration and decomposed through the sequence of steps.

LaCr(C$_2$O$_4$)$_3$. 9H$_2$O -→ LaCr(C$_2$O$_4$)$_3$ + 9H$_2$O

LaCr(C$_2$O$_4$)$_3$ -→ 2La$_2$(CrO$_4$)$_3$ + La$_2$O$_3$.CO$_2$ + 2LaCrO$_4$ + 35CO + 12CO$_2$

LaCr(C$_2$O$_4$)$_3$ + La$_0$O$_3$.CO$_2$ + 2LaCrO$_4$ -→ 8LaCrO$_4$ + CO$_2$ + 3/2 O$_2$

8LaCrO$_4$ -→ 8LaCrO$_3$ + 4O$_2$

Such steps for the thermal decomposition of La-Cr mixed oxalate are as follows ultimately yielding LaCrO3 above 800C. Though the stoichiometry of the reaction concluded from the TG curve indicated the formation of LaCrO3 at this temperature, the product obtained was poorly crystalline. The same mixture on heating in microwave oven produced crystallined LaCrO3 at 500C. TG and DTA plots for the above reactions are presented in figures 10 and 11.
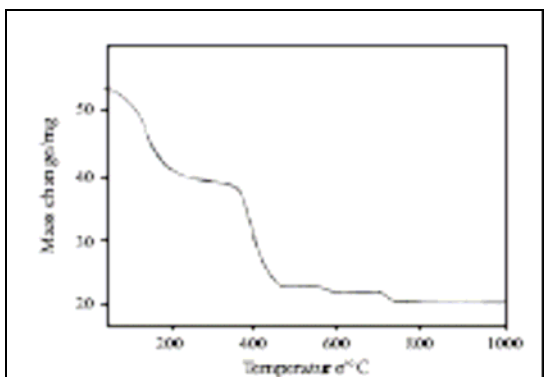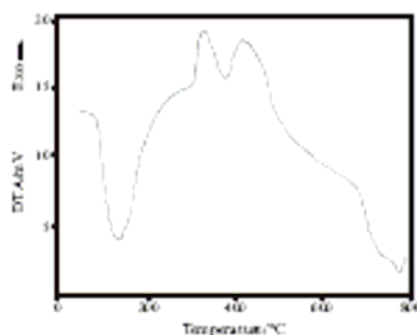

Figure.10

Figure.11

It can be seen from these figures that the dehydration of mixed oxalate of chromium in air is followed by the decomposition of anhydrous oxalate releasing heat due to oxidation of evolved CO in air, thereby increasing the local temperature of the reaction, which could

augment the reaction rate. Similar observations made on the thermal decomposition of mixed cobalt oxalate hydrate[30] enabled understanding of the lowering of the reaction temperature and enhancement of the rate for the formation of $LaCoO_3$ in the presence microwave field.

XRD patterns of LaCoO3 and LaCrO3

- XRD patterns for the products obtained in microwave and resistance heated furnaces are presented in Figures 12 & 13.

- It is important to note that in the case of transition metal oxides containing the unpaired 'd' electrons the oxygen vacancies in concert with the unpaired 'd' electrons will augment the rate of solid state synthesis in microwave processing.
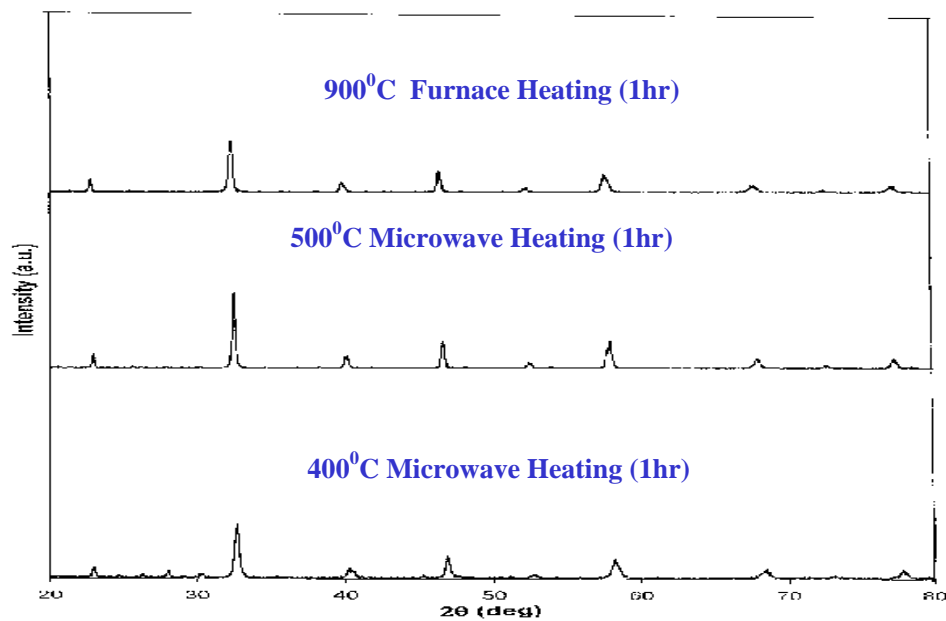

Figure12. XRD patterns of $LaCrO_3$ formed by heating the precursor
   a) In Microwave Heating System at 400C for 1hr
   b) In Microwave Heating System at 500C for 1hr
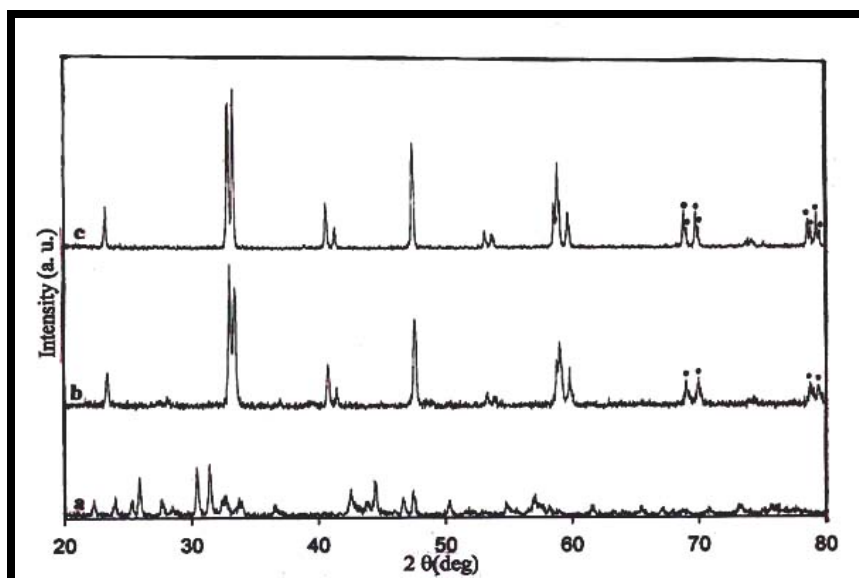   c) In Conventional Furnace at 900C for 1hr

Figure 13: XRD patterns of LaCoO$_3$ formed by heating the precursor

a) in Conventional Furnace at 800C for 1hr

b) In Microwave Heating System at 400C for 1hr

c) In Microwave Heating System at 800C for 1hr

Preparation of Thermodynamically stable Sodium Zirconium Phosphate (NZP) for fixation of High Level Nuclear Waste

NaZr2P$_3$O$_{12}$ considered as a thermodynamically stable matrix for the fixation of high level nuclear waste was prepared by heating the mixture of Na2CO3, ZrO(NO$_3$)2.5H2O and NH4.H$_2$(PO)$_4$ in microwave system at 450°C[32,33]. The simultaneous TG-DSC plots for this reaction mixture are shown in Fig.14. It is clear from this figure that the initial endothermic peak due to dehydration is followed by a series of major and minor exothermic peaks which could be due to oxidation of the evolved ammonia during the course of decomposition and crystallographic transitions in ZrO2. This local exothermicity could be useful in the augmentation of the reaction rate in the presence of the microwave field. The possible sequence of the reactions which could be involved in the formation of NZP from the reaction mixture could be represented by the following equations
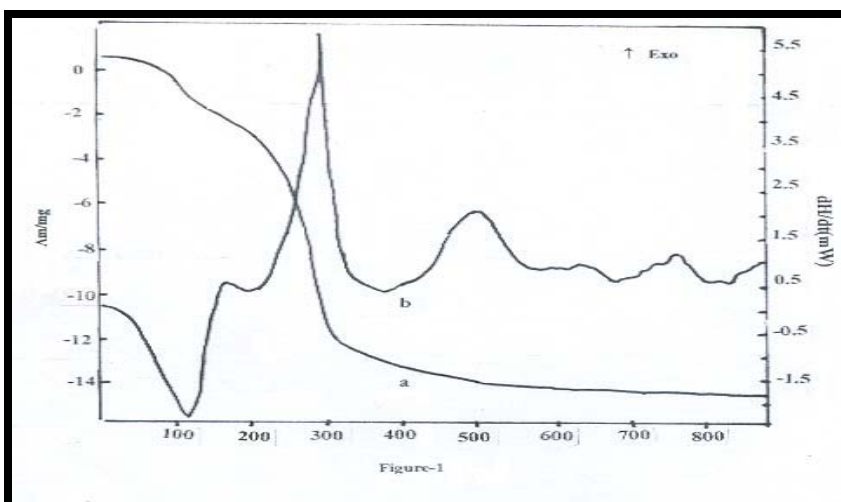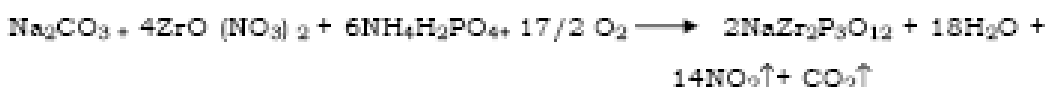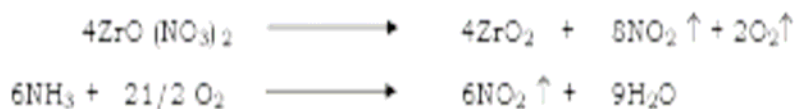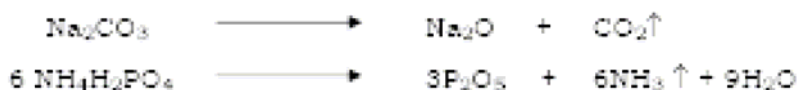
Figure. 14. Simultaneous TG-DSC plot for the thermal decomposition of the reaction mixture:

$$Na_2CO_3 \longrightarrow Na_2O + CO_2\uparrow$$

$$6\,NH_4H_2PO_4 \longrightarrow 3P_2O_5 + 6NH_3\uparrow + 9H_2O$$

$$4ZrO\,(NO_3)_2 \longrightarrow 4ZrO_2 + 8NO_2\uparrow + 2O_2\uparrow$$

$$6NH_3 + 21/2\,O_2 \longrightarrow 6NO_2\uparrow + 9H_2O$$

$$Na_2CO_3 + 6\,NH_4H_2PO_4 \longrightarrow Na_2O + 3P_2O_5 + 4ZrO_2$$
$$+ 4ZrO\,(NO_3)_2 + 17/2\,O_2 \qquad\qquad + 18H_2O + 14NO_2\uparrow + CO_2\uparrow$$

$$Na_2CO_3 + 4ZrO\,(NO_3)_2 + 6NH_4H_2PO_4 + 17/2\,O_2 \longrightarrow 2NaZr_2P_3O_{12} + 18H_2O +$$
$$14NO_2\uparrow + CO_2\uparrow$$

The air dried reaction mixture subjected to simultaneous TG-DSC analysis indicated that the total mass loss involved in the reaction was complete by 600°C.The DSC pattern was however complex and consisted of the initial endothermic peak due to dehydration followed by a sequence of exothermic peaks due to denitration, deammoniation and subsequent oxidation by air of evolved ammonia to nitric oxide. Some of the minor exothermic peaks could also result from the crystallization of the amorphous product formed from the overall decomposition reactions.

The material obtained by heating the reaction mixture in MW oven at 450°C was highly crystalline. Heating the same mixture in conventional furnace required temperatures in excess of 650°C for its synthesis by the same reaction.
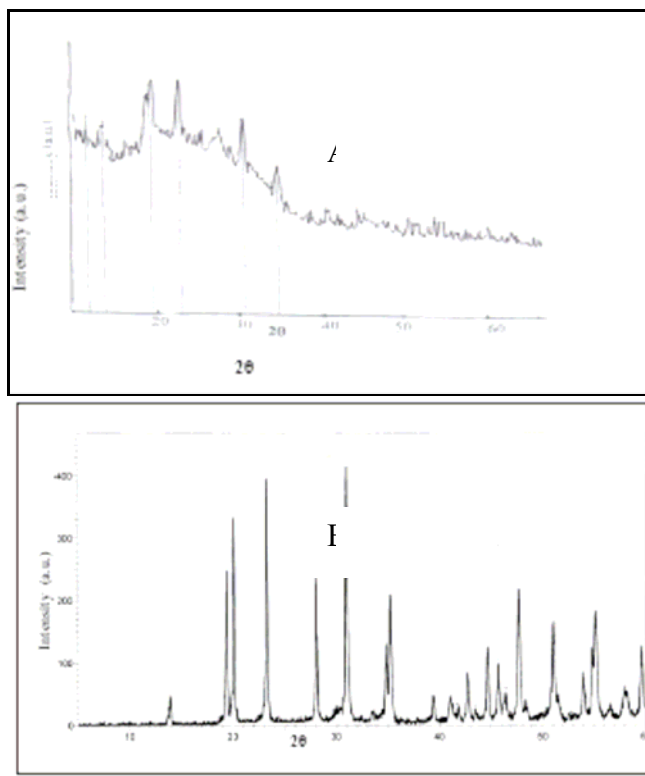
Figure 15. XRD patterns of the reaction mixture heated in conventional resistance furnace(A) and microwave oven(B) at 450C.

XRD patterns of NZP obtained by heating the reaction mixture in MW oven and conventional resistance furnace at 450^{0}C are presented in Figure 15A and 15B.

Partial reduction of the Zr+4 to Zr+3 by ammonia evolved during the course of reaction would create unpaired'd' electrons and also oxygen vacancies in ZrO2 which would facilitate strong electric as well as magnetic interactions with the microwaves, thereby increasing the reaction rate. The local exothermicity of the reaction resulting from the oxidation of ammonia could further augment the reaction rate and bring down the reaction temperature.

Case Study of the Solid State Synthesis of CaTiO$_3$ and BaTiO3

CaTiO$_3$ was synthesized by heating calcium titanyl oxalate (CTO) in a microwave oven around 500°C in air for one hour.[34].The sequence of steps in which CTO transforms to the final product is shown typically in the Thermogravimetric (TG) and Differential Thermal Analysis (DTA) curves recorded on the sample (Figure 16).
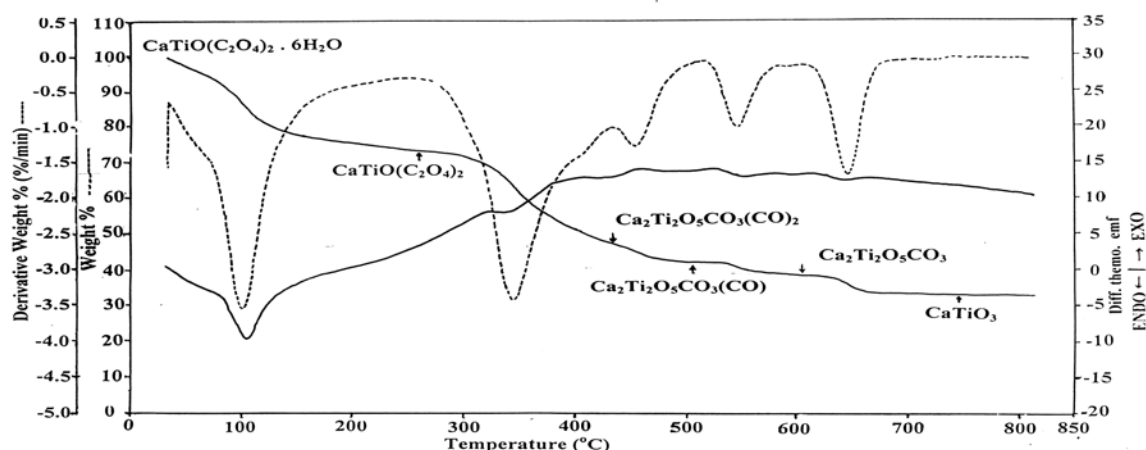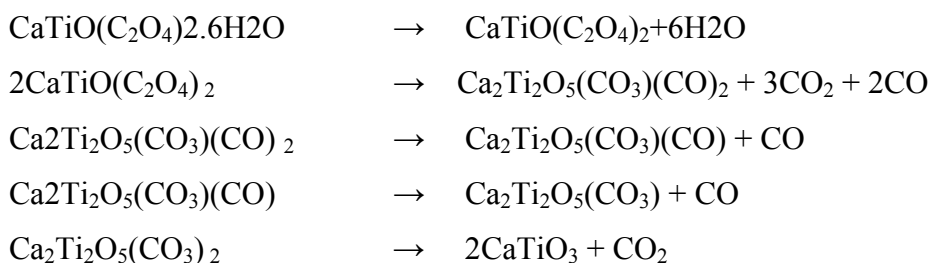
Figure 16. Simultaneous TG-DTG-DTA curves recorded for the thermal decomposition Of calcium titanyl oxalate hydrate [34].

It can be concluded from this figure that CTO on thermal decomposition in air in a conventional resistance heated furnace transforms to $CaTiO_3$ above 650^oC

The formation of $CaTiO_3$ from Calcium titanyl oxalate precursor (concluded from the TG curve) involved the following sequence of steps:

$CaTiO(C_2O_4)2.6H2O$ $\rightarrow$ $CaTiO(C_2O_4)_2 + 6H2O$

$2CaTiO(C_2O_4)_2$ $\rightarrow$ $Ca_2Ti_2O_5(CO_3)(CO)_2 + 3CO_2 + 2CO$

$Ca2Ti_2O_5(CO_3)(CO)_2$ $\rightarrow$ $Ca_2Ti_2O_5(CO_3)(CO) + CO$

$Ca2Ti_2O_5(CO_3)(CO)$ $\rightarrow$ $Ca_2Ti_2O_5(CO_3) + CO$

$Ca_2Ti_2O_5(CO_3)2$ $\rightarrow$ $2CaTiO_3 + CO_2$

Formation of highly crystalline CaTiO3 could however be observed from the CTO precursor heated in microwave oven at temperature as low as 500^oC for one hour. The results are presented in Figure . 17

Similar observations were made in our recent investigation on the microwave assisted solid state synthesis of BaTiO3[35].

XRD patterns of CaTiO₃ obtained by conventional and MW heating

Reducing atmosphere created by evolved CO 'in situ' could have reduced Ti (III) producing oxygen vacancies in TiO_2. This could also introduce unpaired electron in 'd' orbital in Ti ion, which could also contribute to the enhancement of the reaction rate, due to the interaction of the magnetic component with the unpaired electron.
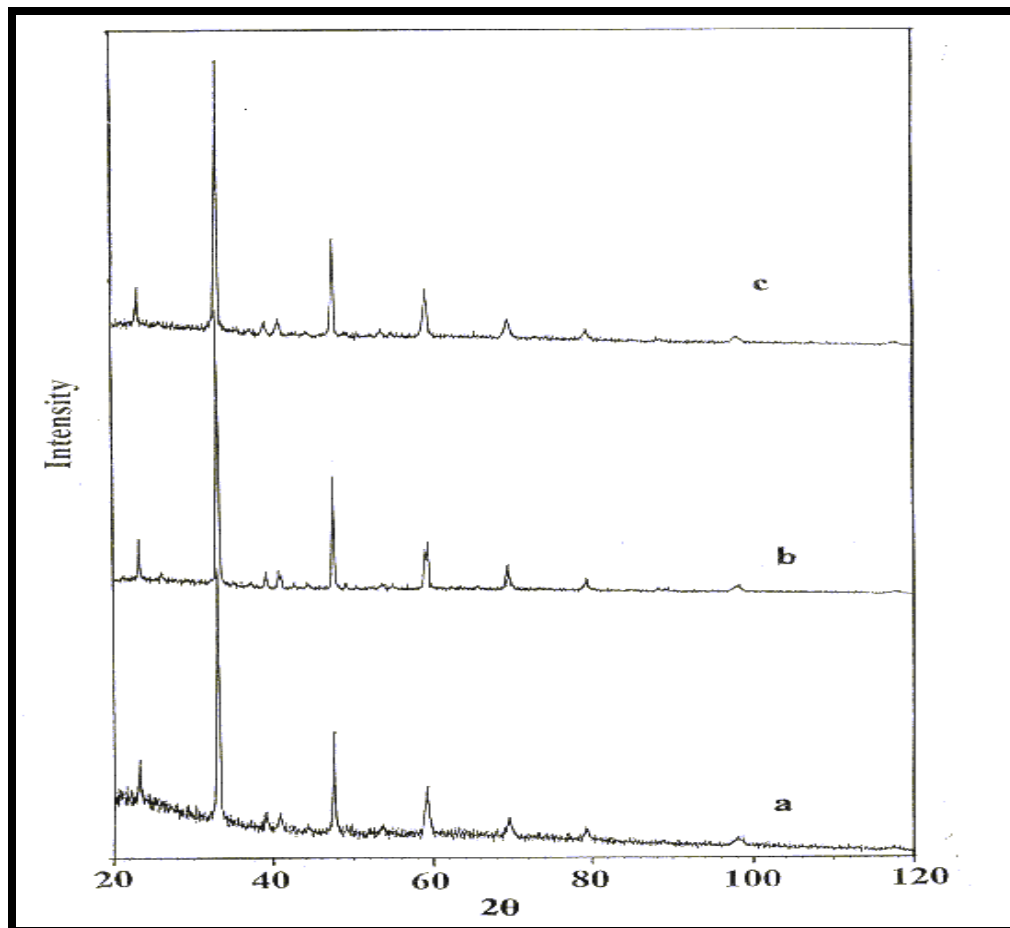

Figure.17: XRD pattern of CTO heated at
    a) 500°C for one hour in microwave heating system ,
    b) 700°C for one hour in microwave oven and
    c) 700°C for one hour in conventional resistance heated furnace

Preparation of Calcia Stabilized Zirconia (CSZ) from mixed oxalate precursor by MW heating

The calcia stabilized zirconia, an important solid oxide electrolyte was prepared from the mixed oxalate containing 15 mole % of calcia precipitated from the aqueous solution of the mixture of nitrates [36]. The simultaneous TG-DTA curve recorded on the mixed oxalate is presented in Figure.18
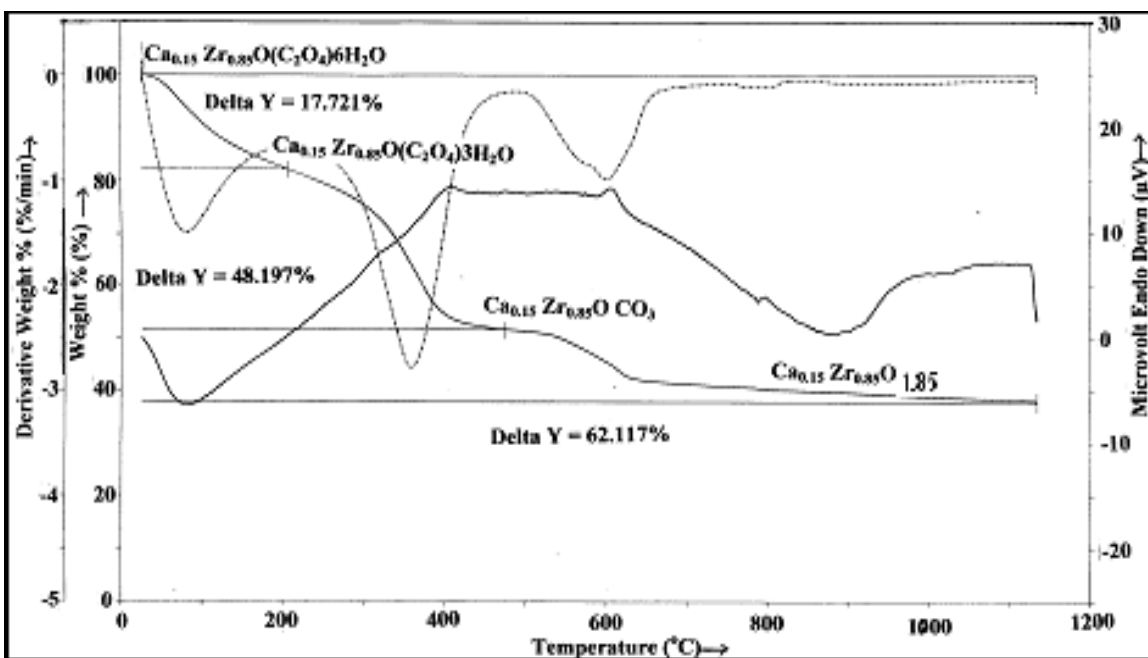

Figure 18: Simultaneous TG-DTA curve recorded on the mixed oxalate

The TG-DTA plots indicate near completion of the formation of solid solution from the precursor above $700^{o}C$ in N_2 atmosphere.

XRD patterns of CSZ prepared in MW and resistance heated furnace showed that

1. The air dried oxalate precursor on heating in microwave system at $400^{o}C$ yielded cubic stabilized zirconia (Figure.19).
2. The conventional heating technique required temperatures above $600^{o}C$ with repeated grinding of the reaction mixture. (Fig.20)
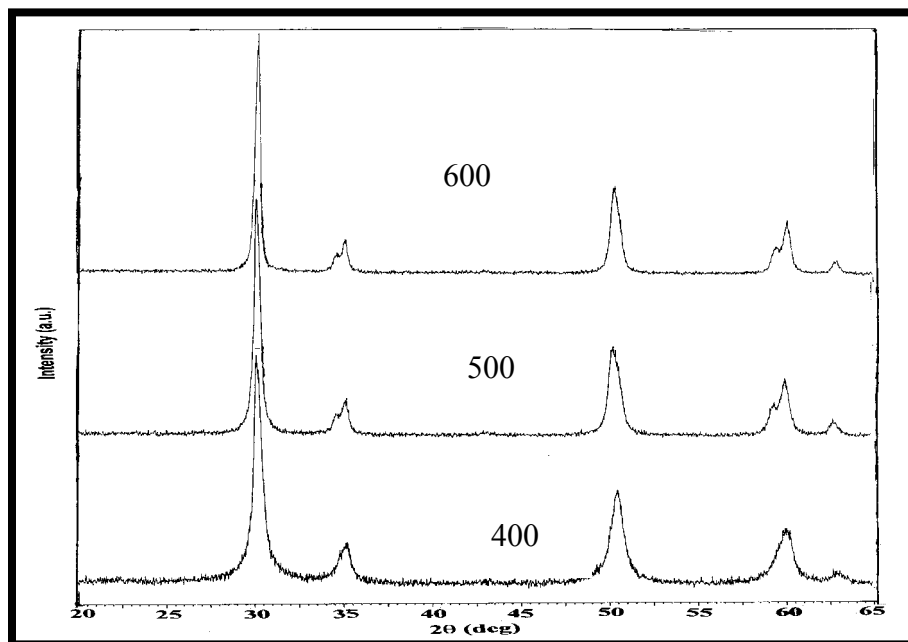
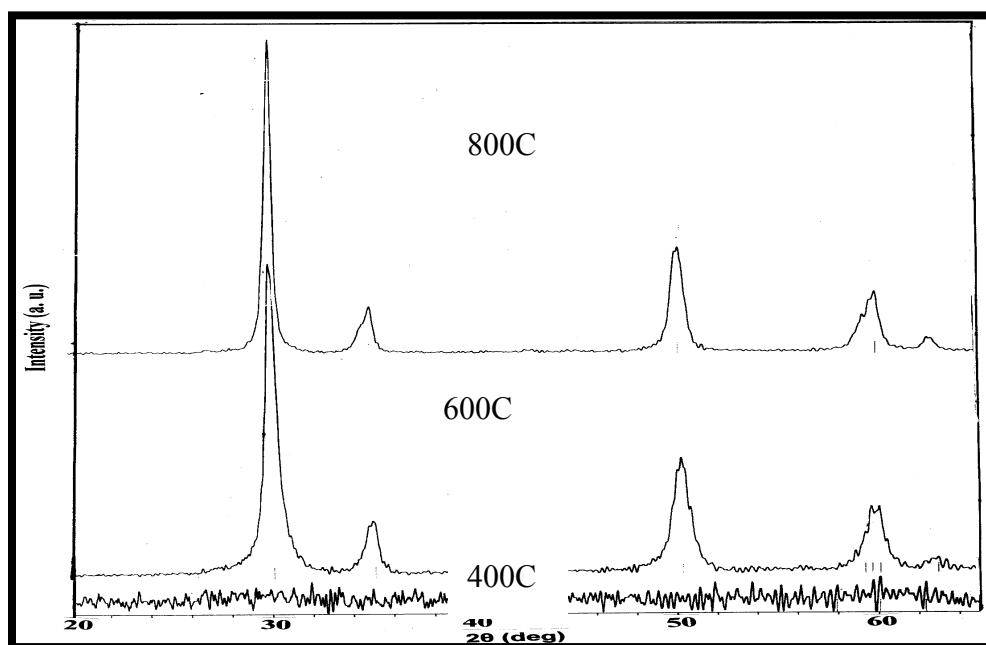**Fig. 19: XRD of Ca $_{0.15}$ Zr $_{0.85}$ O$_{1.85}$prepared by microwave heating**

Fig. 20: XRD of Ca $_{0.15}$ Zr $_{0.85}$ O$_2$ prepared by conventional heating

The oxygen vacancies produced by the substitution of Zr+4 by Ca+2 and by partial reduction of Zr+4 to Zr+3 by evolved CO could facilitate the formation of CSZ at low temperature.

The oxygen vacancies and the unpaired'd' electron in Zr+3 would contribute to the dielectric and magnetic heating respectively.

SUMMARY OF THE OBSERVATIONS

The results of the investigations reported here indicate that thermal analysis of various precursors and the reaction mixtures greatly facilitate the optimization of the temperature of the microwave processing. The temperature of completion of the reaction as indicated by TG under normal heating conditions indicates the maximum heat treatment temperature in the microwave field, which could in fact be much lower, later determined by actual experimentation. The other important information obtained is on the local heating of the material due to exothermicity of the reactions and also the temperature of dehydration in the case of hydrates. The presence of water present in the reactants facilitates heating, by virtue of their electric dipoles and the exothermicity observed for the thermal decomposition in air suggests the evolution of the oxidizable gaseous species formed in the reaction which could be responsible for the introduction of the defects such as oxygen vacancies in the 'in situ' generated reactants formed by the decomposition of the precursors.

The reducing atmosphere created during the thermal decomposition of the precursors facilitates formation of the oxygen vacancies, particularly in the case of TiO2 and ZrO2, which interact strongly with the microwaves and provide most effective local heating.

The reduction of Ti and Zr to the lower oxidation state also produces unpaired electrons which can interact more strongly with the magnetic component of the microwave radiation.

In the case of cobalt and chromium, the number of unpaired electrons in cobalt in +3 state are more than those in chromium +3. Hence, cobalt interacts more strongly with the microwaves and the product is obtained at relatively lower temperature.

In the preparation of $LaCoO_3$ and $LaCrO_3$ the reducing atmosphere may not augment the reaction rate, if unpaired electrons are the only species responsible to enhance the rate of reaction.

Attempts are underway to utilize mixed hydroxide precursors in place of mixed oxalate to rule out the role of lower oxidation states of Co and Cr in the synthesis of these compounds.

All the observations reported here and elsewhere in the cited references indicate that though there is pronounced increase in the reaction rate in the microwave field, the microwave processing of materials is however applicable to only few systems in which the reactants and the products are microwave active.

CONCLUSIONS AND COMMENTS

The results of the solid state reactions presented in this work confirm the role of microwave heating in both, altering the course of the reaction as well as enhancing its rate. The observation of reduction in reaction temperature suggests the lowering of the kinetic barrier for the reaction in presence of the microwave field. Several reactions thermodynamically favorable at low temperatures are found not to occur at any measurable rate at these temperatures. The classic example is that of combination of hydrogen and oxygen to form water which is thermodynamically feasible at room temperature, but never takes place in the absence of catalyst which lowers the kinetic barrier for the reaction.

It has been claimed that compared to the conventional heating, the microwave processing of materials is economically viable since the process involves only selective heating of the material to be processed. Several questions however have to be answered prior to the adoption of this technique for commercial exploitation. One of the most

important is the efficiency of electrical energy conversion to microwave radiation, which is subsequently used for the heating purpose. Opinions differ on efficiency of conversion of the electrical energy to microwave. It is assumed that the energy loss involved in the conversion of electrical energy to microwave is not more than 30% [37] and that this loss can be more than compensated by the phenomenal increase in the reaction rate in the microwave field and lowering of the reaction temperature. Das and Curlee [38] in brief communication discussed the energy conservation potential and economic feasibility of switching to microwave heating and concluded that the cost of energy will be higher and the economic feasibility of the new process will depend on the potential effects the process may have on non energy inputs and on improved product quality.

Metaxas and Meredith[39] observed that in commercial applications of microwave heating the overall efficiency is in the range 50 to 70%. The energy saving arising from the use of microwave energy was considered on the basis of the energy cost for the entire process.

It was concluded that the economic benefit of microwave processing is difficult to define in a general way. The decision to use microwave processing for any application has to be based on an analysis of the specific process. Important factors include the location of the processing facility; the product requirement; possible property improvements; alternative sources of energy; availability of capital and the balance between energy cost, labor costs, capital cost and the value added to the product. In most successful applications of microwave processing; improvement of the productivity and material properties, and saving in time, space and capital equipment, are probably the best bases for selecting the microwaves over conventional processes.

The other intriguing question pertains to the definition of temperature in such reactions. This ambiguity in defining temperature is also applicable to some extent for the reactions taking place in conventional heating systems. The temperature measuring probe is seldom located in the bulk of the sample but always in its close vicinity, irrespective of the conventionally heated or microwave heated sample. The huge temperature gradients between the reactant particles, stated to be responsible for the pronounced increase in the reaction rate [4] would eventually even out to yield the average temperature of the system, undergoing the transformation at the set temperature.

References:

1. W.H. Sutton ,Ceram. Bull. 68, (1989) 376

2. J. D. Katz, Ann. Rev. Mater.Sci., 22 (1992) 153 and ref.3,11 and 12 therein

3. D K Agrawal, Current Opinion in Solid State and Mater. Sci. (1990) 480

4. J.Cheng, R.Roy and D.K.Agrawal, Mater.Res.Innov.,5[2001]170

5. R D .Peelamedu, R Roy, L. Hurutt, J. Cheng, D K Agrawal, Mater.Res. Innov. 6 (2002) 128

6. W. Hertl, J. Am. Ceram. Soc., 71 (1988) 879

7. H. S. Potdar, S. B. Deshpande, P. D. Godbole and S. K. Date, Ind. J. Chem., A31 (1992) 870

8. H. S. Potdar, S. B. Deshpande, S. R. Sainkar, A. Mitra and S. K. Date, Ind. J. Chem., A37 (1998) 674

9. Y. B. Khollam, A. S. Deshpande, H. S. Potdar, S. B. Deshpande, S. K. Date and A. J. Patil, Mater. Lett., 55 (2002) 175

10. H. S. Gopalkrishnamurthy, M. Subbarao and T. R. Narayanan Kutty, Thermochim. Acta, 13 (1975) 183

11. S. R. Dhage, Y. B. Khollam, H. S. Potdar, S. B. Deshpande, B. D. Sarwade and S. K. Date, Mater. Lett., 56 (2002) 564

12. A. S. Deshpande, Y. B. Khollam, A. J. Patil, S. B. Deshpande, H. S. Potdar and S. K. Date, Mater. Lett., 51 (2001) 161

13. K. Nag and A. Roy, Thermochimica Acta, 17 (1976) 247

14. H. S. Gopalkrishnamurthy, M. Subbarao and T. R. Narayanan Kutty, J. Inorg. Nucl. Chem., 38 (1976) 417.

15. J.A.Hedvall, in "Solid State Chemistry", Elsevier,Amsterdam, 1966

16. K. S. Madiyasni, C. T. Lynch and J. S. Smith, J. Am. Ceram. Soc., 48 (1965) 372

17. H. Dishlich, Angew. Chem. Intn. Edn., 10 (1971) 367

18. D K Agrawal and J H Adair , J am Cer Soc. 73 (1990) 2153

19. S. Mukasyan, C. Costello, K. P. Sherlock, D. Lafarga and A. Varma, Separation and Purification Technology, 25 (2001) 117

20. S. T. Aruna, M. Muthuraman and K. C. Patil, Mater. Res. Bull., 35 (2000) 289

21. M. A. Sekhar and A. Halliyal, J. Am. Ceram. Soc., 81 (1998) 380

22. S. T. Aruna, M. Muthuraman and K. C. Patil, J. Mater. Chem., 7(12) (1997) 2499

23. S. Bhaduri, S. B. Bhaduri and E. Zhou, J. Mater. Res., 13 (1998) 156

24. H. Nayak and D. Bhatta, Thermochim. Acta 362 (2000) 99-105

25. J. Jach in " Reactivity of Solids", Ed. J. D'Boer, Elsevier, Amsterdam, 1961,pp334

26. R.D.Peelamedu , R Roy, D K Agrawal ,J.Mater. Res.,16 (2001) 277

27. R.D.Peelamedu , R Roy, D K Agrawal, Mater. Res Bull., 36 (2001)2723

28. R.Roy,Y.Feng,D.K.Agrawal, J.Am.Ceram.Soc.,88(2005)16

29. Y.S.Satpute, S.A.Borkar and S.R.Dharwadkar, Bull.Mater. Sci.,26(2003)667

30. Y.S.Malghe, A.V.Gurjar and S.R.Dharwadkar, J.Thermal. Anal. and Calorimetry,78(2004)

31. Y.S.Malghe and S.R.Dharwadkar, J.Thermal.Anal. Calorimetry 2007(in press)

32. A.H.Naik,N.V.Thakkar,V.Venugopal and S.R.Dharwadkar, J.Thermal Anal. and Calorimetry,78(2004)707

33. A.H.Naik,N.V.Thakkar, V.R.Palkar,K.D.Singh Mudher,V.Venugopal and S.R.Dharwadkar, Radiochim.Acta,94(2006)335

34. B.M.Patil, R.S.Srinivasa and S.R.Dharwadkar, Bull.Mater.Sci.,30(2007)1.

35. Y.S.Malghe,A.V.Gurjar and S.R.Dharwadkar, Bull.Mater.Sci.27(2004)217

36. Y.S.Malghe and S.R.Dharwadkar (Unpublished work)

37.D.K.Agrawal,(Private communication)

38. S.Das and T.R.Curlee , Ceramic Bull., 66(1987)1093

39. A.C.Metaxas and R.J.Meredith in "Industrial Microwave Heating" (1983), Institute of Electrical Engineers,London,, Peter Peregrinus Ltd.